

# Design, fabrication and testing of support structures for biomimetic water filters

**Vogel, Jörg**

*Publication date:*
2011

*Document Version*
Publisher's PDF, also known as Version of record

# Design, fabrication and testing of support structures for biomimetic water filters

PhD Thesis

Dipl.-Ing. Jörg Vogel

Aquaporin A/S and DTU-Nanotech

AQUAPORIN

DTU Technical University of Denmark

# Abstract

The demand for technological development in water purification is tremendous and the possibilities numerous, both in traditional reverse osmosis (RO) and in the upcoming field of forward osmosis (FO). RO is a well developed field and works on the principle of pressing water through a semi-permeable membrane against the osmotic pressure generated by the solute concentration difference in the separated aqueous solutions. The generation of the hydrostatic pressure is energy intensive and demands on membrane stability and salt rejection are high and can only partially be satisfied by state-of-the-art membranes. FO uses the osmotic pressure as a driving force but is a field that just recently has received a higher degree of interest and thus suffers from a lack of optimized setups and specially designed membranes. Big advancements can be made in these water purification techniques by introducing new high performance membranes and also specialized setups in the case of FO. Aquaporin protein based membranes offer a great opportunity in the development of novel high-performance membranes. In this thesis I present the development of support structures and experimental setups that are needed for the technological advancement of such aquaporin based membranes. On one hand there is the flat sheet membrane for RO. Here, I developed a support structure for bilayer lipid membrane formation. This was refined and tested in different experimental chambers. Furthermore, we improved bilayer stability with the introduction of a porous support. The developed sandwich resembles a thin-film composite membrane as known from classical RO membrane technology. On the other hand, a liquid membrane for FO was developed by Aquaporin A/S. To house this membrane and to make it possible to test its performance a novel multi-purpose FO chamber was designed, fabricated and tested. For an additional investigation of the interaction of the liquid membrane with its environment an observation device was developed. Since the development is ongoing this thesis does not include data on actual filtration by aquaporin proteins.

# Resumé

Behovet for teknologisk udvikling indenfor rensning af vand er massivt i disse tider og mulighederne for forskellige løsninger er talrige både indenfor traditionel omvendt osmose samt det nye felt direkte osmose. Omvendt osmose er et veletableret forskningsfelt og princippet bag omvendt osmose processen har været kendt længe: Et hydrostatisk tryk påtrykkes en opløsning med høj koncentration (for eksempel opløse salte) på den ene side af en semi-permeabel membran, og som følge af det påførte tryk presses vand gennem membranen imod den osmotiske gradient. Det er energikrævende at generere et hydrostatisk tryk højt nok til modvirke den osmotiske gradient i omvendt osmose processer. Desuden stilles der høje krav til membran stabilitet samt saltafvisningsegenskaber, noget der kun til dels opfyldes i state-of-the-art membraner i dag. Direkte osmose anvender et osmotisk tryk som drivende kraft, men grundet af den relativt unge alder af dette forskningsfelt lider det af manglen på optimerede forsøgsopsætninger samt specialdesignede membraner. Store fremskridt kan potentielt realiseres i dette forskningsfelt gennem udviklingen af nye højtydende membraner samt specialiserede forsøgsopstillinger. I denne henseende er Aquaporin baserede membraner en oplagt kandidat til en ny type højtydende membran. I denne afhandling præsenterer jeg udviklingen af støttemembraner og forsøgsopsætninger som muliggør den teknologiske udvikling indenfor Aquaporin baserede membraner til rensning af vand. Udviklingen har været delt i to spor – det ene har omhandlet en membran til omvendt osmose, mens det andet har omhandlet en ny type flydende membran til direkte osmose. I udviklingen af en membran til omvendt osmose udviklede og optimerede jeg membranens støttestruktur samt forskellige eksperimentelle kamre til test af membraner. Endvidere optimerede vi membranstabiliteten gennem indførslen af et porøst supportmateriale i støttestrukturen. Den endelige version af membranen til omvendt osmose ligner en tynd-film ”composite” membran, som det kendes fra klassisk omvendt osmose membranteknologi. I udviklingen af en flydende membran til direkte osmose var det nødvendigt at designe producere og teste et nyt multifunktionelt kammer til test af denne type membran. For yderligere at undersøge samspillet mellem den flydende membran og dens umiddelbare omgivelser udviklede jeg en visualiseringsenhed. Udviklingen af en flydende membran til direkte osmose er en del af den igangværende forskning I Aquaporin A/S, hvorfor denne afhandling ikke inkluder faktiske data på aquaporin medieret vandfiltrering.

# List of Publications

**Paper I.** *A support structure for biomimetic applications*
**J. Vogel**, M. Perry, J. S. Hansen, P.-Y. Bolinger, C. H. Nielsen and O. Geschke; Journal of Micromechanics and Microengineering 19 (2009)

**Paper II.** *Development of an automation technique for the establishment of functional lipid bilayer arrays*
J. S. Hansen, M. Perry, **J. Vogel**, T. Vissing, C. R. Hansen, O. Geschke, J. Emnéus and C. H. Nielsen; Journal of Micromechanics and Microengineering 19 (2009)

**Paper III.** *Large scale biomimetic membrane arrays*
J. S. Hansen, M. Perry, **J. Vogel**, J. S. Groth, T. Vissing, M. S. Larsen, O. Geschke, J. Emnéus, H. Bohr, C. H. Nielsen; Anal Bioanal Chem (2009) 395:719–727

**Paper IV.** *Biomimetic membrane arrays on casted hydrogel supports*
M. Roerdink Lander, S. Ibragimova, C. Rein, **J. Vogel**, K. Stibius, O. Geschke, M. Perry, C. Hélix-Nielsen; to be submitted to Langmuir

**Paper V.** *Novel multi-purpose module for forward osmosis*
**J. Vogel**, M. Perry, C. Rein, P. P. Szewczykowski, M. Gruber, C. Hélix- Nielsen, J. Emnéus, O. Geschke; to be submitted

**Appendix I.** *Scaffold for composite biomimetic membrane*
**J. Vogel**, M. Perry, J. S. Hansen, P.-Y. Bolinger, C. H. Nielsen, P. H. Jensen and O. Geschke; WO/2009/074155 (2008)

**Appendix II.** Microfluidic formation and regeneration of highly stable biomimetic membrane arrays; K. Pszon-Bartosz, M. Perry, J. S. Hansen, **J. Vogel**, C. Hélix-Nielsen, J. Emnéus, O. Geschke; to be submitted

# The story of the papers

The papers presented with this thesis reflect the work that has been done throughout the three years of the PhD project. All have the focus on mechanical design, fabrication and optimization of components needed for the investigation and development of a novel type of water filtration device based on biomimetic membranes containing aquaporin proteins.

***Paper I***

Paper I describes the first step of the development of a flat sheet membrane for use in RO. Here, a suitable scaffold with apertures for biomimetic lipid membrane type applications was developed. This work was a continuation of an investigation carried out during my final Diploma project where I selected a scaffold material and production method and was able to fabricate apertures with a diameter of 84 µm. The results of the first experiments with lipid bilayers indicated that it would be beneficial if the support structure would have apertures with a diameter > 100 µm. The fabrication of apertures with a diameter of 300 µm as well as their analysis is presented here. Scaffold topography and diameters were investigated with the help of polydimethylsiloxane (PDMS) replicas and laser confocal microscopy. During $CO_2$ laser ablation melted material accumulated around the area of ablation. This bulge formation was closer investigated and the bulges were found to be smooth and found to be beneficial for lipid bilayer creation. The usability of this support structure was then shown by successfully establishing lipid bilayers across the apertures.

***Paper II***

The usability of the fabricated support from Paper I was further investigated by the formation of lipid bilayers using a novel automation technique. Here, bilayer arrays were formed with a success rate of 95 %. Lifetimes and reproducibility were further increased by pre-treatment with an air-brush where a lipid composition was evenly sprayed onto the support structure. The functionality of the formed lipid bilayer membranes was proven by the incorporation of the ionophoric peptide valinomycin which was shown by the recording of ionic currents. Furthermore, these currents could be blocked again by the introduction of tetraethylammonium.

***Paper III***

Paper III shows the further refinement of the lipid bilayer membrane formation technique by introducing a horizontal chamber. It was developed to gain more control over the lipid bilayer formation by immediate visual inspection. This was made possible by placing the chamber onto a microscope stage. It also allowed for physical access to the actual lipid membrane formation process. The $CO_2$ laser ablation of the ethylene-tetrafluoroethylene (ETFE) substrate was further optimized so that the perforated area of the support structure could be increased from arrays of 64 apertures arranged in a

square lattice and spanning an area of 0.21 $cm^2$ to arrays of 576 apertures corresponding to an area of 1 $cm^2$ which were either arranged in square or hexagonal lattices. The hexagonal lattice further increased the perforation level. Successful bilayer formation experiments proved that the fabricated platform was suitable for further developments of sensitive biosensor assays, and furthermore demonstrated that the design could conveniently be scaled up to support planar lipid bilayers in large square centimeter partition arrays.

***Paper IV***

After successful formation of planar, free-standing bilayer lipid membranes (BLMs) on the hydrophobic multi-aperture partitions from Paper I in the vertical (Paper II), and horizontal chamber (Paper III) the next step towards a biomimetic water filtration system was to investigate how an increased stability could be achieved. Paper IV describes the design and integration of a porous hydrophilic support, called poly-2-hydroxyethyl methacrylate (PHEMA), into the apertures of the membrane scaffolds to stabilize the membrane by dampening membrane vibrations caused by flow close to the freestanding membrane. The polymeric material was bound to the support by functionalizing the surface of the ETFE. It was shown that the PHEMA porous support promoted rapid self-thinning of lipid bilayers suitable for hosting membrane-spanning proteins. A successful incorporation of α-hemolysin demonstrated that the BLMs were fully functional in close proximity to the polymeric material. With this approach, rapid fabrication of large arrays of BLMs that allow large flux transport across the supported membranes should be feasible.

Parallel to the BLM formation and stability extension experiments novel strategies for controllable and reliable reconstitution of membrane proteins into artificially made membranes were explored by my colleagues in Aquaporin A/S. These studies resulted in the development of a method to create giant protein vesicles (GPV) that could be used as a liquid membrane. Here, the principle of FO was applied and the osmotic pressure used as a driving force.

***Paper V***

In parallel to the investigation of bulk liquid membrane, a novel multi-purpose module for FO membrane development was designed, fabricated and tested. Paper V describes this multi-purpose chamber together with the accompanying flow and measurement recording setup. The setup provides automated weight and conductivity measurements that can later on be used to calculate the flux and the salt flux. The chamber in itself can hold a standard flat sheet membrane, but provides also the basic requirements for experiments involving liquid membranes. It has a defined space in between two membranes where an emulsion can be injected. The multi-purpose chambers' characteristics were investigated on the basis of the FO membrane from Hydration Technology Innovations (HTI). The experiments showed that the performance of the module compares well with currently used setups and therefore no disadvantages in comparability from our new module design to state-of-the-art systems is expected.

***Appendix I***

After having shown that the formation of stable BLMs in arrays is possible, the hydrophobic laser ablated support structure was protected with a patent.

***Appendix II***

After using manual membrane formation and thinning in our horizontal chamber setup a next step was to investigate if an automated BLM formation was possible utilizing micro-fluidics. Here, a microfluidic device was developed which enabled the formation and recreation of an array of lipid bilayers across a perforated ETFE partition by utilizing the flow to thin the thick lipid-solvent to a lipid bilayer. Additionally, electrical measurements of BLMs were performed within the micro-fluidic system. To evaluate if the functional lipid bilayers were established in the microfluidic device incorporation of the pore-forming heptameric α-HL membrane protein was conducted.

# My contributions to the papers

Paper I. I designed and performed the experiments. Apart from the bilayer lipid membrane experiments, I performed all analysis and characterization work. I wrote most of the manuscript.

Paper II. I fabricated, analyzed and characterized the support membrane. I participated in the writing of the manuscript.

Paper III. I fabricated the support membrane and took part in the experiments.

Paper IV. I participated in design and performance of the experiments. I investigated, performed and analyzed methods to apply the PHEMA support material to the perforated scaffold. I participated in the writing of the manuscript.

Paper V. I had a significant role in the design, performance and analysis of the experiments. I wrote the manuscript.

Appendix I. I designed, performed and analyzed the experiments regarding the support structure. I had a significant role in writing the patent.

Appendix II. I fabricated and analyzed the support membrane.

# Contents

# 1 Introduction

The ever increasing demand for high quantities of water coupled with increasing water quality demands has in recent years led to an accelerated development of water treatment and the exploitation of new water sources. The demand for technological development in this area is huge and the possibilities numerous. One way is the development of new high-performance biomimetic membranes as presented in this thesis.

Water is the dominating element on earth. Everywhere we go we need it and everywhere we want to go we look for it – in short, it affects all aspects of life. It secures our survival and is essential for food production, energy generation and the economy in general. Water can be found everywhere; in fact it covers 70 % of our planet's surface. It is present in oceans, the atmosphere, plants, and rivers – almost everywhere but most of it is saline and thus only a tiny fraction is fit for human consumption. Even in our industrialized world of today 1.2 billion people lack access to safe drinking water. Millions of people die annually (3900 children a day) from diseases transmitted through unsafe water [1, 2]. The lack of clean water also hinders the development of modern industry and economies which is essential in the course of building a modern society with suitable living standards. Already today, agriculture, livestock and energy are consuming more than 80 % of the water that is fit for human consumption [2]. This number will increase with the increasing world population. In addition, with more countries becoming industrialized the energy component will increase drastically. The development of new materials and chemicals adds new pollutants to the water cycle. Increasing amounts of micro pollutants and pesticides are present in the water resources, which make them unfit for human consumption. Water is thus becoming a scarce resource, not only in developing countries, but industrialized countries are also affected. For example, Israel already now uses more water than what can naturally be replenished [3]. When taking a closer look, it can be seen that industrialized countries not only require water for human consumption but also for their economy where the requirements for water quality are particularly high.

Water can be cleaned to various degrees of purity and making water sources fit for human use often involves disinfection and decontamination. These processes are based on chemical treatment of contaminated water. Examples of chemicals used in this process are ozone, hydrochloric acid, chlorine compounds and ammonia [2]. For industrial use, purity levels have to be even higher than for those for drinking water and sometimes they have to be as high as possible. We then refer to the production of so called Ultra Pure Water (UPW). Compared to potable water with a cleanliness of 1 ppm (parts per million) of impurities, UPW contains only 1 ppb (parts per billion). UPW is used in high-technology applications such as medico, biotech and in the production of semiconductors and flat panels. The latter production uses ever increasing amounts of UPW every day. Since its start in 1960, the semiconductor industry has been one of the fastest growing branches of technology (16 % annual growth). It is characterized by a fast development and widespread use of its products and requires high grade components for its production lines. UPW is essential for rinsing processes and is extensively used in the

production of wafers. The production of UPW, however, is energy intensive (high pressures or elevated temperatures are needed for production) and requires a sophisticated infrastructure. Therefore, UPW production solves water problems for modern industries and the economy only.

In contrast, the exploitation of new water sources for human use requires lower purity levels and less sophisticated equipment, but is nevertheless non-trivial. This process is tightly connected with the accelerated progress in desalination. As mentioned before, most of earth's water resources are saline and to make them fit for human consumption they have to be desalinated. Desalination is the conversion of non-potable seawater and saline aquifers to potable water by removing salt ions. At first, desalination was hard to implement because of its high energy consumption and difficult process conditions which made it inefficient and expensive. In 1970, only 0.8 million $m^3$/day freshwater were produced by desalination [3]. With the development of more efficient processes and new membranes combined with an increased need for desalination, the worldwide production increased significantly to a total volume of desalinated freshwater of 59 million $m^3$/day today. The energy consumption of a desalination process today is 3 to 4 times lower than it was 30 years ago. And it is mostly countries in arid areas that drive the development. Israel and Saudi Arabia are the main producers of desalinated water with Saudi Arabia alone producing 10 million $m^3$/day [3]. The main technique in the field of desalination is RO with more than 50 % of all installed capacity [2]. In RO, water is pressed through a semi-permeable membrane by a hydrostatic pressure that must be higher than the osmotic pressure generated by the difference in solute concentration of the two aqueous solutions on either side of the membrane. This hydrostatic pressure can easily exceed 40 bar. Despite the progress made in the last 30 years desalination is still a very capital and energy intensive process. Salt water has to be pumped to and away from the plant, the intake or feed has to be pretreated and the concentrated feed has to be disposed. Last but not least, the desalination process has to be maintained. Here, creating and maintaining high pressure is one of the main energy consumers.

Alternative methods to RO have been attracting more and more attention in recent years. One of them is FO which has the potential of performing desalination at low energy [2, 4] and could even be used for power generation [5]. FO uses the osmotic pressure gradient to transport water across a semi-permeable membrane. This gradient is established by a difference between the solute concentration in the feed (low concentration) and draw (high concentration). However, no large scale water treatment on the basis of FO has been implemented yet. This is mainly because three main challenges remain [6]. The first challenge is to find suitable draw solutions. Here, different solutions exist but they are either hard to separate from the filtered substance or are damaging the membrane material itself. The second challenge is to design and produce suitable process equipment. RO membranes cannot simply be substituted with FO membranes; the whole processing equipment around has to be modified as well to adapt to the changed working principle. The third and from my point of view the most important challenge is to find a suitable membrane. Standard RO membranes cannot be used as FO membranes due to low flux as well as other side effects. Here, new kinds of membranes have to be designed and until now only one such membrane has been commercialized.

The FO membrane that is commercially available today has a reported flux of about 6 to 8 L/m$^2$h [4, 7] which is far less than the flux in RO processes where that can reach 70 L/m$^2$h (although 30 L/m$^2$h are typical [7]). A closer look at the two processes, RO and FO, will be given in chapter 4 and 5.

The overall global water market has a volume of 480 billion USD with the market for purified water being the second largest in terms of volume and the third largest in terms of turn-over behind only energy and oil. In addition, the water market is constantly growing with desalination having one of the biggest growth rates (55 % in the last 5 years) and a capital expenditure of 11 billion USD today. This is expected to grow to 18 billion USD in 2018 [3] with membrane technologies as one of the significant players. Process equipment and standard membranes are cheap, but energy costs are rising with the reduction of power consumption as one of the great topics of our time. Therefore, incentives for further membrane development exist and the big market will make development profitable.

In summary there is a huge market and a great potential for water purification and desalination but until now we have either high energy consuming RO or low flux FO at our disposal for water treatment and purification. Both methods can however be significantly improved by introducing new and better membranes for enhancing flux and decreasing energy consumption. The designs and investigations undertaken within this PhD project were a part of exactly such a membrane development process. The aim was to support the development and fabrication of a novel water filtration system based on biomimetic membranes with aquaporin proteins. The aquaporin protein is nature's own water filtration channel where in principle nothing else than water can pass. Incorporating these into a membrane should thus result in an effective water filter with manifold possibilities. The company that was founded based upon this idea to use aquaporin proteins in water purification and desalination is Aquaporin A/S (DK). Founded in 2005 the main goal of this Cleantech company is to develop the Aquaporin membrane technology™ capable of purifying water from all other compounds to a new standard. As previously mentioned, the basis for this technology is aquaporin proteins integrated into an artificial water filtration membrane. The unique water transport properties of the aquaporin proteins offer the possibility of developing a membrane with high salt rejection (high purity of product) and low energy consumption for UPW production and desalination.

All facts presented in this introduction show that the development, investigation and fabrication of a novel water filtration membrane is not only driven by the need to tackle water scarcity but for a company, it also is beneficial from an economical point of view. Being an industrial PhD, both points were of great importance because they provided motivation (being part of a growing research field and helping tackle modern worlds challenges) and the environment (having the company as a supporter and partial guide in the research) to what I did and how I did it.

# 2 Definition of goals and structure of the thesis

The overall goal of this PhD project was the investigation and development of support structures and experimental setups for the development of a biomimetic aquaporin based water filtration membrane. Due to the novelty of the concept of using aquaporins in industrial filtration previous work from different scientific areas had to be combined. This is reflected in the presented work in which microfabrication, metrology, biophysical chemistry, and membrane technology can be found. However, the focus was kept on mechanical support structures, chambers, test setups and micro-fabrication technologies that could be utilized in the constantly changing matrix of parameters that is typical for a new field of research.

In the beginning of the project the task was to invent a new perforated support structure for biomimetic membrane formation. To this point most existing ways of fabricating membranes aimed either at single apertures [8, 9] or arrays of apertures with a diameter of less than 1 µm [10]. We, however, wanted to work with arrays of apertures with the size of 50 µm or bigger. This decision was taken due to the fact that for industrial sized water filtration the available area should be maximized. However, apertures could not be too big (mm size) because then bilayer formation would be difficult and rupture of the membrane likely. Therefore, it was necessary to investigate different materials and technologies that could be used for fast and cost-efficient production of such support structures (or scaffolds) with the aim to produce polymeric partitions for industrial use. This development was accompanied with a continuous characterization and optimization of the chosen fabrication process. Furthermore, the application and bonding of additional mechanically stabilizing components, like porous supports, to the scaffold had to be investigated, characterized and tested. These additions were necessary to increase the stability of the biomimetic structure when wanting to expose it to the same challenges (e.g. increased pressure and mechanical stress) as membranes in conventional membrane technology. This included a continuous optimization and redesign of existing experimental setups according to changing specifications and the ongoing development of the biomimetic components provided by my colleagues.

One of the bigger changes underway was the switch from the development of a flat sheet membrane for RO to an aquaporin based liquid membrane for FO. This change was caused by new discoveries in liquid membrane formation developed by Aquaporin A/S. It led to a completely new research track within the water filtration membrane development. The investigation of this new type of membrane required the construction of a novel experimental environment. This included chambers that can house a liquid membrane as well as modules where the interaction of the liquid membrane with its environment could be studied.

This thesis gives a closer insight into the development of support structures for aquaporin based biomimetic membrane for water filtration. Due to the interdisciplinary character of the PhD project, I will start by giving the necessary background information including biomimetic membranes, an

introduction to aquaporins and the principle of osmosis (Chapter 3). Chapter 4 and 5 present the actual work that has been performed within the two different membrane tracks. Chapter 4 starts by giving a close look at RO and the state-of-the-art of membranes. It continues with the development of a flat sheet membrane based on aquaporins including the invention and fabrication of a support structure, the maturation of experimental chambers and the increase of membrane stability by the introduction of a porous support. The second research track comprising the investigation of an aquaporin based liquid membrane is presented in Chapter 5. It starts by explaining the basic principle of FO and the membranes that are used and a basic explanation of liquid membranes. This is followed by the introduction to the observation device that was invented for bulk liquid membrane / aqueous phase interaction and a novel multi-purpose module for FO.

The last part of the thesis (Chapter 6) is a summary of the achieved goals and an outlook into possible future directions.

The papers published during this PhD project can be found in the last part of the thesis. They show the invented support structure (Paper I and Appendix I), its applicability to lipid bilayer formation (Paper II and III and Appendix II), the integration of a porous support (Paper IV) and the novel multi-purpose FO chamber (Paper V).

# 3 Background

## 3.1 Biomimetic membranes and aquaporins

The novel water filtration system envisioned by Aquaporin A/S will be based on aquaporin proteins. To have them fully functional, meaning correctly folded, they have to be in a suitable environment. In nature, aquaporins are incorporated in the cell membrane, which separates the cell from the external environment, consisting of a lipid bilayer. This means that to use the abilities of aquaporins one needs first to establish an artificial membrane that mimics the natural cell membrane, a so called biomimetic membrane.

### 3.1.1 Biomimetic membranes

Biomimetic membranes for technological applications require high membrane stability as well as membrane compatibility to peptides and transmembrane proteins. Both membrane stability and protein compatibility put high demands on the choice of membrane components. In nature, cellular membranes are a complex mix of amphiphilic molecules (such as lipids), transmembrane proteins and other membrane bound components [11]. These organize themselves in a bilayer structure in which a double layer of amphiphilic molecules arrange themselves with their polar moieties facing outwards and their hydrophobic moieties buried inside the double layer [11]. The highly unfavorable packing of water molecules around non-polar substances is the major driving force for the packing of amphiphilic molecules into a bilayer. Besides this, so called hydrophobic forces, van der Waals forces, forces due to hydrogen bonding, and Coulomb interactions in the case of charged molecules, also stabilize the overall structure [12]. Since membranes in nature exhibit mechanical and chemical stability to a wide range of different external stresses they have been a primary source of inspiration for artificial biomimetic membrane systems. Therefore lipids – both natural and synthetic - are extensively used as membrane components and were also the main components used in the experiments to create an artificial water filtration membrane. In parallel, also polymer building blocks such as triblock copolymers have been used as membrane building blocks [13, 14]. Depending on which building block is used artificially formed bilayers are referred to as bilayer (black) lipid membranes (BLM) or black polymer membranes (BPM). BLMs and BPMs can be formed on top of a solid support (Figure 1 A), across an aperture (Figure 1 B) or as spherical shells, so called vesicles (Figure 1 C). The latter represent one of the most widely used methods for studying membrane proteins in biomimetic model membranes. They are called liposomes when lipids are used and polymerosomes when they are formed by synthetic polymers [15, 16]. Vesicles containing reconstituted protein are called proteoliposomes and have been used for delivery of stable protein to lipid or polymer matrices (BLM or BPM) (for review see [17]). Depending on the way the vesicles are formed they are typically divided into 4 categories. There are multilamellar vesicles (MLV), which are vesicles that contain multiple lipid bilayer vesicles inside each other. The second group is small unilamellar vesicles (SUV) that consist of a single lipid bilayer. Typical SUVs have a size in between 4 –

20 nm and resemble the sizes of biological vesicles, carrying neuro-transmitters in the nerve synapses. The third category is large unilamellar vesicles (LUV). These vesicles also consist of a single lipid bilayer but are defined by having sizes between 50 nm and up to 10 µm. The last type of vesicles is giant unilamellar vesicles (GUV), also known as cell-size unilamellar vesicles, because their size approximately mimics biological living cell sizes of ≥ 10 µm.

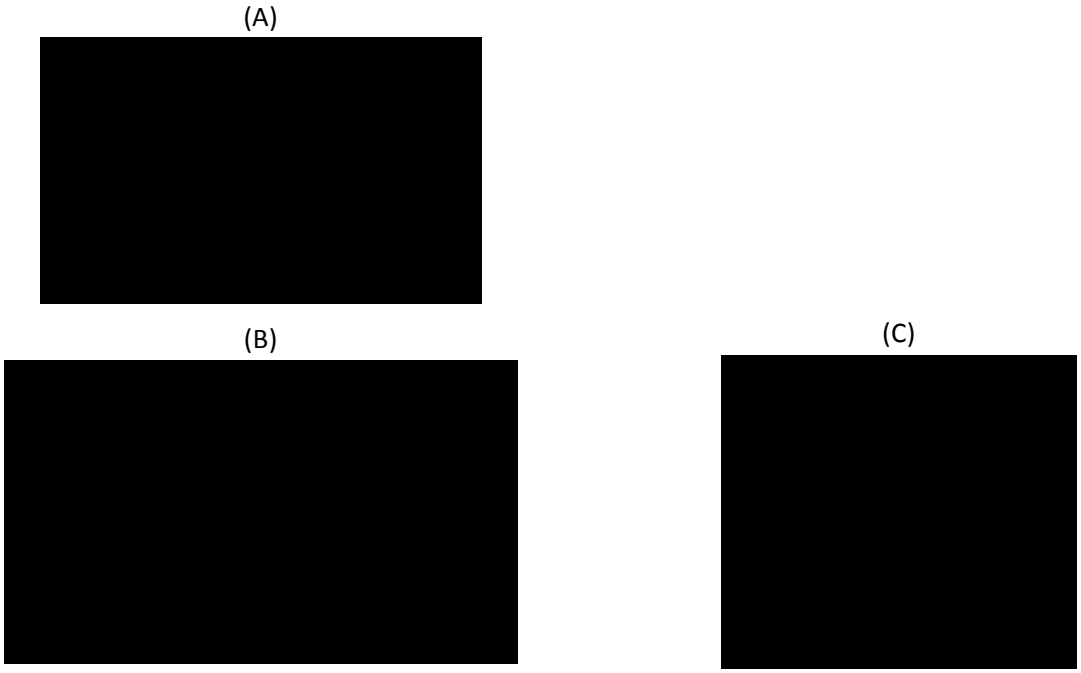


**Figure 1:** Schematic of BLMs on a solid substrate (A), across an aperture in a hydrophobic support (B) or as vesicular structures (C); the solid or perforated support is depicted in green whereas lipids are red.

A tight lipid bilayer, be it as a flat membrane or in vesicles, is only slightly permeable to water and impermeable to ions, and other polar solutes [18]. However, a cell cannot survive without substantial exchange of solutes. The exchange of water is, for example, used by the cell to regulate its volume and internal osmotic pressure depending on the pressure differences over the membrane. This and other transport mechanisms are realized by various proteins, channels and transporters. Water transport for example, is facilitated by aquaporin water channel proteins [19].

### 3.1.2 Aquaporins

The aquaporin protein was first identified by Peter Agre's group in 1988. The protein was thought to function as a channel and was therefore termed "Channel-forming Integral Protein of 28 kDa (CHIP28). In a break-through experiment in 1992, Agre [19] was able to demonstrate that CHIP28 was a water channel (Figure 2). Shortly after, homologous proteins were identified in mammals, plants and bacteria. At the same time, the term aquaporins was coined as a descriptive name for members of this protein family. Several studies [19, 20] have reported that most aquaporins prevent any large molecule or ions to enter the cell interior. Furthermore, even hydronium ($H_3O^+$) and hydroxyl ions ($OH^-$) can be blocked. One exception is for example aquaglyceroporin [21] where also glycerol or urea can pass through. This all happens with a high water permeation rate which can go up to ~$10^9$ molecules of $H_2O$ per second per

channel [20]. This means, that 1 g of aquaporin can transport an amount of up to 700 liter of water per second. The combination of this high permeation rate and strict water selectivity makes aquaporin molecules highly interesting for biomimetically based water filters.

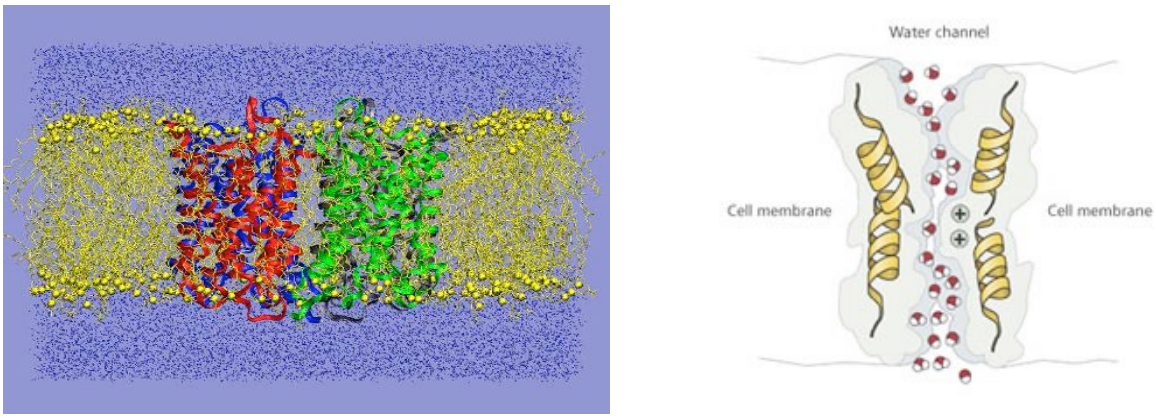


**Figure 2:** Schematic structure of an aquaporin protein; (A) Tetrameric model of SoPIP2;1 (green and red) embedded in a fully hydrated (POPE) and/or phosphatidylcholine (POPC) lipid bilayer (yellow); (B) simplified depiction that shows the water transport through an aquaporin molecule where positively charged ions are deflected by the positive charged amino acid residues at the centre (picture taken from http://www.rsc.org/chemistryworld/Issues/2003/November/theflow.asp).

However, to actually fabricate a working water filter based on aquaporin proteins we have to analyze and understand the principles behind the techniques that are used today to clean and purify water. As mentioned before RO is the governing application when it comes to purifying or desalinating water. In RO a hydrostatic pressure is used to press water through a semi-permeable membrane. The hydrostatic pressure is needed to overcome the osmotic pressure that exists across the membrane due to a concentration gradient.

## 3.2 Osmosis

Osmosis, in general, is a natural process in which concentration differences between two aqueous solutions that are separated by a semi-permeable membrane cause water transport from the side with a low solute concentration to the side with a high solute concentration. This can be explained by the second law of thermodynamics which states that over time a difference in pressure, temperature or concentration in an isolated physical system will equilibrate. This pursuit of maximum entropy leads to irreversible changes in the system. Usually the two differently concentrated aqueous solutions would mix and solute would diffuse equally in the system. By introducing a semi-permeable membrane that does not allow solute transport the only way for the system to equilibrate is by water transport from the side with higher solute concentration to the side with lower solute concentration [22]. This concentration difference across the membrane is reflected as the osmotic pressure by the classic van't Hoff equation:

$$\pi = RT\Delta C_S \tag{3.1}$$

where $R$ is the gas constant, $T$ the absolute temperature and $\Delta C_S$ the difference in molar solute concentration between the two aqueous solutions. This formula has to be modified when a non-ideal (no complete solute rejection) membrane is introduced. Here, the correction factor $\sigma$ is introduced.

$$\pi = \sigma RT\Delta C_S \tag{3.2}$$

Osmosis may be used directly to achieve separation of water from a feed solution containing unwanted solutes. In this process called FO only the osmotic pressure difference ($\Delta\pi$) across the membrane is used as a driving force for transport of water through the membrane. When a hydrostatic pressure is applied to the feed ($\Delta P$), but$\Delta P < \Delta\pi$, water still flows from the dilute solution to the concentrated solution. This so called pressure-retarded osmosis (PRO) can be used to generate electrical power by harvesting the energy created by the osmotic pressure. When the applied pressure exceeds the osmotic pressure, the water flows from the concentrated solution to the dilute solution. We then talk about RO. Figure 3 and Figure 4 further illustrate the pressure-dependent behavior of the flux over the membrane for each individual process. Every separation process, be it osmosis or any other filtration technique can be characterized by a flux over the membrane. In the processes considered in this report, the flux describes the flow of mass (e.g. water, solute etc.) through a unit area per unit time. The substance going through a membrane is also called permeate. Therefore, flux describes the amount of permeate that crosses the membrane over time.

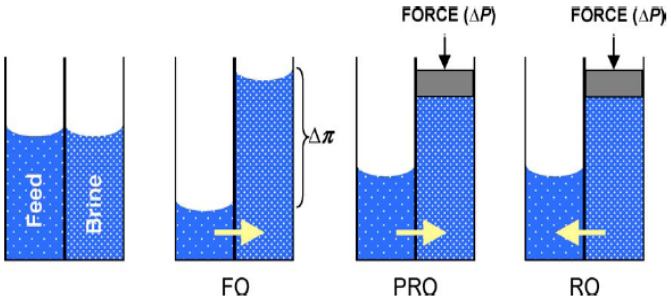


**Figure 3:** Solvent flows in FO, PRO, and RO. For FO, $\Delta \boldsymbol{P}$ is approximately zero and water diffuses to the more saline side of the membrane. For PRO, water diffuses to the more saline liquid that is under positive pressure ($\Delta\boldsymbol{\pi} > \Delta\boldsymbol{P}$). For RO, water diffuses to the less saline side due to hydraulic pressure $\Delta\boldsymbol{P} > \Delta\boldsymbol{\pi}$. Figure adapted from [4].

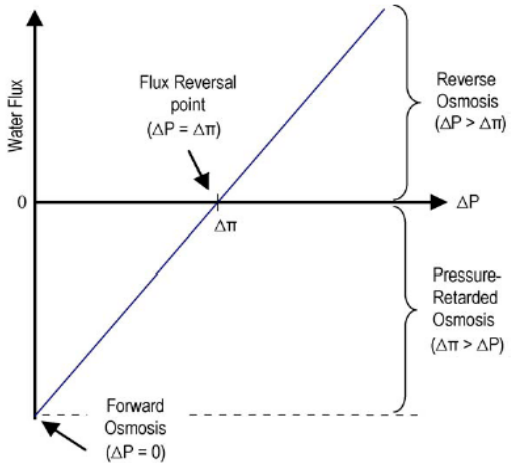


**Figure 4:** Direction and magnitude of water flux as a function of applied pressure in FO, PRO and RO. FO takes place when the hydraulic pressure difference is zero. The PRO zone is where the applied pressure difference is between zero and the flux reversal point, and the RO zone is where the applied pressure difference is greater than the osmotic pressure difference. Figure adapted from [4].

# 4 Flat sheet membrane for reverse osmosis[1]

## 4.1 Reverse Osmosis

### 4.1.1 Application

At present, RO is the main technique when looking at water purification and desalination – in desalination, for example, it makes up over 50 % of all installed capacity [2]. It is used in both, direct seawater and brackish water desalination. The salt concentration of the feed water defines which membranes can be used and how high the recovery rate is. The latter defines the ratio of product flow rate over feed flow rate, meaning how much product volume can be recovered from the supplied feed. Compared to a feed of brackish water with recoveries of 70 – 90 % the desalination of seawater only has typical recoveries of 35 – 45 %. This is due to the higher initial salt concentration of around 35 g/L in seawater compared to only 2 – 10 g/L in brackish water [23]. For reaching the salt concentration of potable water recommended by the World Health Organization (WHO) of 0.5 g/L, less salt has to be removed from brackish water than from seawater. Therefore, when using the same membrane more water with the desired salt concentration can be achieved in brackish water desalination. Higher initial salt concentrations also lead to higher osmotic pressures that need to be overcome. Whereas, pressures between 55 and 70 bar are used in seawater desalination only 20 bar are used for brackish water desalination.

Another high volume application of RO is the production of ultra pure water (UPW) which is widely used in the semiconductor industry. In fact, a factory producing 40 000 wafers per month uses around 8 million liters of UPW each day [24]. UPW has a cleanliness of only a few ppb of impurities. To reach these purity levels several steps like ion-exchange and UV sterilization have to be undertaken with RO being the key technique [23]. Tap water with a purity level of around 200 ppm is used as the feed. The already lower level of impurities minimizes the amount of processing steps and results in a recovery of typically 90 % at applied pressures that range in between 3.5 and 14 bar.

Both application areas are big markets with high volume throughput and RO is a widely known and well investigated technique.

### 4.1.2 Basics of RO

The most important characteristic in RO is an externally applied hydrostatic pressure. It has to be bigger than the osmotic pressure so that water can be pushed through the membrane against a concentration

[1] Parts of this chapter are taken from the chapter “Formation of large scale biomimetic membrane arrays” (M. Perry, C. Rein, J. Vogel) from the book “Biomimetic membranes for sensor and separation applications” which will appear at Springer Verlag in 2011

gradient. The basic setup of a RO filtration system therefore consists of a pressurized feed side with dissolved salts and a low pressure, low salt permeate side. RO as a way to remove salts from water has been investigated for over 100 years. It started with the first experiments of Pfeffer and Traube with ceramic membranes in 1850 and was first patented for desalination in 1931 [25]. Since then technology has advanced fast with the development of new membranes, the optimization of process equipment and the decrease in energy consumption. However, due to a lack of low energy and equally efficient alternatives RO still is today's main technology for desalination.

The water flux $J_w$ that can be achieved with RO depends strongly on the applied hydrostatic pressure $\Delta P$. This can be expressed as:

$$J_w = L_p * (\Delta P - \Delta\pi) \tag{4.1}$$

where $L_p$ is the hydraulic conductivity or hydraulic membrane permeability which expresses how leaky a membrane is. $\Delta P$ describes the applied pressure difference and $\Delta\pi$ the osmotic pressure difference. When permeating the membrane not all salt and dissolved matter will be retained which leads to a salt flux $J_S$:

$$J_S = B * c_{S_0} \tag{4.2}$$

where $B$ defines the salt permeability constant and $c_{S_0}$ is the concentration of salt in the feed solution. However, if a salt flux occurs then 4.1 is not entirely correct anymore because $\Delta P$ and $\Delta\pi$ would not produce identical volume flows [22]. Therefore, a correction factor, the so called reflection coefficient $\sigma$ is introduced to 4.1:

$$J_w = L_p * (\Delta P - \sigma\Delta\pi) \tag{4.3}$$

In membrane technology $\sigma$ is converted into a percentage and called the retention rate $\mathbb{R}$. An ideal membrane that is impermeable to solute would have a retention rate of $\mathbb{R}= 100$ %. However, an ideal membrane does not exist and thus retention rate is used to characterize membrane performance. It can be calculated as followed [23]:

$$\mathbb{R} = \left[1 - \frac{\rho_i * B}{L_p * (\Delta P - \Delta\pi)}\right] * 100\% \tag{4.4}$$

Here, $\rho_i$ describes the density of water [g/cm$^3$]. This equation shows that a membrane can become more selective when applying a higher pressure. But not only the applied pressure, also time and temperature can influence salt rejection and flux. Baker [23] showed that a temperature increase of 30°C can double the flux but decrease the salt rejection however he does not explain the exact reason for this effect. Possible reasons are that an increase in temperature causes a decrease in water density and viscosity. In addition, thermal expansion of the membrane material would result in a widening of the pores. Larger pores and lower viscosity could explain the increase in water flux with increasing temperature. Another influence on water flux and rejection is membrane lifetime. Due to factors that are beyond the scope of this thesis (compaction, fouling, degradation from hydrolysis and membrane

cleaning), a standard RO membrane looses 20 % of its flux over the first three years. This is accompanied by a drop in rejection rate of 0.2 - 0.3 % [23].

These facts point out that not only the pure rejection rate and the flux has to be taken into consideration when choosing a membrane for RO but that also its long-term stability plays a decisive role.

### 4.1.3 Membrane designs

First of all, to withstand the applied pressure the membrane should be mechanically stable which places a certain requirement on its thickness. Typically RO membranes are about 150 µm thick. The flux through a membrane is approximately inversely proportional to the membrane thickness, and 150 µm thick membranes with pore sizes of less than 2 nm would have an unacceptably low flux. In order to increase the flux, RO membranes have an asymmetric structure with a thin (approx. 1 µm) dense toplayer supported on a porous thicker (50 – 150 µm) sublayer (Figure 5). The membrane selectivity is determined by the dense toplayer and the flux by the properties of the sublayer. For the sublayer of RO membranes, it is important to consider the surface porosity and pore size distribution of the material. Two different membranes with asymmetric structure can be distinguished: integral asymmetric membranes and composite membranes. In integral membranes both layers consist of the same material, whereas in composite membranes the materials used for the toplayer and the sublayer are different. The first high performance RO membranes were made of cellulose acetate and belong to the category of integral asymmetric membranes. They are robust, easy to fabricate and resistant to degradation. Especially, they can withstand low concentrations of chlorine that is used to sterilize feed water. The flux and the salt rejection over cellulose membranes depend on their exact chemical structure (e.g. the degree of acetylation) – meaning that a denser structure results in high rejection but low fluxes. So with reasonable fluxes this membrane type typically achieves a salt rejection of 98-99 %, which is too little for direct seawater desalination where a rejection of 99.3 % is needed. Therefore, since 2000 all new desalination plants are equipped with interfacial composite membranes [23]. These are made by interfacial polymerization and can achieve a flux of 50 $l/m^2h$ with a salt rejection of 99.5 % at a pressure of 55 bar. Their greatest flaw, however, is that they are losing their selectivity rapidly when exposed to even trace amounts of chlorine (few ppb). Other materials like non-cellulosic polymer membranes (e.g. polyamide) are produced as hollow fibers and have a good salt rejection (99.5 %), but a low flux (1.8 to 5 $l/m^2h$) and are also unstable when being exposed to chlorine.

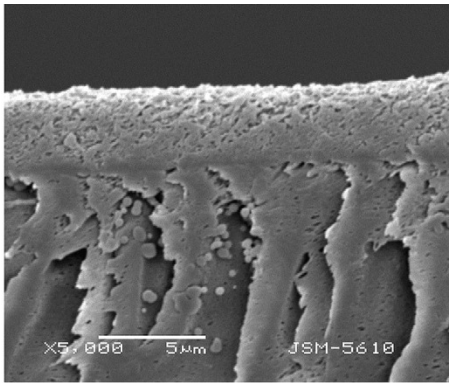


**Figure 5:** Example of thin-film composite (TFC) seawater RO membrane with a thin, dense active toplayer made of polyamide-urethane and a porous polysulphone support layer (picture taken from [26]).

A salt rejection of ≥ 99.3 % is only needed in single step saltwater desalination. When processing brackish water, lower rejection rates are acceptable. Even lower levels are possible in UPW production where membranes with rejection rates of down to 80 % are being used due to the low solute concentration in drinking water. However, it has to be remembered that the higher the salt rejection, the higher the recovery will be. Therefore, RO membranes are continuously refined. One of the best membranes so far was developed by Kurihara et al. [27] which had a salt rejection of 99.9 % with a flux of 20 $l/m^2h$ at a pressure of 69 bar. Unfortunately, this membrane was very susceptible to chlorine and dissolved oxygen and due to these problems the membrane is not commercially available anymore [23].

Summarizing the state of the art in RO membranes two major points become apparent that need to be addressed in the further membrane development – pairing a high rejection rate with a high flux and the resistance to chlorine or other dissolved compounds. Since the discovery of the first high-performance RO membrane in the 1960s [28] different materials, material combinations and techniques have been developed, improved and optimized but the improvements achieved with polymeric materials are decreasing. Many research groups concentrate on improving membranes regarding their fouling and lifetime characteristics by applying surface modifications like plasma treatment [29] and grafting [30] or by optimizing production parameters [31]. Higher resistance against chlorine can also be achieved by the application of different coating processes [32]. However, despite being more stable when exposed to chlorine, salt rejections do not surpass the before mentioned 99.9 % achieved by Kurihara [27]. Therefore, to make the next big step in the development of RO membranes new materials have to be addressed. One opportunity is to integrate aquaporin water channels and thus create a semipermeable membrane. Incorporated into a lipid bilayer these proteins are more resistant to dissolved compounds than existing RO membrane materials and do not degrade when in contact with chlorine [23]. With a reported salt rejection of ≥ 99.999 % [6] they surpass even today's best commercially available RO membrane by a factor of 10 and more. Aquaporins combine high salt rejection with a high water flux capability. When incorporating aquaporins into his polymeric membranes Kumar [33] reports of an increase of productivity (permeability per time and pressure) from 2 µm/(s*bar) to 167 µm/(s*bar). However, this observation was the result of using aquaporins in block-copolymer vesicles in stopped-flow light-scattering experiments. This method enabled Kumar et al. [33] to show the potential of an aquaporin containing membrane but it did not show how to construct a functioning RO membrane.

Here, the difficulty lies within the creation of a biomimetic membrane that can be subjected to the same operational parameters as membranes in conventional membrane technology where parameters like resistance to fouling, interfacial polarization and stability are the most important [17]. Fouling and interfacial polarization are well known challenges in membrane technology and several different solutions for optimized setups exist that could be applied to biomimetic membrane filtration as well. Stability, however, has to be addressed directly during the membrane development. A lipid bilayer has a thickness of only 3 to 6 nm and thus needs to be supported if it should withstand hydrostatic pressure. Therefore, a structure as shown in Figure 6 could be imagined as an aquaporin based flat sheet membrane for RO applications. Here, the lipid bilayer is formed across predefined, round and evenly spaced apertures on a hydrophobic support. To make the membrane more stable and the support better suited for BLM formation an additional surface treatment could be applied. The aquaporin proteins are then incorporated into those bilayer regions. The structure is mechanically stabilized by the porous support. Having this support close to the membrane (e.g. by filling the apertures halfway) would make the operation under pressurized conditions possible. In its overall structure, this biomimetic membrane sandwich is comparable to any commercially available asymmetric RO membrane with the active layer being the lipid bilayer with incorporated aquaporins and its porous support as the porous sublayer.

**Figure 6:** Schematic of the supported biomimetic aquaporin membrane sandwich; the aquaporins (white dots) sit inside a lipid bilayer (red), which is formed across the apertures in a perforated hydrophobic support (green). This perforated scaffold can be modified via surface treatment (yellow) and rests upon a porous hydrophilic support (grey).

## 4.2 Scaffold designs for biomimetic membranes

The initial starting point for the development of the described biomimetic membrane sandwich was to find a suitable perforated support structure. The geometry of such a micro-porous structure plays a key role in establishing a long-lasting and stable biomimetic membrane. Preferably, the surface of the entire support structure should be smooth and hydrophobic. The apertures themselves need to have a smooth, round edge to facilitate the formation of a biomimetic membrane and to stabilize the contact between the membrane components and the aperture rim [34]. Furthermore, for the application in water purification devices based on aquaporin proteins embedded in a lipid bilayer, it is important to densely pack the apertures in arrays to ensure a high water flux across the membrane.

### 4.2.1 General production techniques

The production of such support membranes can be carried out using the full spectrum of known micro technologies in combination with polymers and/or silicon. The simplest of techniques is to use a hot needle in a plastic cup [35] or by micro-drilling a small hole into a polymeric material. However, the quality of these apertures is low. They suffer from burrs, rough edges and an uneven overall shape (Figure 7).

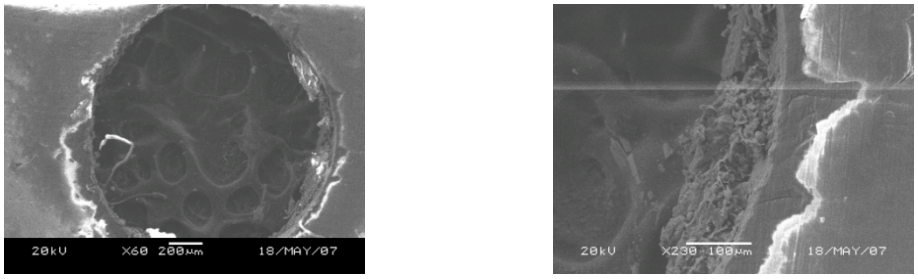


**Figure 7:** Micro drilled hole with a diameter of 1 mm; the close up of the edge (right) shows that the drilling results in rough edges which are sharp and uneven. The porous structure that can be seen underneath is carbon tape that secures the foil on the stage and ensures electrical contact. Pictures were taken using a Jeol JSM 5500 LV SEM from GNNettest.

Other techniques include photolithography and etching to produce submicron apertures in silicon [36] or silicon nitride [37], spark erosion where an electrical spark is used to burn a hole in a polymer membrane as well as the multitude of techniques within the field of polymer micro-technology. For example, Mayer *et al* [38] report of the fabrication of arrays by the casting of thin Teflon films onto a PDMS mould. With this technique precisely placed apertures with a wide controlled range of diameters (2–800 µm) could be fabricated. Kitta [39] reports of well defined high quality apertures for BLM formation that are made in Teflon films using a heated tip. However, spark erosion as well as the approaches by Mayer and Kitta suffer from a limited overall perforation area and long production time (4–24 h). In our lab we used laser ablation in order to achieve drastically decreased production times and easily reproduced results.

### 4.2.2 Laser ablation - Basic principle

The basic setup for a laser consists of a gain medium, which is situated in a resonator that offers the possibility to couple the laser light out on one side. The first of its kind was constructed in 1960, but the principle of stimulated emission has been known since 1916 when discovered by Albert Einstein. The basic principle gave rise to the acronym: Light Amplification by Stimulated Emission of Radiation. The light emitted by a laser is bundled and directed and the energy of the resulting light beam is carried by photons. Laser processing is based on two basic light-matter interactions – absorption and stimulated emission. Absorption means that incoming energy is absorbed and transformed into other forms of energy. Absorption is used in the actual ablation process. The opposite effect is called emission and describes the creation of a photon when excited atoms fall back to lower energy levels. Stimulated emission is when the transition from an excited state to a lower energy level is caused by another photon. The incoming photon forces the emitted photon to go into the same mode. This stimulated emission is the heart of a laser. To create a sufficiently strong laser beam this has to happen many times.

Therefore, the gain medium is inside a closed cavity with mirrors at either end. By travelling back and forth inside this cavity the beam is amplified. This amplification does not happen without losses. Several different causes are known but the main losses occur when photons exit through the front mirror of the cavity or are lost due to scattering. Therefore it is important that a higher amount of photons should be generated than lost. This can be achieved by having more atoms in the upper energy level than in the lower level. This phenomenon is called population inversion and can be achieved by 'pumping' the gain medium of the laser. Pumping describes the process of constantly applying energy to the gain medium so to have enough atoms in an excited state.

The resulting laser beam is monochromatic and most of its power is concentrated in a small area. Laser beams have a good focusability, a small optical bandwidth and are able to form collimated beams with very low divergence. During its way back and forth inside the resonator only some frequencies experience sufficient gain. The limited dimensions of the resonator allow constructive interference only for natural oscillations, or modes. These modes are defined as self-consistent electric field distributions and can be characterized by the arrangement of their electric and magnetic fields. Since they have no electric or magnetic field in the direction of propagation they are called Transverse ElectroMagnetic (TEM) –modes and are characterized by their number of roots (nm) perpendicular to the direction of propagation. The most commonly and most used is the $TEM_{00}$ – mode which can be also referred to as the Gaussian beam. The intensity of the Gaussian beam spreads circular from the optical axis. In doing so, the highest energy is concentrated in the middle of the beam (Figure 8). Important to know is, that the beam stays Gaussian even after passing simple optical elements like lenses and such that are used to focus the beam.

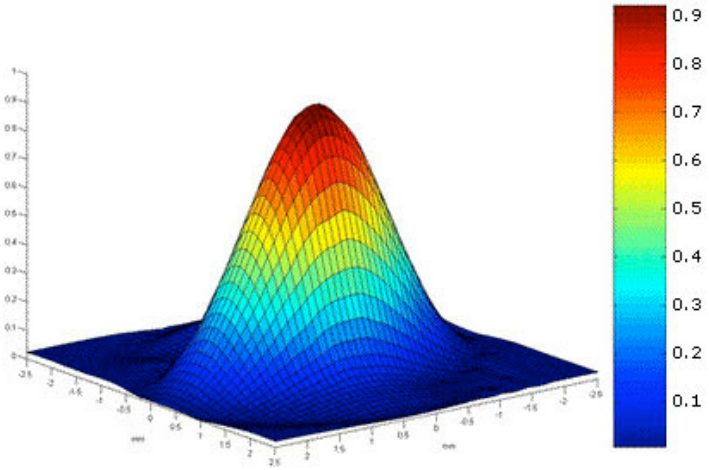


**Figure 8:** Profile of a laser beam in $TEM_{00}$ - mode and Gaussian intensity distribution; the highest intensity is concentrated in the middle of the beam (red area) (picture taken from[40]).

Focusing of the beam is essential for having a defined area of ablation. When leaving the resonator the beam is relatively broad and it has to pass through optical elements like lenses to be useful in a precise production process. The simplest approach to calculate to what extend the beam can be focused by the elements available is to look at ray optics where it is assumed that light propagates in rays rather than in waves. The ray is always normal to the wavefront. The fundamental law here is Snell's law of refraction:

$$\frac{\sin\theta_1}{\sin\theta_2} = \frac{n_2}{n_1} \qquad (4.5)$$

where $\theta_1$ is the incoming angle and $\theta_2$ the transmitted angle. The material in which the light propagates is characterized by the refractive indices $n_x$. Applying 4.5 with a lens with the curvature $R$ and paraxial rays, the focal length can be calculated to be:

$$\frac{1}{f} = \frac{n_2 - n_1}{n_1}\left(\frac{1}{R_1} - \frac{1}{R_2}\right) \qquad (4.6)$$

The term paraxial states that the rays have to have a small angle with the optical axis, meaning $\sin\alpha \approx \alpha$. Laser beams have the advantage of having small divergence angles and therefore fulfill this requirement. However, when working with lasers 4.6 can only be used for calculating the focal plane in which the beam will hit the substrate. It cannot be used for calculating the focal spot diameter since instead of normal rays the beam consists of a Gaussian profile where the intensity distribution is described as:

$$I(r,z) = \frac{P}{\pi w(z)^2/2}\exp\left(-2\frac{r^2}{w(z)^2}\right) \qquad (4.7)$$

with $P$ being the power of the beam. $w(z)$ describes the beam radius to a distance where intensity drops to $1/e^2$ (~13.5 %) of the maximum value. When focusing a beam with a Gaussian profile the minimal achievable spot size is limited by diffraction which is expressed by the angle of diffraction:

$$\theta = \frac{\lambda}{\pi w_0} \qquad (4.8)$$

The Rayleigh length $z_0$ is the distance on which the beam stays focused (Figure 9).

$$z_0 = \frac{\pi^2 w_0^2}{\lambda} \qquad (4.9)$$

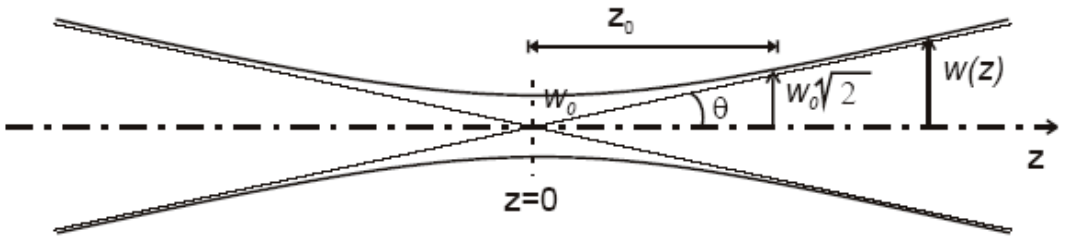


**Figure 9:** Focal point of a laser beam with the characteristics of a Gaussian beam; the minimum beam width is located at z=0; θ characterizes the divergence of the beam [41].

### 4.2.3 Laser ablation of bilayer support structure

When using a laser in the production of apertures care has to be taken which diameters and which surface characteristics want to be achieved and which materials processed. These factors influence the type of laser that has to be chosen. When the laser beam is directed at the surface of the substrate its

energy is absorbed and transformed. Depending on the type of laser used, different processes take place in the material. One example of a laser used in scaffold production is the Excimer laser. With its wavelength of 196 nm (ArF) or 248 nm (KrF) it decomposes the material through a complex mix of chemical and thermal processes. Basically, the chemical bonds between the molecules are broken by photon absorption as well as by heat from vibrating molecules. In contrast, a $CO_2$ laser works with light in the infrared range ($\lambda = 10.6\ \mu m$) and vaporizes and melts the material within its focal spot. The aperture characteristics, range of applicable material and production time depend on the choice of laser. Sandison et al [42] fabricated apertures in PTFE, PMMA, FET and PET foils using an Excimer laser. Here, the best results could be achieved for PMMA (Figure 10 left).

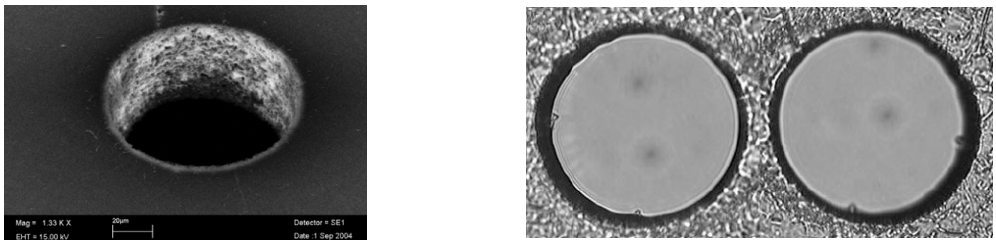

Sandison O'Shaughnessy

**Figure 10:** Excimer laser ablated 100 µm apertures in PMMA by Sandison et al [42] (left) and in PC by O'Shaughnessy [43]. Pictures were acquired using a SEM (right).

Also O'Shaughnessy *et al* [43] report of Excimer laser ablated apertures in PC (Figure 10 right). Here, the production of one aperture with a diameter of about 100 µm took about 30s. The relatively long production time is caused by the layer-by-layer ablation typical for the Excimer laser. In contrast, a $CO_2$ laser can generate an aperture with a single shot. Using $CO_2$ laser ablation I developed a $CO_2$ laser fabricated array of apertures in ethylene-tetrafluoroethylene (ETFE) [44]. It consists of 64 apertures with a diameter of 300 µm and a centre-to-centre distance of 400 µm. This array could be fabricated in only 0.8 s. The typical characteristics of apertures ablated via $CO_2$ laser are smooth and round edges, bulges that are formed around the aperture rims and diamond-shaped pockets formed between adjacent apertures (Figure 11, Figure 12). These characteristics are generated by melted material that is ejected from the focal spot of the laser and redeposited around the edge of the generated aperture. The diameter of the apertures is mainly defined by the lens that is used to focus the beam but can also be varied by adjusting the different parameters of the laser like Spot Lase Time, power and the Off Vector Delay. The Spot Lase Time defines the time the beam is focused on one spot. Together with the chosen laser power this setting defines the amount of heat that is introduced in one given spot. The Off Vector Delay describes the time when the laser is switched off between two production steps. This gives the mirrors time to settle over the starting point of a new structure before starting a new ablation process. When this delay is too short it can cause the formation of tails (ablation starts before the mirrors are adjusted) and if too long the whole production process is slowed down unnecessarily. Due to the Gaussian shape of the beam in a $CO_2$ laser these parameters can be used to make structures that are smaller than the initial focal spot diameter of the laser lens. I was able to proof this theory with the production of apertures with a diameter of 84 µm that were produced with a lens with a focal spot diameter of 116 µm [45].

Standard arrays of 300 µm apertures that were used in BLM experiments consisted of 64 apertures that were arranged in a square lattice of 8 by 8 spanning an area of 0.21 $cm^2$. Using the full working area of the available laser setup production was upscaled to arrays of 576 apertures in an area of 1 $cm^2$ (Paper III) and finally to hexagonal arrays of 7280 apertures covering an area of 10 $cm^2$.

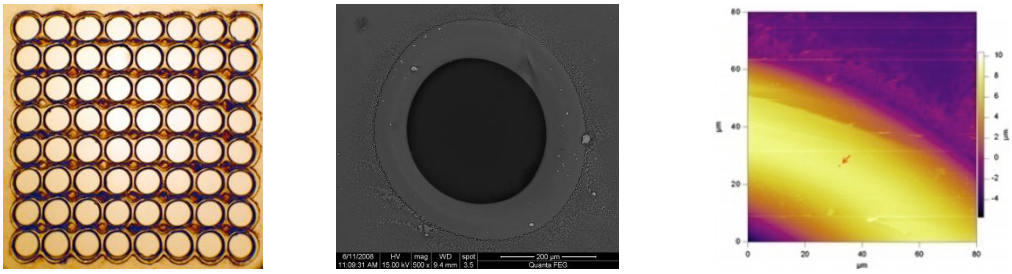

**Figure 11:** ETFE partition with an 8x8 array of apertures with a diameter of 300 µm (A), a SEM picture of a single aperture in ETFE and a close up AFM picture of the smooth bulge surrounding the aperture – here the red arrow indicates a sample area where a surface roughness of 3.5 nm was measured.

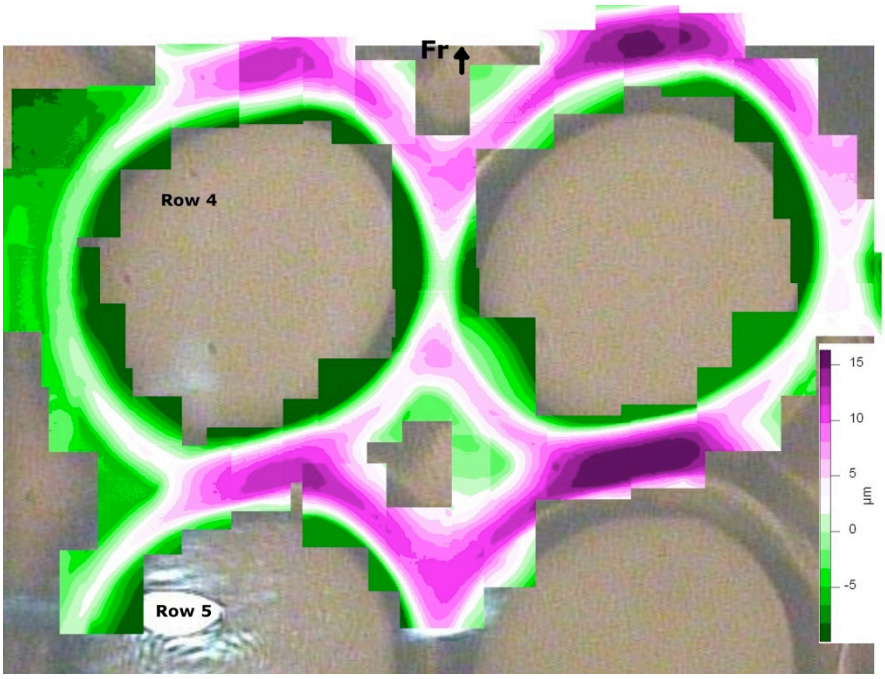


**Figure 12:** Optical image of the front side (side facing the $CO_2$ laser) of a $CO_2$ laser ablated ETFE rectangular array overlaid with 37 AFM topological maps. The mosaic image clearly shows the presence of a diamond-shaped pocket between the apertures.

## 4.3 Chamber designs

The $CO_2$ laser fabricated support structure was tested in bilayer formation experiments. Since we designed and produced a complete novel system we also had to adapt the experimental setup according to our support. Typically, biomimetic membranes in hydrophobic scaffolds are formed in chambers where the scaffold separates two aqueous compartments [46]. There are essentially two methods available for establishing large scale biomimetic arrays. The first method is based on “painting” the matrix across apertures submerged in aqueous solution [47]. Here, lipid dissolved in a low molecular

weight hydrocarbon is spread across the support. Repeated swiping (e.g. with a small artist paint brush) across the bulk lipid above an aperture leads to a thinning which will result in the formation of a lipid bilayer (Figure 13). The second method is based on folding two monolayers of amphiphiles at an air-water interphase across the apertures of a scaffold lowered into the aqueous phase [48] or by lowering and raising an lipid containing solution in one compartment of a two compartment cell that is separated by a small aperture [49] (Figure 14). The technique to be applied depends strongly on the design of the chamber that is envisioned. Whereas the painting method is carried out in a horizontal setup the folding technique requires a vertical configuration. A typical setup consists of two reservoirs/chambers (*cis* and *trans*) that contain buffer solution, a support membrane with one or multiple aperture and two electrodes that are used for electrical characterization.

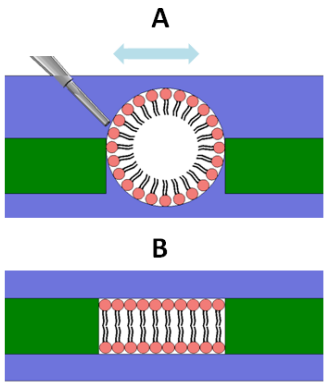


**Figure 13:** Schematic of the membrane painting method; lipids are applied in bulk to the aperture (A) and consequently thinned out to form a bilayer with a thin pipette or brush (B).

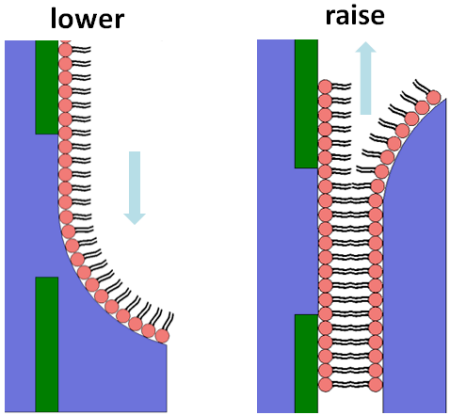


**Figure 14:** Schematic of the membrane folding method; the compartment containing the aqueous solution with the lipid monolayer is lowered and raised so that a bilayer is formed along the wall and over the aperture separating the two fluid compartments.

### 4.3.1 Standard chamber for creating painted membranes

Our simplest chamber design consists of two Teflon parts, which can be clamped together via screws. When assembled with the support scaffold placed in the interface between the two Teflon parts an open two-chamber system is created where electrodes can be inserted into the aqueous solutions from above. Due to its simplicity, this setup is cheap to fabricate. However, we have observed that silicone grease used for sealing tends to dissolve due to the organic solvents (i.e. decane) used in the biomimetic membrane matrix. This results in both loss of sealing over time (usually within a couple of hours) as well as partial coverage of scaffold apertures with grease which greatly reduces both the quality (i.e. electrical tightness) and the lifetime of the biomimetic membranes.

### 4.3.2 Auto-Painted-Membrane (APM) chamber

Recently, we developed an improved chamber design for biomimetic membrane formation (Figure 15) in the laser ablated ETFE partitions presented in paragraph 4.2.3. The main advantages of this design are the reduced amount of silicone grease used for sealing and the possibility of semi-automating membrane formation resulting in a higher degree of reproducibility between experiments. When

properly assembled it is possible to maintain a low leak current for several days and even weeks between the two chamber compartments [50].

The complete chamber setup consists of a main Teflon chamber with two axisymmetrically drilled holes of different diameter, a cylindrical Teflon tube, two circular Teflon inter spacers where one has a slit, six Viton (DuPont Fluopolymers, US) O-ring seals, two cover slip glasses where one is cut and a brass screw to tighten the bilayer chamber (Figure 15 B). Both chamber compartments have identical volumes. Porous regenerated cellulose is used to further stabilize the biomimetic membrane from mechanical agitation. The complete assembled biomimetic membrane chamber can be seen in Figure 15 A. Electrodes for membrane recording are inserted through the top large diameter inlets. The small diameter inlet is used to inject biomimetic matrix solution.

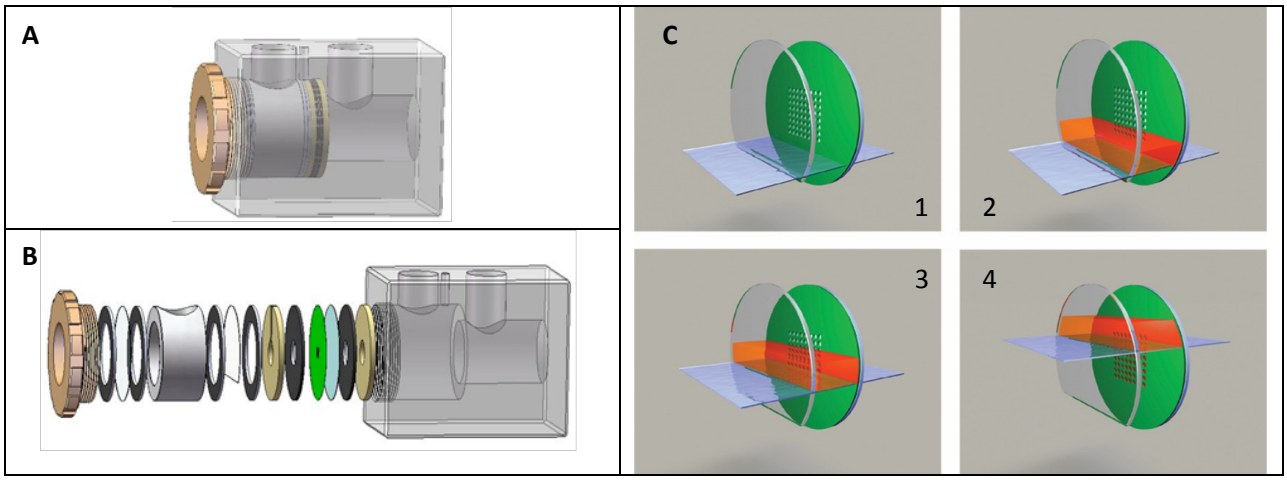


**Figure 15:** Biomimetic membrane chamber design and assembly. (A) The biomimetic membrane chamber fully assembled. (B) The assembly of the main Teflon chamber. The component order of the assembly into the main Teflon chamber (grey – Vink A/S, DK) is from right to left: a Teflon spacer (tawny – Vink A/S, DK), a Viton O-ring (black – DuPont, US), a circular cellulose sheet (light blue – Alfa Laval, DK), an ETFE LZ200 partition (green – DuPont, US), a Viton O-ring (black), a Teflon spacer with a slit (tawny), a Viton O-ring (black), a cut glass cover slip (transparent – VWR-Bie & Berntsen, DK) and another Viton O-ring (black). (C) Principle of the automation technique for the establishment of multiple bilayers in the array. The aqueous electrolyte solution is filled up to the cut glass cover slip (1) and a small amount of the matrix is added to the space between the glass and the scaffold with apertures (2). The aqueous electrolyte solution is then slowly applied to the cis chamber thereby raising the bilayer-forming solution across the multiple aperture partition to form an array of lipid bilayers (3)–(4).

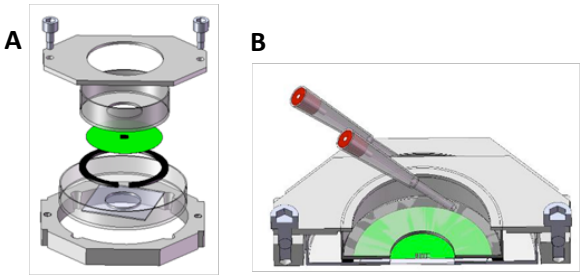


**Figure 16:** The horizontal lipid membrane formation chamber (A) The chamber is assembled by first inserting the big dish into the bottom holder, placing the Viton ring in its center, placing the to the smaller dish glued partition on top and finally clamping the system with the upper metal plate and screws; (B) shows a cross section of the assembled chamber with inserted electrodes.

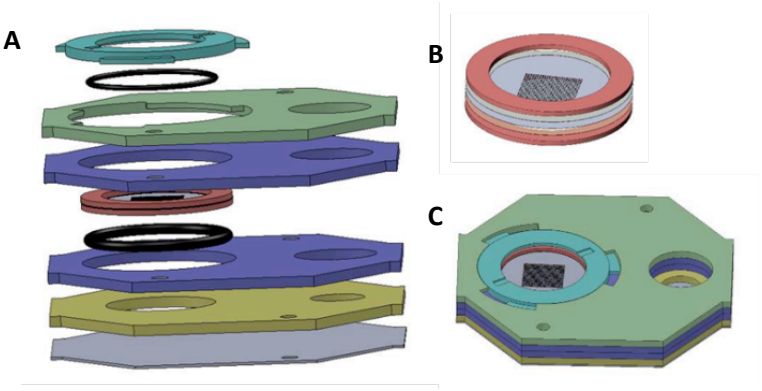


**Figure 17:** Biomimetic membrane formation chamber in an exploded view (A), and as a complete assembly (C) with clamp (turquoise) and PaR (B).

### 4.3.3 Horizontal chamber

Both chambers presented in 4.3.1 and 4.3.2 support formation of biomimetic membranes over vertically placed apertures. In experiments where visual inspection of membrane arrays is needed (i.e. fluorescence) it is necessary to place the arrays horizontally. This also allows for physical access to the actual lipid membrane formation area which is difficult to obtain with the simple membrane formation chamber and close to impossible with the APM chamber. Therefore, we developed another chamber design where the partition is placed horizontally [51].

The entire chamber design with all its components can be seen in Figure 16. It is made from commercially available culture dishes, where the bigger dish constitutes the lower and the smaller dish the upper compartment. An ETFE partition is glued to the upper dish. This gluing functions as a seal from upper to lower chamber. The custom made Viton ring is then used as a spacer so that two separate chambers are created. The slit in the Viton ring functions as the connection between the area underneath the array and the lower reservoir. A reusable, homemade metal sample holder is used to clamp the upper dish to the lower and ensure sealing and proper alignment. The chamber is made to fit onto a microscope stage which makes it possible to combine electrical measurements with fluorescence microscopy.

### 4.3.4 Horizontal chamber with removable membrane unit

All the previously mentioned chambers had one drawback in common – the partition where the biomimetic membrane is formed is fixed within the chamber. If however, the biomimetic membrane should be further used another chamber design has to be considered. The further use can for example include the incorporation of aquaporin proteins and the application of that setup as a water filtration device. A common setup to test the flow through a membrane is a flow cell. Here, the sample is placed onto a sample holder and clamped into the cell. Afterwards, the reservoir is filled with water and pressure is applied and thus the flow through the sample is tested.

Biomimetic membrane formation directly in this flow cell was not tested but was deemed impractical by my colleagues in Aquaporin A/S. This means that the bilayer had to be created in a special partition that could be taken out of the membrane formation chamber. To make the device cheap and disposable,

PMMA (Nordisk Plast, Randers, DK) rings were fitted via double sided adhesive tape onto a perforated partition (Figure 17 B). This assembly of partition and ring (PaR) can then be clamped into a custom made chamber and the bilayer created. Afterwards, the PaR with bilayer can be removed from the chamber and used for further testing. This bilayer formation chamber needs to have a *trans* and a *cis* chamber which both should be accessible by electrodes. Furthermore, it needs to make a tight seal between PaR and chamber.

The developed chamber consists of $CO_2$ laser structured PMMA parts that are bonded via double sided adhesive and O-rings for sealing (Figure 17 A and C). The clamp mechanism consists of a rotatable lid with three noses that fit underneath three counterparts that are situated at the top of the chamber and thus clamp the PaR. The lower chamber is accessible via a channel in the bottom chamber.

## 4.4 Integrating membrane hydrophobic scaffolds with a porous, hydrophilic support

A successful formation of planar, free-standing BLMs on the presented hydrophobic multi-aperture partitions using the previously mentioned chambers was shown [51, 52]. The next step towards a biomimetic water filtration system was to investigate how an increased stability could be achieved. Increasing the stability of large scale biomimetic membrane arrays is one of the major challenges in filtration and separation applications where long term use of the systems under potentially harsh operating conditions is a key factor in reducing the operational cost. Similar considerations apply for biosensing and drug screening applications. Traditionally, biomimetic membrane arrays to be used for the aforementioned applications have been freestanding for free access to either side of the membranes [47]. This complicates the task of stabilization compared to supported biomimetic membrane systems where the matrix components can be physically coupled to the underlying support [53]. In our lab we work with unit cells where the 5 nm thick fluid membrane system spans a 300 µm aperture. If these dimensions are scaled up, the challenge of stabilizing a freestanding biomimetic membrane system is intimidating. Imagine being given the job of making sure a 1m thick and almost 3000 $km^2$ free-standing sheet spanning a 60 km wide canyon does not collapse over an extended period of time under operating conditions such as an applied hydrostatic pressure or mechanical agitation. Just to mention some of the numerous possibilities here are 3 strategies for increasing stability:

1. Coating of the membrane scaffolds through plasma treatment to improve the affinity between the scaffold surface and the matrix components. Plasma treatment was considered most feasible by my co-workers in making a hydrophobic surface more hydrophilic.

2. Integrating a porous hydrophilic support into the apertures of the membrane scaffolds to stabilize the membranes by dampening membrane vibrations caused by flow close to the freestanding membrane.

3. Building a cushion layer of poly-electrolytes on top of the porous hydrophilic support and physically coupling selected matrix components to the cushion. Ultimately this construction could resemble the cytoskeleton seen in nature to stabilize membrane systems [54].

During the PhD project I concentrated on strategy number two – integration of a hydrophilic porous support. Looking back at Figure 6 it can be seen that this support lies beneath the lipid membrane support structure assembly. In a future application this support would be used to protect the fragile bilayer from external forces.

Prior to constructing the support we specified the following demands on the material:

- The support should be integrated on the trans side of the membrane scaffold and adhere sufficiently to the scaffold surface so no delamination takes place under operating conditions such as application of hydrostatic pressure from the cis side.

- The support should fill the apertures halfway or more in order to bring the hydrophilic surface in close proximity to the biomimetic membrane areas. This becomes especially important in cases where a cushion layer is added on top of the hydrophilic support and coupled to matrix components.

- The support should have a highly porous structure that does not create a bottleneck for water flux in filtration and separation applications.

The surface of the support should be smooth and flat on a micrometer scale in order to provide a well defined platform for further modifications. From a basic reasoning point of view we also believe a flat smooth surface to be the preferred geometry since the bilayer itself has an inherent propensity towards adopting a fleet sheet structure and any deviation from this will cause internal stresses that could potentially destabilize the membrane.

### 4.4.1 Choice of material and integration of porous support

To ensure that the support material does not create a bottleneck for water flux we use a highly permeable hydrogel formed by in situ radical polymerization of an aqueous solution of 2-hydroxyethyl methacrylate (HEMA), 1,4-butanedioldiacrylate (BDDA) and poly(ethylene glycol) dimethacrylate (PEG-DMA) and in the presence of silica particles. HEMA constitutes the bulk polymeric part of the material while BDDA and PEG-DMA work as crosslinkers increasing the material strength and flexibility. We have shown that the presence of silica particles in the polymer hydrogel greatly enhances both the mechanical stability of the gel and the flux of water through the hydrogel. Radical polymerization is initiated through the ammonium persulfate (APS) / *N*,*N*,*N'*,*N'*-Tetramethylethylenediamine (TEMED) redox pair initiator system.

Adhesion between the hydrogel support material (hereafter referred to as PHEMA) and the structured ETFE array functioning as the membrane scaffold is achieved by plasma treating one side of the ETFE array with the HEMA (Paper IV).

### 4.4.2 The actual process of integration

Depending on the material there are, in our experience, three different ways of integrating a porous, hydrophilic support with a structured membrane scaffold. The results of these different techniques regarding filling were characterized by focus-variation optical scanning of the surface topography (InfiniteFocus, Alicona Instruments, GmbH, Graz, Austria).

**I- Clamping**

If the desired support material already exists in a solid state it can be clamped onto the back of the partition. Here, the support material will function mainly as a mechanical carrier. In some cases, if it is soft enough, it might penetrate slightly into the apertures and thus also works in the desired way of giving the biomimetic membrane more stability. However, clamping always induces mechanical stress and tension and this might actually pose a hindrance to membrane formation.

**II – Direct Integration**

Here, the porous support is applied directly to the structured membrane in its liquid state and is then cured. In order to achieve halfway filling of the apertures either a mold or a thinly spread (e.g. spin coated) layer of porous support solution is needed. In the mold method (Figure 18) liquid polymer solution is applied to a pre-defined reservoir and an assembly consisting of two poly-methylmethacrylate (PMMA) rings is placed on top. That way the polymer solution can penetrate halfway into the apertures before cross-linking. Spin-coating proved to be not suitable for the application of PHEMA to our substrates due to either an uneven distribution of the polymer solution throughout the array or total penetration of the apertures by the PHEMA.

**III – Negative Plug**

This procedure aims at creating a well-defined plug inside the apertures. It is called negative plug because it forms the counterpart or template for the PHEMA support, which is applied in its liquid state to the partition/negative plug construct. Once cured, the sacrificial plug material (e.g. PDMS (polydimethylsiloxane), PVA (polyvinyl acetate)) is removed leaving a smooth and flat support surface inside the apertures.

The following example illustrates the negative plug technique, which has yielded the best overall results in our lab with regards to the 4 success criteria listed in the beginning of this chapter.

The first step involves spin-coating a PDMS onto a silicon wafer to create an approximately 80 to 100 µm thick layer. Immediately after spin-coating the ETFE membrane scaffolds are placed on the PDMS layer. The degree of filling is visualized by laser-scanning-confocal-microscopy (LSCM) (Figure 20 A). To produce the final composite material, the PHEMA precursor solution is mixed rapidly with a solution of the APS/TEMED redox pair, poured onto the PDMS-plugged scaffold and cured. Upon curing, the PDMS plug is removed from the scaffold yielding the final product (Figure 20 B). Negative plug formation by PDMS proved to give the best results in regards to filling and surface quality of the casted so formed plug. However, a drawback is that PDMS tended to creep onto the backside of the ETFE support

structure and covered it with a thin layer. This meant that the PHEMA that was casted on the backside later on could not be bound to the support structure. Therefore, the mold method was preferred in the fabrication of the envisioned membrane sandwich and by optimization of this technique even surfaces in almost halfway penetrated apertures was achieved (Figure 19).

The so assembled supported lipid bilayer with additional porous support was then tested in the horizontal chamber with removable membrane unit. This chamber proved to be exceptionally well suited to form supported BLMs. Here, we had the possibility to take the support membrane that was clamped into two PMMA rings, apply the porous support and then transfer it into the prepared BLM formation chamber where the bilayer was formed and analyzed.

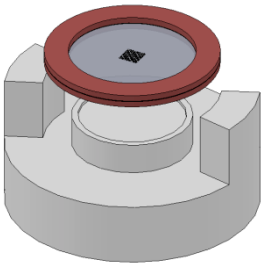

**Figure 18:** Schematic of ETFE scaffold with PMMA rings and the Teflon mold for casting of PHEMA support.

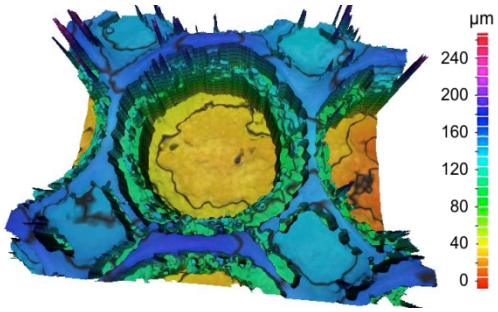


**Figure 19:** Alicona scan of a single aperture with PHEMA, the green ring inside the aperture is the sloping wall of the aperture – it is wrongly displayed in the measurement due to data averaging (the spikes are measurement artifacts due to missing data).

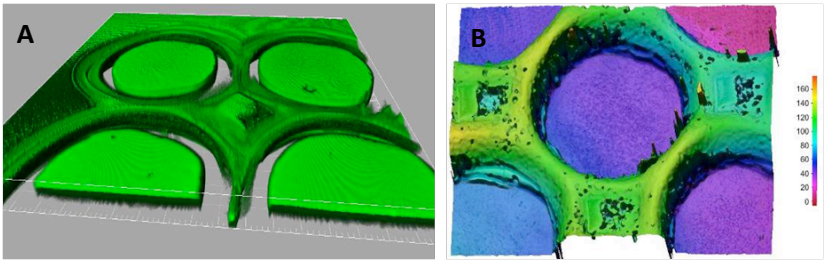


**Figure 20:** Negative plug approach – (A) shows a Laser Scanning Confocal Microscopy image of the surface of the PDMS that was used to generate a negative plug inside apertures with a diameter of 300 µm, (B) shows an optical surface scan image (achieved via InfiniteFocus, Alicona) of the surface of the porous support after pouring it onto the plug and removal of the PDMS (the spikes are artifacts from the measurement).

# 5 Aquaporin based liquid membrane for forward osmosis

Parallel to the BLM formation and stability extension experiments novel strategies for controllable and reliable reconstitution of membrane proteins into artificially made membranes were explored. These studies resulted in the development of a method to create giant protein vesicles (GPV). The advantages of the GPV formation method are, among others, that GPV can be formed in high densities and the amount of protein incorporated into the GPV can be controlled. The high densities in which GPV could be formed led to the speculation of whether this was sufficient to constitute a bulk liquid membrane that could be used for separation applications. The definition of a bulk liquid membrane is a bulk organic, water-immiscible liquid phase that can act as a semi-permeable phase separator between an aqueous feed solution and a receiving aqueous solution [55]. In our case, aquaporin GPV would constitute the bulk organic, water-immiscible liquid phase which in principle should be permeable only to water molecules due to the function of aquaporins combined with the barrier properties of biomimetic membranes. This membrane type could then be used in an FO application.

## 5.1 Forward Osmosis

### 5.1.1 Basic working principle

When looking back at Figure 3 in chapter 3.2, it can be seen that FO solely uses the osmotic pressure to force water through the semi-permeable filtration membrane. No external hydrostatic pressure is used or needed. In basic words FO can be described as a process where water penetrates a semi-permeable membrane due to the differences in solute concentration between the two liquids on either side of the membrane – for example when water molecules are exchanged between the draw and the feed solution.

As in every other filtration process, the feed solution refers to the solution which enters the filtration system as the feed stream and which contains molecules that should be separated from the rest of the solution. The draw solution, which is also called osmotic agent or driving solution, generates the driving force for the FO separation process. It is a concentrated solution on the permeate side. Due to the difference in concentration between the permeate side and the feed stream, a high osmotic pressure is induced on the draw side which leads to a transport of molecules across the semi-permeable membrane. This means that the draw solution becomes diluted whereas the feed solution becomes more concentrated. The basic principle of FO can also be seen in Figure 21.

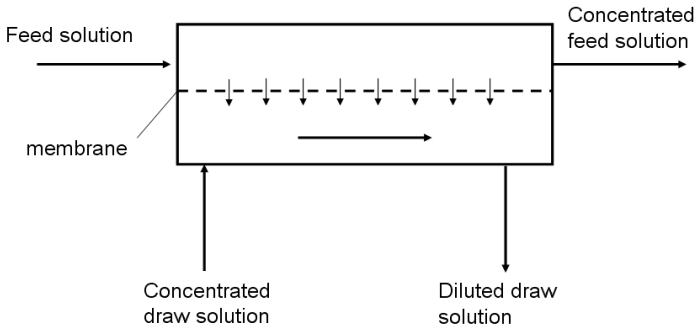


**Figure 21:** Principle of FO – a feed solution and a concentrated draw solution are separated by a dense, non-porous, selectively permeable membrane. Molecules from the feed are drawn in to the concentrated draw solution by the osmotic pressure caused by the concentration gradient between the two solutions. The output of a FO process is a concentrated feed and a diluted draw solution.

The main advantage of FO compared to other filtration/separation processes is that only minimal or no external hydrostatic pressure is required. This means that since the only pressure that is involved in the process is due to the flow resistance of the semi-permeable membrane the rest of the equipment can be rather simple. No-high pressure valves, fittings or tubing are needed and no additional components that pressurize the feed have to be installed. Furthermore, literature reports that FO may have a lower membrane fouling propensity than pressure-driven membrane processes [4, 56]. Low pressure and low temperature processing, for example, are two advantages that benefit the food industry. Here, juices can be upconcentrated without damaging vitamins or taste. Also the pharmaceutical industry benefits from these advantages especially when temperature sensitive drugs are to be upconcentrated. Another advantage with high economic value is that FO has low energy demands. No additional pressure has to be generated and thus no additional pumps are required to generate high pressures as in RO. Most of the required energy in a FO process is consumed by the recovery process. This process refers to the extraction of the desired molecules from the draw solution and the reconstitution of the draw so that it can be reused in the FO process.

### 5.1.2 Applications

Today, FO still is a minor technology when it comes to volume but it is used in several smaller applications. In wastewater treatment for example, FO is used as a high level pretreatment step for the concentration of diluted industrial wastewater, landfill leachate or digested sludge liquids [4]. This is done to remove excess water from the waste to improve the efficiency of the subsequent processes. Another purpose is direct water extraction or purification. Here, a process where FO is successfully applied is in hydration bags where a concentrated sugar solution in combination with a selective membrane extracts water from contaminated water sources [57]. These bags are one of the few commercial applications of FO. Food processing is another application where FO is used to concentrate beverages or liquid foods. A direct water purification method that is under investigation is called direct osmotic concentration (DOC) [58] and is developed by NASA. The goal is to gain fresh water for long-term space missions by reusing the available wastewater from urine, hygiene wastewater and humidity

condensate. The cleaning process should be reliable, durable, lightweight and energy efficient which makes FO an interesting option. However, work is still ongoing in this application.

Despite the simple working principle and the wide application possibilities the lack of optimized membranes and effective recovery processes for the draw solutions prevent FO from becoming more exploited. Therefore, it is important to take a closer look at what membranes are currently used in FO processes.

### 5.1.3 Membrane designs

In general, every dense, non-porous, selectively permeable material could be used as a membrane. The requirements for such a membrane are a high solute rejection, low internal concentration polarization, hydrophobicity and high mechanical strength. Internal concentration polarization (ICP) describes the accumulation of solutes from feed or the dilution of the draw inside the porous support [56]. This effect lowers the effective driving force for water transport across the membrane. High solute rejection can be achieved by a high density of the active layer, as can be found in composite membranes for RO. To minimize concentration polarization (Paper V for additional information) the membrane has to be thin with a high porosity of the support layer. This would minimize ICP and increase the water flux through the membrane. Hydrophobicity also contributes to an increased water flux due to reduced membrane fouling [59]. Since RO membranes like the thin film composite (TFC) membranes as described in chapter 4.3 are well characterized, they were also tested for their FO applicability. However, they suffer from highly reduced flux when operated in FO mode [60]. The thick support layer that stabilizes these membranes against hydrostatic pressure causes severe ICP, which results in the low water flux [56, 61]. Therefore, the development of membranes specially designed for FO is needed. The first example was introduced by Osmotek Inc. (now HTI) in the 1990s. This membrane has been successfully tested in laboratories as well as in commercial applications and proven to be superior to existing RO membranes. The exact composition of the membrane is protected, but it is believed to be made of cellulose triacetate (CTA) [4]. It is less than 50 µm thick and has an embedded polyester mesh that gives the membrane mechanical stability. Figure 22 shows a cross-sectional view of this CTA membrane. Other membranes are under development and show promising performance improvements [60, 62, 63] but are still only applied in laboratory scale experiments. Chou et al. [62] for example report of a polyethersulfone hollow fiber that had a water flux of up to 42.6 $L/m^2h$ and Yip et al. [60] developed a flat thin film composite membrane [60] with a water flux of 18 $L/m^2h$. These novel membranes were only tested under laboratory conditions and the CTA membrane from HTI is to date still the only commercially available FO membrane.

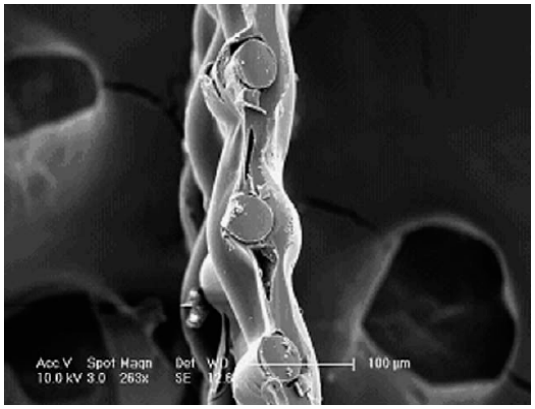


**Figure 22:** Cross sectional view of CTA membrane by HTI. An embedded polyester mesh is used to mechanically support the membrane, which is less than 50 µm thick (picture taken from [4]).

However, the CTA membrane's rather thick support layer is prone to internal concentration polarization, which again would lead to a decrease in flux. To overcome this shortcoming an alternative to standard solid filtration membranes are liquid membranes. Depending on the type of liquid membrane they can be applied without a support layer and thus are less affected by ICP. In addition, they exhibit a high selectivity and flux [55]. As explained in the end of chapter 3 Aquaporin A/S developed a method to make dense GPV networks which could be used as a bulk liquid membrane for separation applications.

## 5.2 Liquid membranes

All membranes, in their basic definition, are semipermeable phase separators – meaning a barrier between two phases (e.g. liquid) that allows only certain solutes to pass. This barrier can be made out of solid materials like polymers and ceramics or it can be a liquid phase. Examples of organic liquid membranes (LM) of an immiscible phase can be found everywhere in nature – be it a layer of oil on water, foam on soap or beer froth. A liquid membrane has the purpose to build up a thin gaseous or liquid barrier between two miscible liquids or gases and thus regulate the mass transfer between both phases. The membrane strips one phase (feed phase) of a component or solute and transports it across to the other phase (stripping phase) where it releases the transported component again. The development of liquid membranes for filtration purposes has experienced a significant increase in interest over the last two decades. This is due to the great potential these membranes exhibit - high selectivity combined with a high permeability and an efficient use of energy [64, 65]. The high selectivity can be reached with the help of the components that are in the liquid membrane. These can be more selective than the openings in a polymeric membrane. Since diffusion in liquid is orders of magnitude higher than diffusion through solid polymers [64] also permeability can be improved by using liquid membranes. Despite this great potential only few applications have found their way into industry yet. The main reason that prohibits the widespread use of liquid membranes so far is to ensure a sufficient stability. However, research in this field is ongoing and the application spectrum is broad. Potential users are companies in the analytical, inorganic and organic chemistry, chemical engineering, biotechnology, biomedical engineering and in wastewater treatment. Liquid membrane separation can be useful in gas

separation, the recovery of valued or toxic metals, for the removal of organic compounds, the recovery of fermentation products or even the water purification and desalination industry [55, 66].

### 5.2.1 Transport mechanism

The basic transport mechanism in liquid membrane separation is solution diffusion. This means that a solute is dissolved in the liquid membrane and then diffuses across it due to a concentration gradient. This transport can be further enhanced by introducing carrier agents that react rapidly and reversibly with the desired solute. This leads to three main basic permeation mechanisms that are most common – simple transport, facilitated transport and coupled counter- or cotransport. The simple transport (Figure 23 A) is comparable with the permeation in polymeric membranes. The solute is transported across the membrane solely by diffusion due to a concentration gradient and the permeation stops when equilibrium is reached. By introducing carrier agents (Figure 23 – B) the transport of solutes can be enhanced. The solute now reacts with these carriers on the feed side and facilitated transport is initiated. The formed complexes are then transported across the membrane by said carriers and released on the receiving side. Simple transport is still present but the main permeation is caused by the carriers. The coupled counter- or cotransport (Figure 23 C) is another form of facilitated transport where either two species of solutes are transported at the same time or where the energy that is gained by transporting one species with the concentration gradient is used to transport another against this gradient. Which of these transport mechanisms is present depends on the components that the liquid membrane contains. Mostly, they consist of a mixture of organic compounds e.g. oil and various chemicals that can act as carriers or facilitate transport.

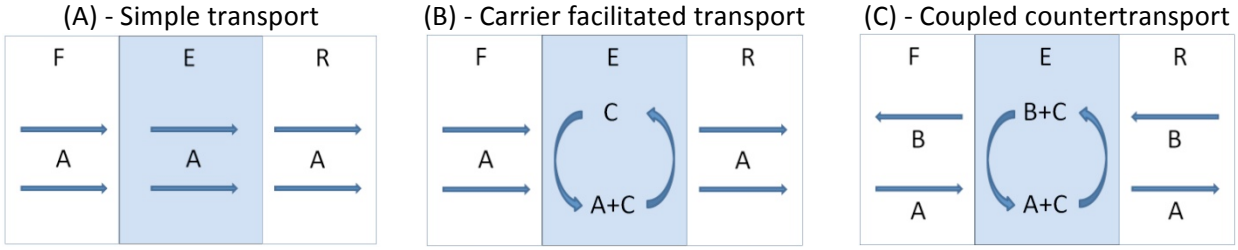


**Figure 23:** Schematic of three main transport mechanism in liquid membranes; A is the desired solute in the feed, C the carrier, F the feed solution, E the liquid membrane emulsion and R the receiving phase; the coupled counter or cotransport is displayed on the example or counter-transport.

### 5.2.2 Types of liquid membranes

Next to the transport mechanism, configuration is another major difference between the different types of liquid membranes that can be used for different applications. In general, there are three main configurations. There are several more existing but they are then mainly variations of the three basic setups. The first one is emulsion liquid membranes (ELM). This method was first mentioned by Li [67] in 1960 and describes an emulsified liquid membrane that is immersed in the feed phase Figure 24. The so achieved high surface to volume ratio and the short diffusion distance (thin membrane) in this method result in a very high efficiency. The main parameters influencing the separation and permeability are the thickness of the membrane and its composition, the temperature and pH and the ratio of emulsion to external phase. Furthermore, stirring enhances the mixing of the LM with the feed and creates smaller liquid membrane droplets and thus enhances the separation. ELM is well suited for dilute feed solutions

since a high solute concentration leads to rapid saturation and thus lowers the transport [55]. However, there are two major drawbacks with ELM. On one side it is a multiple step process because after the separation is done the emulsified liquid membrane has to be removed from the feed and the desired solute has to be extracted from the emulsion. On the other hand there is the stability of the LM. It should be as stable as possible so that rupture or bursting inside the feed phase can be avoided. This, however, goes against the need for easy break down of the emulsion after extraction from the feed. This delicate balancing is one of the main inhibitors for ELM to become widely used in industry.

Supported or immobilized liquid membranes (SLM) have already solved one of these problems by eliminating the extraction process. Here, the LM is trapped inside the pores of a support membrane that is placed in between the feed and the receiving phase. This means that the desired solute is continuously transferred to the receiving phase, which is flowing past the membrane and thus is directly available to the user. This bears a great potential in energy saving and low capital and operating costs. Due to the small volumes that are needed even expensive chemicals can be used as parts of the LM formulation. The first application of SLM was reported by Ward and Robb in 1967 [68] where they used an immobilized bicarbonate-carbonate solution to separate $CO_2$. In SLM the liquid membrane is held inside the pores of a microporous solid support by capillary forces Figure 24. An ideal support material should be highly hydrophobic, have a high porosity and be as thin as possible [55]. Here, the main reason is that the diffusion path for the solutes should be as short as possible. However, the membrane should still be thick enough to mechanically withstand pressure differences. This delicate balancing of short diffusion path and thus high flux and stability is already one challenge in the production and use of SLMs. Other points are the stability of the liquid membrane in itself and the coherence of LM and support. Since the liquid membrane is held inside the support by capillary forces only, the application of flow and pressure can lead to rupture and the development of a leak. In addition, the membrane in itself might leak out of the support and add impurities into the feed or receiving phase. Stabilization by increased thickness is realized in the last form of liquid membrane configuration – bulk liquid membrane.

Compared to the other two configurations bulk liquid membranes have a low carrier loss, longer lifetimes and the possibility of applying different driving forces. As in SLM, bulk liquid membranes work continuously and are a one step process with compact equipment. This configuration consists of a bulk liquid membrane that separates the feed from the receiving phase. The liquid phase can be directly in contact with the two solutions or it can be contained in between two encapsulation membranes (Figure 24). The latter is the more common because it provides more stability. Several different versions of bulk liquid membranes are known like hollow fibre liquid membranes, flowing liquid membranes and multimembrane hybrid systems [55]. All base on the same principles – the bulk liquid membrane is injected in between two encapsulation membranes where it is held in place. The encapsulation membranes should not have an active role in the selectivity and flux behaviour of the process. The hydrophobicity of the membrane defines where the interphase between liquid membrane and feed or receiving solution is. A hydrophobic membrane is wetted by the liquid membrane emulsion which has a higher affinity to go through the pores [55]. The aqueous solution is then brought into contact with the membrane and by adjusting the flow velocity and the pressure, the liquid membrane is kept from

leaking out of the encapsulation membrane but is in direct contact with the feed or receiving solution. The opposite is true for hydrophilic membranes where the aqueous solution wets the membrane and meets the liquid membrane on the inside of the encapsulation membrane. Flow and pressure have to be adjusted carefully so that the liquid membrane is not washed out. Other challenges in bulk liquid membranes are similar to those in SLM including the leakage of liquid membrane into the aqueous phase and the stability and lifetime of the carrier agent. Lower selectivity and the low diffusion rate of larger molecules combined with the longer diffusion path also have to be taken into consideration.

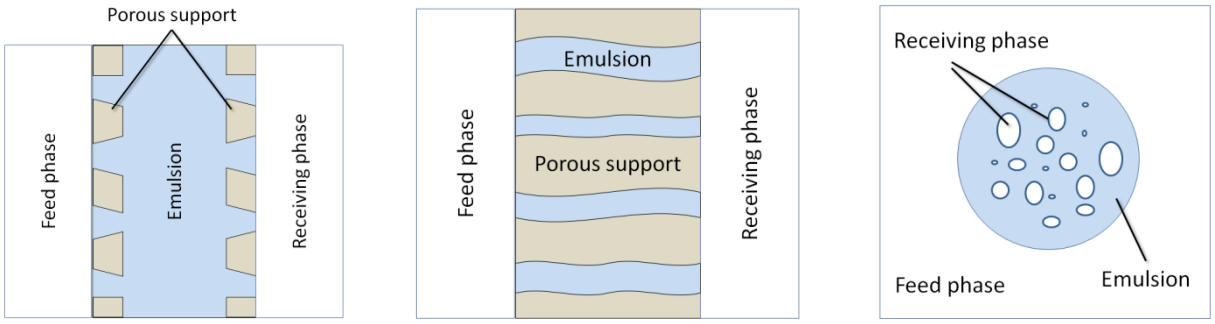


**Figure 24:** Schematic of the different liquid membrane types; in a bulk membrane the emulsion is trapped between two encapsulation membranes whereas it is trapped inside a porous membrane in a supported liquid membrane; in an emulsified liquid membrane the emulsion is immersed in the feed phase.

Several of the above mentioned challenges can be solved when introducing aquaporin proteins into the liquid membrane phase. No carriers are needed and the transport relies solely on the concentration gradient introduced by the draw solution. A liquid membrane based on these proteins resembles more a conventional polymeric or ceramic membrane than an actual liquid membrane but has the same advantages of high selectivity and high flux. Here, the aquaporin proteins are like pores in a normal solid membrane that connect the feed to the receiving side (Figure 25). However, the danger of leakage and washing out is still present with the aquaporin based liquid membrane. Another challenge is how to apply the liquid membrane to a system. Mostly standard components can be used for connecting a chamber to the feed and draw solution but when applying the liquid membrane and its encapsulation membranes the clamping method usually used in membrane modules is difficult to apply. The challenge is to have a chamber where the LM solution can be injected in between the encapsulation membranes without leakage. For that reason, commercially available filtration modules using solid membranes cannot or only to a certain extend be used in connection with LM.

As a result, the main task to make aquaporin based liquid membranes work in FO was to investigate the basic components and behaviour of this novel membrane type. A first step involved the stability and leakage characteristics of the liquid membrane. To investigate if leakage occurs when applying feed and draw solution an observation device was designed and produced that could be beneficial in the process of choosing the right encapsulation materials and membrane formulations.

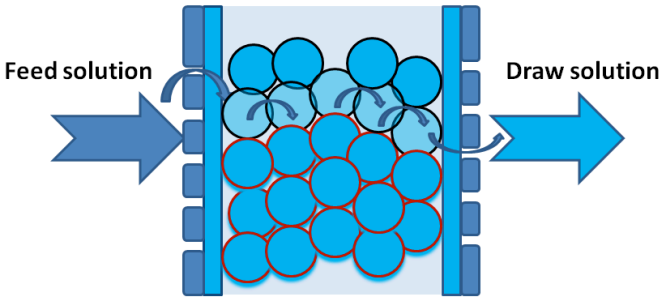


**Figure 25:** Schematic of a possible scenario of water transport through an aquaporin based liquid membrane; the water transport is realized by aquaporin proteins that sit in the outer membrane of vesicle. By having a dense network water transport from vesicle to vesicle is realized.

## 5.3 Observation device for bulk liquid membrane / aqueous phase interaction

Designing and developing a FO membrane on the basis of an aquaporin based liquid membrane involves several challenges, like finding the right membrane formulation, characterizing the membrane and its interactions with its surroundings and building a suitable test setup. The membrane formulation will not be further discussed here because it is handled as confidential information. A suitable multi-purpose module for FO to house the liquid membrane and to enable FO experiments and measurements will be presented in Paper V. This leaves another very important parameter to focus on – the interaction of the membrane with its surroundings. Here, the aim was to optically investigate how the encapsulated liquid membrane behaves when brought into contact with the feed and draw solutions.

### 5.3.1 Motivation

As explained in the beginning of this FO chapter, there are three major kinds of liquid membranes. Those are the emulsion liquid membranes introduced by Li in 1960 [67], the solid support liquid membrane used by Ward and Robb [69]and the bulk liquid as well as several different sub-types that are under development. Every single type can be used in one or more applications like the removal of metal from waste water [70-72] or even desalination [66]. However, despite their great potential only few applications using liquid membranes have found their way into industry yet. The main reasons that prohibit the widespread use of liquid membranes so far are problems with the stability of the emulsion [73-76]. An aquaporin based liquid membrane would be based on the principle of bulk liquid membranes. Here, the emulsion containing aquaporin proteins would be encapsulated in between two commercially available polymeric membranes. The stability of the membrane and many of the challenges concerning encapsulation membranes and interaction with those are similar in bulk and in solid support liquid membranes. Kocherginsky [74] lists the main reasons for membrane degradation as the pressure difference over the membrane, the progressive wetting of the pores in the support membrane by an aqueous phase, the mutual solubility of species from the aqueous phase and liquid membrane phase and the blockage of membrane pores. Also the feed and draw solution [77] as well as the type of membrane and its pore size [78] have an influence on membrane stability. Dzygiel and Wieczorek [55] propose 3 ways to confront these issues and so to increase membrane stability. First of all the membrane thickness should be increased to have a greater area of interaction between the

emulsion and encapsulation membrane. A second recommendation is to use less flow of the aqueous phase which would decrease the shear forces on the liquid membrane / encapsulation membrane / aqueous phase interphase. Both points, however, would lead to a decrease in flux due to a longer diffusion path and an increased risk of concentration polarization so the right equilibrium has to be found. Last of all they propose a regulation of temperature and so to control the solubility of the used components. These are only some suggestions and one can see that the investigation of those factors influencing membrane stability would be a first basic step to the development of novel membrane type for FO based on aquaporin containing liquid membranes. Therefore, a device for bulk liquid membrane / aqueous phase interaction was designed and fabricated.

The observation device should fulfil various criteria to make it a simulation tool as close to reality as possible. It has to contain three compartments – one for the feed phase, one for the receiving phase and one for the liquid membrane itself. The encapsulation membranes separating the liquid membrane from feed and draw should be exchangeable, and the whole device reusable. An additional point was that the device should be small enough to fit onto a microscope stage for optical inspection of the interaction of liquid membrane and aqueous phase. This also demands that the reservoirs and the centre piece are made from a transparent material. Ideally, the whole setup should have been cross flow compatible but due to time restrictions and for reasons of simplification this point has been left out. The major challenge was to seal the device against leakage, which posed a serious problem because of the necessary assembly of three chambers into one structure and the exchangeability of the encapsulation membranes.

The final device than comprised a centre piece made of a rubber like transparent material (PDMS) and a simple pushing and clamping system to make three tight chambers.

### 5.3.2 Materials and Methods

The centre piece, which contains the liquid membrane and the sealings for the reservoir chambers were made in PDMS (Sylgard® 184 Silicone Elastomer Kit, Dow Corning, Michigan, USA). These parts were cast into moulds and cured at room temperature over night. After removal of the parts from the moulds they were further treated for 24 hours in 100 °C to remove leftover radicals from the chemical curing process. The moulds and all other parts were micro-milled.

**Micro-milling**

Micro milling uses a small, mainly metallic, rotating tool to remove material from the substrate. The important factor when going down to micrometer levels is that the common finishing techniques, which are used to improve the surface roughness after the milling process, are difficult or even impossible to apply on microstructures. Therefore, surface roughness will depend directly on the used tool and milling parameters. However, compared to other micro-structuring techniques micro milling has several advantages like flexibility in materials and geometries. Rectangular channels for example can be produced with high aspect ratios. With the help of computerized numeric control (CNC) milling patterns can be easily transferred from 3D CAD programs to the machine itself. However, milling with small tools in small dimensions always puts limitations on machining speed. High aspect ratios take time because

deep channels require multiple passes. Wear and tool breakage are two other factors that put restraints on the machining speed, also called feed. In simple terms the feed can be estimated taking into account tool rotation and depth of cut.

The accuracy of the milling process is further influenced by run-out and chip load [79]. Run-out occurs due to imperfect tool alignment, asymmetric tool geometry or vibrations. As can be seen in Figure 26, run-out influences the precision of the milling process which causes an inhomogeneous removal of material on the channel walls. These inaccuracies of some micrometer are negligible in macro scale milling but become very important when milling microstructures. Due to the fact that the tool is not orthogonal to the surface, one side of it cuts deeper than the other. A reduction of the run-out effect can be achieved by using shorter tools and tool holders as well as a stiffer tool holder. Unfortunately run-out is a function of machine and tool design and cannot be influenced by changing machine parameters. In contrast, the chip load or feed per tooth can be influenced by optimization of the machining parameters. Lee and Dornfeld [79] found that chip load has a great influence on surface roughness, and that the relation between the two is "linear at lower cutting speeds and lower chip loads", which means that a better surface can be achieved with smaller chip load. Chip load is also called feed per tooth. It can be calculated by:

$$feed\ per\ tooth = \frac{feed\ cut}{n \cdot z} \qquad (5.1)$$

Here $n$ is the rotation speed and $z$ the amount of tooth of the tool. By choosing the optimal parameters for the milling process the surface roughness can be minimized. Another important parameter is the cutting speed where the tool diameter $d$ and the rotation speed $n$ are taken into account.

$$cutting\ speed = \pi \cdot d \cdot n \qquad (5.1)$$

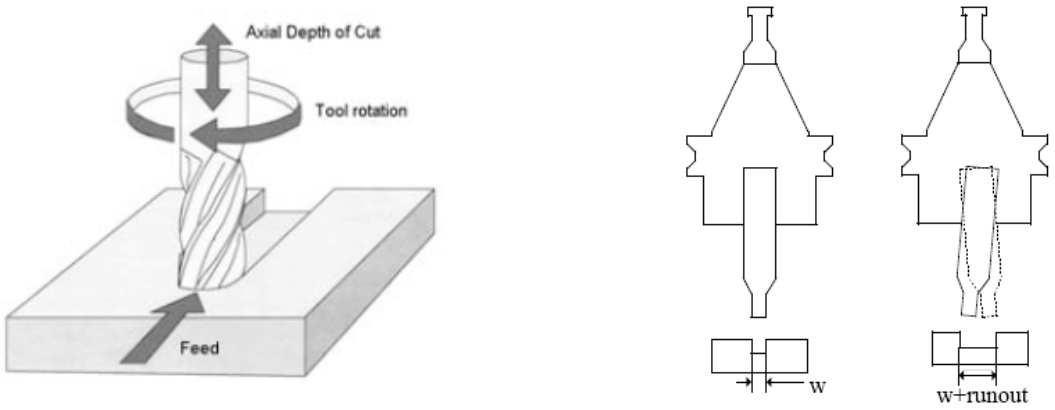


**Figure 26:** Schematic of the milling process with its main parameters feed cut, depth and rotation speed (left) [8] and an example of the run-out effect (right) – the first picture shows the production of an ideal channel where the tools cuts straight into the material. With run-out the tools starts to vibrate and the channels gets wider.

**Device fabrication**

The production of the device presented here, was carried out using a Mini-Mill 3/Pro (Minitech, Norcross, GA, USA) milling machine equipped with a 50,000 rpm (rotations per minute) brushless electrical spindle (EM-501 from NSK America Corp., Schaumburg, IL, USA) (Figure 27 left). End mills with diameters down to 5µm from PMT (Performance Micro Tools, Janesville, WI, USA) are conventionally available but only end mills with a diameter down to 500µm were used during production (Figure 27 right). The materials used for the observation device allowed feed speeds of up to 400 mm/minute. PMMA (NordiskPlast, DK) was used for the reservoir and most clamping parts as well as for the reinforcement bars. This material requires cooling to prevent the material from melting. Melting would lead to an accumulation of material on the milling tool and thus a decrease in surface quality. The two holder parts were made out of polycarbonate (PC). This material was chosen because it allowed the direct incorporation of durable threads so that screws could be fixed without the use of nuts. Table 1 gives an overview over all parts and materials used in the device. The M3 screws and bolts that were used are commercially available parts. The various encapsulation membranes were commercially available and were custom cut via $CO_2$ laser ablation.

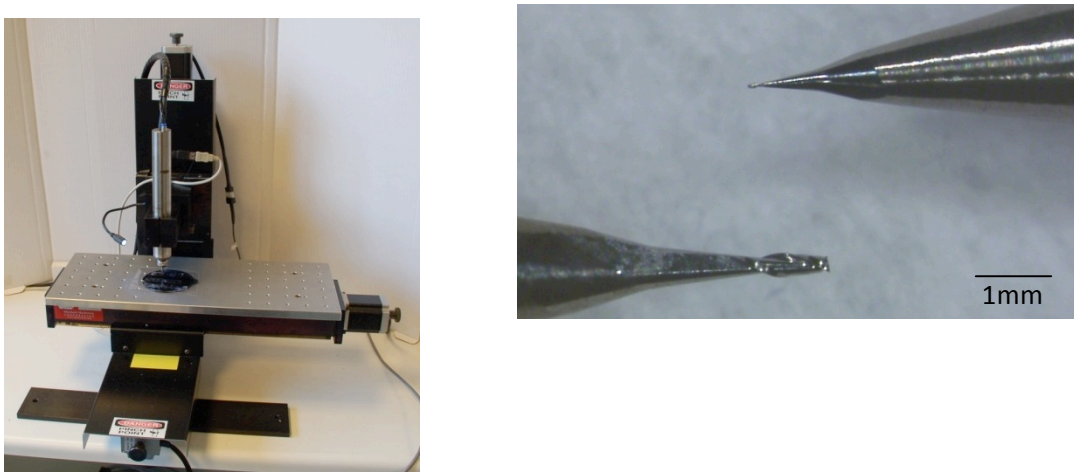


**Figure 27:** Left: Mill 3/Pro (Minitech, Norcross, GA, USA); right: comparison between 25µm and 200µm tool.

### 5.3.3 Results

The dimensions of the overall device are 105 x 60 x 11 mm. The reservoirs have a volume of 616 $mm^3$ which means that 616 µl of fluid can be injected. The emulsion needed to fill the centre piece entirely is 84 µl. All parts and a 3D construction drawing of the chamber can be seen in Figure 28. The principle to seal the chambers is a simple clamping mechanism. The reservoir chambers are assembled using a PDMS seal in between two PMMA plates. The reservoirs are then pressed against the encapsulation membranes and the centre piece via the pusher system. To prevent any of the parts from dislocating and to ensure a tight fit the top piece of the holder is screwed slightly on top before pushing. After the seal between the membranes and the reservoirs has been made the reinforcement bars are added and all screws in the holder are tightened to clamp the whole assembly and to ensure a tight seal.

**Table 1:** Overview over custom made parts for the observation device, the numbers in brackets refer to the disassembled observation device in Figure 28 left.

| Part | Material used | Production method |
|---|---|---|
| bottom and top holder (4,5) | PC | micro-milling |
| reservoir plates (7) | PMMA | micro-milling |
| pusher screw holder (6 middle) | PC | micro-milling |
| all other pusher components (6) | PMMA | micro-milling |
| reinforcement bars (1) | PMMA | micro-milling |
| centre piece (2) | PDMS | casting |
| reservoir seals (8) | PDMS | casting |
| encapsulation membranes (3) | various | $CO_2$ laser ablation |

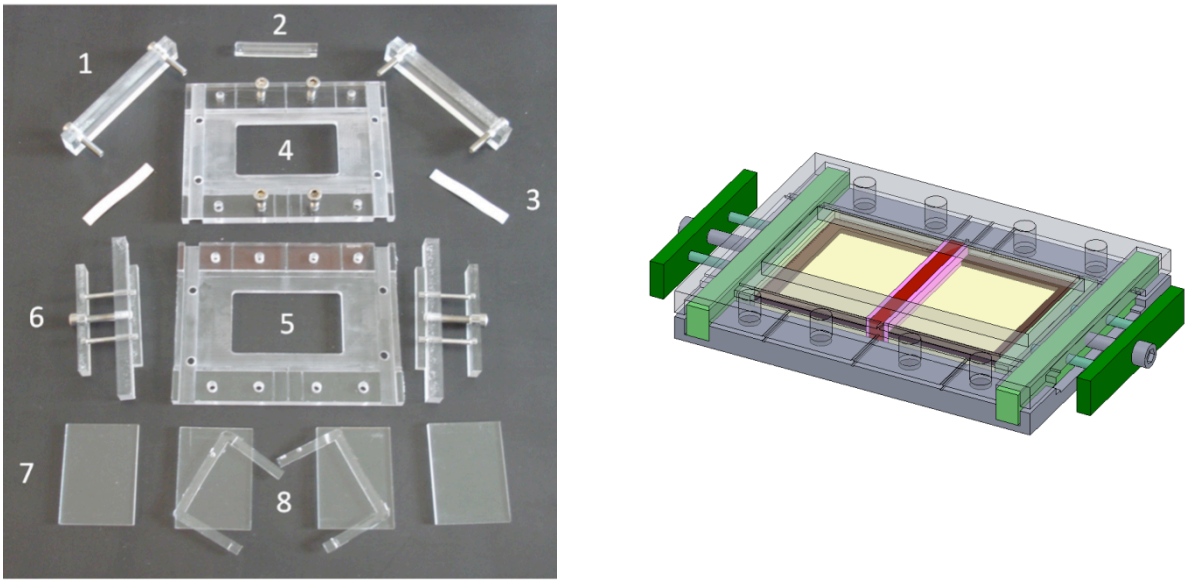


**Figure 28:** Observation device for liquid membrane / aqueous phase interaction inspection as a 3D construction drawing (right) and disassembled (left): 1) reinforcement bar, 2) PDMS center piece (red), 3) encapsulation membrane (pink), 4) holder top (transparent grey), 5) holder bottom (grey), 6) pusher system (green), 7) reservoir plates (yellow), 8) reservoir seals (brown).

Sealing tests were carried out using green food colour dissolved in Mili-Q water. Using mostly transparent components inside the chamber the green colour made it easy to spot any leaks. First tests showed a repeated leak in the back of the reservoirs. A closer inspection revealed that the middle of the clamp in the back of the device bulged up and thus created an area of low pressure where water could leak out in between the reservoir plates and the reservoir seal. This problem was solved by introducing the reinforcement bars, which stiffened the back of the holder and thus prevented it from bulging. This led to a more even pressure distribution along the seal and therefore to a tighter seal.

First experiments with liquid membrane emulsion were performed as well. 1M NaCl was used as a draw solution (receiving phase) and MiliQ as a feed phase. The emulsion was injected as a first step. After injecting both feed and draw phase the device was left for several hours with the camera of the microscope taking pictures in predefined intervals (Figure 29 A).

The first experiments aimed at the investigation of the influence of liquid membrane injection into a by encapsulation membranes confined space. Here, it could be seen that when injecting too fast pressure

builds up in the device which sometimes lead to a leak. When having a tight seal it could be observed that, depending on the membranes used, droplets form on the outside of the encapsulation membranes and thus liquid membrane leaks out into the reservoirs. This can be seen by a droplet formation on the surface of the encapsulation membrane (Figure 29 B). A slower and gentler injection prevented this from happening (Figure 29 C).

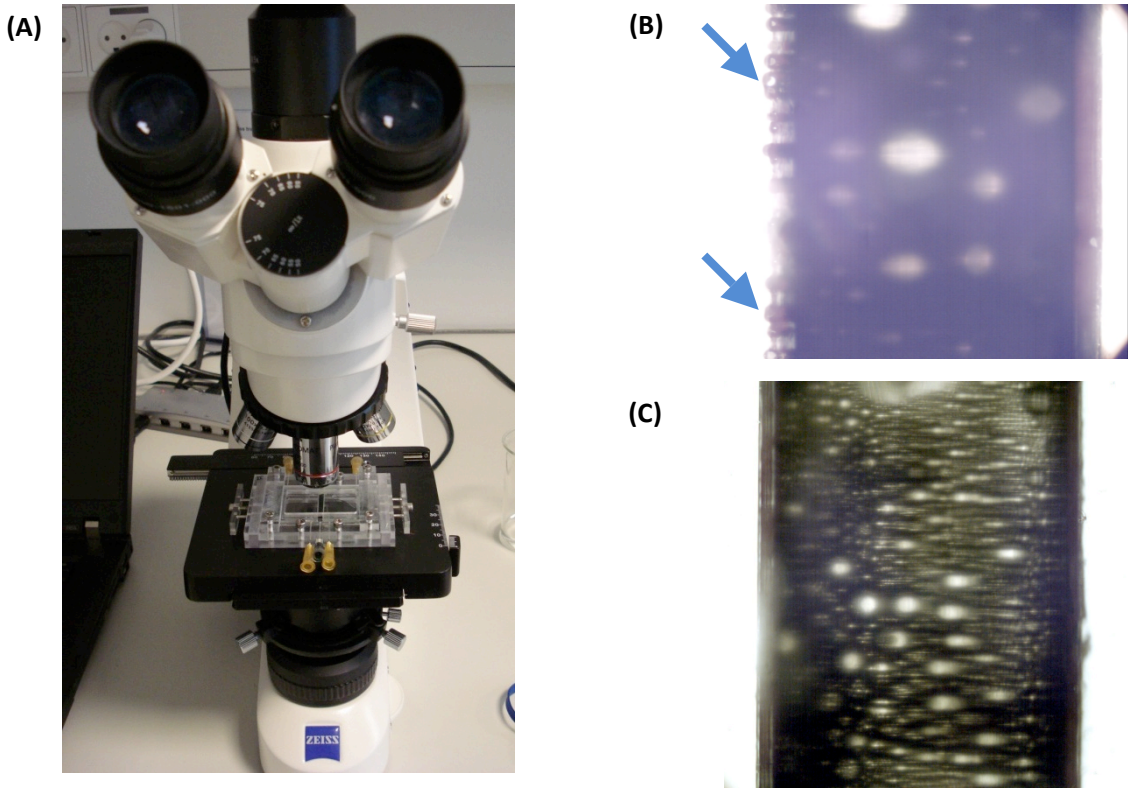


**Figure 29:** (A) Observation device for liquid membrane / aqueous phase interaction inspection under a microscope with automated recording of images in pre-defined intervals; figures (B) and (C) show the PDMS center piece filled with liquid control membrane in between two encapsulation membranes - (B) when pressure built-up during injection becomes too high, liquid membrane emulsion is pushed through the encapsulation membrane which form droplets on its surface (left side, droplets indicated with arrows); (C) a slower injection and thus lower pressure prevents this effect. The injected liquid membrane with its GPV fills up the whole interspace between the encapsulation membranes (thicker lines on both sides of the emulsion). Injection tests were carried out with empty feed and draw chamber.

### 5.3.4 Discussion

When looking at the pictures of the first liquid membrane tests one minor drawback can be noticed. The single vesicles that form the emulsion can only be dimly seen. This is due to the fabrication method of the PDMS centre piece. The mould for casting is made by micro-milling which leaves all surfaces with a certain roughness and milling marks. The PDMS is capable of reproducing structures down to nanometre scale and therefore every unevenness in the mould is replicated. This then diffuses light that is shown through the structure and the result is a milky image Figure 29 B and C. Here, solutions could involve the incorporation of a glass plate either in the mould or the centre piece directly, a splitting up of the centre piece into components or the use of a different mould. Another critical point is the choice of PDMS in itself. Several studies have reported that PDMS has an affinity to absorb small molecules (e.g. lipids) and to have residues of curing agent left inside the material [80-84]. Residues can be removed by thermal

aging [80]. Therefore, PDMS pieces used in this device were cured in the oven at 100 °C for at least 24 h. However, the affinity to small molecules is still a major concern because it could affect the liquid membrane, depending on its constitution. Therefore, for a later device other materials have to be investigated. Here, liquid Teflon would certainly be a viable alternative (e.g. SHIN-ETSU SIFEL®, Shin-Etsu Chemical Co., Ltd., Japan). Even with these problems left the device already showed its potential for the investigation of liquid membranes and their surroundings. A first example was observed during emulsion injections, which led to a bleed of liquid membrane into the reservoir chambers when applying too much pressure. Different encapsulation membranes showed different amounts of that bleeding, always depending on pore size, hydrophobicity and thickness.

### 5.3.5 Conclusion and Outlook

The preliminary tests showed that the developed observation device has the potential to be a versatile tool for liquid membrane / aqueous phase interaction inspection. The micro-milling and casting are methods that are simple and fast. In addition, almost every encapsulation membrane can be cut to size with the $CO_2$ laser. Furthermore, the device is reusable and only the encapsulation membranes and the liquids have to be exchanged. It also fits well onto a microscope stage which was a prerequisite for optical liquid membrane inspection.

The design and production of the device was carried out late in the PhD studies and therefore only the device and first preliminary test could be performed. The device presented here can be used for a basic inspection of liquid membrane / aqueous phase interaction. For more advanced tests involving cross-flow or the application of pressure it is not suited. For that purpose, a new design would have to be made. The best way would be to make a microfluidic chip that contains channels and reservoirs. This could also be fabricated using polymers and micro-milling with an additional bonding step (e.g. thermal bonding) afterwards. This approach would also eliminate the use of PDMS and thus the influence of the material on the experiments. However, the incorporation of exchangeable encapsulation membranes into such a microfluidic device poses a separate challenge in itself and would have to be addressed during the development.

## 5.4 A novel multi-purpose chamber for forward osmosis

In parallel to the investigation of bulk liquid membrane / aqueous phase interaction, a novel multi-purpose module for FO tests was designed, fabricated and tested. This module together with its characterization is presented in Paper V.

# 6 Conclusion and Outlook

This PhD project is part of an ongoing development of a novel kind of water treatment with Mother Nature as a role model. Taking nature's own water filters and making them into an artificial membrane for water treatment in industrial scale is an idea that is as ingenious as it is ambitious. Ingenious because the viability and effectiveness of these water channels has been proven for millions of years in the harshest environments. Plants and humans use these aquaporin proteins for regulating the water transport in and out of their cells. So it is only natural that humans should exploit that technology and make it usable. The project is also ambitious because these proteins have never before been used in an industrial sized filtration system. This is the goal of Aquaporin A/S where aquaporin proteins will be utilized for developing better water filtration systems.

Making aquaporins work in an artificial filter is not only depending on the right biological formulation of the components surrounding the protein and investigating the proteins properties and characteristics. No, it is also about providing a physical support for the protein containing formulation which protects it from the environment and increases its lifetime under industrial conditions. Furthermore it includes ensuring that the novel membrane can be tested and analyzed under conditions as close as possible to the later application. This entails the design and development of completely new, custom made setups and supports and the constant optimization to new findings and changing requirements. This thesis shows such a development. It gives insight into the mechanical side of the Aquaporin membrane technology™. Two different approaches towards a novel aquaporin based water filtration membrane were shown in this thesis.

## 6.1 Flat sheet membrane supports

The first one aimed at the development of a flat sheet membrane for RO applications where the development of the support structure for biomimetic applications was the starting point. The use of $CO_2$ laser ablated arrays of apertures in an ETFE foil resulted in a successful development of a hydrophobic support and thus defined the method and material that was going to be used. The fabrication included apertures ranging from 84 µm up to 500 µm. However, parallel performed bilayer lipid membrane investigations showed that the bilayers were most stable in apertures with diameters of 300 µm. Therefore, the laser fabrication was optimized for the production of arrays of apertures with this diameter (Paper I). This was then followed by further testing of the support structures and proof of their usability by applying stable lipid membranes that could be functionalized (Paper II). The work then continued with an upscaling of production from arrays of 64 apertures arranged in a square lattice and spanning an area of 0.21 $cm^2$ to arrays of 576 apertures in an area of 1 $cm^2$ (Paper III) and finally to hexagonal arrays of 7280 apertures covering an area of 10 $cm^2$. This development was accompanied with the investigation and invention of new BLM formation chambers. To increase stability of the bilayer lipid membranes a porous support was added to the supported bilayer to make it a stable sandwich

structure. To successfully apply this porous material (also referred to as PHEMA) existing coating techniques had to be optimized and manipulated. The result was the fabrication of a stable sandwich structure with halfway filled apertures that showed increased membrane stability (Paper IV).

This development represents a paradigm shift in the field of BLM formation where single aperture experiments are the norm. The creation of tight BLMs on large scale arrays opens up for the possibility for the parallel testing of different transmembrane proteins. One could for example imagine redesigning the array to such an extent that each aperture can be addressed separately and thus create a high throughput drug screening unit. This could be done for example using a microfluidic biomimetic membrane array system based on the scaffold structure. In such a system G-protein coupled receptor (GPCR) ligand interactions and/or ion channel proteins could be studied in a high through-put format using ion currents or electrochemical impedance spectroscopy.

The upscaling of the support structure to 10 $cm^2$ was the limit that could be done with the available $CO_2$ laser setup. This size would be sufficient for a first product like an add-on ultra-pure water filter to existing filtration systems in laboratories and research institutions. However, the demands for ultra-pure water by the semiconductor industry are by far bigger. Here, the fast production of $m^2$ of polymeric support structures would be needed. A possible solution for this problem would be a laser processing system as the Preco Lightning Bolt LB3000 Series Web Cutting system. This machine has a 3 axis scan-head and a processing area of 305 $mm^2$ where the polymer is held in place by a vacuum system. It is fully automated and can process rolls of polymer with a width of 305 mm and a diameter of 400 mm. This makes it suitable for a fast and efficient production of square meters of support structure. However, with an upscaled scaffold production other challenges will arise, like how to form the lipid bilayer on those bigger arrays and on how to fuse aquaporin proteins into them.

## 6.2 Aquaporin based liquid membrane supports

One way to do that would be to integrate aquaporins directly in the lipid matrix that will be used as the active membrane. Here, the second approach of an aquaporin based liquid membrane offers great potential. A liquid membrane can be handled more easily than a flat lipid bilayer membrane. Furthermore, aquaporin proteins can be directly incorporated into the membrane while creating it. With this approach the primary focus is on FO that can be used for various applications like desalination or upconcentration. The field of FO experienced a great increase in interest over the last couple of years but is not yet as fully optimized and developed as RO – for example there is only 1 commercially available FO membrane. The field of liquid membranes shares the same fate – many experiments and investigations are ongoing in labs but only few applications are used in industry. Therefore, to test novel membranes new setups had to be developed. This included a novel multi-purpose FO module (Paper V) and a liquid membrane / aqueous phase interaction observation device. The latter should help us to discover the optimal conditions for a liquid membrane and which encapsulation membranes will be most beneficial.

Compared to current setups for FO [4] where a flat membrane is clamped in between two chambers the introduced novel multi-purpose module offers the possibility to use different membrane types –

regardless if liquid or solid. This enables researchers to consider different approaches to classical solid membranes and broadens the field of possible materials and concepts – as for example an aquaporin based liquid membrane.

The successful testing of an aquaporin based liquid membrane in the novel chamber will be just a first step. This setup is only suited for lab-scale experiments. For the use in industrial scale (e.g. a desalination plant) the active surface area has to be increased. Here, spiral wound modules or hollow fibers offer the greatest potential. One could for example imagine a double-walled hollow fiber where the liquid membrane is injected in the interspace of the two walls and either feed or draw inside the inner core. The small dimensions of these fibers would enable them to be used parallel in a module and thus increase the active filtration area massively.

A working liquid membrane could also be used as a RO membrane. When being able to stabilize and physically bind the liquid membrane inside a support it should withstand the application of a hydrostatic pressure. This way, water could be filtered without the use of an additional draw solution. Other options of liquid membranes without aquaporin proteins will also become more interesting once the encapsulation challenges are solved. For example, a carrier facilitated transport for the extraction of ions is feasible. Here, the most promising advantage is that instead of batch processes as with classical solutions like ion exchange or solvent extraction, continuous operation would be possible. Also here, special hollow fibers could be used.

This thesis has shown two ways of the many possibilities in the development of an aquaporin based water filtration system. However, to get a working water filter for industrial use a lot of work still remains. Nature has used thousands of years to bring its water filtration to perfection. Until now we have only used five, but made considerable progress!

Water, is essential for human life on earth … and beyond.

# Acknowledgements

This Thesis is the summary of three years work and marks the end of my PhD project. These years were packed with learning and the successful end is not my credit alone. On my way I had many helpers that I want to say thank you to.

First, a big thank you to all my supervisors Oliver, Claus and Jenny that were giving me free hand in planning and conducting my activities but nevertheless directed my work into the right channels. I especially have to thank Oliver who has been a great supervisor in different projects for over 4 years. He established the contact with Aquaporin A/S and thus made it possible that I got the chance to have this great experience of being an industrial PhD. Claus, your clear and direct criticism of especially my written work, helped not only in writing articles and this thesis but got me more focused on what a proper publication has to look like. Jenny, thank you for taking over the task as main supervisor so late in the game - your help was very welcome.

Second, I have to thank everyone at Aquaporin A/S. I cannot highlight enough how inspiring and fun it was to do a PhD in this kind of work environment. We had celebrations and discussions and it is fantastic to see that in this company everyone can influence the goals and strategies by throwing in good ideas – nothing is instantly blocked but put forward to discussion. I am delighted that I can continue here and am absolutely certain that we will hit market with our innovative product in the near future. A special thank you goes to Mark, my 'superordinate' project manager. Not only did we advance the technological development of our membranes but you are also a fun person to have around and your constant 'can't we build something like that' kept me busy throughout the years.

Another big thank you goes to my flatmates (present and former) – Lola, Elke, Kåre – I would never have had such a great time living in Copenhagen if it wasn't for you. Coming home is something I always enjoy.

Ali, Emil, Sverrir – the business course, stegt flæsk and life in general would have never been the same without you!

Roland und Ali – super wenn man auch in nem fremden Land mal in seiner Heimatsprache über Gott und die Welt fachsimpeln kann – danke für die vielen spaßigen Abende.

Jan, Maciej and Kamila my office buddies – thanks for fun times during office hours and a helping hand and advice in and outside of the lab.

Stefania, grazie mille for showing me the secrets of the Alicona InfinteFocus.

Thanks to the Danish Polymer Centre, the BIOMICS and POLYMIC group and the rest of DTU-Nanotech for interesting discussions and support.

Thanks to all my friends from all over the world for making my time in Copenhagen unforgettable.

A big thank you also goes to my parents who constantly helped me with psychological support – holidays at home are priceless.

And of course Lea – during my last year you became one of the biggest distractions but every minute with you was, is and will be a minute well spent.

Whoever I have failed to mention – thank you, your help will never be forgotten.

# References


1. Lopez-Gunn, E. and M.R. Llamas, *Re-thinking water scarcity: Can science and technology solve the global water crisis?* Natural Resources Forum, 2008. **32**: p. 228-238.
2. Shannon, M., et al., *Science and technology for water purification in the coming decades.* Nature, 2008. **452**(7185): p. 301-310.
3. Wild, D., M.-O. Buffle, and J. Hafner-Cai, *Water: a market of the future*, in *sam sustainability investing*. 2010, Robeco: Zürich.
4. Cath, T., A. Childress, and M. Elimelech, *Forward osmosis: Principles, applications, and recent developments.* Journal of membrane science, 2006. **281**(1-2): p. 70-87.
5. Achilli, A. and A. Childress, *Pressure retarded osmosis: From the vision of Sidney Loeb to the first experimental installation--Review.* Desalination, 2010.
6. Hélix-Nielsen, C., *Osmotic Water Purification: Insights from Nanoscale Biomimetics.* Environmental Nano Technologies, 2010. **March-April**: p. 58-66.
7. Xu, Y., et al., *Effect of draw solution concentration and operating conditions on forward osmosis and pressure retarded osmosis performance in a spiral wound module.* Journal of membrane science, 2010. **348**(1-2): p. 298-309.
8. Ogier, S., et al., *Suspended planar phospholipid bilayers on micromachined supports.* Langmuir, 2000. **16**(13): p. 5696-5701.
9. Wilk, S., et al., *Integrated platform for ion channel sensing.* Sensors, 2005 IEEE, 2006: p. 4.
10. Favero, G., et al., *Membrane supported bilayer lipid membranes array: preparation, stability and ion-channel insertion.* Analytica Chimica Acta, 2002. **460**(1): p. 23-34.
11. B. Alberts, A.J., J. Lewis, M. Raff, K. Roberts, P. Walter, *Molecular Biology of the Cell, 4.ed*. 2002.
12. Gennis, R.B., *Biomembranes molecular structure and function*. 1989.
13. Graff, A., *Insertion of membrane proteins in artificial polymer membranes.* PhD Thesis, 2006.
14. Ho, D., et al., *Hybrid protein-polymer biomimetic membranes.* Nanotechnology, IEEE Transactions on, 2004. **3**(2): p. 256-263.
15. Lorenceau, E., et al., *Generation of Polymerosomes from Double-Emulsions.* Langmuir, 2005. **21**: p. 9183-9186.
16. Rosenkranz, T., et al., *Observing Proteins as Single Molecules Encapsulated in Surface-Tethered Polymeric Nanocontainers.* ChemBioChem, 2009. **10**: p. 702-709.
17. Hélix-Nielsen, C., *Biomimetic membranes for sensor and separation applications.* Anal. Bioanal. Chem., 2009. **395**(3): p. 697-718.
18. Pohl, P., *Combined transport of water and ions through membrane channels.* Biological chemistry, 2004. **385**(10): p. 921-926.
19. Preston, G., et al., *Appearance of water channels in Xenopus oocytes expressing red cell CHIP28 protein.* Science, 1992. **256**(5055): p. 385.
20. Agre, P., M. Bonhivers, and M. Borgnia, *The aquaporins, blueprints for cellular plumbing systems.* Journal of Biological Chemistry, 1998. **273**(24): p. 14659.
21. Viadiu, H., T. Gonen, and T. Walz, *Projection Map of Aquaporin-9 at 7 Å Resolution.* J. Mol. Biol., 2007. **367**: p. 80-88.
22. Evans, D.H., *Osmotic and Ionic Regulation - Cells and Animals*. 2009, Boca Raton: CRC Press.
23. Baker, R.W., *Membrane Technology and Applications*. Second Edition ed. 2008, Hoboken: John Wiley & Sons, Ltd.

24. Williams, E.D., R.U. Ayres, and M. Heller, *The 1.7 kilogram Microchip: Energy and Material Use in the Production of Semiconductor Devices.* Environ. Sci. Technol, 2002. **36**(24): p. 5504-5510.
25. Horvath, A.G., *Water Softening*. 1931: US Patent.
26. Liu, L., et al., *A new helical membrane module for increasing permeate flux.* Journal of membrane science, 2010. **360**(1-2): p. 142-148.
27. Kurihara, M., et al., *Development of the PEC-1000 Composite Membrane for Single Stage Sea Water Desalination and the Concentration of Dilute Aqueous Solutions Containing Valuable Materials.* Desalination, 1981. **38**: p. 449.
28. Loeb, S. and S. Sourirajan, *Sea Water Demineralization by Means of an Osmotic Membrane*, in *Saline Water Conversion II*, R.F. Gould, Editor. 1963, American Chemical Society: Washington. p. 117-132.
29. Cohen, Y., *Surface-structured RO membranes.* Membrane Technology, 2010. **July**: p. 7.
30. Wei, X., et al., *Surface modification of commercial aromatic polyamide reverse osmosis membranes by graft polymerization of 3-allyl-5,5-dimethylhydantoin.* Journal of membrane science, 2010. **351**: p. 222-233.
31. Liu, M., et al., *Impact of manufacture technique on seawater desalination performance of thin-film composite polyamide-urethane reverse osmosis membranes and their spiral wound elements.* Journal of membrane science, 2010. **348**: p. 268-276.
32. Colquhoun, H.M., et al., *Chlorine tolerant, multilayer reverse-osmosis membranes with high permeate fux and high salt rejection.* Journal of Materials Chemistry, 2010. **20**: p. 4629-4634.
33. Kumar, M., et al., *Highly permeable polymeric membranes based on the incorporation of the functional water channel protein Aquaporin Z.* 2007. **104**(52): p. 20719-20724.
34. White, S.H., *Analysis of the torus surrounding planar lipid bilayer membranes.* Biophys J, 1972. **12**(4): p. 432-45.
35. Wonderlin W F, F.A.a.F.R.J., *Optimizing planar lipid bilayer single-channel recordings for high resolution with rapid voltage steps* Biophys J, 1990. **58**: p. 9.
36. Simon, A., et al., *Formation and stability of a suspended biomimetic lipid bilayer on silicon submicrometer-sized pores.* J Colloid Interface Sci, 2007. **308**(2): p. 337-43.
37. Rijn, C.J.M.v., Nijdam W, Kuiper S, Veldhuis G J, Wolferen H v, Elwenspoek M, *Microsieves made with laser interference lithography for micro-filtration applications* Journal of Micromechanics and Microengineering, 1999. **9**: p. 3.
38. Mayer, M., et al., *Microfabricated teflon membranes for low-noise recordings of ion channels in planar lipid bilayers.* Biophys J, 2003. **85**(4): p. 2684-95.
39. Kitta, M. and H. Tanaka…, *Rapid fabrication of Teflon micropores for artificial lipid bilayer formation.* Biosensors and Bioelectronics, 2009.
40. CascadeTechnologies. 2008 [cited 2010; Available from: http://www.ctscientific.com/images/Beam_Profile.jpg.
41. Jensen, M., *Laser Micromachining of Polymers*. PhD Thesis. 2005.
42. SANDISON, M.E., *Artificial Bilayer Lipid Membranes (BLMs) on-Chip for Single Molecule Sensing.* Nanotechnology II; - Proceedings of SPIE - The International Society for Optical Engineering, 2005.
43. O'Shaughnessy T J, H.J.E., Kulp J L,III, Daly S M, Ligler F S, *Laser ablation of micropores for formation of artificial planar lipid bilay-ers.* Biomedical Microdevices 2007. **9**: p. 6.
44. Vogel, J., et al., *A support structure for biomimetic applications.* Journal of Micromechanics and Microengineering, 2009. **19**: p. 025026.
45. Vogel, J., *Development of a thin, perforated and hydrophobic membrane to incorporate aquaporins*, in *Mechanical Engineering & Electrical Engineering and Information Technology & DTU - Nanotech*. 2007, DTU & Chemnitz Technical University p. 127.

46. H. T. Tien, A.O.-L., *Planar Lipid Bilayers (BLMs) and their applications.* Electrochimica Acta, 2003. **48**(28): p. 3.
47. Mueller, P., et al., *Reconstitution of cell membrane structure in vitro and its transformation into an excitable system.* Nature, 1962. **194**: p. 979-80.
48. Montal, M. and P. Mueller, *Formation of bimolecular membranes from lipid monolayers and a study of their electrical properties.* Proc Natl Acad Sci U S A, 1972. **69**(12): p. 3561-6.
49. Castellana, E. and P. Cremer, *Solid supported lipid bilayers: From biophysical studies to sensor design.* Surface Science Reports, 2006. **61**(10): p. 429-444.
50. HANSEN, J., et al., *Development Of Novel Biomimetic Membrane Designs For Separation And ….* Biophysical Journal, 2009.
51. Hansen, J.S., et al., *Large scale biomimetic membrane arrays.* Anal. Bioanal. Chem., 2009. **395**: p. 719-727.
52. Hansen, J.S., et al., *Development of an automation technique for the establishment of functional lipid bilayer arrays.* Journal of Micromechanics and Microengineering, 2009. **19**: p. 025014.
53. Janshoff, A. and C. Steinem, *Transport across artificial membranes-an analytical perspective.* Anal Bioanal Chem, 2006. **385**(3): p. 433-51.
54. Gratzer, W.B., *The red cell membrane and its cytoskeleton.* Biochem J, 1981. **198**(1): p. 1-8.
55. Kislik, V.S., *Liquid Membranes - Principles & Applications in Chemical Separations & Wastewater Treatment*. 2010, Oxford: Elsevier.
56. Tang, C.Y., et al., *Coupled effects of internal concentration polarization and fouling on flux behaviour of forward osmosis membranes during humic acid filtration.* Journal of membrane science, 2010. **354**(1-2): p. 123-133.
57. HTI. Hydration Technology Innovations - homepage [cited 2010; Available from: http://www.htiwater.com/.
58. Marlaire, R.D. *NASA Space Technology Could Transform Life on Earth*. Oct. 20, 2010 [cited 2010; Available from: http://mynasa.nasa.gov/centers/ames/news/releases/2010/10-88AR.html.
59. Mulder, M., *Basic Principles of Membrane Technology*. 1996, Dordrecht: Kluwer Academic Publishers.
60. Yip, N.Y., et al., *High Performance Thin-Film Composite Forward Osmosis Membrane.* Environ. Sci. Technol, 2010. **44**: p. 3812-3818.
61. Wang, Y., et al., *Direct Microscopic Observation of Forward Osmosis Membrane Fouling.* Environ. Sci. Technol, 2010. **44**: p. 7102-7109.
62. Chou, S., et al., *Characteristics and potential applications of a novel forward osmosis hollow fiber membrane.* Desalination, 2010. **261**(3): p. 365-372.
63. Wang, R., et al., *Characterization of novel forward osmosis hollow fiber membranes.* Journal of membrane science, 2010. **355**(1-2): p. 158-167.
64. Franken, T., *Liquid membranes-academic exercise or industrial separation process.* Membrane Technology, 1997. **1997**(85): p. 6-10.
65. San Romãn, M.F., et al., *Liquid membrane technology: fundamentals and review of its applications.* J. Chem. Technol. Biotechnol., 2010. **85**(1): p. 2-10.
66. Naim, M.M. and A.A. Monir, *Desalination using supported liquid membranes.* Desalination, 2003. **153**: p. 361-369.
67. Li, N.N., *Liquid surfactant membranes.* US Patent No. 3,410,794, 1968.
68. Ward 3rd, W. and W. Robb, *Carbon dioxide--oxygen separation: facilitated transport of carbon dioxide across a liquid film.* Science (New York, NY), 1967. **156**(781): p. 1481.
69. Ward , W.J. and W.L. Robb, *Carbon dioxide--oxygen separation: facilitated transport of carbon dioxide across a liquid film.* Science (New York, NY), 1967. **156**(781): p. 1481.

70. Kedari, C.S., et al., *Removal of $^{241}$Am from aqueous nitrate solutions by liquid surfactant membrane containing 2-ethylhexyl phosphonic acid mono-2-ethylhexyl ester as ion carrier.* Chemosphere, 2010. **80**: p. 433-437.
71. Reddy, T.R., et al., *Selective transport of copper across a bulk liquid membrane using 8-hydroxy quinoline as carrier.* Journal of membrane science, 2010. **351**: p. 11-15.
72. Ren, Z., et al., *Extraction separation oc Cu(II) and Co(II) from sulfuric solutions by hollow fiber renewal liquid membrane.* Journal of membrane science, 2010. **365**: p. 260-268.
73. Danesi, P., L. Reichley-Yinger, and P. Rickert, *Lifetime of supported liquid membranes: the influence of interfacial properties, chemical composition and water transport on the long-term stability of the membranes.* Journal of membrane science, 1987. **31**(2-3): p. 117-145.
74. Kocherginsky, N., Q. Yang, and L. Seelam, *Recent advances in supported liquid membrane technology.* Separation and Purification technology, 2007. **53**(2): p. 171-177.
75. Neplenbroek, A., D. Bargeman, and C. Smolders, *Supported liquid membranes: instability effects.* Journal of membrane science, 1992. **67**(2-3): p. 121-132.
76. Takeuchi, H., K. Takahashi, and W. Goto, *Some observations on the stability of supported liquid membranes.* Journal of membrane science, 1987. **34**(1): p. 19-31.
77. Zha, F., A. Fane, and C. Fell, *Effect of surface tension gradients on stability of supported liquid membranes.* Journal of membrane science, 1995. **107**(1-2): p. 75-86.
78. Chiarizia, R., *Stability of supported liquid membranes containing longchain aliphatic amines as carriers.* Journal of membrane science, 1991. **55**(1-2): p. 65-77.
79. Lee, K. and D. Dornfeld, *A study of surface roughness in the micro-end-milling process*. 2004, University of California. p. 44.
80. Eddington, D.T., J.P. Puccinelli, and D.J. Beebe, *Thermal aging and reduced hydrophobic recovery of polydimethylsiloxane.* Sensors & Actuators B: Chemical, 2006. **114**(1): p. 170-172.
81. McDonald, J.C. and G.M. Whitesides, *Poly(dimethylsiloxane) as a Material for Fabricating Microfluidic Devices.* Accounts of Chemical Research, 2002. **35**(7): p. 491-499.
82. Mukhopadhyay, R., *When PDMS isn't the best. What are its weaknesses, and which other polymers can researchers add to their toolboxes?* Anal Chem., 2007. **79**(9): p. 3248-3253.
83. Regehr, K.J., et al., *Biological implications of polydimethylsiloxane-based microfluidic cell culture.* Lab on a Chip, 2009. **9**: p. 2132-2139.
84. Toepke, M.W. and D.J. Beebe, *PDMS absorption of small molecules and consequences in microfluidic applications.* Lab on a Chip, 2006. **6**: p. 1484-1486.

# Paper I

Reprinted from Journal of Micromechanics and Microengineering **19** (2009) 025026 (6pp), with permission of IOP Publishing

J. Vogel, M. Perry, J. S. Hansen, P.-Y. Bolinger, C. H. Nielsen and O. Geschke;
***A support structure for biomimetic applications***

J. Micromech. Microeng. **19** (2009) 025026 (6pp) doi:10.1088/0960-1317/19/2/025026

# A support structure for biomimetic applications

**J Vogel[1,2], M Perry[1], J S Hansen[1,2], P-Y Bolinger[1], C H Nielsen[1,3] and O Geschke[2]**

[1] Aquaporin A/S, Diplomvej 377, DK-2800 Kongens Lyngby, Denmark
[2] Department of Micro- and Nanotechnology, Technical University of Denmark, DTU Nanotech Building 345 East, DK-2800 Kongens Lyngby, Denmark
[3] Department of Physics, Technical University of Denmark, Quantum Protein Centre, DTU Physics 309, DK-2800 Kongens Lyngby, Denmark

E-mail: jvo@aquaporin.dk

Received 12 September 2008, in final form 6 November 2008
Published 26 January 2009
Online at stacks.iop.org/JMM/19/025026

**Abstract**
Water filtration on the basis of aquaporin molecules incorporated in an artificial lipid bilayer requires a microporous support membrane. We describe a new microfabrication method based on $CO_2$-laser ablation to generate support membranes with homogeneous apertures ranging from 300 $\mu$m down to 84 $\mu$m in diameter. They are arranged in arrays with the densest packaging having a perforation level of up to 60%. The apertures are surrounded by a smooth bulge that is formed by melted material ejected from the aperture during laser ablation. Polydimethylsiloxane (PDMS) replicas were used to visualize and analyse these bulges. The overall area covered so far has been 4 $cm^2$ but upscaling to larger footprints, e.g. square metres, is currently being investigated.

## 1. Introduction

Water with a purity grade of more than 99% is crucial in several applications. In particular, the semiconductor industry needs large amounts of ultra-pure water for the rinsing and cleaning of wafers and chips. The purification steps to achieve this ultra-pure water (UPW) typically involve repeated distillation, ion exchange or reverse osmosis—all powerful purification techniques but generally slow and characterized by high-energy consumption.

So research in improved separation techniques continuously attracts much attention. Among emerging techniques, biomimetic-membrane-based approaches show great potential. In the development of a biomimetic filtration device, a special class of membrane proteins is especially interesting-–the aquaporins. Aquaporins are transmembrane water-selective channels, effectively impermeable to charged species (Preston *et al* 1992). Aquaporins are versatile tools that can be chemically modified or genetically engineered, giving extensive control over membrane transport properties. However, the use of aquaporins in a biomimetic filter requires a suitable support material to establish and stabilize the lipid bilayer or block-copolymer-based biomimetic matrix against hydraulic pressure driven forces (figure 1).

The geometry of such a microporous structure plays a key role in establishing a long-lasting and stable lipid bilayer. Preferably, the surface of the entire support structure should be smooth and hydrophobic. The apertures themselves need to have a smooth, round edge to facilitate the formation of the lipid bilayer and to stabilize the contact between the lipid bilayer and the aperture rim (White 1972). Furthermore, for the application in water purification devices based on aquaporin proteins embedded in a lipid bilayer, it is important to densely pack the apertures in arrays to ensure a high water flux across the membrane.

Partitions can be fabricated by using the full spectrum of known microtechnologies in combination with polymers or silicon. These can be as simple as using a hot needle (Wonderlin *et al* 1990), but also as time consuming and expensive as making submicron apertures in silicon (Simon *et al* 2006) or silicon nitride (van Rijn *et al* 1999). But these technologies suffer either from a limited number of apertures or a costly production process. Mayer *et al* (2003) report the fabrication of arrays by the casting of thin Teflon films onto a PDMS mould. Despite having precisely placed apertures

 

**Table 1.** Specification of the lenses.

| Name | Focal length | Nominal field (mm) | Working distance (mm) | Spot size ($\mu$m) |
|---|---|---|---|---|
| FLA200 | 200 mm | 110 × 110 | 190 ± 3 | 290 |
| FLA80 | 80 mm | 27 × 27 | 74 ± 1 | 116 |

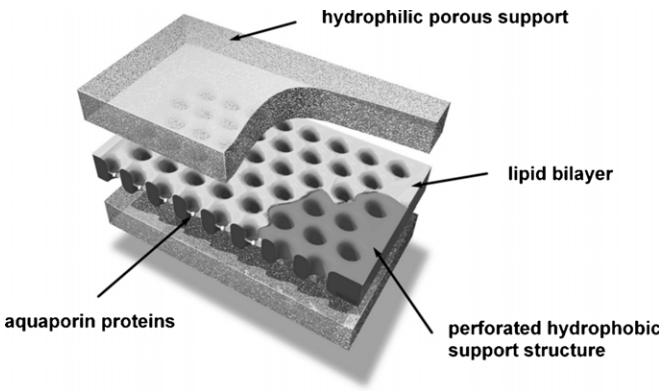


**Figure 1.** Schematic view of an aquaporin-based water purification membrane: the aquaporin proteins (white spots) are embedded in a lipid bilayer (grey) that is generated in a perforated hydrophobic support structure (black). To stabilize the fragile lipid bilayer, it will be encapsulated in a hydrophilic porous support material (grey/white).

with a wide controlled range of diameters (2–800 $\mu$m), this technique suffers from a limited overall perforation area and a long production time (4–24 h). Laser ablation offers a dramatic decrease in production time—mostly using excimer lasers. O'Shaughnessy *et al* (2007) report the fabrication of laser-ablated apertures (4–105 $\mu$m) in polycarbonate (PC). The PC was structured using a UV excimer laser with nanosecond-scale pulse width. However, the production was limited to the PC. So, for example, Teflon, which is widely used as a support material for BLM formation, could not be processed with the excimer laser. The fabrication time was 30 s for a single aperture—still too long for a fast production of highly dense arrays.

Here, we describe a new support membrane microfabrication method based on $CO_2$-laser ablation. This technique allows a fast fabrication of densely perforated support structures. Moreover, it is a well-known production technology with the potential to be scaled up. We were able to generate dense arrays of homogeneous apertures with well-controlled diameters ranging from 84 $\mu$m to 302 $\mu$m in thin ethylene-tetrafluoroethylene (ETFE) films. A partition with 64 apertures could be fabricated within 0.79 s.

## 2. Materials and methods

### *2.1. Material*

To ensure the improved bilayer formation and a potential for use in a large-scale production, the support structure had to consist of a thin polymeric material with a hydrophobic surface. The substrate also needed to absorb light in the operating region of the $CO_2$ laser (10.6 $\mu$m). ETFE (ethylene-tetrafluoroethylene) from DuPont (Detroit, USA) fulfils both these requirements. It has a contact angle with water of around 105° and a transmittance of 88.2% at a wavelength of 10.6 $\mu$m. Two different thicknesses were investigated, namely Tefzel 100LZ (thickness: 25.4 $\mu$m) and Tefzel 200LZ (thickness: 50.8 $\mu$m).

The polymer film was structured by laser ablation using a SYNRAD Inc. (Mulkiteo, WA, USA) 48–5 S Duo Lase carbon dioxide laser with a specified output power of 50 W. It creates a laser beam with a Gaussian intensity distribution and a wavelength of 10.6 $\mu$m. The beam was positioned within the working area using two x/y mirrors and focused by two different lenses (table 1). This made it possible to use different spot diameters and working areas in accordance with the final diameter of the apertures. The post-objective focusing ensured that the focus of the lens remained within the same focal plane over the whole working area.

PDMS (Polydimethylsiloxane–Sylgard® 184 Silicone Elastomer Kit) from DowCorning (Midland, USA) was used to fabricate inverse replicas of the ablated arrays.

### *2.2. Laser ablation*

Laser ablation denotes the fabrication of apertures via laser machining by simply 'shooting' holes through the substrate material. Neither the x/y mirrors nor the stage on which the substrate is placed moves while the structuring takes place. The substrate material was placed in a homemade sample holder made of PMMA (polymethylmethacrylate) which ensured that the underlying surface of the stage would not influence the production. Using a stage that was mechanically adjustable in the $z$-direction, the sample was then positioned within the working distance of the lens. Here, the beam is in focus.

First test series were carried out producing single apertures in ETFE films with a thickness of 25.4 $\mu$m. This was continued with the fabrication of arrays of ETFE films using both thicknesses and different centre-to-centre distances. The apertures were either arranged in rows and columns or in a hexagonal grid. The later configuration enables the densest packaging of apertures and thus the highest perforation level. The arrays were produced row by row always starting from the same side of each row.

Intensity, spot lase duration (SLD) and off vector delay (OVD) were the main parameters to be changed for successful production. The SLD defines the time the beam is focused on one spot and times up to 30 ms were used. The OVD describes the time when the laser is switched off between two production steps. This gives the mirrors time to get settled over the starting point of a new structure before starting a new ablation process. When the OVD is too short it can cause the

formation of tails and if too long the whole production process is slowed down unnecessarily. Here, OVDs from 1 $\mu$s to 8000 $\mu$s were under investigation. These parameters were tuned according to the lens and the final aperture diameter.

### *2.3. Characterization of apertures*

The material is transparent to visible light, thin and non-conductive and therefore a closer characterization of the ETFE support membrane by optical microscopy or scanning electron microscopy (SEM) proved to be rather difficult. So PDMS replicas of the structured ETFE were produced. For easy handling the thickness of the PDMS replicas was chosen to be 3.5 mm. The sample was fixed onto a glass plate with a double-sided tape to prevent the PDMS flowing beneath the structure. Then PDMS was poured on top, cured and released. The PDMS replica was then placed in a Rhodamine B solution to make it fluorescent for further analysis with laser scanning confocal microscopy (LSCM).

Weight measurements for determination of the loss of weight during laser ablation were performed using three ETFE 200LZ sheets of 100 × 100 mm$^2$. Each had to be cut into nine pieces to fit entirely on the scale. They were cleaned with ethanol and weighed. Afterwards, each was structured with an array of 24 × 24 apertures, cleaned and weighed again. The theoretical loss of weight when all material within the apertures is evaporated could be calculated by $m_{\text{theory}} = V \times \rho \times n$, where $V$ defines the volume within the aperture, $\rho$ the density of the material and $n$ the number of apertures made.

The diameter was measured by taking pictures of apertures or the whole array using a Leica DML optical microscope and a built-on Canon Power Shot S40. The pictures then were analysed using the freeware software ImageJ. The diameter of the apertures could be measured using the built-in measurement function and relating the acquired length in pixels to a scale. This way of measuring the diameter means that a tolerance of ±5 $\mu$m has to be accepted. To calculate the average diameter of an array, 25% of all apertures were measured twice. Higher magnifications (40×, 50×) were used for analysing single apertures. Here, at least six measurements were performed to determine the diameter.

### *2.4. Preparation of black lipid membranes in a laser-ablated ETFE scaffold*

For detailed information on the novel automation technique for establishing black lipid membrane arrays (BLMs) on a laser-ablated ETFE scaffold refer to Hansen *et al* (2009). Briefly, BLMs were produced in a custom-designed two-compartment system containing 200 mM KCl electrolyte solution in each compartment. BLMs were established between the two compartments by raising a DPhPC/decane solution (50 mg ml$^{-1}$) across the aperture array. This technique in effect traps a small droplet of DPhPC/decane solution between two aqueous solutions which results in lipid bilayer self-assembly within each aperture of the array.

**Table 2.** Overview over the settings used to produce arrays of apertures, depending on the lens used. It was necessary to change settings within the arrays to fabricate uniform apertures.

| Location | Intensity | SLD | OVD |
|---|---|---|---|
| FLA 80 | | | |
| First aperture of each row | 0.4 W | 5 ms | |
| Rest of the array | | 4 ms | 1 $\mu$s |
| FLA 200 | | | |
| First row | 4.4 W | 5 ms | 1000 $\mu$s |
| Last row | 4.2 W | 4 ms | |
| Rest of the array | 4.4 W | 4 ms | |

## 3. Results

Various lenses and laser settings were used depending on the final diameter of the apertures. During the production of arrays, however, certain characteristics were similar despite using different thicknesses of ETFE and both lenses in the laser set-up. Less energy (intensity and SLD) was needed to structure apertures with the same diameter in arrays than was necessary when making single apertures. And in an array, parameters had to be changed to achieve a uniform structure (table 2). So, for example, if we used the same settings for the whole array when structuring the ETFE with the FLA80 lens, apertures at the start of a row were 15% smaller in diameter than apertures in the middle of the array. We also had to change the settings to achieve uniform shapes and diameters when using the FLA200 lens. After several experiments it was found that to fabricate uniform arrays it is necessary to change the settings within the structure. Not only the starting apertures had to be changed, but also whole rows had to be addressed individually.

### *3.1. FLA 80*

Using the FLA80 lens with a focal spot diameter of 116 $\mu$m, arrays could be fabricated that consisted of apertures with diameters down to 84 $\mu$m. In the end, dense arrays covering an area of 2 × 2 cm$^2$ were produced using an intensity of 0.4 W, a SLD of 4 ms and an OVD of 1 $\mu$s. However, the minimum diameter depended not only on the laser settings, but also on the design of the array. To achieve the densest structure, a hexagonal arrangement of apertures was chosen. With decreasing centre-to-centre distances, a decrease in diameter and a change in the shape of the apertures could be seen. The apertures tended to have a more box-like shape the smaller the centre-to-centre became. The diameter decreased almost constantly from 91 $\mu$m at 140 $\mu$m centre-to-centre distance to 88 $\mu$m at 130 $\mu$m and finally to 84 $\mu$m at 120 $\mu$m in the smallest array (figure 2).

The overall shape of the apertures themselves is also closely related to the centre-to-centre distance and the arrangement, as well as to the machine direction (MD) of the polymer film itself. During the process of melt extrusion, the polymer is stretched and the molecules tend to align in a parallel form (Rosato 1989). This direction is called the machine direction and is material related. In contrast, the production direction (PD) defines the direction

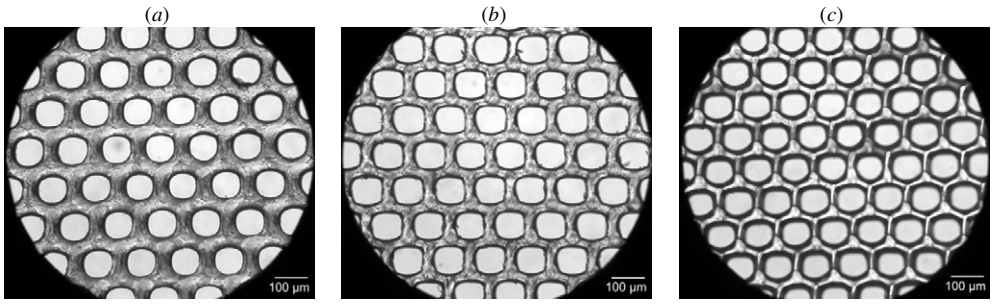


Diameter: 91 µm
c-c distance: 140 µm

Diameter: 88 µm
c-c distance: 130 µm

Diameter: 84 µm
c-c distance: 120 µm

**Figure 2.** Overview of the smallest arrays produced—the shape and diameter of the apertures depended on the centre-to-centre (c–c) distance.

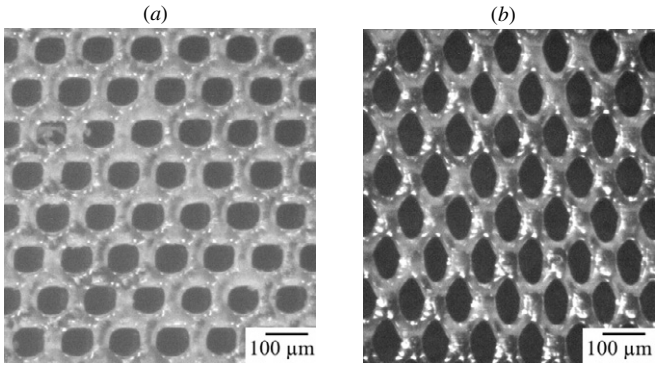


**Figure 3.** Effect of anisotropy of the ETFE film on the example of apertures with a diameter of 84 $\mu$m and a centre-to-centre distance of 120 $\mu$m; (*a*) production of apertures parallel to MD leaves apertures almost round; (*b*) production of apertures perpendicular to MD results in an oval shape.

in which the laser structures the material. Therefore, PD is process related. During the experiments it could be observed that when the centre-to-centre distance was reduced, the PD had to be parallel to MD. If MD was perpendicular to PD the apertures tended to become oval (figure 3). The smaller the final diameter of the apertures, the more pronounced this characteristic. With a smallest aperture of 84 $\mu$m, this anisotropy of the ETFE film became important already at a centre-to-centre distance of 140 $\mu$m. That means that the division bar between the apertures equalled 78% of the overall aperture diameter. In contrast, the anisotropy did not influence the fabrication of apertures with a diameter of 300 $\mu$m until the division bar fell below a value of 33% of the aperture diameter. Furthermore, it should be noted that the apertures produced with MD were no longer completely round at low centre-to-centre distances. They tended to be more hexagonal and formed an array which can be compared to a honeycomb.

### *3.2. Characterization of an aperture rim*

Due to the nature of $CO_2$ laser micromachining, bulges are formed along the edges around the apertures. They are a result of the thermal ablation process. When the laser beam hits the surface, optical energy is transferred into thermal energy,

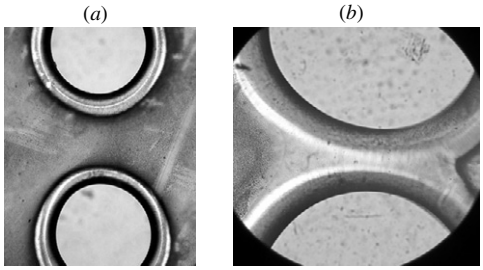


**Figure 4.** Comparison between the behaviour of bulges in arrays with different centre-to-centre distances using the FLA 200 lens; (*a*) no interference of the bulges can be observed with 600 $\mu$m distance; (*b*) superposition of bulges at 400 $\mu$m distance.

which heats up the material. The material in the middle of the focal spot of the beam (point of highest energy impact) evaporates and builds up a high pressure. The substrate in the immediate surrounding area melts and the pressure of the vaporized material ejects this melted part which itself cools down very fast when subjected to air. In consequence, bulges are formed along the edges of the aperture. This feature made the $CO_2$ laser ablation the process of choice, because the melted and deposited material forms smooth and round rims around the apertures (figure 4(*a*)).

The height of these bulges was measured using PDMS replicas of the arrays dyed with Rhodamine B and laser-scanning confocal microscopy. The structures used were arrays of 64 apertures arranged in eight rows and eight columns with a centre-to-centre distance of 400 $\mu$m and an average diameter of 302 $\mu$m. The height value strongly depends on the arrangement and the centre-to-centre distance of the apertures. At a certain distance, the bulges start interfering with each other and superimposing (figure 4(*b*)), which leads to greater heights. This becomes more pronounced the denser the array is, e.g. with hexagonally arranged apertures.

The different height of the bulges between single apertures and closely spaced arrays could be clearly seen on the scans with the LSCM. The bulge on the outside of an array equals the one from a single aperture. This offers a direct comparison of single aperture bulge and superimposed bulge within the same picture. Here, the outer bulge has a height of 9 $\mu$m whereas the one between two apertures amounts up to 15 $\mu$m (figure 5).

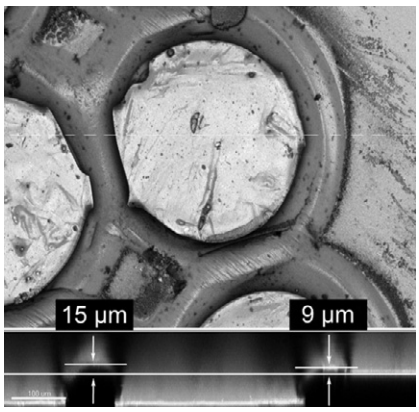


**Figure 5.** Cross section of PDMS replica of an 8 × 8 array of 300 $\mu$m apertures by laser-scanning confocal microscopy—outside (similar to single aperture) the bulge has a height of 9 $\mu$m; due to the superposition of material from two apertures the bulge within an array has a height of 15 $\mu$m.

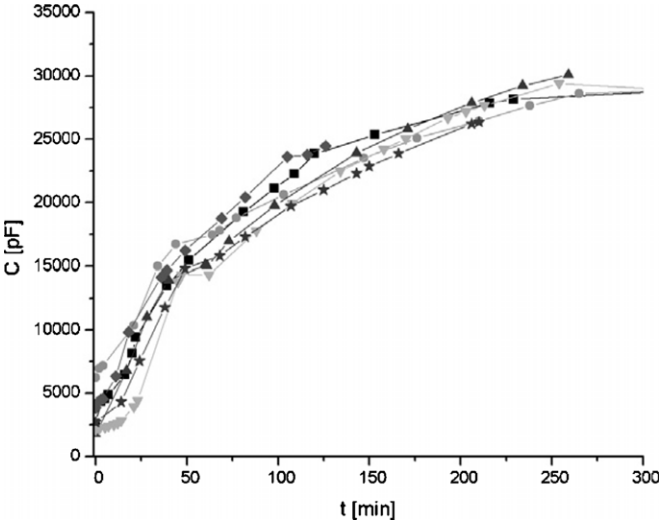


**Figure 6.** Capacitance versus time of six individual free-standing membrane systems created under identical experimental conditions. Membrane systems were formed from a 1,2-diphytanoyl-*sn*-glycero-3-phosphocholine (DPhPC)/decane solution using a new automation technique for simultaneous formation of multiple lipid bilayers. 8 × 8 arrays with 300 $\mu$m apertures served as membrane scaffolds, and regenerated cellulose as an additional support.

Due to the nature of the ablation process, material within the focal spot diameter of the laser melts and evaporates. So weight measurements were done to investigate how much of the original material from the void contributes to the formation of the bulge around the edges of the apertures. The tests showed that around 90% of the weight that theoretically could be removed from the sample by total evaporation of the material within the apertures is actually removed. That means that the bulge formation is made up of only 10% of the volume.

### *3.3. BLM experiments*

Black lipid membrane arrays were prepared in the two-chamber system by the method described in 2.4. The simultaneous formation of BLMs within all of the individual apertures in the ETFE scaffold creates an electrical seal between the electrolyte solutions of the two-chamber system. By applying a square-shaped electrical signal across the BLM membranes separating the two chambers, and measuring the resulting response, the total capacitance of the BLM membrane array can be calculated.

Measurements were performed on an array of apertures with an average diameter of 302 $\mu$m. Using the FLA 200, an array of 64 apertures arranged in eight rows and eight columns with a centre-to-centre distance of 400 $\mu$m could be produced in just 0.79 s.

Figure 6 shows capacitance measurements performed with such a support structure with 64 apertures of 302 $\mu$m in diameter. It proves that lipid bilayer formation with good reproducibility is possible on the $CO_2$-laser-ablated structures. For detailed information on electrophysiological measurements of BLMs, see Hansen *et al* (2009).

## 4. Discussion

A typical characteristic of the $CO_2$-laser-ablated structures is the smooth bulge around the rims. These bulges are formed by default and consist of melted and deposited material and therefore create a smooth and round surface. The height of these bulges strongly depends on the design of the array itself. With closely spaced apertures, the bulges start superimposing and therefore form higher bulges. The loss of weight showed that just 10% of the original material removed from the aperture contributes to the formation of bulges. However, it is believed that the volume of the melted, ejected and deposited polymer increases. This is caused by a lowering of the material's density during the heating process where polymer chains are cut into shorter chains without being ablated (Snakenborg *et al* 2004). This means that to estimate the resulting bulge height further investigations on the density and the volume change within the ETFE will be needed. Until then, laser scanning confocal microscopy offers a reliable tool to determine the height of the bulges.

The anisotropy of the material clearly influenced the production of the support membrane. While there is almost no difference observable at 200 $\mu$m, it gets more pronounced at 140 $\mu$m and is significant at 120 $\mu$m. Clearly visible is the more elliptical shape of the apertures when the array is produced at an angle of 90° to the machine direction. The tendency to form elliptical apertures can be explained by the orientation of the molecules in the polymer. As already mentioned they tend to align parallel after the melt extrusion. During laser ablation high thermal energy is induced which breaks bonds between the polymer chains. In the immediate focal spot of the laser this causes melting and vaporization of the material. The surrounding area is also affected by this thermal energy, plus the energy induced while drilling the neighbouring apertures within a short span of time. When producing perpendicular to MD, the bonds between the parallel chains break and cracks develop. That is why the aperture extends in this direction and becomes elliptical. However,

when fabricating with MD, this effect does not occur because within a very short time ($\sim$1 $\mu$s) a neighbouring structure was drilled and additional material was placed on the partition between the two apertures. So the polymer chains cannot drift apart to form cracks that would result in elliptical apertures. The broadening of the apertures in MD is also impeded by the production of the neighbouring structure where the dividing wall is pushed against the direction where the cracks would develop.

The ETFE tested is a promising material for the chosen application because it absorbs light at 10.6 $\mu$m and its hydrophobicity helps the later stage of bilayer formation. Furthermore, even when perforated, ETFE provides good mechanical stability and therefore easy handling of the structured partitions.

By using different lenses and careful adjustment of the laser parameters (most important: intensity, spot lase time, off vector delay), apertures with diameters from 84 $\mu$m to 300 $\mu$m can be easily fabricated. A hexagonal arrangement of the apertures ensures the densest structure and therefore the optimal perforation level which is necessary for a high water flux across the membrane.

Successful BLM experiments have been performed on arrays of apertures made by $CO_2$ laser ablation. This proves that this microfabrication process offers a fast and inexpensive way of producing support structures for biomimetic applications.

## Acknowledgments

This work was carried out by DTU Nanotech and DTU Physics at the Technical University of Denmark in collaboration with the company Aquaporin A/S, Denmark. The project was partially funded by the Danish National Advanced Technology Foundation (023-2007-1), the Danish National Research Foundation and MEMBAQ (NMP4-CT-2006-033234). Special thanks go to all the employees of Aquaporin who tested and evaluated the partitions with regard to their usability in BLM formation.

## References

Hansen J S, Perry M, Vogel J, Vissing T, Hansen C R, Geschke O, Emnéus J and Nielsen C H 2009 Development of an automation technique for the establishment of functional lipid bilayer arrays *J. Micromech. Microeng.* **19** 025014

Mayer M, Kriebel J K, Tosteson M T and Whitesides G M 2003 Microfabricated Teflon membranes for low-noise recordings of ion channels in planar lipid bilayers *Biophys. J.* **85** 2684–95

O'Shaughnessy T J, Hu J E, Kulp J L III, Daly S M and Ligler F S 2007 Laser ablation of micropores for formation of artificial planar lipid bilayers *Biomed. Microdevices* **9** 863–8

Preston G M, Carroll T P, Guggino W B and Agre P 1992 Appearance of water channels in xenopus oocytes expressing red cell CHIP28 protein *Science* **256** 385–7

Rijn, Cees J M, van Nijdam W, Kuiper S, Veldhuis G J, Wolferen H v and Elwenspoek M 1999 Microsieves made with laser interference lithography for micro-filtration applications *J. Micromech. Microeng.* **9** 170–2

Rosato D V 1990 *Plastics Processing Data Handbook* (New York: Van Nostrand Reinhold)

Simon A, Girard-Egrot A, Sauter F, Pudda C, Picollet D'Hahan N, Blum L, Chatelain F and Fuchs A 2007 Formation and stability of a suspended biomimetic lipid bilayer on silicon submicrometer-sized pores *J. Colloid Interface Sci.* **308** 337–43

Snakenborg D, Klank H and Kutter J P 2004 Microstructure fabrication with a $CO_2$ laser system *J. Micromech. Microeng.* **14** 182–9

White S H 1972 Analysis of the torus surrounding planar lipid bilayer membranes *Biophys. J.* **12** 432–45

Wonderlin W F, Finkel A and French R J 1990 Optimizing planar lipid bilayer single-channel recordings for high resolution with rapid voltage steps *Biophys. J.* **58** 289–97

# Paper II

Reprinted from Journal of Micromechanics and Microengineering **19** (2009) 025014 (11pp), with permission of IOP Publishing

J. S. Hansen, M. Perry, J. Vogel, T. Vissing, C. R. Hansen, O. Geschke, J. Emnéus and C. H. Nielsen; ***Development of an automation technique for the establishment of functional lipid bilayer arrays***

J. Micromech. Microeng. **19** (2009) 025014 (11pp) doi:10.1088/0960-1317/19/2/025014

# Development of an automation technique for the establishment of functional lipid bilayer arrays

**J S Hansen[1,2,5], M Perry[2,5], J Vogel[1,2], T Vissing[2], C R Hansen[2,3], O Geschke[1], J Emnéus[1] and C H Nielsen[1,4,6]**

[1] DTU Nanotech, Technical University of Denmark, DK-2800 Kgs. Lyngby, Denmark
[2] Aquaporin A/S, Diplomvej 377, DK-2800 Kgs. Lyngby, Denmark
[3] Nano-Science Center, Copenhagen University, DK-2100, Copenhagen, Denmark
[4] Quantum Protein Centre, Technical University of Denmark, DK-2800 Kgs. Lyngby, Denmark

E-mail: Claus.Nielsen@fysik.dtu.dk

Received 30 September 2008, in final form 18 November 2008
Published 14 January 2009
Online at stacks.iop.org/JMM/19/025014

**Abstract**

In the present work, a technique for establishing multiple black lipid membranes (BLMs) in arrays of micro structured ethylene tetrafluoroethylene (ETFE) films, and supported by a micro porous material was developed. Rectangular 8 × 8 arrays with apertures having diameters of 301 ± 5 $\mu$m were fabricated in ETFE Teflon film by laser ablation using a carbon dioxide laser. Multiple lipid membranes could be formed across the micro structured 8 × 8 array ETFE partitions. Success rates for the establishment of cellulose-supported BLMs across the multiple aperture arrays were above 95%. However, the time course of the membrane thinning process was found to vary considerably between multiple aperture bilayer experiments. An airbrush partition pretreatment technique was developed to increase the reproducibility of the multiple lipid bilayers formation during the time course from the establishment of the lipid membranes to the formation of bilayers. The results showed that multiple lipid bilayers could be reproducible formed across the airbrush-pretreated 8 × 8 rectangular arrays. The ionophoric peptide valinomycin was incorporated into established membrane arrays, resulting in ionic currents that could be effectively blocked by tetraethylammonium. This shows that functional bimolecular lipid membranes were established, and furthermore outlines that the established lipid membrane arrays could host functional membrane-spanning molecules.

(Some figures in this article are in colour only in the electronic version)

## Abbreviations

| | |
|---|---|
| AFM | atomic force microscopy |
| BLM | black lipid membrane |
| DPhPC | 1,2-diphytanoyl-*sn*-glycero-3-phosphocholine |
| ETFE | ethylene tetrafluoroethylene; |
| NBD-PC | 1-Oleoyl-2-[6-[(7-nitro-2–1,3-benzoxadiazol-4-yl)amino]hexanoyl]-*sn*glycero-3-phosphocholine |
| ROI | region of interest |
| SEM | scanning electron microscopy |
| TEA | tetraethylammonium |

[5] Shared first authorship.
[6] Author to whom any correspondence should be addressed.

## 1. Introduction

Artificially made lipid bilayers suited for the insertion of functional molecules, such as ion channel peptides or membrane proteins, have potentials in a diverse range of technical applications, including cell adhesion and ligand–receptor interaction studies [5], screening platforms for drug discovery [9], development of nanobiosensor devices [3, 18], immuno-assays [16] and bioremediation platforms in environmental biology.

 

BLMs are typically formed by painting a solvent containing lipid solution across a hydrophobic partition material (typically Teflon) with an aperture of up to 1 mm in diameter [17], or by the folding technique where solvent-free lipid monolayers of each side of a partition aperture are spread and raised across the aperture (diameters of 50–100 $\mu$m) to produce a BLM [15]. Both methods for producing artificial lipid membranes are commonly produced in a single aperture partition separating two Teflon compartments each containing a saline solution.

Although multiple aperture partitions in a hydrophobic partition material can be produced, both the painting and the folding techniques are only useful in the preparation of a BLM in a single aperture or a small number of apertures [11, 19], and they are not straightforward to scale into large aperture arrays. Establishing a folded membrane often requires multiple lowering and raisings of the aqueous solutions, which may compromise the simultaneous formation of membranes across multiple apertures. Formation of painted membranes requires manual painting of the single partition aperture and for this reason the membrane painting technique is not easy to scale into multi-aperture partitions.

Various mechanical fabrication methods for producing a partition having a single aperture have been described previously including micro drilling [4], puncturing the scaffold film with a needle [12], a heated wire [29, 2, 15], or an electrical spark [14]. Of these mechanical aperture production methods, only micro drilling could be suitable for scale up into aperture arrays. However, it is difficult to produce consistently sized and closely positioned apertures using micro drilling. Moreover, micro machined apertures commonly exhibit microscopic burr and groin edges resulting in poor experimental reproducibility.

A soft lithography technique based on casting of amorphous Teflon to create partitions with multiple apertures (up to 15) was described by Mayer *et al* [11]. This technique has the ability to produce precisely positioned and sized (2–800 $\mu$m) apertures, but the technique is time intensive with the casting time for the partition being between 4 and 24 h [11].

Recently, UV excimer laser ablation has been described for the fabrication of multiple apertures in thin polycarbonate films (20 $\mu$m) and polymethyl methacrylate with aperture diameters of 4–105 $\mu$m and 50–100 $\mu$m, respectively [23, 19]. Common for the UV excimer laser ablation technique for fabricating multi-array apertures is that the technique is highly reproducible, apertures are precisely positioned, but the UV excimer laser technology is costly and a major drawback is the inability to use Teflon films [19] with this technology. Moreover, excimer lasers are in general slow due to the pulse lasing technique and for this reason are not suited for the fabrication of large aperture arrays.

In the current work, laser ablation was applied to produce ETFE partitions with aperture diameters of 301 $\pm$ 5 $\mu$m as 8 $\times$ 8 multiple aperture arrays using a $CO_2$ laser. Three main criteria made this method to be preferred for the production of a support structure. First, the $CO_2$ laser is able to ablate Teflon films with different thicknesses (25 $\mu$m to above 1 mm) by varying the lasing parameters. Second, the apertures can be positioned in a precise and controlled manner giving high reproducibility. Third, the $CO_2$ laser offers a cost efficient and fast production with fabrication times in the range of milliseconds–seconds. Moreover, this technique supports easy scale up [24].

To enable the simultaneous formation of cellulose-supported multiple lipid bilayers in an array, a novel modified painting method was established. We show by voltage clamp experiments that multiple BLMs can be reproducible formed across 64 aperture arrays by this method, and that established membrane arrays are suited for the functional insertion of membrane-spanning molecules.

Our results are discussed in the context of current developments in free-spanning artificial membrane platform technologies.

## 2. Material and methods

### *2.1. Materials*

Tefzel ethylene tetrafluoroethylene (ETFE) LZ200 for the fabrication of multi-aperture partitions, and Viton A fluoroelastomer for production of rubber chamber sealing O-rings were from DuPont Fluopolymers (Detroit, U.S.A.). Solid Teflon (polytetrafluoroethylene) blocks to the manufacture of the lipid bilayer chambers were supplied by Vink A/S (Randers, Denmark). Sheets of regenerated cellulose (DSS-RC70PP) were purchased from Alfa Laval (Nakskov, Denmark). Round glass cover slips (30 mm) were from VWR—Bie & Berntsen (Herlev, Denmark). The lipids 1,2-diphytanoyl-*sn*-glycero-3-phosphocholine and 1-oleoyl-2- [6-[ (7-nitro-2–1, 3-benzoxadiazol-4-yl) amino]hexanoyl]-*sn*-glycero-3-phosphocholine were from Avanti Polar Lipids Inc. (Alabaster, AL, USA). The potassium ion-selective cyclodepsipeptide valinomycin (SIGMA), the channel blocker tetraethylammonium (Fluka) and *n*-decane (Fluka) were purchased from Sigma-Aldrich Denmark (Brøndby, Denmark). All other chemicals were purchased from commercial sources.

### *2.2. Micro structuring of ETFE membrane scaffold arrays*

A Synrad Duo 48–5 S Duo Lase carbon dioxide laser with a specified power output of 50 W (Mulkiteo, WA, USA) and equipped with a 200 mm focal length lens was used to fabricate partitions with rectangular arrayed apertures in ETFE LZ200 film (50.8 $\mu$m thickness). The EFTE film was laser ablated into 29 mm diameter discs, where the aperture array was placed in the middle hereof. The apertures within the structure had a distance from center to center of 400 $\mu$m. The apertures were produced with an intensity of 4.4 W, a spot lase time (impact time of the beam) of 4 ms and an off vector delay of 1 ms, respectively. The ETFE film was placed in a custom-produced sample holder made of polymethyl methacrylate. A clearance was situated in the middle of this fixture where the lasers beam impact on the sample. Thereby, it was assured that no underlying material interfered with the production process.

### *2.3. Scanning electron microscopy of produced Teflon partitions*

The scanning electron microscope (SEM) used was a Jeol JSM 5500 LV SEM from GN Nettest. It is capable of a lateral resolution down to 30–50 nm and a magnification up to ×300 000. The acceleration voltage can be set between 1 and 30 kV. The SEM used has a reproducibility and accuracy in lateral distance measurements better than 5%.

### *2.4. Atomic force microscopy of produced Teflon partitions*

Topographic measurements of the laser-ablated aperture arrays were carried out using atomic force microscopy (AFM). The equipment used was a model: MFP-3D, atomic force microscope (Asylum Research) with an Olympus Silicon Nitride tip (AC240, k ∼2 N m$^{-1}$) used in tapping mode. The sample used for AFM was an ETFE LZ200 partition with a rectangular 3 × 3 partition array with 300 $\mu$m diameter apertures having a center-to-center distance of 400 $\mu$m. The average surface roughness of a region of interest (ROI) was calculated using

$$\mathrm{SD}_{\mathrm{average}} = \frac{1}{V_{\mathrm{ntp}}} \sum_{i=0}^{V_{\mathrm{ntp}-1}} |Y_i - \overline{Y}|,$$

where $\mathrm{SD}_{\mathrm{average}}$ is the average surface deviation of the ROI, $V_{\mathrm{ntp}}$ is the total number of pixels of the ROI, $Y_i$ is the height of each pixel and $\overline{Y}$ is the average pixel height.

### *2.5. The lipid bilayer chamber design*

The lipid bilayer chamber design is depicted in figure 1. The complete chamber setup consists of a main Teflon chamber with two axisymmetrically drilled holes having diameters of 20 and 30 mm respectively, a 30 mm diameter cylindrical Teflon tube (5 mm thickness), two 30 mm circular Teflon inter spacers where one has a 2 mm slit, six Viton O-ring seals, two cover slip glasses where one is cut and a brass screw to tighten the bilayer chamber (figure 1(*A*)). The inner elements consisting of porous regenerated cellulose, micro structured ETFE partition array, Teflon spacers, circular glass cover slips and Viton O-rings (figure 1(*B*)) fit into the cylindrical 30 mm diameter tube of the *cis* chamber, and rest upon the ledge created by the interface of the *trans* chamber and the cylindrical 20 mm diameter tube of the *cis* chamber (figures 1(*A*) and (*B*)). The 5 mm thick cylindrical Teflon tube provides the link to the annular brass screw (perimeter thickness 7 mm) generating sufficient pressure from the exterior of the chamber to obtain a water tight sealing (figure 1(*C*)). Thus the *cis* and *trans* chambers have identical volumes. A circular, 2 mm thick Teflon spacer with a 2 mm slit is positioned with the opening at the top of the chamber that allows bilayer-forming solutions to enter into the lipid bilayer chamber with a Hamilton syringe (figures 1(*A*) and (*B*)).

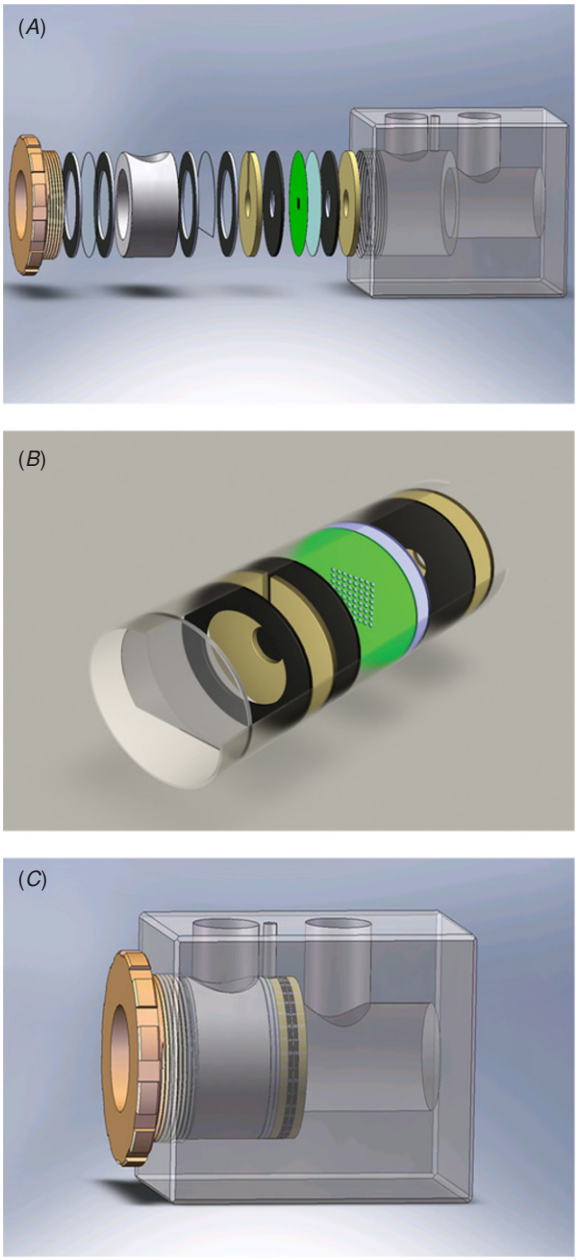


**Figure 1.** Lipid bilayer chamber design and assembly. (*A*) The assembly of the main Teflon chamber. The component order of the assembly into the main Teflon chamber (grey) is from right to left: a Teflon spacer (tawny), a Viton O-ring (black), a circular cellulose sheet (light blue), an ETFE LZ200 partition (green), a Viton O-ring (black), a Teflon spacer with a slit (tawny), a Viton O-ring (black), a cut glass cover slip (transparent) and another Viton O-ring (black). Following this, a cylindrical Teflon tube (grey) is placed onto to the inserted components, and a glass cover slip (transparent) is clamped between two Viton O-rings (black) to create a window for visual inspections into the assembled chamber. Finally, an annular brass screw is used to clamp all of the components to ensure a tight chamber. (*B*) The inner elements of the *cis* chamber. Indicated are the cut glass cover slip (transparent grey), the Teflon spacers (tawny), the Viton O-rings (black), the cellulose support (light blue) and the ETFE partition (green). (*C*) The lipid bilayer chamber fully assembled.

### *2.6. Preparation of lipid solution for BLM experiments*

The lipid solution for the pre-treatment of ETFE LZ200 partitions (prepainting) and for the bilayer formation consisted of 1,2-diphytanoyl-*sn*-glycero-3-phosphocholine (DPhPC) in *n*-decane (50 mg ml$^{-1}$). DPhPC (2 ml) in chloroform

(10 mg ml$^{-1}$ stock) was evaporated under nitrogen gas and the dry lipid was resuspended in 400 $\mu$L *n*-decane. For fluorescent microscopy the lipid solutions were added 1 mol% of 1-oleoyl-2-[6-[(7-nitro-2–1,3-benzoxadiazol-4-yl)amino]hexanoyl]-*sn*-glycero-3-phosphocholine (NBD-PC). The lipid solutions were prepared the day before, and stored at −20 °C until use.

### 2.7. Partition pretreatment

The prepainting of ETFE partitions was carried out by the addition of approximately 2 $\mu$L of prepainting solution using a glass Pasteur pipette to both sides of the ETFE partition. The ETFE partitions were left to dry for 10 min followed by applying a gentle stream of nitrogen gas to both sides of the partition to ensure that the apertures were not clogged. The prepainting step was repeated five times, and the pretreated ETFE partitions were stored in a vacuum desiccator for 30 min before use.

Another prepainting strategy was developed to provide a more controlled and uniform deposition of the prepainting solution (50 mg ml$^{-1}$ DPhPC in *n*-decane) to the ETFE partition aperture arrays. This was based on airbrushing the prepainting solution onto the ETFE partition sides. The airbrush setup consisted of an airbrush (type: MAS G41, TCPGlobal) pressurized by a nitrogen gas flask, and mounted onto an aluminium track with a ruler. The airbrush was positioned at a distance of 45 mm from the airbrush nozzle to the ETFE partition. The partition was mounted on a perforated brass housing connected to a low-capacity vacuum pump. Partitions were placed on the brass housing and the vacuum applied keeping the partition in position during the prepainting procedure.

The 0.6 ml gravity-fed cup of the airbrush was filled with the prepainting solution (100 $\mu$l) and the prepainting solution was deposited onto the ETFE partitions as a fine mist using a nitrogen pressure of 1 bar. The partitions were applied on the prepainting solution on each side for 20 times with 30 s intervals to give a thin uniform coverage of the prepainting solution on the ETFE partitions.

### 2.8. Fluorescence microscopy

Fluorescent imaging was performed on a Zeiss Axiovert 200 M epifluorescence microscope (Carl Zeiss, Jena, Germany) equipped with a monochrome Deltapix DP450 CCD camera (Deltapix, Maalov, Denmark). The images were acquired using Deltapix DpxView Pro acquisition software (Deltapix, Maalov, Denmark). The objectives used were air corrected Plan-Neofluar 2.5 ×/0.075 Numerical Aperture (NA), 10 ×/0.25 NA and 20 ×/0.40 NA, respectively.

### 2.9. Formation of BLMs across multi-aperture ETFE partitions

The lipid bilayer chamber was assembled with a 8 × 8 multi-aperture ETFE partition (300 $\mu$m diameter apertures, center-to-center distance of 400 $\mu$m) and a circular regenerated cellulose sheet (DSS-RC70PP, Alfa Laval). Once assembled, the ETFE partition was by design located at the center of the circular interface between the *trans* and *cis* chambers (figure 1).

The *trans* and *cis* chambers were filled with 7.5 ml of a saline solution (0.2 M KCl), and the lipid bilayer chamber was then placed in a Faraday cage and the silver/silver chloride electrodes were placed in the electrode wells.

The level in the *cis* chamber was lowered to the beginning of the cut glass cover slip by aspiration of approximately 7 ml of the aqueous electrolyte solution using a plastic Pasteur pipette (figure 2(*A*)). A Hamilton pipette was filled with 100 $\mu$l of DPhPC in *n*-decane (50 mg/ml), and the bilayer forming solution was applied to the space between the cut cover slip glass and the ETFE partition of the *cis* chamber through the 2 mm slit in the circular Teflon spacer (figure 2(*B*)). The level of the aqueous electrolyte solution in the *cis* chamber was slowly raised by re-adding approximately 7 ml of the saline solution using a plastic Pasteur pipette (figures 2(*C*) and *(D)*). During the raising of the saline solution the formation of BLMs in the partition aperture arrays was recorded by measurements of the capacitance and conductance signals.

### 2.10. Data acquisition

The experimental setup consisted of a Model 2400 Patch Clamp Amplifier with a head stage containing 10 G/10 M feedback resistors (A–M Systems, Inc., WA, USA) and a Thurlby Thandar Instruments model TG2000 20 MHz DDS function generator (RS Components Ltd, Northants, UK). The electrodes were placed in the *trans* and *cis* compartments of the bilayer formation chamber with the ground electrode positioned in the *trans* compartment. Data acquisition was done with a combined oscilloscope/analog–digital converter (ADC-212/50, Pico Technology, Cambridgeshire, UK) connected to a laptop computer. The sampling frequency was 50 Hz.

Capacitance and conductance measurements were performed by applying 1 Hz triangular (2 Vpp) and rectangular (20 mVpp) voltage clamp wave forms, respectively. Reference measurements of the combined regenerated cellulose and perforated ETFE partition were made prior to the formation of the multiple BLMs. Membrane capacitance ($C = 1/I \cdot \mathrm{d}U/\mathrm{d}t$) was determined by measuring the peak-to-peak amplitude of the square-shaped response signal, while the membrane conductance ($G = I/U$) was determined from the post-transient steady-state amplitudes. The capacitance and conductance amplitudes were converted into currents using the appropriate head stage conversion factor. The results are given as mean ± SD of a minimum of five experiments for each measurement.

### 2.11. Incorporation of valinomycin

Valinomycin was dissolved in 96% ethanol to yield a 1.8 mM working solution, which was stored at 4 °C until use. Tetraethylammonium (TEA) working solution (16 mM) was prepared in 0.2 M KCl immediately before use. Valinomycin (1.8 mM) was added (10 $\mu$l) to the small chamber volume between the ETFE partition and the first glass cover slip

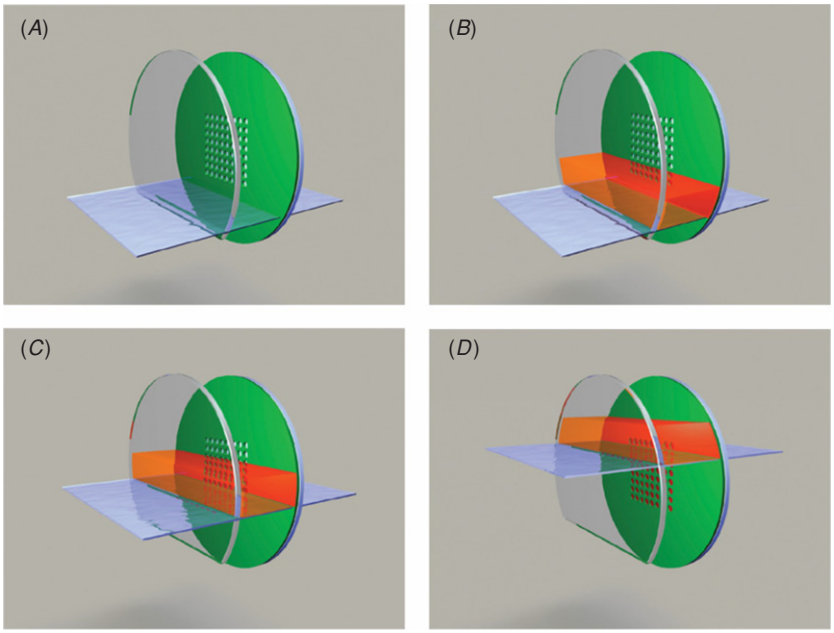


**Figure 2.** Principle of the automation technique for the establishment of multiple bilayers in the array. The aqueous electrolyte solution (0.2 M KCl) is filled up to the cut glass cover slip (*A*) and the bilayer forming solution (50 mg ml$^{-1}$ DPhPC in *n*-decane) is applied from the top through the slit in the front Teflon spacer (*B*). The aqueous electrolyte solution is then slowly applied to the *cis* chamber thereby raising the bilayer-forming solution across the multiple aperture partition to form an array of lipid bilayers (*C*)–(*D*).

in the chamber setup (volume 0.5 ml). This corresponds to an estimated valinomycin concentration of about 36 $\mu$M in close proximity to the membrane array, provided that no diffusion occurs from the small chamber to the rest of the *cis* chamber. Valinomycin incorporation was only performed on multiple BLMs displaying constant membrane characteristics for more than 60 min. To reverse the valinomycin-induced conductance, a TEA working solution was added (200 $\mu$l) to the small chamber volume, corresponding to an estimated final concentration of 4.5 mM TEA close to the membrane array.

## 3. Results

In the following, the development of an automation technique to enable reproducible establishment of multiple bilayers across micro structured membrane scaffolds will be presented.

### *3.1. $CO_2$ laser-ablated multi-array ETFE partitions*

ETFE LZ200 films having a thickness of 50.8 $\mu$m were micro structured into partition aperture arrays using a carbon dioxide laser. The arrays consisted of 8 $\times$ 8 apertures with an average diameter of 301 $\pm$ 5 $\mu$m (number of experiments, $n = 5$), which were positioned in a rectangular array with an aperture center-to-center spacing of 400 $\mu$m (figure 3). SEM images of the ETFE partition arrays showed that the apertures were symmetrically positioned with slight elliptical apertures that exhibited nicely rounded edges (figure 3).

To further investigate the topography of the edge of the aperture rims, AFM topographical measurements were carried out (figure 4). In order to calculate the topographic roughness around the rim edge, a 470 $\times$ 470 nm$^2$ ROI without artifacts such as scan lines was selected (figure 4). On this basis, the average surface roughness of the aperture edge was determined to be approximately 3.5 nm. The micro structured apertures were expected to be suited for accommodation of lipid bilayers, based on the overall geometries obtained by the combination of SEM and AFM imaging, respectively, of the fabricated partition apertures [28].

### *3.2. Automation technique for simultaneous formation of multiple lipid bilayers*

Current methods for lipid bilayer formation are not straightforward to scale up to simultaneous establishment of multiple lipid bilayers in arrays. Therefore, the aim was to develop an automation technique for the establishment of functional lipid bilayers in rectangular arrays.

The bilayer formation strategy chosen was the formation of lipid bilayers from hydrocarbon containing bilayer-forming solutions, which was essentially based on the ease of lipid bilayer formation, membrane thickness and stability (reviewed in [13]). On this basis a two-cell Teflon chamber was designed to accommodate the micro structured partition arrays (figure 1). In this design the cut glass cover slip and the Teflon spacer with the 2 mm slit provide a small accessible chamber within the *cis* chamber that functions to contain the bilayer-forming solution (figures 1(*A*) and (*B*)). This prevents spreading of the bilayer-forming solution to the rest of the *cis* chamber and minimizes the volume required to establish multiple aperture membranes. The Viton fluoroelastomer was custom fabricated into sealing O-rings, thereby removing the need for silicone grease (figure 1).

Regenerated cellulose was included in the multiple bilayer formation technique to provide a micro porous support

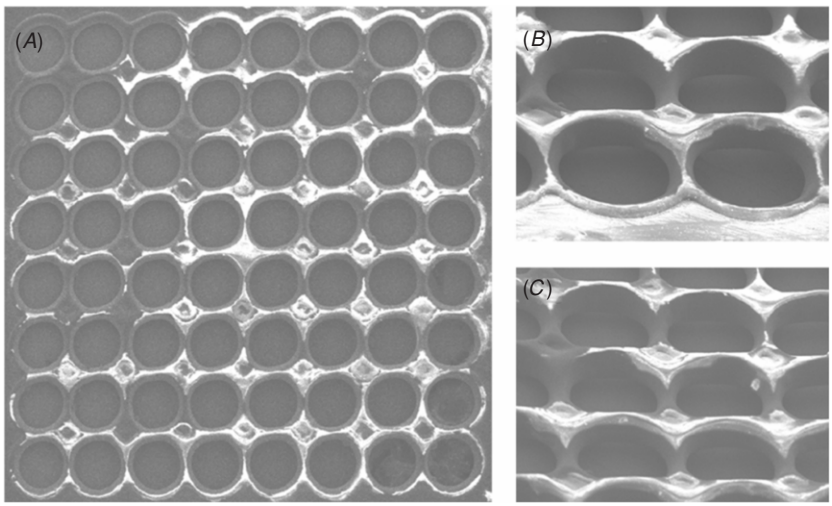


**Figure 3.** SEM images of $CO_2$ laser ablated multi-array aperture partitions. (*A*) SEM image of 8 × 8 apertures in a rectangular array with average aperture diameters of 303 ± 5 $\mu$m. The center-to-center spacing of the micro structured apertures is 400 $\mu$m. The same multi-aperture partition is tilted at a 55° angle to show (*B*) the intermediate stage from the unmodified ETFE film to the $CO_2$ laser ablated apertures and (*C*) the mid section of the partition array.

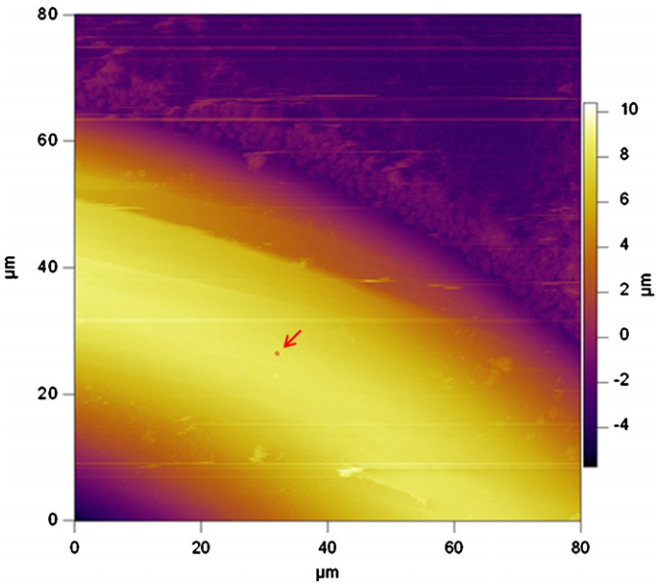


**Figure 4.** AFM image of the edge topography of an aperture rim in a partition array. The ROI (red square) indicated by the red arrow was used for the surface roughness calculation. The left lower corner of the image is the edge nearest to the aperture.

structure for bilayer formation (figures 1(*A*) and (*B*)). This semi-supported bilayer formation strategy was chosen to prevent fluid flow through the apertures from the *trans* to the *cis* chamber upon establishment of lipid bilayers (figure 2).

The technique for multiple bilayer formation was based on raising the aqueous electrolyte solution in the *cis* chamber in front of the glass cover slip leading to the raising of the bilayer-forming solutions between the cut glass cover slip and the multi-aperture partition (figure 2). The process of multiple bilayer formations could in this manner be established automatically by raising the bilayer-forming solution across the partition aperture array (figure 2).

### *3.3. Formation of planar lipid bilayers across multiple aperture ETFE partitions*

We evaluated the capacitance and conductance contributions of the regenerated cellulose, and of ETFE film without apertures plus the regenerated cellulose mounted in the bilayer chamber, respectively. The regenerated cellulose had a conductance of 9165.9 ± 23.0 nS and no measurable capacitance ($n = 5$), whereas the non-perforated ETFE film plus cellulose had a conductance of 127.0 ± 1.6 nS and a capacitance of 2336.4 ± 19.0 pF ($n = 5$). Thus the values for ETFE film and cellulose are regarded as the background. In line with this multiple aperture bilayer experiments had initial conductance values in the range of 250–900 nS and capacitance values in the range of 2000–6000 pF. The fluctuations in the initial conductance and capacitance values were found to be variations in chamber assembly (e.g., tightening of the brass screw).

Following lipid membrane sealing across the apertures, lipid bilayers start to form and expand inside the apertures. The thinning of lipid membranes into bilayers gives rise to an increase in capacitance values above the background (figure 5(*A*)). The time-dependent increase in capacitance above the background values is interpreted as thinning of lipid membranes into lipid bilayers [27], and is thus also taken as evidence for the establishment of functional bilayers. Conversely, an increase in conductance is observed when the sealing properties of the BLMs start to fail (figure 5(*B*)).

Although multi-array membranes could consistently be formed, the membrane thinning curves varied considerably for the membranes established across Pasteur pipette prepainted ETFE partition apertures. Average capacitance and conductance values were 31 600 ± 13 400 pF and 2950 ± 2900 nS ($n = 5$) at 250 min (figures 5(*A*) and (*B*)).

A subset of membranes (∼10%) exhibited a capacitative discharge and recharge cycling behavior with a time course of approximately 500 min, which is also reflected in the time course of the conductance. This behavior of BLMs

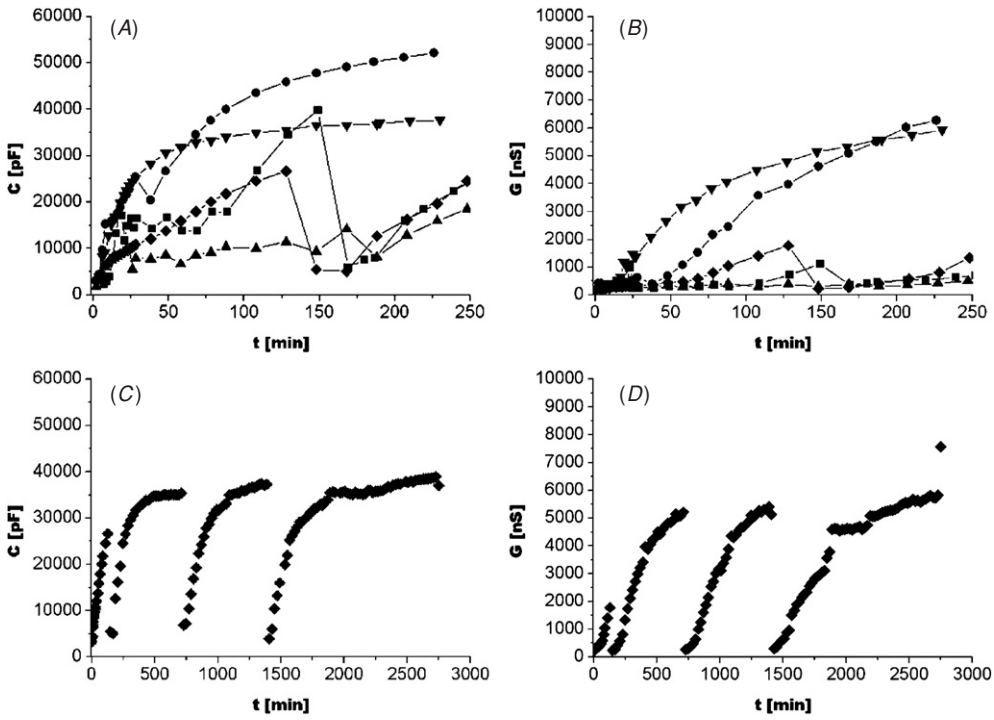


**Figure 5.** Time course characteristics of bilayers formed across multiple apertures. Bilayers were formed across Pasteur pipette pretreated ETFE partition arrays. (*A*) Capacitance and (*B*) conductance time course characteristics (250 min) of the bilayer formation across ETFE partitions with an 8 × 8 rectangular array of averaged 300 $\mu$m diameter apertures. The individual symbols represent independent experiments carried out under the same conditions. (*C*) Capacitance and (*D*) conductance of multi-aperture array BLMs exhibiting membrane discharge and recharge behavior during a time course of 50 h.

formed across multiple aperture partitions was observed as a repetitive cycling in capacitance and conductance values from the initial lipid bilayer formation values of around 2000–6000 pF and 250–900 nS, and to the lipid bilayer values of 26 000–38 000 pF and 2500–5800 nS, respectively (figures 5(*C*) and (*D*)).

### *3.4. Improved membrane reproducibility by controlled partition pretreatment*

In order to improve membrane reproducibility, the deposition of prepainting solution onto the ETFE aperture arrays was assessed. Fluorescent images were acquired of 8 × 8 array ETFE partitions following prepainting using the traditional Pasteur pipette application method with DPhPC in *n*-decane (50 mg ml$^{-1}$) added 1 mol% of the fluorescent lipid NBD-PC. The results showed that the prepainting solution was inhomogeneously deposited on the partition surface, and several apertures were consistently partial or completely occluded by the prepainting solution in spite of the applied nitrogen to open the apertures (figure 6).

To circumvent this inhomogeneous lipid deposition and to improve reproducibility, an airbrushing pretreatment technique was developed. Fluorescent images of the airbrush pretreated partitions showed that this technique was able to deposit lipids onto the ETFE partition in a homogeneous and controlled manner (figure 6).

Following a short lag phase (∼2–10 min) multiple formed lipid membranes established across airbrush pretreated ETFE partition arrays thinned in a time-dependent manner reaching the maximum capacitance values of 28500 ± 1400 pF at around 250 min ($n = 5$) (figure 7(*A*)). The conductance values were relatively stable (541 ± 128 nS) during the time course of 100 min at which point the conductance increased during the time course from 100 min to 250 min to values of 2300 ± 461 nS (figure 7(*B*)).

Compared with the bilayer characteristics obtained with the traditional prepainting method, a significantly increased reproducibility could be achieved by applying the prepainting solution to the ETFE arrays in a controlled manner (figure 8).

### *3.5. Incorporation of valinomycin into multiple formed lipid bilayers*

To ensure that bilayers were formed across the aperture arrays the potassium ion-selective cyclodepsipeptide valinomycin was added (10 $\mu$l, 1.8 mM stock solution) to lipid bilayers displaying stable membrane properties for more than 60 min [25]. Following the addition of valinomycin to the chamber an abrupt increase in conductance was immediately observed indicating a functional reconstitution of valinomycin cyclodepsipeptides into the bilayers formed across the array of 8 × 8 apertures (figure 9(*A*)). The effect of valinomycin could effectively be reversed by the addition of the channel blocker TEA (200 $\mu$l, 16 mM stock solution) (figure 9(*A*)). Before valinomycin incorporation the near-square response to the triangular wave form reflects the capacitative properties of the bilayers. The capacitance response signal becomes

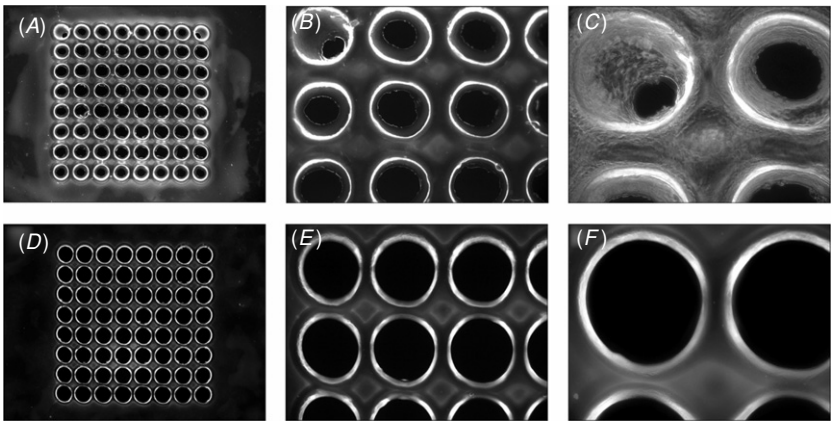


**Figure 6.** Fluorescent images of Pasteur pipette and airbrush-applied prepainting solution onto ETFE partition arrays. (*A*), (*B*) and (*C*) Pretreatment of ETFE partitions by the traditional prepainting method using a glass Pasteur pipette for five times on both sides. Objectives used were (*A*) 2.5×, (*B*) 10× and (*C*) 20×. (*D*), (*E*) and (*F*) Pretreatment of ETFE partitions by the airbrushing technique. The prepainting solution was airbrushed onto both sides of the ETFE partition array for 20 times with 30 s intervals. The objectives used were (*D*) 2.5×, (*E*) 10× and (*F*) 20×. The prepainting solution consisted of 50 mg ml$^{-1}$ DPhPC in *n*-decane with 1 mol% of NBD-PC. The ETFE partition aperture diameters are 301 ± 5 $\mu$m.

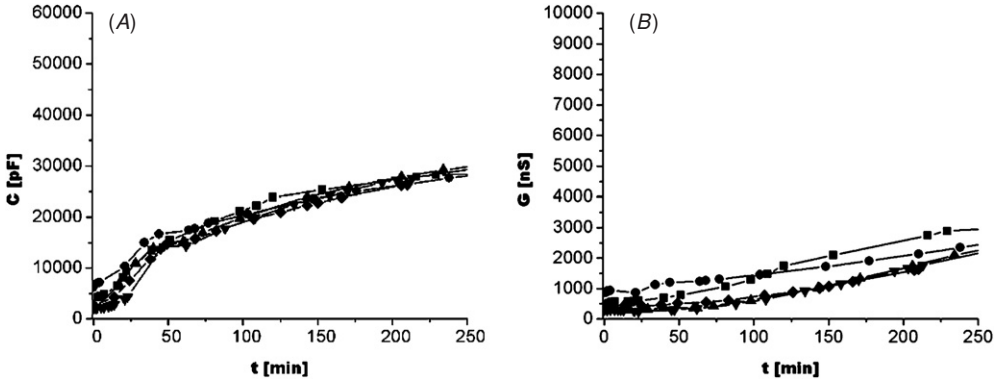


**Figure 7.** Time course characteristics of bilayers formed across airbrush pretreated ETFE partition arrays. (*A*) Capacitance and (*B*) conductance time course characteristics (250 min) of bilayer formation across ETFE partitions with 8 × 8 rectangular array pretreated for 20 times with prepainting solution (50 mg ml$^{-1}$ DPhPC in *n*-decane) using the airbrush prepainting technique. The individual symbols represent independent experiments carried out under the same conditions.

more triangular upon functional valinomycin incorporation into established bilayers reflecting ionic currents through the bilayers and reverts following the channel blockage by TEA (figure 9(*B*)). In contrast, the addition of ethanol or TEA alone to preformed lipid bilayers to final chamber concentrations of up to 1% and 5.9 mM, respectively, did not significantly affect the membrane characteristics (data not shown).

Combined, these results strongly indicate that stable lipid bilayers are in fact formed across the multi-array aperture partitions, and that lipid bilayer spanning channels can be functionally inserted into the formed lipid bilayers.

## 4. Discussion

Current design criteria for free-spanning biomimetic membrane platform technologies are low leak currents (i.e., good membrane sealing); long-lasting membranes (i.e., lifetimes > 1 day); absolute reproducibility with a high success rate; a scaffold consisting of multiple functional units for effective up-scaling; the ability to reconstitute membrane spanning proteins/peptides; robustness (i.e., stable during transportation/handling); and cost effective in production [21]. For mass transfer flow and high throughput screening applications additional design criteria must be met. These include a high perforation level of the membrane scaffold material, the functional membrane units are arranged in arrays to facilitate a screening platform (e.g., for microplate readers) and the artificial membrane platform is scalable to meet various requirements for individual technical applications.

The criteria of a high perforation level of the membrane scaffold material and the fabrication of functional membrane units were in this study achieved by micro structuring ETFE films using a carbon dioxide laser. The positioning of averaged 300 $\mu$m diameter apertures in 8 × 8 rectangular arrays with a center-to-center distance of 400 $\mu$m yielded a perforation level of 43.6%, and created a total aperture area of 0.045 cm$^2$. This area is about 150 times larger compared to a recently published silicon nitride nano-structured array chip which had impressive 960 000 nanometer-sized apertures [6].

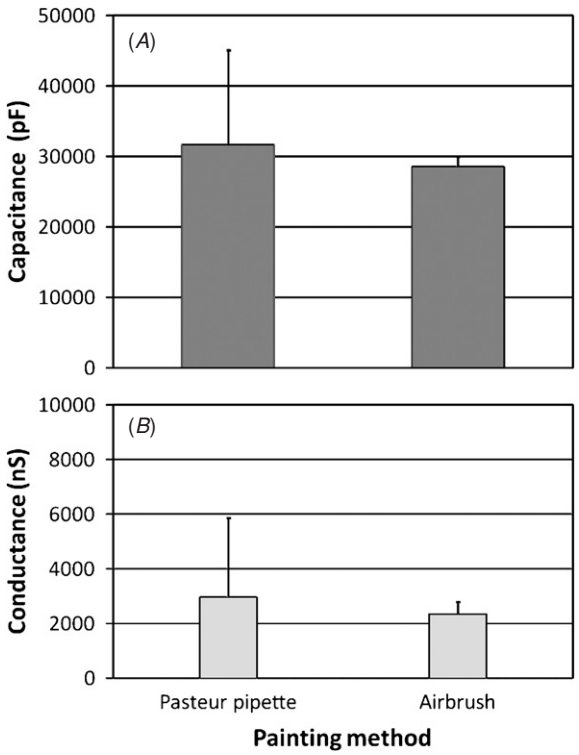


**Figure 8.** Comparison of bilayer characteristics between prepainting techniques. (*A*) Capacitance and (*B*) conductance values at 250 min for bilayers established on Pasteur pipette or airbrush prepainted ETFE arrays. Standard deviations are indicated.

The automation technique for multiple bilayer formations was created to meet the above-mentioned design criteria of stable, scalable and reproducible membranes for establishing planar artificially made membranes in arrays (figures 1 and 2). Generally, the 8 × 8 arrayed lipid bilayers were established by a single lowering and raising of the aqueous electrolyte solution in the chamber design (figure 2). The success rates for multi-array bilayer experiments exceeded 95%. Moreover, the technique is easy to scale and the bilayers have been created in single aperture, 5 × 5, 8 × 8 and 30 × 21 arrays having average aperture diameters of 300 $\mu$m. Multi-array lipid bilayers were in general stable for 200–300 min before breakdown, while 40% of the established bilayer membranes lasted for 1–3 days when left with voltage potentials $\leqslant \pm$ 100 mV. A few membranes lasted for more than a week and up to 14 days.

Reproducible multiple aperture bilayer experiments were achieved by the development of an airbrush partition pretreatment technique for controlled surface pre-coatings of the aperture arrays (figures 7 and 8). Our results indicate that the substrate for the establishment of lipid bilayers is very important in order to achieve highly reproducible biomimetic membrane platforms. This notion is supported by Ries *et al* who showed that the reproducibility of bilayer formations was strongly influenced by the substrate material, e.g., delrin, polyethylene or silicon wafers, respectively [22].

Although a high reproducibility was achieved in the automation technique for the establishment of multi-array bilayers, the life span of bilayers was not increased correspondingly. The low leak currents of established multiple bilayers across partition arrays could only be maintained for approximately 100 min. Following a gradual decrease in the overall membrane sealing properties until membrane rupture was observed (figure 7(*B*)). Therefore, the membrane stability issue needs to be further addressed.

Evidence for the formation of functional bilayers in the multiple aperture bilayer experiments was provided by the obtained capacitance values of 28 500 ± 1400 pF (figure 7(*A*)). Giving a total aperture area of 0.045 cm$^2$ for 64 apertures with average diameters of 300 $\mu$m and literature values of the specific capacitance of 0.4–0.6 $\mu$F cm$^{-2}$ for the solvent containing lipid bilayers [2], the capacitance for multiple formed lipid bilayers was expected to be in the range of 18 100–27 100 pF. Therefore, the capacitance values could indicate that the total lipid bilayer area is somewhat 4.9–36.6% larger than expected with a specific bilayer capacitance of 0.4–0.6 $\mu$F cm$^{-2}$. This discrepancy is however regarded as a technical capacitance measurement artifact. The membrane capacitances were consistently determined by measuring the peak-to-peak amplitude of the square-shaped signal in response to applying a triangular pulse. Any leak current in the setup (e.g., if individual bilayers start to fail) will therefore give rise to an ohmic contribution to the square capacitance response signal, and thus an overestimation of the obtained capacitance values. Therefore, it is reasonable to assume that the specific capacitance values of thinned lipid bilayers in our multiple aperture experiments lie within the range of 0.4–0.6 $\mu$F cm$^{-2}$ for solvent-containing lipid bilayers.

Further evidence for the establishment of lipid bilayers was the functional reconstitution of valinomycin into formed bilayers, and the blockage of ionic currents by the addition of TEA (figure 9). These results showed that the established bilayers in array were accessible to the reconstitution of transmembrane spanning molecules, which is also an important design criterion for the construction of a free-spanning artificial membrane platform. In this regard experimental results have recently shown that there is no practical hindrances in the use of hydrocarbon containing lipid bilayers compared with the solvent-free folded membranes regarding the reconstitution of transmembrane proteins through proteoliposome vesicle fusion events [1].

The transportation robustness of the presented method has not been addressed here. However, recent advantages in bilayer encapsulation methods suggest that a robust portable artificial membrane platform can be produced [7, 8, 10, 20, 26].

An unresolved issue is to understand the cycling membrane characteristic behavior exhibited in roughly 1 out of 10 membranes, where repeated events of gradual decreases in membrane tightness followed by sudden resealing were observed (figures 5(*C*) and (*D*)). We were however not able to record the actual membrane failure events where the overall conductance increases to background levels (in this case ∼8000 nS, figure 5(*D*)) due to our 20 min intervals between samplings. One explanation is that a gradual increase in membrane conductance in a small subset of apertures occurs, most likely a single aperture, followed by membrane failure and subsequent resealing of a single or several apertures.

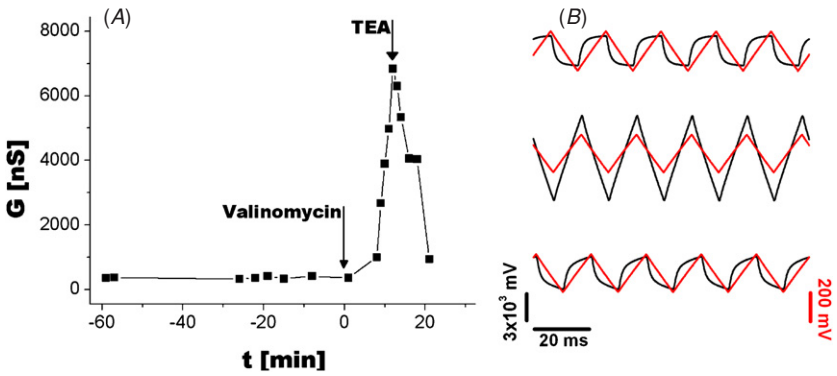


**Figure 9.** Reconstitution of valinomycin and channel blocking in multiple lipid bilayers. (*A*) Time course of conductance values for a bilayer array (8 × 8) alone, reconstituted with valinomycin and subsequently blocked by TEA. (*B*) Capacitative signals of lipid bilayers in the array (top panel), reconstituted with valinomycin (middle panel), and valinomycin blockage by TEA (lower panel). Capacitance signals correspond to $t = -10$, 15 and 20 min in (*A*). Red lines represent the triangular applied voltage clamp wave forms to obtain the membrane capacitance response signals (black lines).

The single aperture failure notion is based on the observation that the cycling behavior of both the capacitance and the conductance displays a high degree of regularity (figures 5(*C*) and (*D*)). If all 64 aperture bilayers went through a membrane failure and resealing event, the observable regular behavior would require that all of the individual membrane events to take place more or less in phase. Therefore, a single (or small subset) aperture event is more probable. Upon the single membrane failure, the electric field across the entire membrane system breaks down causing a global discharge leading to the overall system capacitance dropping to zero in phase with the drop in conductance. The electric field breakdown may subsequently trigger a global membrane thickening event caused by a backflow of bilayer forming solution into the aperture areas from reservoirs (Plateau-Gibbs) present in the surrounding partition landscape. This would explain the gradual increase in membrane capacitance on a global scale following the abrupt single membrane failure and resealing event. If the system as a whole remained unchanged after the resealing event, the increase in capacitance would be solely due to recharging of the system and take place with a considerable smaller time constant compared to what was observed.

Recently, a platform for the individual production of BLMs in 4 × 4 aperture arrays has been described, where each BLM should be established manually. In this method a success rate of 50% could be achieved, and the authors suggested a robotic injection approach to obtain better and more reproducible rates of the BLM formation [30]. We do not see any major obstacles in converting our current automation technique from establishing vertical BLMs to form horizontal BLMs thus enabling a modular design allowing for individual BLM measurements.

In this study we demonstrated that large BLM arrays can reproducible be fabricated with high success rates (above 95%) by an automation technique that does not require sophisticated and expensive robots. We conclude, based on the large capacitance values relative to the background and the reconstitution of valinomycin and subsequent blockage by TEA, that functional multi-array bilayers were established with the presented automation technique. The low leak sealing properties of the established functional bilayers are ideally suited for the design of mass transfer devices based on mass transport through highly selective membrane transport peptides and proteins (e.g., biomimetic filters based on incorporated aquaporins or ion channels).

## Acknowledgments

The work was supported through MEMBAQ, a Specific Targeted Research Project (STREP), by the European Commission under the Sixth Framework Programme (NMP4-CT-2006-033234), by The Danish National Advanced Technology Foundation (023-2007-1) and The Danish National Research Foundation.

## References

[1] Anzai K, Ogawa K, Ozawa T and Yamamoto H 2001 Quantitative comparison of two types of planar lipid bilayers—folded and painted—with respect to fusion with vesicles *J. Biochem. Biophys. Methods* **48** 283–91

[2] Benz R, Frohlich O, Lauger P and Montal M 1975 Electrical capacity of black lipid films and of lipid bilayers made from monolayers *Biochim. Biophys. Acta* **394** 323–34

[3] Eray M, Dogan N S, Reiken S R, Sutisna H, Van Wie B J, Koch A R, Moffett D F, Silber M and Davis W C 1995 A highly stable and selective biosensor using modified nicotinic acetylcholine receptor (nAChR) *Biosystems* **35** 183–8

[4] Ginsburg S and Noble D 1974 The activation enthalpies for ion conductance systems in lipid bilayer membranes *J. Membr. Biol.* **18** 163–76

[5] Goennenwein S, Tanaka M, Hu B, Moroder L and Sackmann E 2003 Functional incorporation of integrins into solid supported membranes on ultrathin films of cellulose: impact on adhesion *Biophys. J* **85** 646–55

[6] Han X, Studer A, Sehr H, Geissbühler I, Di Berardino M, Winkler F K and Tiefenauer L X 2007 Nanopore arrays for stable and functional free-standing lipid bilayers *Adv. Mater.* **19** 4466–70

[7] Jeon T J, Malmstadt N and Schmidt J J 2006 Hydrogel-encapsulated lipid membranes *J. Am. Chem. Soc.* **128** 42–3

[8] Kang X F, Cheley S, Rice-Ficht A C and Bayley H 2007 A storable encapsulated bilayer chip containing a single protein nanopore *J. Am. Chem. Soc.* **129** 4701–5
[9] Kelety B, Diekert K, Tobien J, Watzke N, Dorner W, Obrdlik P and Fendler K 2006 Transporter assays using solid supported membranes: a novel screening platform for drug discovery *Assay Drug. Dev. Technol.* **4** 575–82
[10] Malmstadt N, Jeon J and Schmidt J 2008 Long-lived planar lipid bilayer membranes anchored to an *in situ* polymerized hydrogel *Adv. Mater.* **20** 84–9
[11] Mayer M, Kriebel J K, Tosteson M T and Whitesides G M 2003 Microfabricated teflon membranes for low-noise recordings of ion channels in planar lipid bilayers *Biophys. J.* **85** 2684–95
[12] Melikov K C, Frolov V A, Shcherbakov A, Samsonov A V, Chizmadzhev Y A and Chernomordik L V 2001 Voltage-induced nonconductive pre-pores and metastable single pores in unmodified planar lipid bilayer *Biophys. J.* **80** 1829–36
[13] Miller C 1986 *Ion Channel Reconstitution* (New York: Plenum)
[14] Minami H, Sugawara M, Odashima K, Umezawa Y, Uto M, Michaelis E K and Kuwana T 1991 Ion channel sensors for glutamic acid *Anal. Chem.* **63** 2787–95
[15] Montal M and Mueller P 1972 Formation of bimolecular membranes from lipid monolayers and a study of their electrical properties *Proc. Natl. Acad. Sci. USA* **69** 3561–6
[16] Moran-Mirabal J M, Edel J B, Meyer G D, Throckmorton D, Singh A K and Craighead H G 2005 Micrometer-sized supported lipid bilayer arrays for bacterial toxin binding studies through total internal reflection fluorescence microscopy *Biophys. J.* **89** 296–305
[17] Mueller P and Rudin D O 1969 Translocators in bimolecular lipid membranes: their role in dissipative and conservative bioenergetic transduction *Curr. Top. Bioenerg.* **3** 157–249
[18] Nikolelis D P and Siontorou C G 1995 Bilayer lipid membranes for flow injection monitoring of acetylcholine, urea, and penicillin *Anal. Chem.* **67** 936–44
[19] O'Shaughnessy T J, Hu J E, Kulp J L 3rd, Daly S M and Ligler F S 2007 Laser ablation of micropores for formation of artificial planar lipid bilayers *Biomed. Microdevices* **9** 863–8
[20] Oliver A E, Kendall E L, Howland M C, Sanii B, Shreve A P and Parikh A N 2008 Protecting, patterning, and scaffolding supported lipid membranes using carbohydrate glasses *Lab. Chip.* **8** 892–7
[21] Reimhult E and Kumar K 2008 Membrane biosensor platforms using nano- and microporous supports *Trends Biotechnol.* **26** 82–9
[22] Ries R S, Choi H, Blunck R, Bezanilla F and Heath J R 2004 Black lipid membranes: visualizing the structure, dynamics, and substrate dependence of membranes *J. Phys. Chem* B **108** 16040–9
[23] Sandison M E and Morgan H 2005 Rapid fabrication of polymer microfluidic systems for the production of artificial lipid bilayers *J. Micromech. Microeng.* **15** S139–44
[24] Snakenborg D, Klank H and Kutter J P 2004 Microstructure fabrication with a CO2 laser system *J. Micromech. Microeng.* **14** 182–9
[25] Stark G, Benz R, Pohl G W and Janko K 1972 Valinomycin as a probe for the study of structural changes of black lipid membranes *Biochim. Biophys. Acta* **266** 603–12
[26] Uto M, Araki M, Taniguchi T, Hoshi S and Inoue S 1994 Stability of an agar-supported bilayer lipid membrane and its application to a chemical sensor *Anal. Sci.* **10** 943–6
[27] White S H 1970 A study of lipid bilayer membrane stability using precise measurements of specific capacitance *Biophys. J.* **10** 1127–48
[28] White S H 1972 Analysis of the torus surrounding planar lipid bilayer membranes *Biophys. J.* **12** 432–45
[29] Wonderlin W F, Finkel A and French R J 1990 Optimizing planar lipid bilayer single-channel recordings for high resolution with rapid voltage steps *Biophys. J.* **58** 289–97
[30] Zagnoni M, Sandison M E and Morgan H Microfluidic array platform for simultaneous lipid bilayer membrane formation *Biosens. Bioelectron.* at press

# Paper III

Reprinted from Analytical and Bioanalytical Chemistry (2009) 395:719–727, with permission of Springer-Verlag

J. S. Hansen, M. Perry, J. Vogel, J. S. Groth, T. Vissing, M. S. Larsen, O. Geschke, J. Emneús, H. Bohr, C. H. Nielsen***; Large scale biomimetic membrane arrays***

Anal Bioanal Chem (2009) 395:719–727
DOI 10.1007/s00216-009-3010-7

ORIGINAL PAPER

# Large scale biomimetic membrane arrays

**Jesper S. Hansen · Mark Perry · Jörg Vogel · Jesper S. Groth · Thomas Vissing · Marianne S. Larsen · Oliver Geschke · Jenny Emneús · Henrik Bohr · Claus H. Nielsen**

Received: 2 July 2009 / Revised: 22 July 2009 / Accepted: 23 July 2009 / Published online: 13 August 2009


**Abstract** To establish planar biomimetic membranes across large scale partition aperture arrays, we created a disposable single-use horizontal chamber design that supports combined optical–electrical measurements. Functional lipid bilayers could easily and efficiently be established across $CO_2$ laser micro-structured 8×8 aperture partition arrays with average aperture diameters of 301±5 μm. We addressed the electro-physical properties of the lipid bilayers established across the micro-structured scaffold arrays by controllable reconstitution of biotechnological and physiological relevant membrane peptides and proteins. Next, we tested the scalability of the biomimetic membrane design by establishing lipid bilayers in rectangular 24×24 and hexagonal 24×27 aperture arrays, respectively. The results presented show that the design is suitable for further developments of sensitive biosensor assays, and furthermore demonstrate that the design can conveniently be scaled up to support planar lipid bilayers in large square-centimeter partition arrays.

J. S. Hansen · J. Vogel · O. Geschke · J. Emneús
DTU Nanotech, Technical University of Denmark,
2800 Lyngby, Denmark

J. S. Hansen
e-mail: jsh@aquaporin.dk

J. S. Hansen · M. Perry · J. Vogel · J. S. Groth · T. Vissing · M. S. Larsen · C. H. Nielsen
Aquaporin A/S, Scion DTU,
Diplomvej 377,
2800 Lyngby, Denmark

H. Bohr · C. H. Nielsen (✉)
DTU Physics, Quantum Protein Center,
Technical University of Denmark,
2800 Lyngby, Denmark
e-mail: claus.nielsen@fysik.dtu.dk

**Keywords** Black lipid membrane · Array · Optical–electrical measurements · Membrane-spanning peptides · Membrane protein

**Abbreviations**

| | |
|---|---|
| α-HL | α-Hemolysin |
| BLM | Black lipid membrane |
| DPhPC | 1,2-Diphytanoyl-*sn*-Glycero-3-Phosphocholine |
| ETFE | Ethylene tetrafluoroethylene |
| FomA | *Fusobacterium nucleatum* outer membrane protein A |
| gA | Gramicidin A |
| LDAO | *N*-lauryl-*N*,*N*-dimethylammonium-*N*-oxide |
| NBD-PC | 1-Oleoyl-2-[6-[(7-nitro-2-1, 3-benzoxadiazol-4-yl)amino]hexanoyl]-*sn*-glycero-3-phosphocholine |
| TEA | Tetraethylammonium |

## Introduction

To create a device that utilizes membrane-spanning molecules, it is necessary to construct an efficient platform to handle biomimetic membranes [1]. The advantages of biomimetic membrane-based applications are, among others, that a lot of information can be achieved with extremely low sample volumes, specific drug interactions with a single target (protein or peptide) can be assessed, and the experimental conditions can be exactly controlled (e.g., buffer, protein amount, and membrane composition) [1].

Biomimetic membrane-based biosensing devices may provide a powerful tool in the early stage of identifying promising drug candidates for a specific membrane protein or peptide [2–5]. Moreover, a reduction in drug candidates

failing at later stages may be expected. The reason for this is the ability to exactly address the specific effects of a drug candidate on a single target, as well as the potential unintended effects that may occur due to the physiochemical properties of the lipid membrane [6]. This reduces the potential of obtaining unintended interactions with secondary receptors or proteins, or potentially indirect effects on the lipid membrane, which may otherwise occur in living-cell-based systems.

Recently, we described a fast and cost efficient method to produce large scale aperture partitions by micro-structuring ethylene tetrafluoroethylene (ETFE) films using $CO_2$ laser ablation [7]. In a parallel study, we constructed a vertical automation technique for the simultaneous establishment of functional bilayers in 8×8 partition arrays [8].

In this study, we created a horizontal biomimetic membrane design supporting optical–electrical measurements of lipid bilayers established across the $CO_2$ laser-ablated ETFE LZ200 partition arrays. The chamber design was created to constitute a low-cost disposable single-use system. Lipid bilayers could efficiently be established across the partition arrays in the chamber design by employing a modified painting method [9]. The success rate for establishing lipid bilayers across the partition array in the presented design was ≥98%. To demonstrate the functionality of the biomimetic membrane design, controllable reconstitution of the biotechnological and physiological relevant peptides valinomycin and gramicidin A (gA), together with the membrane proteins α-hemolysin and FomA was carried out. We show that the design supports low-current (high sensitivity) recordings of membrane peptides and proteins by incorporating gA, α-hemolysin, and FomA into the established lipid bilayers.

Finally, we demonstrate that the design can conveniently be scaled up to 24×24 (576 apertures) rectangular and 24×27 (648 apertures) hexagonal membrane arrays with averaged diameters of 300 μm. The two different geometries of the micro-structured aperture arrays seem to support stable membrane arrays, however, with somewhat different electrical properties.

Our results are discussed in the context of improving the design to create a multifunctional biomimetic platform suitable for the development of biosensing devices.

## Experimental

### Reagent and materials

Tefzel ETFE LZ200 fluoropolymer for the fabrication of multi-aperture partitions, and Viton A fluoroelastomer for the production of rubber chamber sealing rings were from DuPont Fluoropolymers (Detroit, U.S.A.). Uncoated 35- and 50-mm glass-bottom culture dishes were purchased from MatTek Corporation (Ashland, MA, U.S.A.). The lipids 1, 2-diphytanoyl-*sn*-glycero-3-phosphocholine and 1-oleoyl-2-[6-[(7-nitro-2-1, 3-benzoxadiazol-4-yl)amino]hexanoyl]-*sn*-glycero-3-phosphocholine were from Avanti Polar Lipids Inc. (Alabaster, U.S.A.). The potassium ion-selective cyclodepsipeptide valinomycin (Sigma), *Bacillus brevis* gramicidin A (Sigma), *Staphylococcus aureus* α-Hemolysin (Sigma), tetraethylammonium (Fluka), *n*-heptane and *n*-decane (Fluka) were purchased from Sigma-Aldrich Denmark (Brøndby, Denmark). All other chemicals were of analytical grade and purchased from commercial sources.

### Micro-structuring and surface modification of ETFE scaffold arrays

ETFE LZ200 film (50.8 μm thickness) was laser-structured to produce partition aperture arrays as previously described [7]. Partitions produced were rectangular 8×8 and 24×24, and hexagonal 24×27 arrays, respectively. The apertures within the partition structure had average diameters of 301±5 μm and with a nominal distance from center-to-center of 400 μm.

The ETFE surfaces were covalently modified by plasma treatment with lower-carbon-chain-length alkanes, predominantly hexanes, resulting in a hydrophobic surface coating as described by Inagaki et al. [10] and by Park and Inagaki [11]. This surface modification was applied to provide a molecular anchoring for establishing the lipid membranes across the micro-structured arrays.

### Disposable single-use horizontal biomimetic membrane chamber design

A horizontal lipid bilayer chamber was designed for optical imaging that at the same time enabled recording of the electrical membrane properties by voltage clamp. The assembly of the chamber design is schematically depicted in Fig. 1a. The design was inspired from previous work by Hemmler et al. [12] and Wilburn et al. [13], respectively. Our chamber was, however, made from commercially available 35- and 50-mm MatTek glass-bottom culture dishes, where the 35-mm dish constituted the upper and the 50-mm dish the lower compartments, respectively (Fig. 1). The glass cover slip of the 35-mm MatTek glass-bottom dishes was replaced with the ETFE LZ200 partition by first removing the cover slip by adding 0.5 ml *n*-heptane to the dishes for 10 min, and then gluing the ETFE LZ200 partition array on the dish using silicone-based glue (Dow Corning). A reusable aluminum microscope sample holder was designed to clamp the upper and lower compartments (Fig. 1b and c). A 34-mm cut Viton ring was placed between the two Petri dishes to create two independently accessible compartments (Fig. 1c). By design, the chamber components were made of low-cost, commercially available

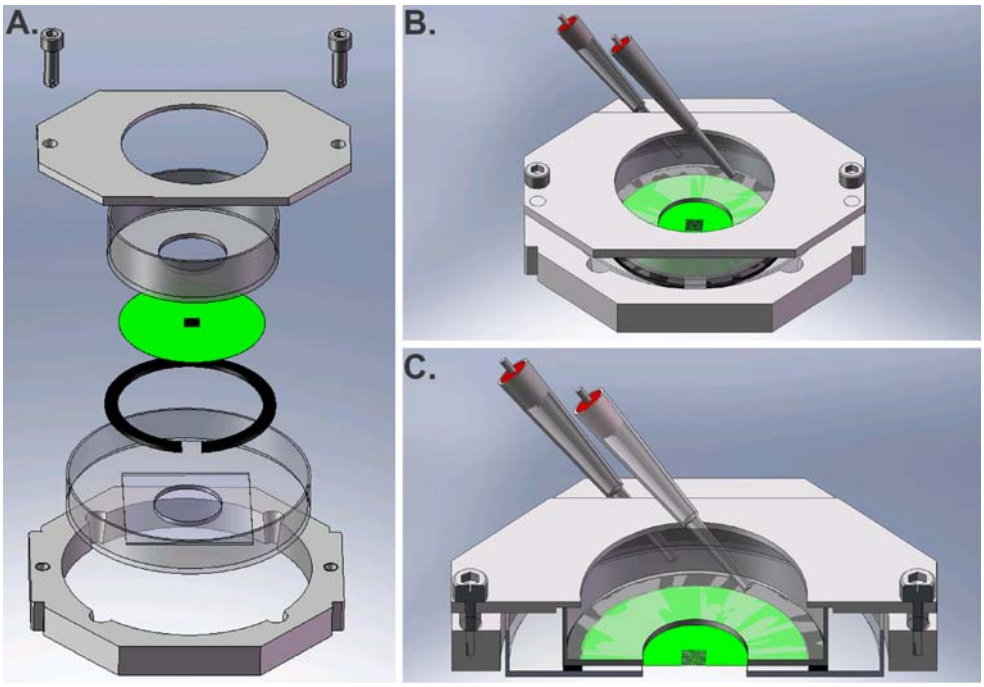


**Fig. 1** The horizontal lipid chamber design. **a** Assembly of the bilayer chamber. The chamber is assembled sequentially from the bottom and up. The upper *cis* compartment consists of a MatTek 35 mm culture dish (transparent) with a micro-structured ETFE LZ200 partition (*green*) glued onto the bottom across the center hole. A MatTek 50-mm-diameter glass-bottom culture dish constitutes the lower *trans* compartment (*transparent*). A cut Viton ring (*black*) is placed between the dishes to create two independently accessible compartments. A custom-designed aluminum sample holder clamps the chamber elements together (*gray*). **b** The assembled lipid chamber. **c** Cross-sectional view of the assembled chamber. The position of the Ag/AgCl electrodes connected to the voltage-clamp setup is indicated in **b** and **c**

components that constituted a convenient disposable single-use chamber design.

## Preparation of lipid solutions for BLM experiments

The lipid solution for bilayer formation consisted of 1, 2-diphytanoyl-*sn*-glycero-3-phosphocholine (DPhPC) in *n*-decane (25 mg/ml) doped with 1 mol% 1-oleoyl-2-[6-[(7-nitro-2-1, 3-benzoxadiazol-4-yl)amino]hexanoyl]-*sn*-glycero-3-phosphocholine (NBD-PC). The lipid solution for bilayer formation is henceforth referred to as the bilayer-forming solution (BFS). The lipid solutions were prepared the day before, and stored at −20°C until use.

## Formation of BLMs across multi-aperture ETFE partitions

Planar lipid bilayers were established across the micro-structured ETFE partition arrays by the lipid bilayer painting technique [9], which was modified essentially, as previously described [12]. Briefly, ~0.5–5 µl (depending on the array size) of the BFS was deposited onto the partition array. To thin the membranes into bilayers, a sterile plastic inoculation loop with a 1 µl loop capacity (Sarstedt) was used. The thinning process was carried out by gently sweeping the inoculation loop across the entire ETFE partition array.

## Fluorescence microscopy visualization

Fluorescent imaging was performed on a Zeiss Axiovert 200M epifluorescence microscope (Carl Zeiss, Jena, Germany) equipped with a monochrome Deltapix DP450 CCD camera (Deltapix, Maalov, Denmark). Images were acquired using Deltapix DpxView Pro acquisition software (Deltapix, Maalov, Denmark). Objectives used were air-corrected Plan-Neofluar 2.5×/0.075 Numerical Aperture (NA) and 10×/0.25 NA, respectively.

## Voltage-clamp data acquisition and processing

The experimental setup consisted of a Model 2400 Patch Clamp Amplifier with a head stage containing 10 GΩ/10 MΩ feedback resistors (A-M Systems, Inc., WA, USA) and a Thurlby Thandar Instruments model TG2000 20 MHz DDS function generator (RS Components Ltd, Northants, UK). The Ag/AgCl electrodes were placed in the *trans* and *cis* compartments of the bilayer formation chamber with the ground electrode positioned in the *trans* compartment. Data acquisition was done with a combined oscilloscope/analog–digital converter (ADC-212/50, Pico Technology, Cambridgeshire, UK) connected to a laptop computer. Sampling frequency was 50 Hz.

Capacitance and conductance measurements were performed as previously described [8]. The results are given as means±S.D. for five individual experiments unless otherwise stated. Off-line analysis was done using custom made software.

To measure channel incorporation electrically, a current potential of +60 mV or +150 mV was applied, and the resulting membrane output current was filtered through 1 kHz on the amplifier and subsequently further filtered through a low-pass Bessel filter with 50 Hz cutoff (Frequency Devices, IL, USA) before data acquisition.

### Reconstitution of transmembrane peptides and proteins

Valinomycin dissolved in ethanol (1.8 mM) was added (10 µl) to the top horizontal chamber to yield a final concentration of 12 µM in close proximity to the lipid bilayer array. To reverse the valinomycin-induced current increase, tetraethylammonium (TEA, 16 mM) was added (200 µl) to the top horizontal chamber. The aqueous chamber solution consisted of 0.2 M KCl. The applied potential across the partition arrays was +60 mV.

Incorporation of *B. brevis* gramicidin A (gA) into established membrane arrays was carried out by the addition of 5 µl gA dissolved in ethanol (120 nM) to both the *cis* and *trans* horizontal chambers. The aqueous solution in the bilayer chamber consisted of HCl (1 N) adjusted to pH 1.0, while the potential applied across the bilayers was +150 mV.

*S. aureus* α-hemolysin (α-HL) was reconstituted into 8×8 bilayer arrays by adding 10 µl of a 50 µg/ml stock solution to the *cis* chamber, while 20 µl of a 0.5 mg/ml stock solution was used for the large arrays. The aqueous solution in the chamber consisted of 1.0 M KCl for the 8×8 partition arrays, while a 0.2 M KCl saline solution was used for the large partition arrays. The applied potential across the partition arrays was +60 mV.

The *F. nucleatum* outer membrane protein A (FomA) was kindly provided by Dr. Jörg H. Kleinschmidt (Universität Konstanz, Germany). Incorporation of FomA into established lipid bilayer arrays was carried out by adding 2 µl of refolded FomA (9.6 mg/ml) in *N*-lauryl-*N*,*N*-dimethylammonium-*N*-oxide (LDAO) micelles (LDAO/FomA ratio=800 mol/mol) to the *cis* chamber compartment as previously described [14]. The *cis* and *trans* chamber were filled with a saline solution consisting of 1.0 M KCl, and the applied potential across the partition arrays was +60 mV.

## Results and discussion

We created a horizontal biomimetic membrane chamber based on commercially available MatTek glass-bottom culture dishes to make an inexpensive and easily assembled design. Thus, the main chamber parts constitute a disposable single-use biomimetic membrane chamber, where only the custom-designed aluminum sample holder is reusable, and which does not require cleaning prior to re-assembly (Fig. 1).

The design allows for combined optical imaging and voltage-clamp recordings of established bilayers across the micro-structured ETFE LZ200 partition arrays (Fig. 1). The pair of Ag/AgCl electrodes is positioned in the *cis* and *trans* chamber, respectively (Fig. 1b and c). The electrodes therefore give an overall electrical readout of the complete set of membranes established across the micro-structured ETFE LZ200 partition arrays.

The electrical properties of the biomimetic membrane chamber, with non-perforated ETFE LZ200 films, were evaluated. The capacitance ($C$) and conductance ($G$) contributions of the chamber setup with non-perforated ETFE LZ200 film were 132±13 pF and 2.5±0.5 nS, respectively. These values of the non-perforated ETFE LZ200 film are defined as the baseline values of $C$ and $G$.

### Establishment of horizontal 8×8 lipid bilayer arrays

Lipid bilayers were established across the micro-structured ETFE LZ200 partition arrays in the horizontal biomimetic membrane chamber by spreading ~0.5 µl of the BFS onto the 8×8 partition array. This resulted in complete lipid membrane coverage of all the partition apertures. In contrast to the previously described establishment of lipid bilayer arrays across vertically positioned ETFE LZ200 partitions [8], the lipid membranes did not thin spontaneously to lipid bilayers in the horizontal setup. In this stage, lipid membranes were stable for days, and could be transported without disrupting the membranes. Manual thinning of lipid membranes was therefore necessary to obtain functional lipid bilayers suitable for insertion of membrane-spanning peptides and proteins. Prior to the manual-thinning process, the deposited membranes were equilibrated for 15 min with the micro-structured ETFE partition. The thinning of the membranes was carried out by gently sweeping a sterile plastic inoculation loop (1 µl capacity) across the entire ETFE partition array. This manual-thinning process took approximately 30 s per array. Repetitions of the sweeping motions across the membranes were required if the bilayer in a single or a few individual apertures ruptured, or if excess BFS flowed back from the surroundings into the actual aperture array positioned in the center of the ETFE partition. The fact that bilayers could be easily re-established if they ruptured during the membrane thinning process resulted in a success rate of ≥98% for establishing bilayers across the partition arrays. The establishment of bilayers in the ETFE arrays could

furthermore be carried out by untrained personnel with no previous experience in establishing black lipid membranes following a short instruction behind the principle of the manual-thinning technique.

To adapt the current manual processes of lipid bilayer formation to a fully automated system for industrial scale applications a robotic deposition technique or a micro fluidic system is envisaged.

The fluorescent lipid analog NBD-PC (1 mol%) included in the BFS provided a convenient visual control over the thinning process, and the Plateau–Gibbs border of the individual bilayers could easily be visualized (Fig. 2).

Following the manual-thinning process, the resulting lipid bilayers were equilibrated for another 15 min in order for the established bilayers to stabilize before carrying out experimentation.

The lipid bilayer arrays established under these conditions had average lifetimes of 1 h with voltage potentials less than or equal to ±100 mV, and exhibited C and G values of 9,750±515 pF and 61±11 nS, respectively. This indicated that the bilayer area constituted around 36–54% of the aperture area [15].

To demonstrate that functional lipid bilayers were established across the horizontal 8×8 arrays the potassium-selective cyclodepsipeptide valinomycin was added to the *cis* chamber to a final concentration of 12 μM [16]. The resulting increase in the current trace recording indicated functional reconstitution of valinomycin, which could effectively be reversed by the addition of the channel blocker TEA (Fig. 3a). This strongly suggested that functional lipid bilayers were established in the horizontal setup.

## Sensitivity of current trace recordings of membrane molecules

The current noise increases strongly with the aperture diameters and the recording bandwidth [17]. This could affect the ability to resolve low-conductance events by voltage-clamp recordings in the bilayers established across the horizontal 8×8 partition arrays.

The current noise of the bilayers established in 8×8 arrays was determined to be in the range 3–5 pA peak-to-peak with a frequency bandwidth of 50 Hz. This scale of current noise would be expected to be acceptable for resolving low-conductance events of a wide range of membrane-spanning peptides and proteins, provided that the experimental conditions are optimal (e.g., ionic strength) for the given peptide or protein. We therefore addressed the sensitivity of the bilayers established in the 8×8 partition arrays by incorporating biotechnological or physiological relevant membrane peptides and proteins (Table 1).

The well-characterized peptide gA from *B. brevis* is a cation-selective channel formed by transbilayer association of pentadecapeptide subunits residing in each monolayer of the lipid bilayer [18]. We reconstituted gA into established bilayers by adding gA dissolved in ethanol to both the *cis* and *trans* bilayer chambers. Reconstituted gA peptides exhibited a high channel activity, where multiple gA channel opening and closures could be observed during the current trace (Fig. 3b). The current of single-channel activity with the chosen experimental conditions was expected to be ~20 pA [19]. Channel events with these current values could be distinguished in the current traces

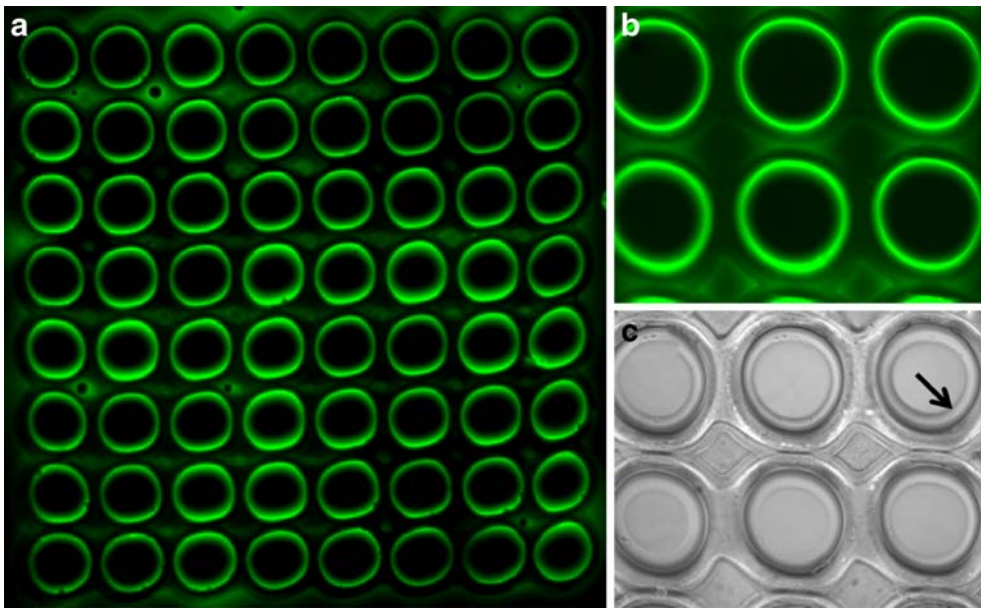


**Fig. 2** Fluorescent and bright-field images of established horizontal 8×8 bilayer arrays. **a** Fluorescent image of established 8×8 bilayer array with 25 mg/ml DPhPC in *n*-decane doped with NBD-PC (1 mol%). Image was acquired with a 2.5× air-corrected objective. **b** Fluorescent image acquired with a 10× air-corrected objective, and **c** the corresponding brightfield image. Indicated is the visual appearance of the Plateau–Gibbs border (*black arrow*)

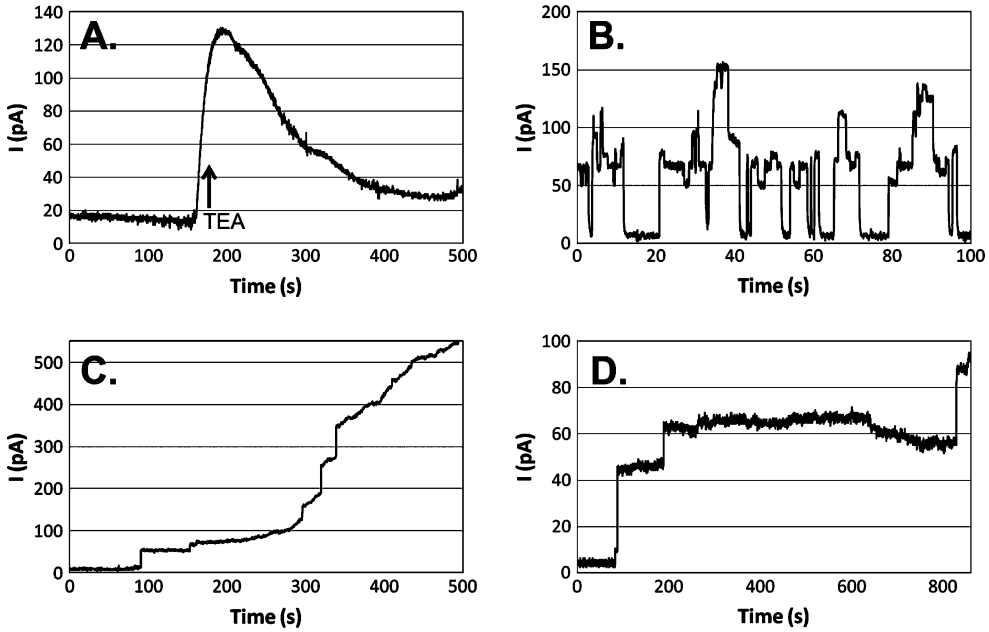


**Fig. 3** Current traces of reconstituted membrane peptides and proteins in established 8×8 bilayer arrays. **a** Insertions of valinomycin and blocking by TEA. TEA was added ($t$=180 s) when the current increased as a consequence of functional valinomycin insertions. **b** Traces of gA channel activities. High channel activities are seen during the current trace with simultaneous opening and closure of multiple channels. Single-channel opening and closure could be distinguished with current values of ~20 pA **c** Reconstitution of heptameric α-HL pores. Single-channel incorporations had current values of ~35 pA. **d** Incorporation of trimeric FomA porins. Single-channel events had current values of approximately 15 pA. In the current traces of **b**, **c**, and **d** multiple insertions together with single-channel events could be observed. Applied potentials were +60 mV in **a**, **c**, and **d** and +150 mV in **b**

of incorporated gA peptides, although with some conductance heterogeneity (Fig. 3b).

We next evaluated the compatibility of the horizontal bilayers in the 8×8 arrays to support functional incorporation of membrane proteins, and to further characterize the ability to resolve low-conductance events. The pore-forming heptameric α-HL membrane protein from *S. aureus* and the trimeric outer-membrane-embedded porin FomA from *F. nucleatum*, respectively, were reconstituted into bilayers established across the partition arrays. The α-HL pores incorporated into the membranes with single-channel currents of around 35 pA (Fig. 3c), agreeing with previous reports [12]. The voltage-dependent FomA channel porins inserted into the membrane with a current of approximately 15 pA (Fig. 3d), which also agreed with previously published current traces [14, 20]. Simultaneous multiple-channel insertions were also observed in the current traces of both reconstituted α-HL pores and FomA channel porins (Fig. 3c and d).

These results show that the bilayers established in the micro-structured 8×8 ETFE LZ200 partitions support low-current (high sensitivity) recordings.

The individual bilayers are, at present, not electrically addressable. Recent approaches have been described that conveniently allow the integration of a membrane scaffold with planar addressable microelectrode arrays [21, 22]. Further developments of the horizontal biomimetic membrane design could therefore be to develop composite membrane scaffolds enabling the electrical readout of individual bilayers. The lipid bilayers are however optically

**Table 1** Potential applications of selected membrane peptides and proteins

| Name | Type | Biotechnology/pharmacology | References |
|---|---|---|---|
| Valinomycin | Cyclodepsipeptide | Biomedical devices | [30, 31] |
| gA | Peptide | Sensors for drug-induced toxicity, chemical and biochemical analytes, pH and ammonium | [6, 32–34] |
| α-HL | Protein | Stochastic sensing techniques | [35, 36] |
| | | Polynucleotide detection and sequencing | [37–41] |
| FomA | Protein | Drug discovery in Gram-negative bacteria infectious diseases | [42, 43] |
| | | Immunological assays | [44] |

individually addressable and fluorescent-based techniques may be combined with the membrane design in order to characterize specific interactions with membrane peptides or proteins [23, 24]. Moreover, the aperture array geometry (diameters of 300 µm and nominal center-to-center distances of 400 µm) provides a platform that may be adapted to modern array scanners and/or automated imaging and image analysis systems.

## Lipid bilayers across rectangular 24×24 and hexagonal 24×27 partition arrays

The scalability of the array size is a key feature in the successful development of biotechnological applications based on planar biomimetic membranes. We therefore addressed the scalability of our design by scaling up the partition array size from the 8×8 rectangular arrays to 24×24 rectangular and 24×27 hexagonal EFTE LZ200 partition arrays. The total aperture areas were 0.41 $cm^2$ for the 24×24 rectangular and 0.45 $cm^2$ for the 24×27 hexagonal arrays, corresponding to a nine- and ten times area increase, respectively, compared to the 8×8 partition arrays (0.045 $cm^2$).

Lipid bilayers could be established across the large ETFE LZ200 partition arrays in a similar manner as for the 8×8 partition arrays. Modifications were that 5 µl BFS was needed to cover the large partition arrays and an equilibration period of approximately 1 h were required prior to the membrane thinning to obtain stable membranes. In order to obtain a full view of the bilayers established across the large partition arrays, mosaics of twelve images were assembled for each large array (Fig. 4a and b). The membranes could be evenly thinned across the whole partition array as evidenced by the separate bright appearance of the torus of the

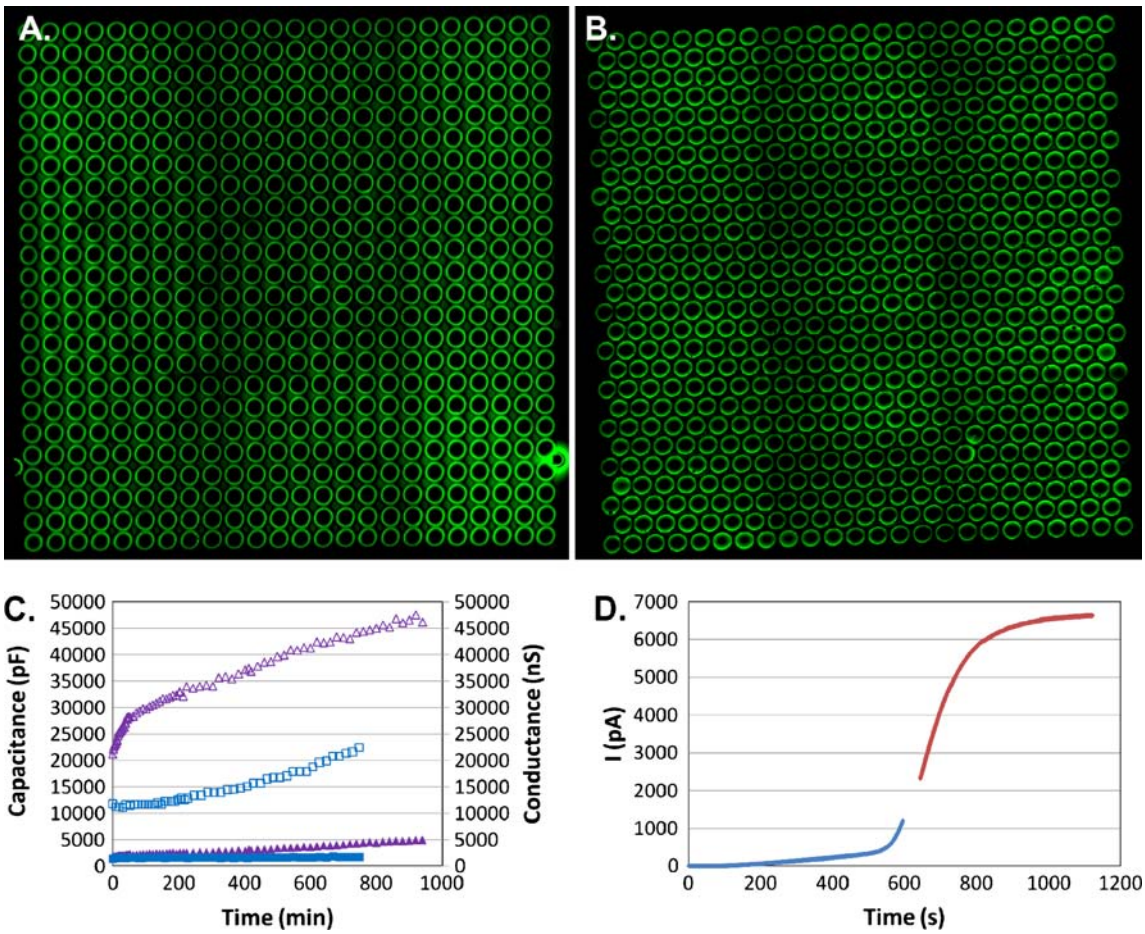


**Fig. 4** Comparison of 24×24 rectangular and 24×27 hexagonal bilayer arrays. **a** and **b** Mosaics comprising 12 fluorescent images of the 24×24 rectangular and 24×27 hexagonal bilayer arrays. **c** Capacitance (*open boxes*) and conductance (*filled boxes*) values during the membrane lifetime of the 24×24 rectangular (*purple*) and 24×27 hexagonal (*blue*) arrays. Time=0 is subsequent a 15 min equilibration period after the manual thinning process. **d** Demonstration of α-HL incorporation into a 24×24 rectangular array. The initial amplifier gain was set to 10× (*blue line*). When the amplifier saturated due to the incorporation of α-HL pores, the gain was adjusted and the trace recording was resumed (*red line*). The aqueous solution in the horizontal bilayer chamber consisted of a 0.2 M KCl. The applied potential was +60 mV

individual bilayers (Fig 4a and b). Although the large arrays also needed initial manual thinning, they spontaneously continued the thinning process (Fig 4c). The maximum capacitance values that could be achieved were around 50,000 pF for the 24×24 rectangular arrays, while considerably lower values were obtainable for the 24×27 hexagonal arrays (Fig. 4c).

The bilayers exhibited relatively stable conductance values ranging between 2,000–5,000 nS, depending on the array type, throughout the bilayer lifetimes, indicating good sealing properties of the large arrays (Fig. 4c).

The current noise of the bilayers established across the large arrays was also assessed, and determined to be in the range of 10–20 pA peak-to-peak for both the 24×24 rectangular and the 24×27 hexagonal arrays, respectively.

Surprisingly, the bilayers established across the large partition arrays were considerably more stable than the bilayers established across the 8×8 partition arrays with membrane lifetimes up to around 16 h for both the rectangular and hexagonal arrays. The reason might be that bilayer breakages often appeared at the edges of the partition array. The percentage of bilayers residing at the edges is ~44% for the 8×8 partition arrays, whereas this fraction only constitutes ~16% for the 24×24 arrays and ~15% for the 24×27 arrays, respectively.

To evaluate the functionality of the large bilayer arrays, α-HL was reconstituted into the large arrays (Fig. 4d). The α-HL incorporated exponentially exhibiting a sigmoid current shape, indicating that α-HL incorporated into the bilayers in a cooperative manner (Fig 4d). The large arrays therefore comprised functional bilayers suitable for incorporation of membrane proteins, preferentially in large scale amounts.

Although evenly thinned bilayers could be consistently obtained across the large partition arrays, the spontaneous thinning process varied between experiments. This could mainly be attributed to the manual handling involved in the establishment of the lipid arrays.

To establish large scale biomimetic membrane arrays in a more reproducible manner, an automation technique needs to be integrated with the current horizontal setup. The automation of bilayer formations can be integrated with the horizontal design by either a robotic-based membrane deposition technique or a micro fluidic-based system.

In this study, we have addressed the electro-physical properties of the micro-structured membrane scaffold and the scalability of the bilayer arrays in the constructed horizontal design.

The transportation robustness of the functional bilayer arrays has not been addressed here. However, the thick precursor membranes could be stored and transported without disrupting the membranes in the stage prior to the manual thinning of membranes to lipid bilayers. Encapsulation of the suspended bilayers would be an expected requirement. Recent advantages in bilayer encapsulation methods suggest that a robust portable artificial membrane platform may be produced [25–29].

We conclude that the electro-physical properties of the micro-structured membrane scaffold combined with the scalability of array sizes enable further development of novel biomimetic membrane-based biosensing devices.

**Acknowledgments** We thank Dr. Jörg H. Kleinschmidt (Universität Konstanz, Germany) for the delivery and guidance with the handling and incorporation of FomA porins. The work was supported through MEMBAQ, a Specific Targeted Research Project (STREP), by the European Commission under the Sixth Framework Program (NMP4-CT-2006-033234), by The Danish National Advanced Technology Foundation (023-2007-1), and The Danish National Research Foundation.

## References

1. Suzuki H, Takeuchi S (2008) Anal Bioanal Chem 391:2695–2702
2. Fang Y, Frutos AG, Lahiri J (2002) J Am Chem Soc 124:2394–2395
3. Fang Y, Hong Y, Webb B et al (2006) MRS bulletin 31:5
4. Fang Y, Lahiri J, Picard L (2003) Drug Discov Today 8:755–761
5. Kaczorowski GJ, McManus OB, Priest BT et al (2008) J Gen Physiol 131:399–405
6. Lundbaek JA (2008) J Gen Physiol 131:421–429
7. Vogel J, Perry M, Hansen JS et al (2009) J Micromech Microeng 19:025026
8. Hansen JS, Perry M, Vogel J et al (2009) J Micromech Microeng 19:025014
9. Mueller P, Rudin DO (1969) Curr Topics Bioenergetics 3:157–249
10. Inagaki N, Narushima K, Lim SK, Park YW, Ikeda Y (2002) Journal of Polymer Science Part B: Polymer Physics 40:2871–2882
11. Y. W. Park N I (2004) Journal of Applied Polymer Science 93:1012-1020
12. Hemmler R, Bose G, Wagner R et al (2005) Biophys J 88:4000–4007
13. Wilburn JP, Wright DW, Cliffel DE (2006) Analyst 131:311–316
14. Pocanschi CL, Apell HJ, Puntervoll P et al (2006) J Mol Biol 355:548–561
15. Benz R, Frohlich O, Lauger P et al (1975) Biochim Biophys Acta 394:323–334
16. Stark G, Benz R, Pohl GW et al (1972) Biochim Biophys Acta 266:603–612
17. Mayer M, Kriebel JK, Tosteson MT et al (2003) Biophys J 85:2684–2695
18. Andersen OS, Koeppe RE 2nd (2007) Annu Rev Biophys Biomol Struct 36:107–130
19. Mobashery N, Nielsen C, Andersen OS (1997) FEBS Lett 412:15–20
20. Kleivdal H, Benz R, Jensen HB (1995) Eur J Biochem 233:310–316
21. Baaken G, Sondermann M, Schlemmer C et al (2008) Lab Chip 8:938–944
22. Lin Z, Takahashi Y, Kitagawa Y et al (2008) Anal Chem 80:6830–6833
23. Hebert TE, Gales C, Rebois RV (2006) Cell Biochem Biophys 45:85–109
24. Lohse MJ, Bunemann M, Hoffmann C et al (2007) Curr Opin Pharmacol 7:547–553

25. Jeon TJ, Malmstadt N, Schmidt JJ (2006) J Am Chem Soc 128:42–43
26. Kang XF, Cheley S, Rice-Ficht AC et al (2007) J Am Chem Soc 129:4701–4705
27. Malmstadt N, Jeon J, Schmidt J (2008) Advanced Materials 20:84–89
28. Oliver AE, Kendall EL, Howland MC et al (2008) Lab Chip 8:892–897
29. Uto M, Araki M, Taniguchi T et al (1994) Analytical Sciences 10:943–946
30. Frant MS, Ross JW Jr (1970) Science 167:987–988
31. Schar-Zammaretti P, Ziegler U, Forster I et al (2002) Anal Chem 74:4269–4274
32. Capone R, Blake S, Restrepo MR et al (2007) J Am Chem Soc 129:9737–9745
33. Borisenko V, Zhang Z, Woolley GA (2002) Biochim Biophys Acta 1558:26–33
34. Nikolelis DP, Siontorou CG (1996) Anal Chem 68:1735–1741
35. Braha O, Gu LQ, Zhou L et al (2000) Nat Biotechnol 18:1005–1007
36. Gu LQ, Braha O, Conlan S et al (1999) Nature 398:686–690
37. Ashkenasy N, Sanchez-Quesada J, Bayley H et al (2005) Angew Chem Int Ed Engl 44:1401–1404
38. Kasianowicz JJ, Brandin E, Branton D et al (1996) Proc Natl Acad Sci U S A 93:13770–13773
39. Kasianowicz JJ, Henrickson SE, Weetall HH et al (2001) Anal Chem 73:2268–2272
40. Vercoutere WA, Winters-Hilt S, DeGuzman VS et al (2003) Nucleic Acids Res 31:1311–1318
41. Winters-Hilt S, Vercoutere W, DeGuzman VS et al (2003) Biophys J 84:967–976
42. Bolstad AI, Jensen HB, Bakken V (1996) Clin Microbiol Rev 9:55–71
43. Jensen HB, Skeidsvoll J, Fjellbirkeland A et al (1996) Microb Pathog 21:331–342
44. Guo M, Han YW, Sharma A et al (2000) Oral Microbiol Immunol 15:119–123

# Paper IV

Reprinted from Langmuir (2011) 27:7002-7007, with permission of ACS Publications

M. Roerdink Lander, S. Ibragimova, C. Rein, J. Vogel, K. Stibius, O. Geschke, M. Perry, C. H. Nielsen; **Biomimetic Membrane Arrays on Cast Hydrogel Supports**

Langmuir

ARTICLE

pubs.acs.org/Langmuir

# Biomimetic Membrane Arrays on Cast Hydrogel Supports

Monique Roerdink Lander,[†,⊥] Sania Ibragimova,[‡,§,⊥] Christian Rein,[§,∥,⊥] Jörg Vogel,[†,§] Karin Stibius,[‡,§] Oliver Geschke,[†,§] Mark Perry,[§] and Claus Hélix-Nielsen*[,‡,§]

[†]DTU-Nanotech and [‡]DTU-Physics, Technical University of Denmark, DK-2800 Kgs. Lyngby, Denmark

[§]Aquaporin A/S, Ole Maaløes Vej 3, DK-2200 Copenhagen N, Denmark

[∥]Nano-Science Center and Department of Chemistry, University of Copenhagen, Universitetsparken 5, DK-2100 Copenhagen Ø, Denmark

**ABSTRACT:** Lipid bilayers are intrinsically fragile and require mechanical support in technical applications based on biomimetic membranes. Tethering the lipid bilayer membranes to solid substrates, either directly through covalent or ionic substrate−lipid links or indirectly on substrate-supported cushions, provides mechanical support but at the cost of small molecule transport through the membrane−support sandwich. To stabilize biomimetic membranes while allowing transport through a membrane−support sandwich, we have investigated the feasibility of using an ethylene tetrafluoroethylene (ETFE)/hydrogel sandwich as the support. The sandwich is realized as a perforated surface-treated ETFE film onto which a hydrogel composite support structure is cast. We report a simple method to prepare arrays of lipid bilayer membranes with low intrinsic electrical conductance on the highly permeable, self-supporting ETFE/hydrogel sandwiches. We demonstrate how the ETFE/hydrogel sandwich support promotes rapid self-thinning of lipid bilayers suitable for hosting membrane-spanning proteins.

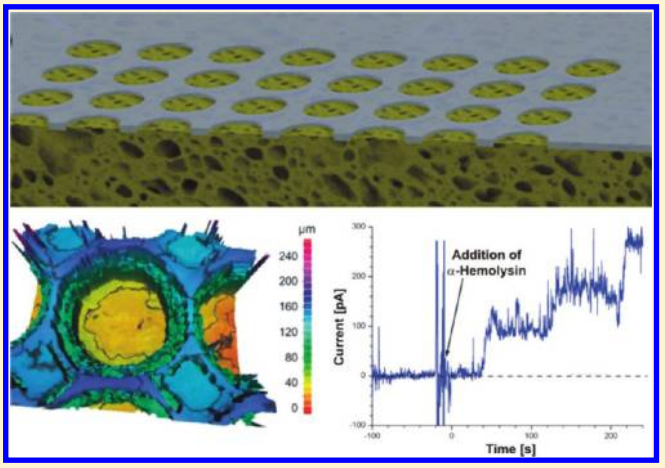


## INTRODUCTION

Biomimetic membranes based on lipid bilayers are increasingly being recognized as a platform not only for the study of reconstituted membrane-associated proteins but also as building blocks in devices for sensor and separation applications.[1,2] Lipid bilayer membranes are extremely fragile and require mechanical support,[3,4] and deposition of planar lipid bilayers onto supports allows for the biofunctionalization of surfaces, providing a natural environment for the immobilization of highly specialized membrane-associated proteins.[5] Support surfaces with nanoscale smoothness based on gold, silicon, or cleaved mica have been investigated intensively with several membrane−protein systems.[6] Such systems are well-suited for biomimetic sensors where the sensor readout is based on, e.g., detecting electrochemical impedance changes induced by ligand binding to membrane-stabilized proteins of the supported membrane−protein complex via gold electrodes or detection based on optical (fluorescence) signals.

Membrane-spanning proteins often have hydrophilic moieties that may hinder optimal support of bilayers with reconstituted proteins on solid surfaces. This has led to the development of "cushions" in the form of polymeric structures that effectively separate the bilayers from the solid surface using, for example, polyacrylamide and agarose as the cushion material.[7−9] In these approaches the bilayers were formed across a single aperture (100−500 $\mu$m diameter), and the cushion supported the membrane in the aperture area. Later developments include the formation of membranes where the bilayer is cushioned by poly(ethylene glycol) (PEG)-conjugated lipids that effectively separate the bilayer from a solid surface.[10,11] A different approach consists of using supports with submicrometer porosity where the bilayers are formed directly on top of, for example, nanoporous alumina substrates.[12,13] Bilayer formation has also been demonstrated using ordered arrays of submicrometer-sized pores formed in silicon substrates with well-defined pore diameters ranging from 250 to 1000 nm.[14,15] In this case, the membranes span the pores without additional support. Supports using hydrogels have also been demonstrated.[16,17]

Applications relying on mass transport across planar biomimetic membranes mediated by transmembrane proteins require that the supported membrane is stable against external forces, such as osmotic and hydrostatic forces, and concomitantly sufficiently porous to allow for vectorial transport of solutes and solvents. Tethering the lipid bilayer membranes to solid substrates, either directly through covalent or ionic substrate−lipid conjugates or indirectly by substrate-supported cushions, provides mechanical support but is not optimal for large-scale

**Received:** December 22, 2010
**Revised:** March 24, 2011
**Published:** April 28, 2011

mass transport across the membrane. Large-scale transport across biomimetic membranes also requires that the entire system is readily upscalable. Approaches using nanoporous alumina require arduous preparation,[13] and the use of nanopore silicon arrays is limited by material cost and wafer size. These are issues that need to be addressed to harness the unique opportunities that lipid bilayer membranes offer in technological applications where large-scale transport is desired.

Previously, we reported the fast fabrication of dense arrays of 300 $\mu$m diameter circular apertures in 50 $\mu$m thick partitions made of ethylene tetrafluoroethylene (ETFE) for biomimetic membranes using a $CO_2$ laser ablation method that is cost-effective and that can be easily scaled up to square centimeters.[18] We also reported successful formation of planar, free-standing black lipid membranes (BLMs) in these hydrophobic multi-aperture partitions.[19,20] In this study we aimed at stabilizing lipid membranes further against pressure-induced disruptions in a construction that tolerates large flux through the supported BLMs using a relatively simple upscalable porous support structure. Specifically, we formulated a composite hydrogel that demonstrates high water permeability. The hydrogel support is formed by in situ polymerization of an aqueous solution of 2-hydroxyethyl methacrylate (HEMA) and poly(ethylene glycol) dimethacrylate (PEG-DMA) in the presence of silicon dioxide particles. The composite hydrogel was cast using a mold such that the polymerized hydrogel would form a supportive layer across apertures formed in an ETFE array as shown in Figure 1A–C. The rationale behind this design was to optimize the lipid–partition interactions at the aperture rim while providing maximal support for the membranes across the aperture arrays. To ensure good contact between the hydrophilic composite hydrogel and the hydrophobic multiaperture ETFE partition, we modified the ETFE surface using a plasma surface treatment on the partition side facing the hydrogel. We demonstrate how the composite support is capable of promoting rapid self-thinning of BLMs and that the supported BLMs are suitable for hosting membrane-spanning proteins.

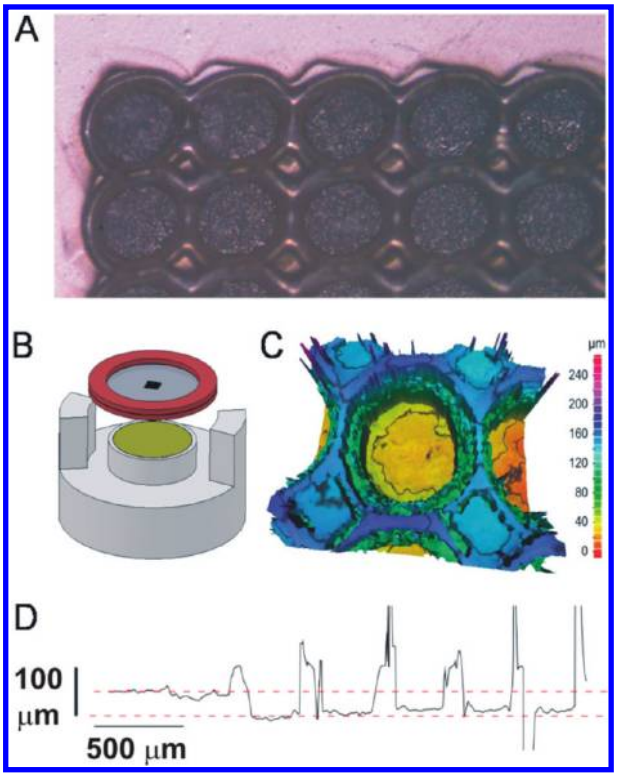


**Figure 1.** (A) Top view of a section of the ETFE/hydrogel sandwich. The composite hydrogel is attached to the back of the ETFE without penetrating the apertures. (B) Schematic of the ETFE scaffold with PMMA rings (red) and the Teflon mold used for casting of the hydrogel support. The hydrogel-forming solution (green) is contained in a reservoir with a depth of 500 $\mu$m. (C) Optical scanning image of a single aperture with the composite hydrogel. The green toroidal structure inside the aperture represents the sloping wall of the aperture. The spikes are measurement artifacts due to missing data points. (D) Profile scan across five apertures. The red dashed lines indicate the surfaces of the ETFE sheet.

## EXPERIMENTAL SECTION

**Materials.** PEG-DMA ($M_w$(PEG block) = 1000 g/mol) was purchased from Polysciences, Inc. (Warrington, PA). *N,N,N′,N′*-Tetramethylethylenediamine (TEMED), α-hemolysin (*Staphylococus aureus*), 10× phosphate-buffered saline (PBS), pH 7.4, HEMA, 1,4-butanediol diacrylate (BDDA), silicon dioxide particles (0.5–10 $\mu$m diameters), ammonium persulfate (APS), *n*-decane, and ethanol were purchased from Sigma-Aldrich Denmark (Brøndby, Denmark). Tefzel ETFE LZ200 for fabrication of multiaperture arrays and Viton A fluoroelastomer used for the production of rubber chamber-sealing O-rings were supplied by DuPont Fluoropolymers (Detroit, MI). 1,2-Diphytanoyl-*sn*-glycero-3-phosphocholine (DPhPC), 1,2-dioleoyl-3-(trimethylammonium)-propane (DOTAP), 1,2-distearoyl-*sn*-glycero-3-phosphoethanolamine-*N*-[biotinyl(poly(ethylene glycol))-2000] (ammonium salt) (DSPE-PEG2000-biotin), and 1-oleoyl-2-[6-[(7-nitro-2,1,3-benzoxadiazol-4-yl)-amino]hexanoyl]-*sn*-glycero-3-phosphocholine (NBD-PC) were purchased from Avanti Polar Lipids, Inc. (Alabaster, AL). All materials were used as received.

**Fabrication of the ETFE/Hydrogel Sandwich.** In the first production step the ETFE partition was plasma-treated on one side of the ETFE with HEMA in a custom-built 50 Hz two-phase plasma chamber[21] using 1 sccm of Ar as the activation/carrier gas with 10 Pa of total pressure and 10 W of plasma power (20 mA, 500 V). The partition and monomer solution were left overnight to cure. Casting was performed with a solution consisting of 23 mg of PEG-DMA, 560 $\mu$L of HEMA, 8 $\mu$L of TEMED, 5 $\mu$L of BDDA, 140 mg of $SiO_2$, and 1000 $\mu$L of Milli-Q water vortexed to create a milky suspension. To 400 $\mu$L of this solution was added 15.3 $\mu$L of an initiator solution (170 mg of APS in 1000 $\mu$L of Milli-Q water). The mixture was vortexed for 10 s and immediately transferred to a reservoir (2 cm diameter, 0.5 mm height) in a Teflon mold (see Figure 1B). A surface-functionalized ETFE partition with 8 × 8 apertures (300 $\mu$m diameter, 400 $\mu$m center-to-center spacing),[18] glued between two custom-made poly(methyl methacrylate) (PMMA) rings, was fitted on top of the mold, resulting in direct contact between the monomer solution and the functionalized side of the ETFE partition. This setup allowed for the monomer solution to cover but not fill up the apertures. After 10–20 min the hydrogel-coated partitions could be removed from the mold and were stored in Milli-Q water. The hydrogel surface topography was characterized by focus-variation optical scanning of the surface (InfiniteFocus, Alicona Instruments, GmbH, Graz, Austria), shown in Figure 1C,D. Before membrane formation, excess water was removed from the hydrogel-coated partitions by blotting with tissue.

**BLM Formation.** The membrane formation chamber used was a modified version of the horizontal chamber design described by Hansen et al.[19] The chamber was assembled by placing the hydrogel-coated partition with the ETFE side up in the *cis* chamber between two O-rings. An open lid sealed the assembly. Both the *cis* chamber and the channel between the *cis* and *trans* chambers were filled with 1 mL of 1× PBS

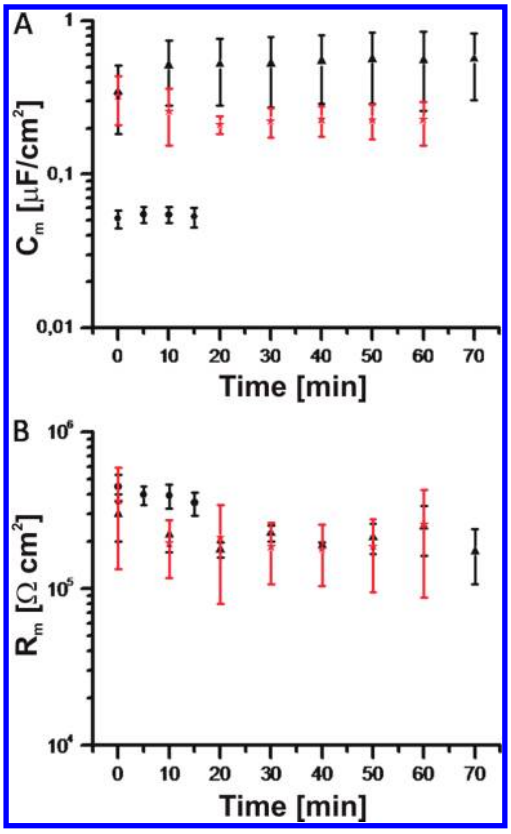


**Figure 2.** (A) Comparison of mean ± SD specific capacitance values $C_m$ of unsupported free-standing (black circles, $n$ = 9) and hydrogel-supported (triangles and asterisks, $n$ = 8) membrane arrays consisting of 8 × 8 individual membranes versus time. Two trends were observed for the hydrogel-supported membranes: (1) development of the specific capacitance to a mean value of 0.3 $\mu$F/cm$^2$ (red asterisks, $n$ = 4); (2) development of the specific capacitance to a mean value of 0.6 $\mu$F/cm$^2$ (black triangles, $n$ = 4). (B) Specific resistance for the membranes shown in (A).

(filtered through a 0.2 $\mu$m filter). The apertures were pretreated by depositing 4 $\mu$L of lipid solution and incubating for 1 h. The lipid solution used in membrane preparation for electrical measurements contained 294 $\mu$L of DPhPC (72 mol %), 61 $\mu$L of DOTAP (18 mol %), and 145 $\mu$L of DSPE-PEG2000-biotin (10 mol %). Lipid solutions in chloroform (10 mg/mL) were dried under nitrogen gas. The dried lipid film was subsequently redissolved in 200 $\mu$L of decane (25 mg/mL). The lipid solution used in membrane preparation for fluorescence measurements contained 292 $\mu$L of DPhPC (71 mol %), 61 $\mu$L of DOTAP (18 mol %), 146 $\mu$L of DSPE-PEG2000-biotin (10 mol %), and 39 $\mu$L of NBD-PC (1 mol %). Lipid solutions in chloroform (10 mg/mL) were dried and redissolved in decane as described above. Lipid solutions were deposited on top of the apertures in 2 $\mu$L aliquots up to 10 $\mu$L. One mL of 1× PBS (filtered through a 0.2 $\mu$m filter) was added to the *cis* chamber, which was subsequently sealed. Membrane formation was monitored by electrical capacitance and conductance measurements using standard electrophysiological methods as previously described.[22] Briefly, the membranes were voltage clamped using AgCl electrodes in each chamber compartment, and transmembrane currents were recorded using a patch-clamp amplifier. The membrane resistance $R$ and capacitance $C$ were measured by applying rectangular and triangular waveforms, respectively ($V_{pp}$= 10 mV). The response signal was low pass filtered at <100 Hz and logged via analog to digital conversion for off-line analysis. Measured total $R$ and $C$ values for the hydrogel-supported membrane were converted into specific values $R_m$ and $C_m$, by normalizing with the combined aperture

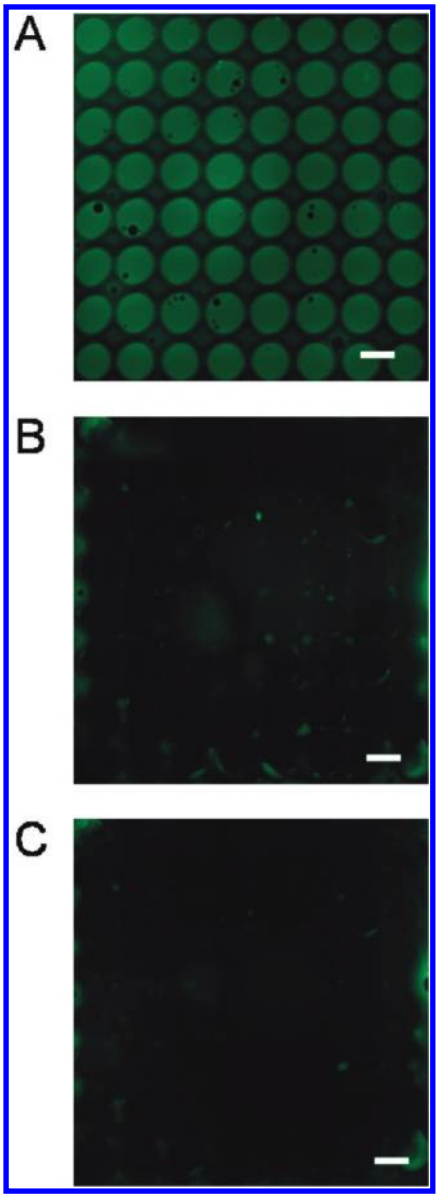


**Figure 3.** (A) Fluorescent images of established unsupported free-standing membranes immediately after formation. (B) Same for hydrogel-supported membrane arrays directly after formation. (C) Same as in (B) but 20 min after formation. Scale bars are 300 $\mu$m.

array area, 0.050215 cm$^2$, neglecting the vanishingly small Plateau–Gibbs regions (see Figure 3B,C) and accounting for the surface area ratio, $S_{dr}$. The empty ETFE/hydrogel sandwich had negligible resistance and capacitance.

**Fluorescence Microscopy.** Fluorescent imaging was performed on a Zeiss Axiovert 200 M epifluorescence microscope (Carl Zeiss, Jena, Germany) equipped with a monochrome Deltapix DP450 charge-coupled device camera (Deltapix, Maalov, Denmark). Images were acquired using Deltapix DpxView Pro acquisition software (Deltapix) and air-corrected Plan-Neofluar 2.5×/0.075 numerical aperture (NA) and 10×/0.25 NA objectives.

**Ion Channel Insertion.** α-Hemolysin was added to the *cis* chamber 10 min after a membrane array was established, resulting in a final concentration of 1 $\mu$g/mL in 10× PBS (filtered through a 0.2 $\mu$m filter). A potential of 60 mV was applied across the membrane, and current traces were filtered at 20 Hz.


dx.doi.org/10.1021/la1050699 |*Langmuir* 2011, 27, 7002–7007

## RESULTS AND DISCUSSION

The presence of silica particles in the polymer hydrogel greatly enhances both the mechanical stability of the gel and the flux of water through the hydrogel.[24] The permeability increased with the amount of silica present in the hydrogel composite. We measured permeabilities up to 24 g $m^{-2}$ $min^{-1}$ at 1 bar for a 1 mm thick slab of composite hydrogel, which contained 44 wt % silica. For comparison, commercial nanofiltration membranes have permeabilities of 1−4 g $m^{-2}$ $min^{-1}$ at applied pressures of 7−30 bar for 0.1 $\mu$m pore size films.

The hydrogel was cast using a Teflon mold to form a hydrogel support in each aperture over the entire array (Figure 1B) as described in the Experimental Section. The surface topography of the hydrogel areas in the ETFE/hydrogel sandwich was characterized by focus-variation optical scanning and revealed the desired backing of the ETFE partition apertures with the composite hydrogel (Figure 1C). We evaluated the arithmetical mean roughness $R_a$ of the hydrogel surface inside each aperture from

$$R_a = \frac{1}{l}\int_0^l |f(x)|\, dx \quad (1)$$

which corresponds to averaging over a section of standard length $l$ sampled from mean value curves (described by $f(x)$) on the optical scan roughness chart. From this the average $R_a$ value of an ETFE/hydrogel surface fabricated using the mold method was determined to be 1.036 ± 0.178 $\mu$m (mean ± SD, $n$ = 5 scans). By comparison, $R_a$ is 0.583 ± 0.088 $\mu$m (mean ± SD, $n$ = 5 scans) for a glass−hydrogel interface prepared on a glass slide. The difference reflects the increased roughness of the mold-cast, air-cured interface of the hydrogel. The surface roughness corresponds to an increment of the interfacial area of the sampled surface area relative to an ideally flat surface. The increment, or surface area ratio $S_{dr}$, of the hydrogel surface relative to the area of the projected $x-y$ surface, can be determined from

$$S_{dr} = \frac{(\sum_{k=0}^{M-2}\sum_{l=0}^{N-2} A_{kl}) - (M-1)(N-1)\,\delta x\,\delta y}{(M-1)(N-1)\,\delta x\,\delta y} \times 100 \quad (2)$$

where $M$ and $N$ represent the numbers of pixels in the $x$ and $y$ directions, respectively, and

$$A_{kl} = \frac{1}{4}\left(\sqrt{\delta y^2 + (z(x_k, y_l) - z(x_k, y_{l+1}))^2} + \sqrt{\delta y^2 + (z(x_{k+1}, y_l) - z(x_{k+1}, y_{l+1}))^2}\right) \times \left(\sqrt{\delta x^2 + (z(x_k, y_l) - z(x_{k+1}, y_l))^2} + \sqrt{\delta x^2 + (z(x_k, y_{l+1}) - z(x_{k+1}, y_{l+1}))^2}\right) \quad (3)$$

The surface area ratio is 11% for the ETFE/hydrogel support. Figure 1A shows the ETFE/hydrogel support. A pore size distribution analysis of the composite hydrogel, based on environmental scanning electron microscopy image analysis, showed a bimodal distribution with some pore diameters of <500 nm and the majority of the pore diameters between 2 and 5 $\mu$m. The smaller pores (with radii less than the surface roughness) reflect some degree of interfacial skin layer formation.[24] However, water flux and electrical properties of the composite hydrogel were not affected by this.[23] The composite hydrogel support covered the apertures with marginal penetration into the apertures (see Figure 1D).

Using the ETFE/hydrogel sandwich support, we established lipid membranes across 8 × 8 aperture arrays. ETFE partition arrays without hydrogel served as the reference. Membranes were formed by manually applying a lipid−decane solution to the apertures.[19] The membrane-forming solution contained DOTAP and PEG-conjugated lipid. The rationale behind including the cationic DOTAP comes from the observation that DOTAP is able to electrostatically "stitch" gel-state bilayers together to form defect-free membranes of several square micrometers; therefore, DOTAP can be seen as a bilayer-stabilizing agent.[25,26] PEG-conjugated lipids were included to provide a soft cushion for the bilayers resting on top of the hydrogel surface.[5] The array electric specific capacitance, $C_m$, and specific resistance, $R_m$, for the free-standing and the hydrogel-supported membranes are shown in Figure 2.

When using apertures without a cast hydrogel support, the membranes appeared thick and did not thin automatically, as evidenced by a stable, low membrane array specific capacitance not exceeding 0.06 $\mu$F/$cm^2$ (Figure 2A). In contrast, $C_m$ values of 0.35 $\mu$F/$cm^2$ were observed for membranes formed on ETFE/hydrogel directly after membrane formation, indicating thin, decane-containing lipid bilayer membranes. Two trends in the specific capacitance values were observed for the hydrogel-supported membranes after membrane formation: (1) the specific capacitance stabilized at $C_m$ = 0.30 $\mu$F/$cm^2$, which is comparable to the 0.3−0.4 $\mu$F/$cm^2$ reported for decane-containing free-standing bilayers;[27] (2) the membranes spontaneously thinned further, and average specific capacitance values of 0.6 $\mu$F/$cm^2$ were observed, occasionally exceeding 0.9 $\mu$F/$cm^2$ (Figure 2A). Theoretical estimates for the specific capacitance of solvent-free lipid bilayers range from 0.75 to 0.81 $\mu$F/$cm^2$, while 0.78 $\mu$F/$cm^2$ was found experimentally for "solvent-free" membranes formed from squalene.[28] Our measurements suggest that the membranes formed in ETFE/hydrogel sandwiches, if not solvent-free, then at least contain only a small solvent fraction. The "solventless" membranes thus formed should be favorable for protein incorporation. On the basis of these results, we conclude that the hydrogel support significantly facilitates the formation of thin BLMs in the aperture arrays without the need for the manual thinning (painting) that is typically necessary to form thin membranes. Alternatively, the increase in specific capacitance observed for the supported BLMs (Figure 2A) could be attributed to an increase in the effective bilayer area due to hydrogel surface corrugation or due to a surface-induced expulsion of hydrocarbon solvent. Since the increment of the interfacial area is ≤11%, we conclude that the increase in capacitance is mainly due to an induced thinning of the lipid film. The average specific membrane resistance $R_m$ was above $10^5$ Ω $cm^2$ for all membranes (Figure 2B), indicating that the thinned membranes formed in the ETFE/hydrogel arrays cover all apertures in the array, as rupture of even a single aperture membrane would lead to a several-orders-of-magnitude increase in membrane conductance.[20,22] Furthermore, both the $C_m$ and $R_m$ values are comparable with reported results obtained for PEG-cushioned bilayers.[10]

Figure 2 monitors the lifetime of the membranes until the first out of 64 membranes ruptures, leading to an immediate increase in total conductance. After 15 min, membrane rupture occurred in the free-standing, non-thinned membranes. By comparison,

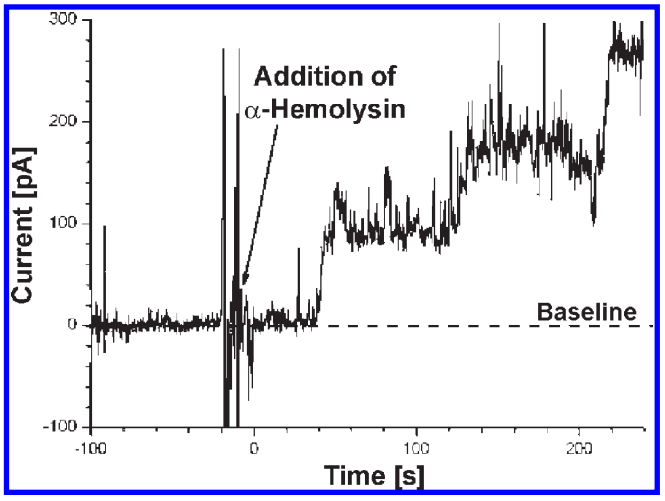


**Figure 4.** Current trace of a hydrogel-supported BLM indicating the formation of α-HL pores (mean step size 57 pA).

the first membrane ruptured after 60 min in the hydrogel-supported membrane arrays. Thus, addition of the composite hydrogel support significantly increased the time until first rupture. Although some membranes lasted for many hours with $C_m$ values >0.9 $\mu$F/cm$^2$, we believe that observing the time of first rupture as a better way to quantify membrane array lifetimes instead of reporting the "best mode" (i.e., the longest living membranes in each case), which may only correspond to a small number of successful experiments.

To obtain further insight into the membrane thinning, we used fluorescence microscopy to image formed membranes (Figure 3). Free-standing lipid films are thick, as indicated by the apertures being evenly filled with fluorescently labeled lipids (Figure 3A), and did not thin spontaneously until the time of first membrane rupture. When using the ETFE/hydrogel sandwich array structure, the lipid bilayer membranes formed immediately upon applying the lipid solution and thinned spontaneously with negligible Plateau−Gibbs tori (Figure 3B,C). The negligible Plateau−Gibbs tori and the apparent reduction in the diamond-shaped lipid area between apertures (compare part A with parts B and C of Figure 3) indicate that excess decane solvent from the lipid solution has been "squeezed out" during the membrane self-assembly and thinning process. The bright, nebulous region in Figure 3B is the residual bilayer-forming solution (primarily decane). In the horizontal chamber used, this solution floats to the water/air interface and thus appears as a diffuse area since the microscope focus plane is kept at the level of the upper surface of the ETFE/hydrogel sandwich. Over time this excess solution accumulates along the inner rim of the chamber outside the microscope field (compare part B with part C of Figure 3). To confirm the existence of thin lipid membranes located in the aperture array and demonstrate the functionality of the hydrogel-supported BLMs, α-hemolysin (α-HL) was added to the *cis* chamber of an existing hydrogel-supported BLM while the current trace of the BLMs was measured. The results are shown in Figure 4. The measurement was performed with a transmembrane potential of 60 mV in 10× PBS to obtain a sufficient signal-to-noise ratio for voltage-clamp recording of the 8 × 8 BLM array. In less than 1 min, α-HL heptamer channel formation in the membrane was observed as indicated by a stepwise increase in the current with a mean single channel current amplitude of 57 pA, which compared well to previously reported values obtained at equivalent ionic strength.[29]

In conclusion, we designed a highly water permeable composite hydrogel support consisting of polyHEMA, PEG, and silica particles to create a support for lipid membranes formed across an array of apertures in an ETFE partition. The hydrogel support significantly facilitates the formation of thin BLMs in the aperture arrays without the need for the manual thinning (painting) that is typically necessary to form thin membranes. The solventless hydrogel-supported membranes form rapidly over arrays of apertures and thin spontaneously with an increase rather than a decrease in membrane array lifetime, as compared to thicker, solvent-containing, free-standing membranes. Successful incorporation of α-hemolysin demonstrated that the BLMs are fully functional in close proximity to the polymeric material. With this approach, rapid fabrication of large arrays of BLMs that allow large flux transport across the supported membranes should be feasible.

## AUTHOR INFORMATION

### Corresponding Author

*Phone: +45 60 68 10 81. Fax: +45 45 93 16 69. E-mail: claus.helix.nielsen@fysik.dtu.dk.

### Author Contributions

⊥Shared first coauthorship.

## ACKNOWLEDGMENT

We thank H. Nørgaard Hansen and S. Gasparin at DTU-Mechanical Engineering for placing the Alicona InfiniteFocus at our disposal and for their help in its operation. This work was supported through MEMBAQ, a Specific Targeted Research Project (STREP), by the European Commission under the Sixth Framework Programme (Grant NMP4-CT-2006-033234), by the Danish National Advanced Technology Foundation (Grant 023-2007-1), and by a grant to DTU-Physics from the Danish National Research Foundation. C.H.N. was also supported by the Environment & Water Industry Development Council of Singapore (EWI) through Project MEWR 651/06/169.

## REFERENCES

(1) Martin, D. *Nanobiotechnology of Biomimetic Membranes*; Springer Verlag: New York, 2007.
(2) Nielsen, C. H. *Anal. Bioanal. Chem.* **2009**, *395*, 697–718.
(3) Tien, H. T.; Ottova, A. L. *J. Membr. Sci.* **2001**, *189*, 83–117.
(4) Ottova, A.; Ti Tien, H. *Bioelectrochemistry* **2002**, *56*, 171–173.
(5) Sackmann, E. *Science* **1996**, *271*, 43–48.
(6) Tamm, L. K.; McConnell, H. M. *Biophys. J.* **1985**, *47*, 105–113.
(7) Kuhner, M.; Tampe, R.; Sackmann, E. *Biophys. J.* **1994**, *67*, 217–226.
(8) Ide, T.; Yanagida, T. *Biochem. Biophys. Res. Commun.* **1999**, *265*, 595–599.
(9) Costello, R. F.; Peterson, I. R.; Heptinstall, J.; Walton, D. J. *Biosens. Bioelectron.* **1999**, *14*, 265–271.
(10) Lin, J.; Szymanski, J.; Searson, P. C.; Hristova, K. *Langmuir* **2010**, *26*, 3544–3548.
(11) Wagner, M. L.; Tamm, L. K. *Biophys. J.* **2000**, *79*, 1400–1414.
(12) Drexler, J.; Steinem, C. *J. Phys. Chem. B* **2003**, *107*, 11245–11254.
(13) Schmitt, E. K.; Vrouenraets, M.; Steinem, C. *Biophys. J.* **2003**, *91*, 2163–2171.

(14) Simon, A.; Girard-Egrot, A.; Sauter, F.; Pudda, C.; D'Hahan, N. P.; Blum, L.; Chatelain, F.; Fuchs, A. *J. Colloid Interface Sci.* **2007**, *308*, 337–343.
(15) Mey, I.; Stephan, M.; Schmitt, E. K.; Muller, M. M.; Ben Amar, M.; Steinem, C.; Janshoff, A. *J. Am. Chem. Soc.* **2009**, *131*, 7031–7039.
(16) Jeon, T.-J.; Malmstadt, N.; Schmidt, J. J. *J. Am. Chem. Soc.* **2005**, *128*, 42–43.
(17) Ibragimova, S.; Stibius, K.; Szewczykowski, P.; Perry, M.; Bohr, H.; Hélix-Nielsen, C. *Polym. Adv. Technol.* DOI: 10.1002/pat.1850 (in press).
(18) Vogel, J.; Perry, M.; Hansen, J. S.; Bolinger, P.-Y.; Nielsen, C. H.; Geschke, O. *J. Micromech. Microeng.* **2009**, *19*, 025026.
(19) Hansen, J. S.; Perry, M.; Vogel, J.; Groth, J. S.; Vissing, T.; Larsen, M. S.; Geschke, O.; Emneus, J.; Bohr, H.; Nielsen, C. H. *Anal. Bioanal. Chem.* **2009**, *395*, 719–727.
(20) Hansen, J. S.; Perry, M.; Vogel, J.; Vissing, T.; Hansen, C. R.; Geschke, O.; Emneus, J.; Nielsen, C. H. *J. Micromech. Microeng.* **2009**, 025014.
(21) Winther-Jensen, B.; Norrman, K.; Kingshott, P.; West, K. *Plasma Processes Polym.* **2005**, *2*, 319–327.
(22) Perry, M.; Vissing, T.; Boesen, T. P.; Hansen, J. S.; Emneus, J.; Nielsen, C. H. *Bioinspir. Biomimetics* **2009**, *4*, 044001.
(23) Roerdink Lander, M., Nielsen, C. H., Geschke, O. Manuscript in preparation.
(24) Pinnau, I.; Koros, W. J. *J. Polym. Sci., Part B: Polym. Phys.* **1993**, *31*, 419–427.
(25) Zhang, L. F.; Spurlin, T. A.; Gewirth, A. A.; Granick, S. *J. Phys. Chem. B* **2006**, *110*, 33–35.
(26) Gurtovenko, A. A.; Parta, M.; Karttunen, M.; Vattulainen, I. *Biophys. J.* **2004**, *86*, 3461–3472.
(27) Benz, R.; Frölich, O.; Läuger, P.; Montal, M. *Biochim. Biophys. Acta* **1975**, *394*, 323–334.
(28) White, S. H. *Biophys. J.* **1978**, *23*, 337–347.
(29) Hemmler, R.; Bose, G.; Wagner, R.; Peters, R. *Biophys. J.* **2005**, *88*, 4000–4007.

# Paper V

Manuscript – to be submitted

J. Vogel, M. Perry, C. Rein, P. P. Szewczykowski, M. Gruber, C. Hélix-Nielsen, O. Geschke; ***Novel multi-purpose module for forward osmosis***

**Novel multi-purpose module for forward osmosis**

*J. Vogel[1, 2], M. Perry[1], C. Rein[1, 3], P. P. Szewczykowski[4], M. Gruber[3], C. Hélix-Nielsen[1, 6], O. Geschke[1, 2]*

[1] Aquaporin A/S, Ole Maaløes Vej 3, 2200 Copenhagen N, Denmark
[2] DTU-Nanotech, Technical University of Denmark, DK-2800 Kongens Lyngby, Denmark
[3] Nano-Science Center and Department of Chemistry, University of Copenhagen, Universitetsparken 5, DK-2100 Copenhagen Ø, Denmark
[4] DTU-Chemical Engineering, Technical University of Denmark, DK-2800 Kongens Lyngby, Denmark
[6] DTU-Physics, Technical University of Denmark, DK-2800 Kongens Lyngby, Denmark

**Abstract:**

Forward osmosis promises to be a versatile tool in the area of membrane technologies. Its potential in seawater and brackish water desalination and upconcentration with minimal energy demand is significant and could help to solve the ever growing demand for fresh water. Thus the area of forward osmosis received a lot of interest in recent years. Several studies have been performed to optimize draw solutions and investigate concentration polarization phenomena. Furthermore, several different membranes were developed and investigated but unfortunately only one forward osmosis membrane is currently commercially available. This is mainly due to polarization issues and low fluxes when using existing membranes (e.g. reverse osmosis membranes). In this paper we developed a specially designed multi purpose forward osmosis module for FO membrane development. It offers the opportunity to use flat sheet membranes as well as alternatives like liquid membranes. In our multi-purpose FO module such a membrane type can be injected into a confined space where it is held in place by encapsulation membranes. The overall performance of the setup was characterized using a standard HTI forward osmosis membrane and the results (flux up to 13 L/m$^2$h) compare well with other studies. Therefore, the novel forward osmosis module presented in this paper is well suited for testing and characterization of various novel FO membranes.

**Introduction:**

In recent years, forward osmosis experienced a great increase in interest. It has been described and investigated in numerous articles as a new low-energy way to water purification and desalination [1-5]. It also shows potential in wastewater treatment, food processing and in the pharmaceutical industry [1]. In contrast to reverse osmosis, forward osmosis solely uses an osmotic pressure difference to force water through a filtration membrane. No external hydraulic pressure has to be applied which keeps the energy consumption to a low level. Forward osmosis can be described as a process where water penetrates a semipermeable membrane due to the differences in solute concentration between the two liquids on either side of the membrane. The feed stream contains molecules (e.g. water) that should be separated from the rest of the solution. The high concentration of molecules in the draw solution (also called osmotic agent or driving solution) generates the osmotic pressure that is needed to transport molecules across the membrane. The result is a dilution of the draw solution and an upconcentration of the feed.

The most important factors to make FO an economically feasible alternative to present filtration techniques are high flux combined with a high rejection rate. Flux defines the amount of permeate going through the membrane over time and the rejection rate tells us how many unwanted particles are rejected by the membrane. Both factors can be influenced by the draw solution and the membrane in itself. Several studies have investigated different draw solutions for various applications [5, 6]. However, what is still lacking are high-performance membranes. Cath [1] described that the desired membrane should have a high density active layer, a thin support, that it should be hydrophilic and have a low affinity to fouling. Several groups tried to use commercially available RO membranes in FO setups but all came to the conclusion that these membranes are not suited for forward osmosis application due to a very limited flux [6, 7]. In comparison, specially designed FO membranes are superior to RO membranes when operated in FO mode [1, 8]. Unfortunately, until now only one commercially available FO membrane exists. It is produced by Hydrations Technology Innovations (HTI) (Albany, Oregon) and has been widely used and investigated within the research community [4-6, 9, 10].

A factor that has to be taken into account when talking about membranes is concentration polarization (CP). It influences the membranes' performance and results in what McCutcheon called a 'lower than expected flux' [4]. In general, CP is a build-up of concentration gradients on both sides of the membrane. Using the boundary layer film model Baxter [11] calculates the concentration polarization modulus $c_{i_o}/c_{i_b}$ as:

$$\frac{c_{i_o}}{c_{i_b}} = \frac{\exp\left(J_v \delta / D_i\right)}{1 + E_o[\exp(J_v \delta / D_i) - 1]} \qquad (1)$$

where $J_v$ is the volume flux over the membrane, δ the boundary layer thickness, $D_i$ the diffusion coefficient and $E_o$ the membrane's intrinsic enrichment. This enrichment factor is defined as:

$$E_o = \frac{\mathrm{c_{i_p}}}{c_{i_0}} \qquad (2)$$

with $\mathrm{c_{i_p}}$ as the concentration of salt in the permeate and $c_{i_0}$ as the concentration of solute in feed at the membrane interphase.

In principle, there are two types of concentration polarization – internal and external. Gray [3] and McCutcheon [9] found that external concentration polarization as often observed in RO applications has minimal influence in FO applications. Here, several studies showed that the application of cross-flow and the use of spacers [12-18] minimize boundary layer and to such an extent that ECP can be neglected. As can be seen in (1), the magnitude of concentration polarization becomes exponentially smaller when decreasing the boundary layer thickness δ.

More important than external CP is the influence of internal CP. Internal concentration polarization can be further divided into dilutive ICP and concentrative ICP. If the active layer of the membrane faces the draw solution, as in PRO applications, solutes accumulate on the feed side inside thee porous support and concentrative internal CP occurs. It is comparable with concentrative external CP but occurs inside the confined space of the membrane. In FO applications where the active layer faces feed, solutes in the draw have to diffuse through the porous membrane to the

active layer. When now water permeates the active layer it dilutes the concentration of solutes at the active layer. This is called dilutive internal CP and causes the concentration at the inner active layer to be smaller than the concentration in the bulk which results in a smaller osmotic pressure and thus in a smaller driving force. A schematic overview over concentration polarization effects in FO can be found in Figure 1. Limiting ICP is of outmost importance in the development of new forward osmosis membranes [19]. McCutcheon [10] proposed two ways to limit ICP – limiting the flux or increasing the diffusion coefficient. Looking at the purpose of FO like desalination or upconcentration a limited flux would be counterproductive. Therefore, increasing the diffusion coefficient of the solute in the osmotic agent would be the better option to choose. One way to do that is to change the draw solution. This however, is something that is often difficult to do due to processing and/or economical limitations. Some draw solutions damage the membrane [20] and others are hard to separate from the permeate. The other option is to tailor the membrane where the porous support should be made thinner or more porous which would increase diffusion of solute to and away from the membrane.

Therefore, the modification of current membranes is a viable option but also the introduction of new types of membranes should be considered. One example would be the introduction of a liquid membrane. A liquid membrane has the purpose to build up a thin gaseous or liquid barrier between two miscible liquids or gases and thus regulated the mass transfer between both phases. The membrane strips one phase (feed phase) of a component or solute and transports it across to the other phase (stripping phase) where it releases the transported component again. The development of liquid membranes for filtration purposes has experienced a significant increase in interest over the last two decades. This is due to the great potential these membranes exhibit - high selectivity combined with high permeability and low energy demand [21, 22].

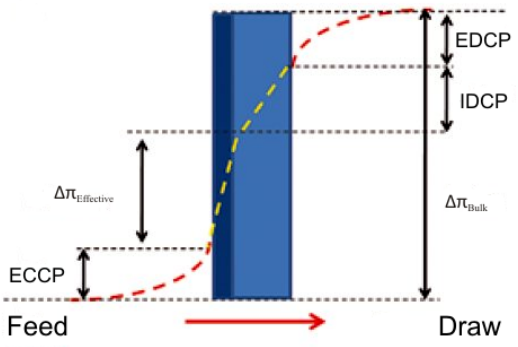


**Figure 1:** Schematic of polarization effects in FO; Instead of the bulk osmotic pressure $\Delta\pi_{Bulk}$ only the effective osmotic pressure defines the driving force for separation. The decrease in pressure is caused by concentration polarization effects in particular external concentrative CP (ECCP) at the active side of the membrane (dark blue) and internal dilutive CP (IDCP) inside the porous support (light blue) and external dilutive CP (EDCP) [20].

To be able to test all these possible candidates it would be beneficial to have a setup where different types of membranes can be easily applied. In the case of liquid membranes it is hard to imagine how those should be applied to current FO setups as described in [1]. This kind of membrane would require space in between two encapsulation membranes where the emulsion can be uniformly injected without leakage. The device, however, should also be easy to handle and cross-flow applicable so as to be able to compare it to current setups.

Here, we present a novel multi-purpose forward osmosis module which fulfils these requirements. Its performance has been tested, analyzed and optimized using the widely studied HTI FO membrane. This ensured

comparability to already published data and therefore to commonly used setups. In addition, the device has been investigated regarding injection of a possible liquid membrane in between two encapsulation membranes.

**Material and Methods**

The chamber has been developed and produced in cooperation of Aquaporin A/S (Copenhagen, DK), Kapacitet A/S (Hellerup, DK) and AR Engineering Systems (Singapore, SG). The clamping system consists of stainless steel and aluminum. The reservoirs are made of polycarbonate (PC). All other components, such as valves and O-rings are standard, commercially available parts. The membrane used to test and characterize the chamber was taken out of a SeaPack from HTI (Albany OR, USA). The feed was ultrapure water (Mili-Q system) and the draw was a 1 M NaCl solution. The active side of the membrane was oriented against the draw solution so as to minimize the influence of internal CP on the flux during the chamber performance experiments. Only trace amounts of ions are present on the porous support side and thus ICP does not occur in significant dimensions. The flux was measured using the increase in weight in the draw reservoir. The scale (Denver Instrument SI-2002) was connected to a computer so that the read-out of the measurements could be fully automated. The fluids were driven by a peristaltic pump (Longer pump BT100-1L, Baoding, CN) at a pumping velocity of 37.45 mL/min. The whole test setup can be seen in Figure 2, top right. The flux measurement to characterize the FO cell were carried out by having one FO membrane with the active side facing draw in the lower part of the centre piece. There was no second encapsulation membrane present at these tests.

A small magnetic stirrer could be added to the draw reservoir of the chamber to promote turbulence and so to minimize external CP. The so created vortexes helped mixing the solution and thus created a stable concentration at the membrane interphase. An additional steel grid was introduced to stabilize the inserted membranes. The grids were provided by Etch A/S (Farum, DK) and consisted of 150 µm thin steel with honeycomb shaped openings of 6 mm in width and a trapezoidal cross-section with the thinner part pointing towards the membrane. The special cross-section was chosen to have a stable grid and to have as less area of the membrane covered as possible. The more membrane area can contribute to the filtration the more permeate will be able to pass the membrane.

Flow simulations were performed using the open source CFD software package OpenFOAM (1.7.x). The computational mesh was constructed with the utility blockMesh and consisted of 551460 cells. To obtain good resolution near the membrane, the main chamber mesh was axially graded such that the first layers of grid points were distanced less than 5 µm from the membrane, which was modelled as a two-dimensional plane separating the feed and draw chamber. Grid independence was ensured by running the simulation on a similar mesh with 2311680 cells. The governing flow equations were assumed to be isothermal, incompressible and Newtonian and a concentration-dependent diffusion coefficient was introduced into the governing solute convection-diffusion equation. Draw and feed inlet velocities were set to 0.1 m/s while NaCl concentrations of 1 M and

0 M were specified at the draw and feed inlet, respectively. The remaining boundary conditions, including those describing salt and water flux through the membrane, were implemented according to previous studies on symmetric membranes [23].

**Results**

*The FO chamber*

The complete setup of the chamber can be seen in Figure 2, top left. It consists of two PC plates with integrated channels that connect the outside to the inner reservoirs (Figure 2, top left A). The inlet channels are split up into three and exit into the reservoir in a 145 degree angle so that they point directly at the membrane to ensure turbulences along its surface. The slope at the outside of the reservoir is used to clamp the O-rings into the centre piece and ensure a tight sealing. The centre piece is the heart of the multi-purpose forward osmosis module (Figure 2, top left B). It holds the encapsulation membranes and enables the injection of liquid membrane emulsion in a defined space. The distance between the encapsulation membranes is kept constant by the balcony inside the centre piece. It has a thickness of 600 µm and two inlets of 300 µm in diameter (Figure 2, bottom). A tight seal and proper clamping is ensured via the clamping system. It consists of a plunger, a clamp and three steel columns that hold the whole device in place. When lowering the ledge the steel columns press the reservoirs together, the reservoir edges slide into the O-rings and ensure that the centre piece is hold in place and tightly sealed from the outside. The only access points are now the inlet/outlet of the feed and draw and the injection channels inside the centre piece.

*Influence of metal support grids*

The metal support grids where added to stabilize the inserted membranes and to prevent them from bulging outwards. Being an additional component, their influence on the flux had to be investigated as well. Several tests were carried out using no grid, the grid in its normal direction (thinner end of trapezoidal structure facing membrane), an inverted grid and the grid glued to the membrane. The glue was added in an attempt to ensure grid and membrane are connected and so to further minimize bulging of the membrane. The metal supports were always put on the active side of the membrane because it was expected that they create additional turbulence and thus help minimize external CP. The results of these tests can be found in Figure 4.

*Influence of stirring*

After ensuring the proper use of the metal grids a second additional component was introduced into the system, namely a magnetic stirrer. It was added in an attempt to investigate if the flux over membrane can be improved by creating additional turbulences inside the draw reservoir. Additional turbulences should further minimize external CP and thus result in a higher flux. During the experiment the speed of the stirring was increased in three steps from 0 rpm to 1600 rpm and the flux was measured continuously. Figure 5 displays the effect that could be achieved.

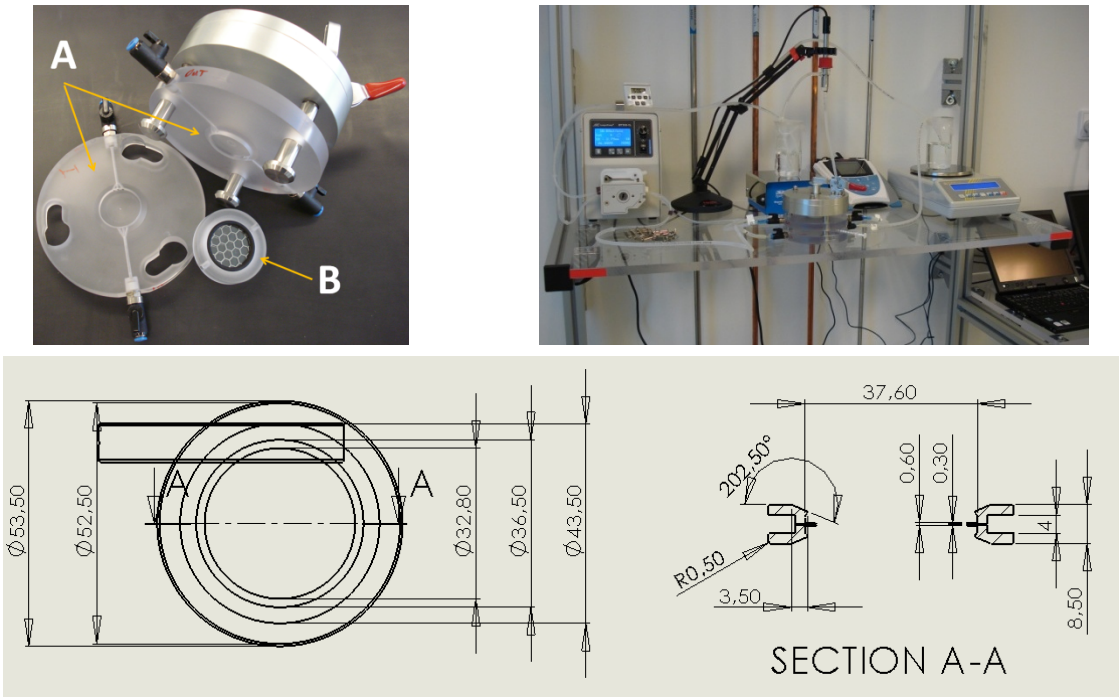


**Figure 2:** Novel multi purpose module chamber for forward osmosis; top left: disassembled chamber with feed and draw reservoir (A) and centre piece with additional metal grid support and O-rings (B); complete FO setup with peristaltic pump, magnetic stirrer for feed reservoir, conductivity meter, scale for draw reservoir and computer for automated recording (from left to right); bottom: technical drawing with dimensions for the centre piece that can be used for single membranes or membrane combinations.

*Influence of flow rate*

Another parameter that had to be investigated within the characterization of the newly designed FO chamber was the influence of flow rate. Here, a higher flow rate should result in a higher flux due to increased formation of turbulence at the membrane interface. In our setup, with MilliQ water as feed, this should further minimize the external CP at the draw side. Within a continuous measurement we changed the flow rate of feed and draw at the same time from 10 mL/min to the maximum value of 37.45 mL/min. No further steps in between were chosen because the envisioned effect should be most prominent when changing from very low to high. As expected, the flux over membrane changed considerably when increasing the flow rate (Figure 6).

*Salt flux*

An additional part of our forward osmosis setup was the continuous conductivity measurement in the feed circuit. This was done to monitor the performance of the membrane and to ensure that no leaks appeared. A rapid increase in salt concentration on the feed side would suggest a leak in the system where NaCl solution can cross the membrane unhindered. The conductivity meter (Orion 3 star conductivity benchtop, Thermo Fisher Scientific Inc., Waltham, USA) was incorporated into the experimental setup at a position directly after the feed exited the FO chamber. The increase in conductivity over time (see Figure 7 for a typical example) was then used to determine the salt flux. Here, we relate the increase of conductivity over time to a concentration of salt in the feed and thus can calculate the overall salt flux from the draw solution into the feed to

monitor the performance of the membrane. After making a standard curve with different concentrations of NaCl in MilliQ the salt flux can be calculated by:

$$J_{NaCl} = \frac{V_{\%\,NaCl} * \rho}{V_{feed} * t * A} \qquad \left[\frac{kg}{m^2 * h}\right]$$

where $V_{\%\,NaCl}$ is determined with the help of a previously prepared standard curve relating conductivity to salt concentration, $\rho$ the density of NaCl, $V_{feed}$ the volume in the feed circuit, $A$ the active area of the membrane and $t$ the passed time.

*Filling of centre*

To demonstrate and investigate the filling of the space between the encapsulation membranes an external clamp was constructed. This allowed us to clamp the centre piece as it would be done in the FO chamber with the difference that an observation of the filling process was possible. A coloured squalene dummy solution was used for this purpose. This was done because squalene has a higher viscosity than water and therefore was better suited to mimic a liquid membrane. For visualization purposes, a transparent polymeric foil was used instead of non-transparent encapsulation membranes.

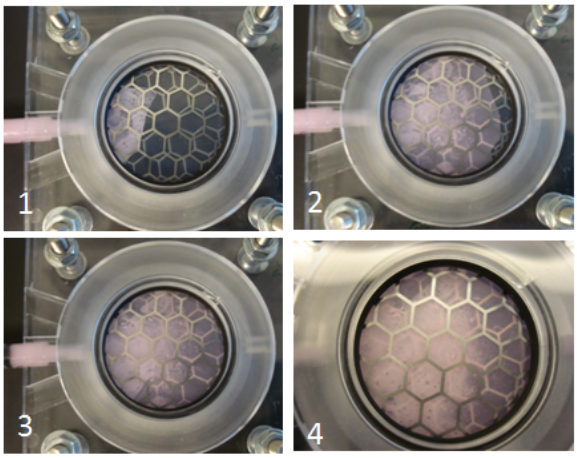


**Figure 3:** Filling of the centre piece with the squalene dummy. From left to right: After starting the injection, the emulsion spreads out evenly throughout the space in between the encapsulation. To visualize the filling a homemade clamp and a transparent polymeric foil as encapsulation membranes was used.

**Discussion**

The fabrication of the multi-purpose module was carried out using standard CNC-milling equipment and is therefore neither time-consuming nor cost-intensive. The only critical component is the centre piece with the small 300 µm hole drilled through a 600 µm thin balcony. Here, our partners that fabricated the device experienced smaller inconveniences in the beginning but were able to overcome those and deliver a constantly high quality. That means that once the production process is established the device can be easily and cost efficiently produced in higher numbers.

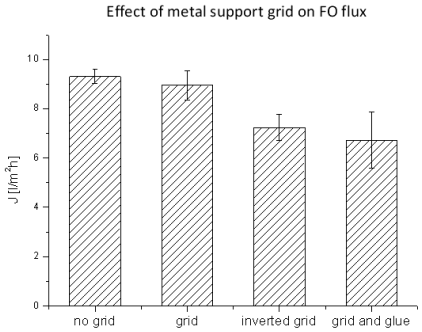


**Figure 4:** Effect on FO flux by including a metal grid and/or gluing of HTI membranes to the grid. HTI membranes were soaked overnight in MilliQ water prior to use. 37.45mL/min flow rate in feed and draw loops. Feed/Draw: MilliQ/1M NaCl. The salt flux was less than 2.5 g/m$^2$*h in all three experiments. Dow Corning 3140 Silicone glue was used to glue membranes to metal grids. The glue was allowed to dry overnight.

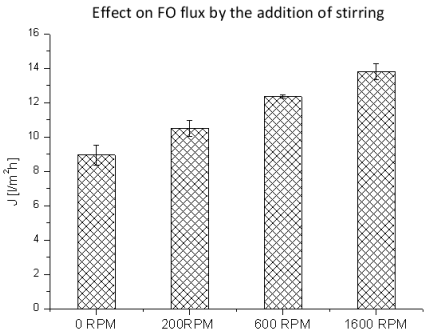


**Figure 5:** Effect of FO flux across a HTI membrane by adding a magnetic stirrer in the draw chamber. The HTI membrane was soaked overnight in MilliQ water prior to use. 37.45 mL/min flow rate in feed and draw loops. Feed/Draw: MilliQ/1M NaCl. The salt flux was less than 2.5 g/m$^2$*h throughout the experiment. The data were acquired in a continuous measurement series of a single HTI membrane.

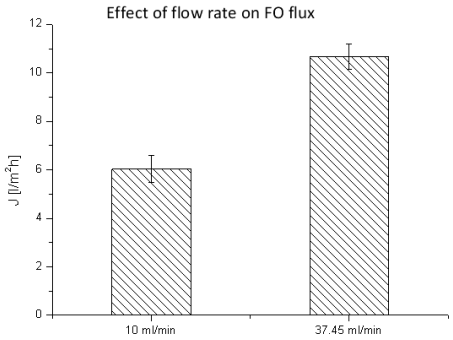


**Figure 6:** Effect of flow rate in feed and draw circuit on FO flux across a HTI membrane. The HTI membrane was soaked in MilliQ water overnight prior to use. A metal support grid was applied on the draw side of the membrane. The flow rate was changed in a continuous measurement.

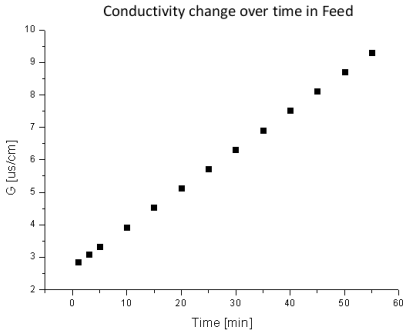


**Figure 7:** Typical example of a continuous measurement of conductivity in the feed circuit. The salt flux in this experiment was 2.38 g/m$^2$*h. The HTI membrane was soaked overnight in MilliQ water prior to use. 37.45 mL/min flow rate in feed and draw loops. Feed/Draw: MilliQ/1M NaCl.

The reference measurements performed with a commercially available FO membrane show that the grids do not hinder the flux considerably. A slight decrease could be observed when introducing a grid but taking the standard deviation of the tests into account this decrease is insignificant. However, this does not hold true when applying the metal support in its reverse configuration or when gluing the grid to the membrane. Here we observed significant decreases of flux of 22 % and 28 % accordingly. This can be explained by a reduced active area. If the grid is applied in the reverse direction more area at the membrane is blocked. Even more membrane area is blocked when introducing glue. Here, the authors suggest that glue seeps into the pores of the membrane, block them and so considerably decrease the area that is available for filtration. Similar flux rates with and without grids is a positive result but also suggests that the metal support does not create additional turbulence at the membrane interface. With a thickness of 150 µm it is likely to be too thin to have greater influence. In contrast, the addition of a magnetic stirrer into the system shows

significant influence on flux over the membrane. This effect is visualized in the presented flux data where an increase in water flux of 54 % from 0 rpm stirring to 1600 rpm stirring could be observed. The big increase in flux can be explained with the introduction of vortexes into the system which cause a reduction of CP. Flow profile simulations inside the reservoirs showed that no vortexes are introduced by the inlet channels. Only small turbulences can be observed in between and on either side of the inlet channels. Figure XX shows that the overall flow profile inside the chamber and along the membrane is linear and CP can take effect unhindered. This changes when introducing the stirrer which causes the flow to be turbulent and a reduction of the unstirred layer at the membrane surface. The magnetic stirrer can be exchanged for a spacer as widely reported in literature [12-14, 18]. The same effect as the stirring has the flow rate of feed and draw. We have shown that a 4 times increase in flow rate results in a 77 % increase in flux. This can again be explained by a reduction of external CP. Furthermore, we have shown that our novel multi-purpose chamber would also be suited for investigating the behaviour of liquid membranes. As documented in

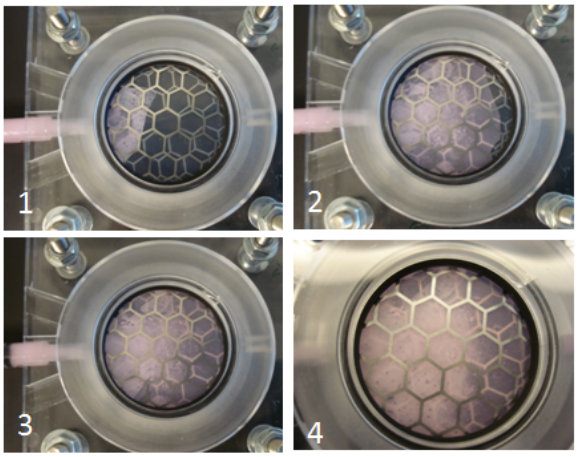


Figure 3, an injected viscous liquid spreads out evenly and fills the entire space in between the encapsulation membranes uniformly. This is necessary to ensure that transport over the membrane is caused by the injected components and not by a leak. The encapsulation membranes are further stabilized by the metal grids. This additional stability is expected to be beneficial because a bulging membrane could lead to a leaky liquid membrane which then would hinder the membrane to perform as expected. A possible scenario is sketched in Figure 9.

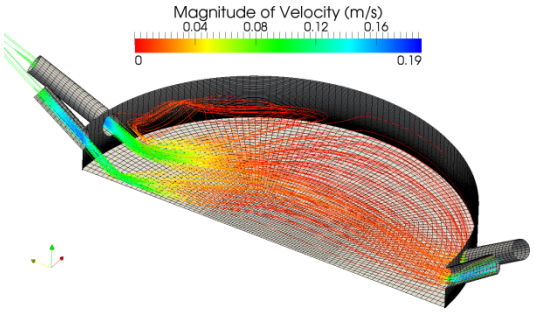


**Figure 8:** Flow profile simulation inside the top reservoir shows that most flow is linear and no vortexes are generated except on both sides of the inlet channels.

The, together with the multi-purpose module, used measurement setup enabled us to make precise and automated experiments without an operator being present at all times. Due to the automated weight and conductivity analysis we were able to reproducibly perform test series that were comparable with each other and existing data from other groups. An advantage of weight over volume measurements is that no additional correction of the measured values in regards to volume increase by temperature has to be performed. The measured weight values can directly be used to determine the flux over the membrane.

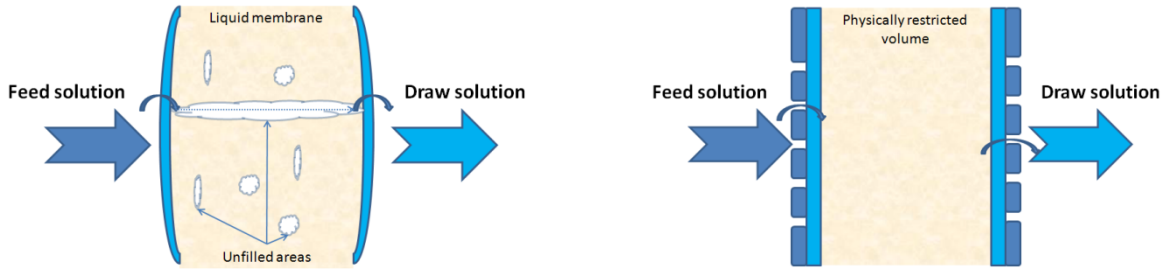


**Figure 9:** schematic of a liquid membrane between two encapsulation membranes. Left: without support the membranes could bulge up uncontrolled and leave free areas where water could pass unfiltered. Right: when properly contained the liquid membrane has no open interspaces and water can only pass the assembly through the liquid membrane

## Conclusion

Our novel multi-purpose module is well suited for FO experiments. The whole setup has proven to give reliable and reproducible results. Similar experiments performed by Xu et al. [5] with a flux at 8 L/m$^2$h for an 0.8 M NaCl draw solution, Gray et al. [3] with a flux of 18 L/m$^2$h for a pressure of 40 atm generated by a NaCl solution and Cath et al. [2] with a flux of 8.29 L/m$^2$h at 49 bar osmotic pressure show that flux values vary considerably and depend strongly on the test setup. With values of up to 13.8 L/m$^2$h our multi-purpose forward osmosis module compares well to existing flat sheet membrane setups. Tests showed that the influence of external CP can be successfully minimized. How the chamber reacts to internal CP needs to be seen and depends strongly on the membranes that will be tested in the setup. Furthermore the specially designed centre piece can also be used for the investigation of the performance of the liquid membranes in forward osmosis. We were able to evenly fill the space in between two membranes with a squalene dummy without leaving any leak. It is therefore assumed that the only way for water to pass the membrane would be actually through the injected components.

## Acknowledgements

We would like to thank Thomas Heinstrup Vikkelsø (Kapacitet A/S) and Andrew Tan (AR Engineering Systems) for their help with the design and production of the FO chamber.

## References

1. Cath, T., A. Childress, and M. Elimelech, *Forward osmosis: Principles, applications, and recent developments.* Journal of membrane science, 2006. **281**(1-2): p. 70-87.
2. Cath, T.Y., J.E. Drewes, and C.D. Lundin, *A Novel Hybrid Forward Osmosis Process for Drinking Water Augmentation using Impaired Water and Saline Water Sources.* 2009: p. 1-84.
3. Gray, G., J. McCutcheon, and M. Elimelech, *Internal concentration polarization in forward osmosis: role of membrane orientation.* Desalination, 2006. **197**(1-3): p. 1-8.
4. McCutcheon, J., R. McGinnis, and M. Elimelech, *Desalination by ammonia-carbon dioxide forward osmosis: Influence of draw and feed solution concentrations on process performance.* Journal of membrane science, 2006. **278**(1-2): p. 114-123.
5. Xu, Y., et al., *Effect of draw solution concentration and operating conditions on forward osmosis and pressure retarded osmosis performance in a*

*spiral wound module.* Journal of membrane science, 2010. **348**(1-2): p. 298-309.
6. Garcia-Castello, E., J. McCutcheon, and M. Elimelech, *Performance evaluation of sucrose concentration using forward osmosis.* Journal of membrane science, 2009. **338**(1-2): p. 61-66.
7. Dertinger, T., et al., *Surface sticking and lateral diffusion of lipids in supported bilayers.* Langmuir, 2006. **22**(22): p. 9339-9344.
8. Yip, N.Y., et al., *High Performance Thin-Film Composite Forward Osmosis Membrane.* Environ. Sci. Technol, 2010. **44**: p. 3812-3818.
9. McCutcheon, J. and M. Elimelech, *Influence of concentrative and dilutive internal concentration polarization on flux behavior in forward osmosis.* Journal of membrane science, 2006. **284**(1-2): p. 237-247.
10. McCutcheon, J. and M. Elimelech, *Influence of membrane support layer hydrophobicity on water flux in osmotically driven membrane processes.* Journal of membrane science, 2008. **318**(1-2): p. 458-466.
11. Baker, R.W., *Membrane Technology and Applications*. second ed. 2004: John Wiley & Sons, Ltd.
12. Balster, J., et al., *Multi-layer spacer geometries with improved mass transport.* Journal of membrane science, 2006. **282**(1-2): p. 351-361.
13. Belfort, G., *Membrane modules: comparison of different configurations using fluid mechanics.* Journal of membrane science, 1988. **35**(3): p. 245-270.
14. Li, F., et al., *Novel spacers for mass transfer enhancement in membrane separations.* Journal of membrane science, 2005. **253**(1-2): p. 1-12.
15. Phattaranawik, J., R. Jiraratananon, and A. Fane, *Effects of net-type spacers on heat and mass transfer in direct contact membrane distillation and comparison with ultrafiltration studies.* Journal of membrane science, 2003. **217**(1-2): p. 193-206.
16. Phattaranawik, J., et al., *Mass flux enhancement using spacer filled channels in direct contact membrane distillation.* Journal of membrane science, 2001. **187**(1-2): p. 193-201.
17. Schwinge, J., D. Wiley, and A. Fane, *Novel spacer design improves observed flux.* Journal of membrane science, 2004. **229**(1-2): p. 53-61.
18. Schwinge, J., et al., *Characterization of a zigzag spacer for ultrafiltration.* Journal of membrane science, 2000. **172**(1-2): p. 19-31.
19. Mccutcheon, J. and M. Elimelech, *Modeling water flux in forward osmosis: Implications for improved membrane design.* AIChE Journal, 2007. **53**(7): p. 1736-1744.
20. Hèlix-Nielsen, C., *Osmotic water purification: Insights from nanocale biomimetics.* ENT Magzine, 2010(March-April).
21. Franken, T., *Liquid membranes-academic exercise or industrial separation process.* Membrane Technology, 1997. **1997**(85): p. 6-10.
22. San Romãn, M.F., et al., *Liquid membrane technology: fundamentals and review of its applications.* J. Chem. Technol. Biotechnol., 2010. **85**(1): p. 2-10.
23. Wardeh, S. and H.P. Morvan, *CFD simulations of flow and concentration polarization in spacer-filled channels for application to water desalination.* Chem.Eng.Sci, 2008. **86**: p. 1107-1116.

# Appendix I

WO/2009/074155 (2008)

Vogel J., Perry M., Nielsen C.H., Hansen J.S., Jensen P.H., Geschke O., Bolinger P.-Y.;

***Scaffold for composite biomimetic membrane***

(12) INTERNATIONAL APPLICATION PUBLISHED UNDER THE PATENT COOPERATION TREATY (PCT)

(19) World Intellectual Property Organization
International Bureau

(43) International Publication Date
18 June 2009 (18.06.2009)

PCT

(10) International Publication Number
WO 2009/074155 A1

(51) International Patent Classification:
*B01D 69/14* (2006.01) *B01D 69/10* (2006.01)
*B01D 69/02* (2006.01)

(21) International Application Number:
PCT/DK2008/050303

(22) International Filing Date:
11 December 2008 (11.12.2008)

(25) Filing Language: English

(26) Publication Language: English

(30) Priority Data:
PA 2007 01771 11 December 2007 (11.12.2007) DK
61/082,087 18 July 2008 (18.07.2008) US

(71) Applicant *(for all designated States except US)*: **AQUAPORIN A/S** [DK/DK]; Diplomvej 377, DK-2800 Kgs. Lyngby (DK).

(72) Inventors; and

(75) Inventors/Applicants *(for US only)*: **VOGEL, Jörg** [DE/DK]; Dortheavej 17, 2nd Floor, No. 9, DK-2400 Copenhagen Nv (DK). **PERRY, Mark Edward** [GB/DK]; Søllerød Park, Block 4, flat 1, DK-2800 Holte (DK). **NIELSEN, Claus Hélix** [DK/DK]; Kærmindevej 1, DK-2630 Høje-taastrup (DK). **HANSEN, Jesper Søndergaard** [DK/DK]; Kildebakkegaards Allé 110, DK-2860 Søborg (DK). **JENSEN, Peter Holme** [DK/DK]; Classensgade 11, 3rd floor, DK-2100 Copenhagen Ø (DK). **GESCHKE, Oliver** [DE/DK]; Høstvej 4, DK-2800 Kgs. Lyngby (DK). **BOLINGER, Pierre-Yves** [CH/CH]; Untere Zelgistrasse 2, CH-8600 Dübendorf (CH).

(74) Agents: **RASMUSSEN, Torben Ravn** et al.; Rigensgade 11, DK-1316 København K (DK).

(81) Designated States *(unless otherwise indicated, for every kind of national protection available)*: AE, AG, AL, AM, AO, AT, AU, AZ, BA, BB, BG, BH, BR, BW, BY, BZ, CA, CH, CN, CO, CR, CU, CZ, DE, DK, DM, DO, DZ, EC, EE, EG, ES, FI, GB, GD, GE, GH, GM, GT, HN, HR, HU, ID, IL, IN, IS, JP, KE, KG, KM, KN, KP, KR, KZ, LA, LC, LK, LR, LS, LT, LU, LY, MA, MD, ME, MG, MK, MN, MW, MX, MY, MZ, NA, NG, NI, NO, NZ, OM, PG, PH, PL, PT, RO, RS, RU, SC, SD, SE, SG, SK, SL, SM, ST, SV, SY, TJ, TM, TN, TR, TT, TZ, UA, UG, US, UZ, VC, VN, ZA, ZM, ZW.

(84) Designated States *(unless otherwise indicated, for every kind of regional protection available)*: ARIPO (BW, GH, GM, KE, LS, MW, MZ, NA, SD, SL, SZ, TZ, UG, ZM, ZW), Eurasian (AM, AZ, BY, KG, KZ, MD, RU, TJ, TM), European (AT, BE, BG, CH, CY, CZ, DE, DK, EE, ES, FI, FR, GB, GR, HR, HU, IE, IS, IT, LT, LU, LV, MC, MT, NL, NO, PL, PT, RO, SE, SI, SK, TR), OAPI (BF, BJ, CF, CG, CI, CM, GA, GN, GQ, GW, ML, MR, NE, SN, TD, TG).

**Published:**
— *with international search report*

(54) Title: SCAFFOLD FOR COMPOSITE BIOMIMETIC MEMBRANE

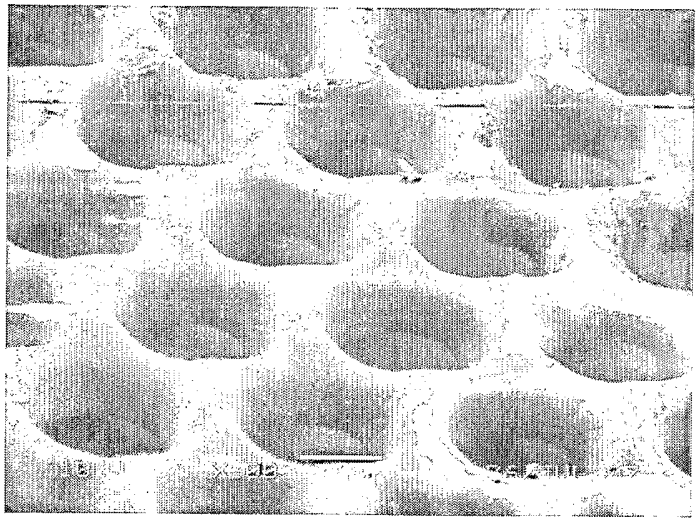

Fig. 2

(57) Abstract: Disclosed herein is a membrane scaffold comprising a planar material having a hydrophobic surface and a functional area comprising a plurality of apertures. The apertures have a diameter of from about 80µm to about 3000µm and the rims of the apertures comprise bulges extending above and/or below the surface level of the planar material. The membrane scaffold is useful in the preparation of a composite biomimetic membrane wherein functional channel forming molecules have been incorporated in said membrane.

WO 2009/074155 A1

# SCAFFOLD FOR COMPOSITE BIOMIMETIC MEMBRANE

## FIELD OF THE INVENTION

The present invention relates to a planar hydrophobic membrane scaffold having multiple apertures suitable for the formation of biomimetic membranes, a method for producing the membrane scaffold, a composite biomimetic membrane comprising said scaffold, a filtration device comprising the composite biomimetic membrane, as well as a method of preparing said composite biomimetic membrane.

## BACKGROUND

Membranes comprising an artificial lipid bilayer with incorporated functional molecules, such as ion channel peptides and transmembrane proteins are useful in a diverse range of technical applications. A common theme for such membranes is the need for stability of the membranes over time and against mechanical, electrical and chemical impacts. Planar lipid bilayers are usually supported in apertures or perforations of a scaffold or septum separating two solution compartments. Various hydrophobic materials have been used as scaffolds, including an amorphous Teflon® (Teflon® AF) film, cf. Mayer et al. (Bio physical Journal Vol 85, Oct. 2003, 2684-2695). Various methods of fabrication of such a scaffold having a single aperture or a plurality of apertures have been described, e.g. puncturing the scaffold film with a needle, or a heated wire and various other mechanical methods. It is reported that useful materials for the preparation of lipid or amphiphilic bilayer membranes are Teflon films and other membrane materials with hydrophobic surface properties. Current methods of preparing BLMs include the solvent free Folded bilayers method described by Montal & Muller (1972, PNAS, 69:3561-3566) which require small apertures (< 100 μM) and the solvent containing Painted bilayers method described by Muller & Rodin (1969, Cur. Top. Bioeng. 3:157-249) which is optimal for apertures of up to 400 μm. Both methods are useful in the preparation of a BLM in a single aperture or a small number of apertures such as less than 5 in a hydrophobic partition, but they are not straight forward to scale into

multi aperture partitions. Establishing a folded membrane often requires multiple lowerings and raisings of the aqueous solutions which may compromise the simultaneous formation of a plurality of membrane units. Formation of painted membranes requires manual prepainting of the single aperture, which, when scaled up will lead to considerable variation in painting quality.

Since the discovery of the aquaporin water transport proteins distinguished by their ability to selectively transport $H_2O$ molecules across biological membranes there has been a certain interest in devising an artificial water membrane incorporating these proteins, cf. published US Patent Application No. 2004/0049230 "Biomimetic membranes" which aims to describe how water transport proteins are embedded in a membrane to enable water purification. The preferred form described has the form of a conventional filter disk. To fabricate such a disk, a 5 nm thick monolayer of synthetic triblock copolymer and aquaporin protein is deposited on the surface of a 25 mm commercial ultrafiltration disk using Langmuir-Blodgett transfer. The monolayer on the disk is then crosslinked using UV light to the polymer to increase its durability. It has been suggested that a water purification technology could be created by expressing the aquaporin protein into lipid bilayer vesicles and cast these membranes on porous supports, cf. James R. Swartz, home page at http://cheme.stanford.edu/faculty/jswartz.html

WO 2006/122566 discloses a membrane for filtering of water comprising a sandwich construction having at least two permeable support layers separated by at least one lipid bilayer comprising functional aquaporin water channels. WO 2006/122566 also discloses a hydrophobic film comprising evenly distributed perforations having a uniform shape and size, where the lipid bilayer is formed in the perforations. It is stated that the hydrophobic material has a degree of hydrophobicity corresponding to a contact angle of at least 100° between a droplet of deionised water and the hydrophobic material, where the contact angle measurement is performed at 20°C and atmospheric pressure, but higher degrees of hydrophobicity are preferred, such as those corresponding to contact angles of at least 105°, 110°, or 120°. A preferred

hydrophobic material is Teflon. The polymer film comprises multiple perforations, wherein said perforations are evenly distributed in the film and substantially all of the same geometric shape in the intermediate plane between the 2 surfaces of the film. The perforations typically have a maximum cross-sectional length in the nm to mm range, such as in the µm range, and the films as such typically have a thickness in the µm to mm range. The geometric shape of the perforations is selected from circular and elliptical, and it is stated that both shapes are easily obtainable when using laser equipment for introducing the perforations in the film. For instance, circular apertures can be obtained by using a stand-still laser beam, whereas movement of the film relative to the laser beam (either by moving the film or the laser beam) during exposure would provide an elliptical perforation. The hydrophobic polymer films of this prior art contains multiple perforations or apertures which are suitable for the support of a biomimetic membrane, such as a bilayer lipid membrane. While it is preferred that the apertures' geometric shape is circular corresponding to a cylindrical form or ellipsoidal corresponding to an elliptic cylinder (rod-like shape) there is a lack of specific teaching as to a preferred or optimal shape of the aperture rim. The present inventors have realised that the characteristics of the aperture rim is highly correlated with the longevity of the biomimetic membranes formed in said apertures and besides, that use of the ETFE material for the formation of aperture arrays enables preparation of highly stable composite biomimetic membranes.

SUMMARY OF THE INVENTION

The present invention relates to a membrane scaffold comprising a planar material having a hydrophobic surface and a functional area comprising a plurality of apertures, wherein the apertures have a diameter of from about 80 µm to about 3000 µm, preferably 800 µm and the rims of the apertures comprise bulges extending above and/or below the surface level of the planar material. The bulging of the rims may contribute to the stabilisation of the scaffold material and/or bilayer membranes, such as BLMs, subsequently formed in the scaffold. Thus, due to the bulging

rims it is possible to position the plurality of apertures close to each other without risking the breakage of the membrane scaffold. Thereby, the present invention offers the advantage of obtaining a highly effective membrane area, i.e. a high perforation area in the functional area, without destabilisation of the membrane scaffold during operation. In addition, the functional scaffold area can be up-scaled to 20 $cm^2$ or more even when fabricated in very thin planar material of less than 200 µm thickness.

The hydrophobic surface of the membrane scaffold usually has a water contact angle larger than 90°, such as larger than about 100°. Specific examples of the planar material include a fluoropolymer film, such as a Teflon (polytetrafluoroethylen, PTFE) or a polyethylenetetrafluoroethylene (ETFE) film including suitable derivatives thereof.

The functional area comprises a plurality of apertures and may be formed using an optically induced or stimulated thermal process. The cross section of said apertures in said planar material is essentially of a circular or approximately circular shape viewed from above and has an essentially perpendicular axis relative to the plane of said planar material. The apertures are characterized by rims, which are smooth and expand to bulges, which are formed onto the surface of said planar material. The functional area of the membrane scaffold may be optimized to obtain a perforation as high as possible while maintaining the physical integrity during operation of the ensuing membrane.

In a certain aspect of the invention, the perforated area of the functional area is 20% or above. In preferred embodiments the perforated area covers from about 30 % to about 60 % of said functional area. In the membrane scaffold according to the invention the aperture rim may have a toroidal bulging which contributes to stabilization of the membranes formed in the apertures. It is presently believed that the bulging rims of the apertures are able to support a sufficiently large torus (or annulus) of fluid amphiphilic lipid membrane forming solution, which probably participates in stabilizing the bilayer membrane.

The diameter of the apertures may vary according to the design needs within the range of 80 to 800 µm and they may be produced with

a diameter of up to 3000 µm. Experiments have shown that bilayer lipid membranes form easily in apertures of 200 µm to about 300 µm, especially 250 µm to about 450 µm. Typically the membranes last from 24 hours to 13 days. The number of apertures in the functional area is normally 25 or more to obtain a high effective membrane area. In a preferred aspect of the invention, the number of apertures is 64 or above, such as 100 or above. The apertures are usually distributed in a certain pattern in the functional area, such as a hexagonal pattern, a triangular pattern or a rectangular or square pattern. A regular pattern may be preferred in the scaffolds of the invention due to the ease of manufacturing and reproducibility.

The bulges of the rims extend above the surface of the planar material to obtain a higher physical stability. When measuring the bulge heights using atomic force microscopy they are found to extend 6 µm or more above the level of the planar material. A typical range of bulge heights is from about 6 to about 20 µm. In a preferred aspect of the invention, the bulges of neighbouring apertures may be merged into a common bulge. In this instance, which is found between apertures in the inner rows and columns of the scaffold array, the bulges can generally be higher, e.g. measured up to about 15 µm (Height of merged bulges (triple point) = 15.3 ± 4.4 µm, and height of merged bulges (center) = 12.7 ± 6.4 µm) for specific 3x3 aperture scaffolds produced in Tefzel 200LZ having a center-to-center distance of 400 µm and an aperture diameter of 295 - 300 µm, and where the outer, non-merged bulges were measured to be 9.7 ± 1.7 µm. The merging of the bulges may be entirely to obtain a single bulge (center) between neighbouring bulges or partly according to which the individual bulges may still be discerned (triple point). The aperture rims are usually smooth to support the longevity of the biomimetic membrane formed in the apertures.The center-to-center distance of neighbouring apertures may vary in a functional area. To obtain a high aperture density, the distance is usually not below 120 µm nor above 4000 µm. In a preferred aspect, the center-to-center distance is from about 150 µm to about 500 µm. The planar material may have any suitable thickness.

Generally, it is suitable to use a planar material that has a thickness of from about 25 µm to about 200 µm. A preferred ETFE film has a thickness of about 50 µm to about 75 µm. The hydrophobic surface of the membrane scaffold material may be covered with a coating, e.g. deposited through chemical vapour deposition. The coating may serve various functions, such as enhancement of the formation of the membrane, stabilisation of the membrane, improvement of the smoothness of the surface, and reinforcement of the membrane scaffold. The coating may be applied onto the scaffold membrane and adhered thereto or chemically bonded to the surface of the scaffold membrane. The coating may for instance be a homogeneous layer of a hydrophobic substance when a lipid bilayer membrane is intended. The initial pre-treatment with a lipid solution ensures a higher stability of the membrane. The lipid layer may be applied by any suitable means including spraying and painting. Usually, the lipid solution is applied several times to the scaffold with intermediate drying periods. According to another embodiment, a compound is chemically bonded to the surface, e.g. by a covalent bonding. As an example, the hydrophobic surface of the planar material may be modified by reaction with sodium naphthalenide as disclosed by Ayurova, O. Zh., et al., Russian Journal of Applied Chemistry, vol. 78, No. 5, 2005, pp. 850-852.

In addition, the present invention relates to a method for producing the membrane scaffold. The method includes the steps of:

a. providing a planar material having a hydrophobic surface,

b. subjecting a spot of a functional area of the planar material to a laser beam having a wave length absorbed by the planar material for a time and a power sufficient for the planar material to melt and/or vaporize at said spot,

c. allowing the melted material to solidify around the spot, thereby forming a bulging aperture rim,

d. displacing the planar material or the laser beam to another spot of the functional area and

e. repeating steps b. to d. until a plurality of apertures have been formed.

The method for production of the scaffold includes the use of a laser beam, which preferably is provided by a $CO_2$ laser, and the planar material is preferably a polyethylenetetrafluoroethylene (ETFE) film or a derivative of ETFE.

In this method it is further preferred that a neighbouring spot is subjected to a laser beam before solidification of the melted material of a previous spot and/or wherein the apertures initially produced are receiving a higher spot lase duration and/or a higher intensity than the subsequently produced apertures. The laser beam and/or the planar material in step d is preferably displaced about 150 µm to about 500 µm.

The planar material partly melts when impacted by the laser beam. The melted material subsequently solidifies, preferably to form smooth bulges. To obtain a merging of bulges it may be preferred that a neighbouring spot is subjected to a laser beam before solidification of the melted material of a pervious spot. The laser beam may have any suitable power (or intensity) and spot lase duration for the apertures of the invention to be obtained. In a preferred embodiment the laser beam is operated at a power of about 3 W to about 8.5 W, and the laser beam is preferably operated at a spot lase duration of between 1 and 7 ms. In accordance with the desired specifications of the bulges the off vector delay is of 1 µs to 1000 µs. The spot lase duration and/or the power may be varied during the production of the functional area. Thus, according to a preferred aspect, the apertures initially produced are receiving a higher spot lase duration and/or a higher power than the apertures subsequently produced to obtain a uniform appearance of the scaffold.

The membrane scaffold is especially useful in the preparation of a composite biomimetic membrane where an amphiphilic membrane forming composition has been deposited in said apertures to form the membrane wherein functional molecules, such as channel forming molecules, e.g. certain peptides or peptide like molecules including amphotericin B, alamethicin, valinomycin, gramicidin A and their dimers, oligomers and analogues thereof; or transmembrane proteins, e.g. aquaporin water channels, Fas protein, DsbB, CFTR, alpha-haemolysin, VDAC, and OmpG, are incorporated.

Thus, the present invention also relate to a composite biomimetic membrane comprising the membrane scaffold described above, and a biomimetic membrane provided in the apertures, wherein functional channel forming molecules have been incorporated in the membrane. In a preferred aspect of the invention, the channel-forming molecule is selected among the aquaporin water channels to make it possible to obtain a composite biomimetic membrane useful in a filtration device for purification of a water source or a liquid, aqueous medium. Other useful applications include a biosensor or for high throughput screening of ligands. The present inventors have found that the membrane scaffold described herein is especially suitable for the formation of bilayer lipid membranes in its apertures, and that said membranes have an increased longevity compared to membranes of the prior art. The biomimetic membrane of the invention is suitable for incorporation of biomolecules that are naturally membrane-bound, e.g. aquaporins, or for incorporation of artificial molecules. The composite biomimetic membranes comprising aquaporins are suitable for transporting water from one side of the membrane to the other side, e.g. when driven by a pressure gradient. The ability to transport water may be utilized in a filtration device for preparing essentially pure water. Other embodiments of the composite biomimetic membrane are suitable as biosensors or for high throughput screening of transmembrane protein ligands. The channel-forming molecules cover in a preferred aspect at least 1% of the membrane surface. Suitably, the membrane is covered with 1 to 10% of the channel-forming molecules.

The invention relates in a further aspect to a filtration device for filtering essentially pure water comprising a composite biomimetic membrane comprising aquaporin water channels as described above. The advantages of using the composite membrane in said filtering device or other applications where upscale is an advantage is closely related to the possibility of up-scaling the functional membrane area by the manufacturing of large, flexible, and relatively thin sheets having a large multitude of discrete membrane units. In addition, the composite membrane ensures that filtering ability is maintained even though one or more dis-

crete membrane units have failed. This situation may especially apply to a filtration device having multi layer stacking of the individual composite membranes or 2D-aperture-arrays.

Furthermore, the invention relates to a novel method of forming auto-painted membranes (APM) in said scaffold to prepare a composite biomimetic membrane, and a chamber for the preparation and holding of said composite biomimetic membrane. Surprisingly, the inventors have found that the principle of the APM technique which uses a narrow reservoir of a concentrated, limited volume of amphiphilic membrane forming solution (e.g. DPhPC lipid mixed with an apolar solvent, e.g. a hydrocarbon solvent) in direct connection with a buffer volume on the front side (cis chamber) of the vertically positioned scaffold/ partition is able to facilitate preparation of a composite biomimetic membrane. When raising said buffer solution the amphiphilic membrane forming solution will be raised completely past the scaffold (Teflon partition) and in the process be deposited into the multiple apertures, which have been prepainted with a solution of amphiphilic substance in an apolar solvent, to create a composite membrane in said scaffold apertures. The hydrophobic nature of the scaffold surface ensures deposition of the apolar membrane forming solution into said multiple apertures. An optional feature of the APM method is that the composite membrane is supported and stabilized on the back side (trans chamber) by a preferably hydrophilic, porous support material that allows fluid connection between the membrane and the buffer solution in the trans chamber.

In addition, the invention relates to an apparatus for testing the function of a transmembrane molecule comprising the composite biomimetic membrane according to the invention and having the following features:

A two-cell chamber wherein each cell has an upper opening to allow access to the cell, and a membrane scaffold according to any one of the claims 1 to 6 comprising said composite biomimetic membrane, which provides a partition between the two cells to form a cis chamber and a trans chamber, a partial separation (7) in the cis chamber which extends from the top of said chamber to below said functional area thus forming a relatively narrow space with said scaffold (4), a porous sup-

port layer (3) which is a functional water barrier at atmospheric pressure opposite the partial separation (7), a first volume of aqueous buffer solution in the trans chamber opposite the partial separation (7) where said volume extends above said central area of said scaffold (4), a second volume of aqueous buffer solution in the cell having the partial separation (7) where said volume does not reach the lower level of said functional area of said scaffold (4), a spacer (5) is provided between said partial separation (7) and said scaffold (4), said spacer having an upper opening to allow insertion of a syringe. The apparatus may further include elastic seals (2, 6) that are inserted between parts 1 and 3, 4 and 5, 5 and 7, 7 and 8, 8 and 9, and between 9 and the annular sealing screw, said elastic seals being of a chemically resistant material, such as a fluoroelastomer, e.g. Viton®. The reference numbers are found in Fig. 12. In the apparatus an electrode may be inserted in each of said upper openings and in contact with said first and second "buffer" solutions.

In a preferred embodiment of the apparatus of the invention said said transmembrane molecule is alpha-hemolysine, and a further aspect of the invention is the use of the apparatus according for the testing of a compound having binding effect on alpha-hemolysine said testing comprising adding a solution of said compound to said cis chamber and measuring conductance through said electrodes.

BRIEF DESCRIPTION OF THE DRAWINGS

Fig. 1 is a drawing showing an overview of geometries needed for theoretical bulge calculation. is an optical microscopy picture of the scaffold with apertures.

Fig. 2 is a SEM micrograph of an ETFE scaffold of the invention showing a close up on apertures turned 60o to show bulges in an array with 140 µm spacing. The rough surface is due to the gold which is sputtered on for better contrast.

Fig. 3 is a SEM photograph showing the central area with apertures of a scaffold according to the invention having 120 µm spacing and turned 45o.

Fig. 4 is a SEM photograph showing a section of a scaffold accord-

ing to the invention having an aperture diameter of about 300 µm and a bulging aperture rim.

Fig. 5 shows a 5x5 array in rectangular design with spacing of 150 µm.

Fig. 6 shows SEM pictures of two scaffold arrays of the invention made in Tefzel 100LZ ETFE film (DuPont) with 140 µm spacing.

Fig. 7 is an SEM picture showing most parts of an entire scaffold of the invention having a central 20 x 20 aperture array in hexagonal design and with 150 µm spacing and an outer nonperforated area.

Fig. 8 is a graph showing a Dektak profilometer measurement of a scaffold having average aperture diameter of 84.6 µm.

Fig. 9 is a drawing showing the APM method of preparing a biomimetic membrane, e.g. a BLM membrane, in the apertures of the scaffold of the invention creating a composite biomimetic membrane. Shown is a sectioned schematic side view through the middle of an assembled two-cell Teflon chamber. In steps 1-3 the buffer level in the cis chamber is raised above the aperture, thus creating a lipid bilayer (red line, step 3) by the parallel raising of the DPhPC/decane layer (red square, step 1-3).

Fig. 10 shows schematically the Folded bilayers method according to Montal & Muller (1972, PNAS, 69:3561-3566).

Fig. 11 shows schematically the Painted bilayers method according to Muller & Rodin (1969, Cur. Top.Bioeng. 3:157-249).

Fig. 12 shows the movable inner parts of an embodiment of the two-cell Teflon chamber. The inner diameter of Viton seals and Teflon spacers is 8mm. A thin layer of silicone grease (High Vacuum Grease, Dow Corning) is applied to the inner Viton seals prior to assembly. An annular sealing screw (not shown) secures sealing from the right end as shown by the arrow. It is possible to visually follow the formation of lipid membrane through the opening in the annular sealing screw.

Fig. 13 is a drawing showing various views of the solid, outer parts of an APM-1 chamber of the invention.

Fig. 14 is a drawing showing the T-ring.

Fig. 15 is a drawing showing the annular sealing screw.

Fig. 16 is a graph showing changes in conductance of a composite

membrane after adding valinomycine and TEA.

Fig. 17 is a graph showing changes in conductance of a composite membrane after adding valinomycine and TEA in a different experiment.

Fig. 18 shows 4 diagrams of capacitance and the conductance for an experiment reported in example 10.

Fig. 19 shows 6 fluorescent images of traditional and airbrush pretreated multiple apertures.

Fig. 20 shows diagrams of the capacitance and the conductance for an airbrush pretreated membrane scaffold.

Fig. 21 discloses a diagram of conductance of a membrane incorporating valinomycin.

Fig. 22 shows 3 SEM images of the scaffold membrane used in example 10.

Fig. 23 shows in 4 sequences the formation of a membrane by the APM method.

Fig. 24 shows the hexagonal configuration of an aperture array of the invention.

Fig. 25 are Photomicrographs of composite biomimetic membranes made in a Fluon 50N scaffold material comprising BLMs in 8x8 arrays in the horizontal chamber setup, 300 micrometre diameter apertures and centre-to-centre distance of 400 micrometres, cf. Fig. 26. The figures show functional incorporation of alpha-hemolysin channels in composite biomimetic membrane array of the invention. 25A is a fluorescence image of an 8x8 BLM array using a 2.5x objective, 25B+C show a transmitted light image and the corresponding fluorescent image using a 10x objective, and 25D is a graph showing conductance in pA of said membrane arrayas a function of time.

Fig. 26 shows combined horizontal imaging and electrical voltage clamp chamber design.

DETAILED DESCRIPTION OF THE INVENTION

One aspect of the invention relates to a membrane scaffold comprising a planar material having a hydrophobic surface (such as an ETFE film) and a central perforated area wherein a plurality of essentially cir-

cular apertures having smooth, bulging rims have been formed using a $CO_2$ laser ablation process. The membrane scaffold has preferably a thickness of from about 25 µm to about 200 µm. The rounded and bulging rims of the apertures in the membrane scaffold of the invention possess several advantages in contrast to apertures having blunt-edged rims, e.g. by/in stabilizing the membrane formed in the apertures against breakdown and in supporting a stable torus or annulus of fluid membrane forming composition, such as an amphiphilic lipid solution, for the sustainability of the fluid biomimetic membrane during evaporation of solvent. A toroidal membrane forming solution reservoir will act as a reservoir in equilibrium with the bilayer membrane allowing for exchange of material necessary for bilayer bulging (e.g. when under pressure) and self-repair.

Definitions:

The term "Biomimetic membrane" as used herein is intended to cover planar molecular structures having an upper and a lower hydrophilic layer and an inner hydrophobic layer resembling the structure of a eukaryotic cell membrane.

"BLM" as used herein means Black Lipid Membrane or Bilayer Lipid Membrane. The term "aperture diameter" as used herein always refers to an average measured diameter of the apertures in the entire scaffold. The term "essentially circular" is used herein to characterize the cross sectional shape of the apertures in the scaffolds of the invention. It is believed that this shape is ideally circular for optimal support of a biomimetic membrane, such as a lipid bilayer. However, various approximately circular forms including ovals or ellipses and rounded tetragonal or box-like forms are intended to be included in the term.

"Buffer" is used herein to describe a solution comprising one or more electrolytes with or without buffering capacity.

"Smoothness" as used herein refers especially to the aperture rims that ideally do not have blunt edges or cracks.

The term "bulge" is used herein to denote the enlarged height of the apertures relative to the thickness of the film in which they are

formed using the laser ablation process. Especially when using a $CO_2$ laser ablation to form the apertures some film material will accumulate along the rim to form the bulge. For the purposes of the invention the bulges have to be smooth and rounded and should not be too high. The geometry of the bulge is described in more detail below.

The term "torus" is used herein to describe a peripheral ring of multilayered amphiphilic lipid solution surrounding the central bilayer membrane formed in the aperture.

"APM" means Auto-Painted Membrane the formation of which is described in Example 2 below.

"Teflon" as used herein includes ETFE, polyethylene-tetraflouroethylene, and modifications and derivatives thereof; ECTFE, polyethylene-chlorotrifluoroethylene, and modifications and derivatives thereof; PTFE, Polytetrafluoro-ethylene and modifications and derivatives thereof; FEP, Fluorinated ethylene propylene and modifications and derivatives thereof. Teflon is used synonymous with flouropolymer. DPhPC means 1,2-diphytanoyl-sn-glycero-3-phosphocholine. EtOH means ethanol.

"ETFE" as used herein includes polyethylene-tetraflouroethylene, and modifications and derivatives thereof;as well as ECTFE, polyethylene-chlorotrifluoroethylene and modifications and derivatives thereof.

"BFS" means bilayer forming solution and is used herein interchangeably with the term "Membrane forming solution" and specifies a mixture of an amphiphilic substance with an apolar solvent to obtain a liquid solution suitable for forming membranes.

The terms "film" and "foil" are used interchangeably herein when describing the planar material used in fabricating the membrane scaffolds, and the term "elastic" is used to characterize sealing means that can be made of an elastomeric material or other rubber-like material.

$CO_2$-Laser: The process used in forming the apertures is preferably a laser ablation (laser photoablation), preferably using a $CO_2$ laser (e.g. Synrad, Inc. 4600 Campus Place Mukilteo, Washington 98275 USA, Laser: 48-of the 48series (50 W laser)) which will secure high reproducibility, well defined aperture diameters, and a high degree of aperture den-

sity in the planar scaffold material. In addition a laser ablation method can easily be upscaled. The membrane scaffold according to the invention is preferably prepared using an optically induced/stimulated thermal process, such as a $CO_2$ laser ablation, where said laser beam is preferably operated at a power of about 3 W to about 8 W or more. An advantage of using a thermal process is the partly melting of the material resulting in forming of the smooth rims without any sharp edges. Further advantages include low power consumption and that the laser itself having small dimensions is mountable on a stage together with other lasers for production of large scale scaffolds, e.g. in $m^2$ scale. The $CO_2$ laser emits infrared light with a wavelength of 10.6 µm in a continuous beam. The decomposition of the planar material takes place due to thermal processes only. When the beam hits the surface of the sample the polymer melts and parts are vaporized. The gas drives the melted polymer out of the void which results in a bulge around the edges of the structure. It is a fast and inexpensive method which is mainly used in direct writing. Every polymer with sufficient absorption in this region can be processed.

The $CO_2$ laser ablation is a mere thermal process. This means that parts of the planar material surrounding the aperture are influenced by the thermal process and bulges are left behind. The minimal structure size depends on the optical components used in the setup. For example with a lens with a focal length of 80 mm apertures of 116 µm were reported to be the minimum (Jensen, M. F., et al. 2003. - Microstructure Fabrication with a $CO_2$ Laser System: Characterization and Fabrication of Cavities Produced by Raster Scanning of the Laser Beam. Lab on a chip. 3pp 302-307). Scaffold material The scaffold material is chosen to be hydrophobic, preferably having a contact angle of more than 90°, or preferably more than about 100° as measured between a droplet of deionised water and the hydrophobic material. The contact angle measurement is performed at 20°C and atmospheric pressure using a contact angle goniometer. Suitable hydrophobic materials include films made of various crystalline or semicrystalline fluoropolymer materials (Teflon®) such as ETFE (ethylene Tefzel® ETFE, DuPont™), Fluon ETFE Film 50N

(by Asahi Glass Company, Ltd.) and Norton ETFE, ECTFE (Saint- Gobain Performance Plastics Tygaflor Ltd.). These film materials are susceptible to the ablation process of the $CO_2$ laser. Crystalline polymers have a relatively sharp melting point where the crystalline lattice is destroyed which is characterized by the crystalline melting temperature Tm. It is desired that the scaffold material is able to absorb infrared light with a wavelength of 10.6 µm, and therefore a relatively low transmittance at this wave length is desirable. A preferred example of a suitable scaffold material is ethylene-tetrafluoroethylene (ETFE) which has an transmittance at 10.6 µm of 88.2 %.

The planar hydrophobic material must be resistant towards the chemicals used in the process of forming the membranes in the apertures. The material must be able to withstand the complex cleaning steps used prior to establishing the biomimetic membrane, e.g. a lipid bilayer. The material needs to withstand, e.g., chloroform, hexane and DPhPC/decane (2.5 wt %). SEM pictures of the apertures were taken before and after this chemical treatment to provide the basis to compare any changes in aperture diameter as well as in the overall appearance of the structure. The chemical resistance tests have shown that the crystalline or semicrystalline Teflon materials, such as ETFE were sufficiently chemically stable. The experiments with the different chemicals did not show any damage on the ETFE scaffold apertures. A comparison between the aperture diameter before and after the treatment confirmed the results from the visual inspection.

Table 1: Properties of various Teflon materials

| Property | Polytetrafluoroethylene (PTFE) | Fluorinated ethylene propylene (FEP) | Ethylene-tetrafluoroethylene (ETFE) |
|---|---|---|---|
| Polymer | Thermo- | Thermo- | Thermo- |

| type | setting | setting | setting |
|---|---|---|---|
| Melt tempera-ture | 327°C | 250 - 280°C | 250 - 270°C |
| Transmitt ance at 10.6 µm | 97.5 % | 97.5 % | 88.2 % |
| Contact angle (water) | 106° | 105° | 105° |
| Manufac-turer | DuPont™ | DuPont™ | DuPont™ |

Scaffold geometry

The membrane scaffold according to the invention has preferably a central functional area having a degree of perforation of about 20 % to about 60 % and more preferably from about 30 to about 50 %. In addition, the membrane scaffold comprises a circumscribing area of unperforated film which is useful when sealing the scaffold into a tight chamber. In the membrane scaffold according to the invention the spacing between the apertures is preferably from about 150 µm to about 500 µm measured as the distance between aperture centres. The spacing is preferably from about 130 % of the aperture diameter to about 500 % of the aperture diameter. It has been found that this spacing will allow bulge formation of the aperture rims, which may further stabilize the membrane formation and/or longevity of the membranes. However, in some embodiments of the invention the interspace between neighbouring apertures is so reduced that two separate bulges cannot be formed. Instead they combine and build up one bulge ranging from the edge of one aperture to the neighbouring one with the highest point approximately in the middle of the interspace, cf. Fig. 2 and Fig. 3 showing a picture of a scaffold having 84 µm aperture diameter and 120 µm spacing where this

phenomenon is visible.

In a specific embodiment of the invention the membrane scaffold has a central perforated area of about 3.1 mm x 3.1 mm having 8 x 8 apertures (diameter 300 µm) and center to center distance of 400 µm in a rectangular arrangement where the scaffold was made from an ETFE film of 0.001 inch (25.4 µm) thickness (Tefzel 100 LZ, DuPont®).

The apertures are preferably of relatively smaller dimensions, such as about 80 to 200 µm, when the composite biomimetic membrane formed using the membrane scaffold is to be used for applications such as biosensors.

In the membrane scaffold according to the invention said planar material has typically a thickness of from about 25 µm to about 300 µm, where the thinner materials are suitable for apertures having the larger diameters, and the thicker materials are suitable for applications requiring applied pressure, such as filtration of water. The planar material having a hydrophobic surface is preferably an ETFE film having a contact angle of about 95°- 106° and a thickness of between about 25 to 100 µm or more preferably of about 50µm to about 60 µm.

Theoretical geometry considerations

The material accumulations during the laser ablation process are of importance for the final shape of the membrane scaffolds. The rims of the apertures desirably are smooth and round and should not be too high to ensure stable lipid bilayer formation. Therefore, a model of the bulge was developed. With these equations and the parameters s and di measured on a SEM picture, the expected height could be determined. Several assumptions have been made to simplify the calculation. First of all, vaporization and increase of volume of the ablated polymer were neglected. Furthermore, it was expected that the bulges will have an elliptical vertical cross-sectional shape and that they are equal all around the aperture. Fig. 1 shows a cross-section of a perforation to the left and a cross section of a bulge to the right.

When "shooting" the aperture hole, all material which can be accumulate in a bulge must be displaced volume from the aperture. This

means the displaced volume is:

$$V = \pi * \frac{d_i^2}{4} h_i \qquad (5.1)$$

This volume is then deposited to form the bulge which surrounds the hole on both sides of the foil. It depends on the diameter of the hole di and the width s of the bulge.

$$V_{bulge} = A * l \qquad (5.2)$$

$$l = U = \pi * (d_i + s) \qquad (5.3)$$

The parameter l describes the perimeter of the circle on which outer side the maximum bulge height was expected. When looking at one side only, the value h is half the length of the major axis of the ellipse.

$$A = \pi * \frac{s}{2} * h \qquad (5.4)$$

By measuring di and s for example on a SEM picture, the height of the bulge then arises from Eq.(5.1), Eq.(5.3) and Eq.(5.4) to be:

$$h = \frac{d_i^{\,2} * h_i}{2 * \pi * s * (d_i + s)} \qquad (5.5)$$

A calculation has been made to find the best suitable arrangement of apertures. As widely known from literature, the highest density which can be achieved is when using a hexagonal structure. This can also be applied to the membrane scaffold of the present invention. The area which is covered by this structure can be calculated by having the spacing between the holes a, the number of apertures within each row x and the number of rows y. This results in the length l and width w which can

be calculated by:

$$l = a * x \quad (7.1)$$

$$w = h * (y - 1) + a \quad (7.2)$$

$$h = \sqrt{3} * \frac{a}{2} \quad (7.3)$$

The final covered area then is:

$$A = l * w \quad (7.4)$$

However, it has to be taken into account that x defines the maximum number of apertures in a row. In a maximum density hexagonal structure this number is different in the even and uneven numbers of rows. This calculation assumes that the used array starts and ends with an uneven row number which has one aperture more than an even one. When having an area which has to be covered with apertures this calculation has to be performed backwards. Then, the amount of apertures for an even row can be calculated by:

$$x = \frac{l}{a} \quad (7.5)$$

The number of rows is defined to be:

$$y = \frac{2 * (w - a)}{\sqrt{3} * a} + 1 \quad (7.6)$$

The resulting values have to be rounded to fulfill the requirements of having integer values and an uneven number of rows. By taking the average diameter d of the apertures into account, the perforation level p can now be calculated by:

$$p = \frac{A_{holes}}{A} * 100\% \qquad (7.7)$$

Here Aholes defines the area where material was removed.

$$A_{holes} = (\frac{1}{4} * \pi * d^2) * z \qquad (7.8)$$

The value z is the overall number of apertures in the area Aholes. Table 2 lists the percentage of perforation for different spacings (center-to center distance) and an aperture diameter of 89 µm in average when filling an area of approximately 2x2 cm.

Table 2: Theoretical level of perforation which can be achieved by hexagonal arrangement of the apertures in a 2x2 cm sample with an average aperture diameter of 89 µm

| spacing a | x | Y | number of apertures z | perforation level p |
|---|---|---|---|---|
| 150 µm | 133 | 153 | 20,273 | 31 % |
| 140 µm | 143 | 163 | 23,228 | 36 % |
| 130 µm | 154 | 177 | 27,170 | 41 % |
| 120 µm | 167 | 191 | 31,802 | 49 % |

Table 3: Perforation level, calculated for rectangular arrangement of the apertures in a sample with an average aperture diameter of 300 µm

| **number of apertures (same in x and y)** | | **8** | **10** | **100** | **1000** |
|---|---|---|---|---|---|
| **level of perforation** | c-c distance = 600 µm | 21,19% | 20,87% | 19,75% | 19,65% |
| **level of perforation** | c-c distance = 400 µm | 43,63% | 43,74% | 44,13% | 44,17% |

| | | | | | |
|---|---|---|---|---|---|
| **level of perforation** | c-c distance = 350 µm | 54,92% | 55,46% | 57,47% | 57,68% |

Table 4: Perforation level, calculated for hexagonal arrangement of the apertures in a sample with an average aperture diameter of 300 µm

| **number of apertures (different in x and y)** | | **8** | **10** | **100** | **1000** |
|---|---|---|---|---|---|
| **level of perforation** | c-c distance = 600 µm | 22,73% | 22,71% | 22,67% | 22,67% |
| **level of perforation** | c-c distance = 400 µm | 46,78% | 47,53% | 50,63% | 50,97% |
| **level of perforation** | c-c distance = 350 µm | 58,87% | 60,24% | 65,92% | 66,56% |

Table 5: Perforation level. Calculation for 2 x 2 cm scaffold, cf. Fig. 24

| | |
|---|---|
| **Rectangular arrangement; Aperture diameter** | **300 µm** |
| **2 $cm^2$ area; c-c distance =** | **400 µm** |
| number of apertures (same in x and y) | $50^2$ |
| level of perforation | 46,01% |
| **Hexagonal arrangement; Aperture diameter** | **300 µm** |
| **2 c $m^2$ area; c-c distance =** | **400 µm (x)** |
| number of apertures in x | 50 |
| number of rows (y = 347 µm) | 57 |

| | |
|---|---|
| number of holes | 2822 |
| level of perforation | 50,80% |

With these densely packed structures and the huge amount of apertures another parameter came into focus – the Off Vector Delay (OVD). By reducing this parameter to a value as low as possible, precious time during production could be saved. For example by reducing OVD from 600 µs to 1 µs with a production volume of 20,273 apertures the production time can be shortened by 12 s. This is an advantage regarding the further up-scaling of the membrane scaffold fabrication where it can result in reduction of considerable production time. However, this reduction of OVD could change the overall parameters because the material would have less time to cool down between production steps.

Anisotropy of the Teflon film used in preparation of the membrane scaffold

The used ETFE film is available on 25 $m^2$ rolls which were processed by conventional melt-extrusion techniques (DuPont™). There are two main directions which are significant in this process. The machine direction (MD) which is oriented along the length of the sheet and perpendicular the transverse direction (TD) which defines the characteristics of the film across the width of the film. During the process of being stretched and pressed, polymer chains tend to align in a parallel form. By the immediate following cooling process this alignment is frozen in. Orientation of the material leads to higher strength in this direction than at right angles. This characteristic of having an orientation should be taken into account when forming the aperture array. It was found for the Tefzel 100LZ film that while lowering the distance between center-to-center of the apertures, the shape of the holes became more and more elliptical. Thus, there is a dependency on the material's orientation for the production of closely spaced arrays. Furthermore, it has to be noted

that the apertures produced with the MD were not completely round when having a low distance. They tended to be more hexagonal and formed an array which can be compared to a honeycomb. The tendency to form elliptical holes can be explained by the orientation of the molecules within the polymer. They tended to align parallel after the film extrusion. When shooting an aperture, high thermal energy is induced which breaks bonds between the polymer chains. In the immediate focal spot of the laser this causes melting and vaporization of the material. The surroundings of the aperture was also affected by this thermal energy, plus the energy induced from neighbouring apertures. When producing perpendicular to MD the bonds between the parallel chains may break and cracks develop. This could explain the elliptical apertures. However, when fabricating with MD this effect did not occur because within a very short time (~1 µs) a neighbouring aperture was produced and additional material was placed on the partition between the two apertures. The fabrication of several closely spaced apertures and the later increase of the perforation level showed that not only the settings of the laser influenced the quality of the aperture. It has been found that the characteristics of the material are important as well. Primarily, this applied for the alignment of the polymer chains due to the fabrication process of the foil. Tests showed that the direction of aperture fabrication is preferably parallel with the machine direction of the ETFE film. This resulted in dense arrays with a honey comb like structure. However, this only applied for the fabrication of the smallest apertures in dense arrays. When producing the apertures with a larger diameter and a larger spacing the optimal production direction changes to be perpendicular to MD. Here, structuring in the machine direction resulted in more oval apertures. Compared to the single aperture approach, the fabrication settings of the $CO_2$ laser itself had to be modified when making arrays. Significant here was the OVD which could be reduced from 600 µs to 1 µs. This change was possible due to the closely arranged apertures. The OVD vs. spacing test revealed that slight changes in diameter and shape were possible with changing time. A higher number of apertures will lead to more time between the fabrications of rows and thus every single aper-

ture will be influenced only by its two immediate neighbours from the same row. Therefore, and considering the time of the fabrication process a minimum OVD was preferred. The second important parameter was the spot lase duration. This value had to be changed within the same structure. Outer apertures (mostly the ones starting a new row) required a higher value than those following. That proved the influence of the heat, coupled in by the ablation process. The thermal energy lowers the threshold of the melting and vaporizing of the ETFE. That made it possible to produce apertures in a shorter time. The first aperture of an array always had to be 5 ms which is higher than the rest but lower than needed to produce a single aperture. Depending on the distance between the apertures, this time could be further reduced down to 4 ms. This effect was also observable when measuring the diameter, for example in the OVD vs. spacing test. Apertures closer to the middle of the array were always bigger than the ones on the outside. Therefore, when determining the average diameter for a structure, only apertures from inside the array were measured. Different center to center distances resulted in different average diameters. This was caused by the thermal energy from the production of previous apertures in the array. As mentioned before, this also led to a decrease in spot lase duration in denser arrays which in turn led to a smaller diameter for shorter spacings.

Channel forming molecule

The membranes formed in the scaffolds of the invention readily incorporate channel forming molecule, e.g. a peptide ionophore such as valinomycin that exists in natural lipid bilayer membranes, cf. Example 8 below or aquaporins, such as bovine AQP-1 and plant plasma membrane aquaporins of the PIP subfamily, e.g. SoPIP2;1. The channel forming molecule may be incorporated in the membrane by direct incorporation at the membrane formation step, where the aquaporin proteins are first incorporated in a suitable hydrophobic spreading solution. The spreading solution can be prepared from aqueous SoPIP2;1 extract emulsified with the lipid, e.g. DPhPC in hydrophobic solvent, e.g. n-decane, cf. Walton et al., Anal. Chem. 2004, 76, 2261-2265. SoPIP2;1 can be obtained in the

form of a heterologously expressed protein, cf. Kukulski W et al. Journal of molecular biology (2005), 350(4), 611-6. Thus, said channel forming molecules are preferably selected from the group consisting of ion channel molecules, such as valinomycin and gramicidin monomers and dimers, transmembrane proteins such as porins e.g. outer membrane protein OmpG, phosphoporin PhoE and aquaporin water channels, connexins e.g. Cx26, Cx30, Cx32, Cx36, Cx40, Cx43, etc., transporters such as light absorption-driven transporters e.g. bacteriorhodopsin-like proteins including rhodopsin and opsin, light harvesting complexes from bacteria, etc., ABC (ATP-binding cassette) transporters facilitating transport of small solutes and molecules such as ions, salts, antibiotics, etc. in a type-dependent manner, ABC subclass A transporting cholesterol, sphingolipids and phospholipids in a type dependent manner (Piehler et al. 2007, Tidsskr. Nor. Laegeforen., Vol. 127, No. 22. Review), Multidrug resistance pumps transporting antibiotics (Alekshun and Levy 2007 Cell Vol. 128), lead and mercury ion pums (e.g. CadA, ZntA and MerC, Rensing et al. 1998, J. Biol. Chem., Vol. 273, No. 49; Sasaki et al. 2005, Biosci., Biotechnol. Biochem. Vol. 69, No. 7), cation diffusion facilitator (CDF) protein family transporting heavy metal ions such as zinc, cobalt, cadmium (e.g. CzcD, Anton et al. 1999, J. Bacteriol., Vol. 181, No. 22), receptors such as neurotransmitter receptors e.g. GABA transporters, monoamine transporters, glutamate transporters, etc., CD-receptors such as CD-95, a receptor for serum Fas ligand, which is a serological marker for different disease states in humans including certain hormone sensitive cancer forms e.g. breast carcinoma, chemosensitivity in colorectal cancer, disease activity and infection states such as malaria or the asymptomatic stage of human immunodeficiency virus infection, etc. (Kuwano et al. 2002, Respirology, Vol. 7 Issue 1.; Kern et al. 2000 Infect. Immun. 68(5); Bahr et al. 1997, Blood, Vol. 90, No. 2), transmembrane CC chemokine receptor for which macrophage-derived chemokine (MDC) is a ligand and whose serum levels are elevated in atopic dermatitis differentiable from psoriasis activity (Kakinuma et al. 2002, Clin. Exp. Immunol., Vol. 127), CXC chemokine receptors, interleukin receptors, olfactory receptors and receptor tyrosine kinases e.g. the matura-

tion-mediating receptor tyrosine kinase Tie-2 whose ligands include soluble angiopoietin-2, which has been identified as a biological marker in serum for non-small cell lung cancer with distant metastasis (Park et al. 2007, Chest., Vol. 132, Fiedler et al. 2003, J. Biol. Chem., Vol. 278, Issue 3). A useful channel protein is POR1 which forms a channel through the cell membrane that allows diffusion of small hydrophilic molecules. The channel adopts an open conformation at low or zero membrane potential and a closed conformation at potentials above 30-40 mV. The open state has a weak anion selectivity whereas the closed state is cation-selective. It is the major permeability factor of the mitochondrial outer membrane. Other interesting membrane proteins include the bacterial DsbB electron donor and the cystic fibrosis transmembrane regulator (CFTR) which functions as a cAMP-activated chloride channel and also regulates a separate protein, the outwardly rectifying chloride channel (ORCC). Other useful channel forming molecules identified from several ORFs are listed in Burri et al. 2006 FEBS Journal Vol. 273. Also preferred is the heptameric channel forming protein alpha-hemolysin.

Biomimetic membrane

In the biomimetic membrane of the invention said lipid is preferably selected from amphiphilic lipids, such as DPhPC or DPPC. WO2006122566, the contents of which are incorporated herein by reference, discloses useful amphiphilic compounds and lipids for reconstitution of aquaporins and formation of lipid bilayers or biomimetic membranes, cf. Table 1 therein. In addition, DPhPC (diphytanoylphosphatidylcholine, Avanti Polar Lipids, Alabaster) and DPPC, SOPC, DOPC, asolecthin, E. coli total lipid extract, SOPE, DOPE, DOPS and derivatives and mixtures thereof are preferred lipids for use in the biomimetic membranes of the present invention. The lipid is preferably dissolved at a concentration of from about 2 mg/mL to about 100 mg/mL in an apolar solvent, such as hexane, octane, decane, tetradecan, hexadecane, etc., in order to obtain a suitably fluid membrane forming composition. Preferred solvents are n-decane, n-tetradecane, and n-hexadecane. Without being bound by any theory it is assumed that the most suitable solvents possess a carbon

chain which is approximately of the same length scale as the acyl carbon chains of the amphiphilic lipids. Said lipid bilayer may further comprise a bilayer stabilising amount of one or more stabilizing substances, such as cholesterol, dextran, or a monosaccharide, a sugar alcohol, a disaccharide, a trisaccharide, an oligosaccharide, a polysaccharide as disclosed in US 2005/0048648.

Useful methods of preparing lipid bilayer membranes in the apertures of the scaffold of the invention to form composite biomimetic membranes are described in WO2006122566 the contents of which is incorporated herein by reference. A preferred method herein is the APM method described in Example 10 below.

In some embodiments of the invention the biomimetic membranes can be formed in the scaffold apertures from solutions of amphiphilic block copolymer simulating a natural environment. Functional membrane molecules can be incorporated in this type of biomimetic membrane. One method of forming a biocompatible membrane, which is preferred for use with block copolymer-based membrane, is as follows: Form a solution of block copolymer in solvent (BC solution). The solution can be a mixture of two or more block copolymers. The solution preferably contains 1 to 90% w/v copolymer, more preferably 2 to 20%, or yet more preferably 20 to 10%, such as 7%. Make a solution of channel forming molecule such as aquaporin in the prepared BC solution, preferably by adding 1.0 to 50.0 mg/mL of the preferred aquaporin, more preferably 1.0 to 10.0 mg/mL. Drop a small volume (e.g., 4 microliter) aquaporin/BC solution onto each aperture or each of a subset of apertures, and allow to dry, thereby removing the solvent. Repeat this step as needed to cover all apertures. The solvent is selected to be miscible with both the water component used in the process and the B component of the block copolymer. Appropriate solvents are believed to include methanol, ethanol, 2-propanol, 1-propanol, tetrahydrofuran, 1,4-dioxane, solvent mixtures that can include more apolar solvents such as dichloromethane so long as the mixture has the appropriate miscibility, and the like. (Solvent components that have any tendency to form proteindestructive contaminants such as peroxides can be appropriately pu-

rified and handled.) Solvent typically comprises 10% v/v or more of the applied aquaporin/ BC solution, preferably 20% or more, and usefully 30% or more. The above-described method of introducing aquaporin or other desirable membrane channels as described herein to a solution containing nonaqueous solvent(s) in the presence of block copolymers serves to stabilize the function of active channels, such as aquaporins. The non-aqueous components can comprise all of the solvent. The mixtures of block copolymers can be mixtures of two or more of the following classes, where the separate components can be of the same class but with a different distribution of polymer blocks: Polymer Source triblock copolymers E/EP/E, of poly(ethylene)(E) and poly(ethylene-propylene)(EP) Triblock copolyampholytes. Among (N,N dimethylamino)isoprene, such polymers are 15 Ai14S63A23, Ai31S23A46, Ai42S23A35, styrene, and methacrylic acid Ai56S23A21, Ai57S11A32. Styrene-ethylene/butylene-styrene (KRATON) G 1650, a 29% styrene, 8000 solution triblock copolymer viscosity (25 wt-% polymer), 100% triblock styrene- ethylene/butylene-styrene (S-EB-S) block copolymer; (KRATON) G 1652, a 29% styrene, 1350 solution viscosity (25 wt-% 20 polymer), 100% triblock S-EB-S block copolymer; (KRATON) G 1657, a 4200 solution viscosity (25 wt-% polymer), 35% diblock S-EB-S block copolymer; all available from the Shell Chemical Company. Such block copolymers include the styrene- ethylene/propylene (S-EP) types and are commercially available under the tradenames (KRATON) G 1726, a 28% styrene, 200 solution viscosity (25 wt-% polymer), 70% diblock S-EB-S block copolymer; (KRATON) G- 1701X a 37% styrene, >50,000 solution viscosity, 100% diblock S-EP block copolymer; and (KRATON) G-1702X, a 28% styrene, >50,000 solution viscosity, 100% diblock S-EP block copolmyer. 30 Siloxane triblock copolymer PDMS-b-PCPMS-b-PDMSs (PDMS = polydimethylsiloxane, PCPMS = poly(3- cyanopropylmethylsiloxane) can be prepared through kinetically controlled polymerization of hexamethylcyclotrisiloxane initiated by lithium silanolate end-capped PCPMS macroinitiators. The macroinitiators can be prepared by equilibrating mixtures of 3- cyanopropylmethylcyclo-siloxanes (DxCN) and dilithium diphenylsilanediolate (DLDPS). DxCNs can be synthesized

by hydrolysis of 3- cyanopropylmethyldichlorosilane, followed by cyclization and equilibration of the resultant hydrolysates. DLDPS can be prepared by deprotonation of diphenylsilanediol with diphenylmethyllithium. Mixtures of DxCN and DLDPS can be equilibrated at 100[deg.] C. within 5-10 hours. By controlling the DxCN-to-DLDPS ratio, macroinitiators of different molecular weights are obtained. The major cyclics in the macroinitiator equilibrate are tetramer (8.6 +- 0.7 wt %), pentamer (6.3 +- 0.8 wt %) and hexamer (2.1 +- 0.5 wt %). 2.5k- 10 2.5k-2.5k, 4k-4k-4k, and 8k-8k-8k triblock copolymers have been characterized. These triblock copolymers are transparent, microphase separated and highly viscous liquids. PEO-PDMS-PEO triblock Formed from Polyethylene oxide (PEO) and poly-copolymer dimethyl siloxane (PDMS). Functionalized poly(2- Angew. Chem. Int. Ed. 39: 4599-4602, 2000; Langmuir methyloxazoline)-block- 16: 15 1035-1041, 2000. These A-B-Apolymers include poly(dimethylsiloxane)-blockversions in which the A components have MW of poly(2-methyloxazoline) triblock approximately 2 kd, and the B component of copolymer approximately 5 kd, and (b) the A components have MW of approximately 1 kd, and the B component of approximately 2 kd Poly(d/1-lactide)("PLA")-PEG-PLA triblock copolymer Poly(styrene-b-butadiene-b-styrene) triblock copolymer Poly(ethylene Such polymers included Pluronic F127, Pluronic P105, or oxide)/poly(propylene oxide) Pluronic L44 from BASF (Performance Chemicals). Triblock copolymers PDMS-PCPMS-PDMS A series of epoxy and vinyl endcapped polysiloxane (polydimethylsiloxane- triblock copolymers with systematically varied molecular polycyanopropylmethylsiloxane) weights can be synthesized via anionic polymerization using LiOH as an initiator. Polydiene-polystyrenepolydiene available as Protolyte A700 from DAIS-Analytic, Odessa, FL. Azofunctional styrene-butadiene- HEMA triblock copolymer Amphiphilic triblock copolymer carrying polymerizable end groups Syndiotactic polymethylmethacrylate (sPMMA)- polybutadiene (PBD)-sPMMA triblock copolymer Tertiary amine methacrylate triblock Biodegradable PLGA-b-PEO-b- PLGA triblock copolymer, Polylactide-b-polyisoprene-b- polylactide triblock copolymer, Poly(isoprene-blockstyrene- block- dimethylsiloxane) triblock copolymer, Poly(ethylene

oxide)-block-polystyrene-block-poly(ethylene oxide) triblock copolymer, Poly(ethylene oxide)- poly(THF)- poly(ethylene oxide) triblock copolymer Ethylene oxide triblock Poly E-caprolactone Birmingham Polymers, Birmingham, AL Poly(DL-lactide-coglycolide) Birmingham Polymers, Poly(DL-lactide) Birmingham Polymers, Poly(L-lactide) Birmingham Polymers, Poly(glycolide) Birmingham Polymers, Poly(DL-lactide-co-caprolactone) Birmingham Polymers, Styrene-Isoprene-styrene triblock Japan Synthetic Rubber Co., Tokyo, Japan; MW = 140 kg/mol; copolymer Block ratio of PS/PI = 15/85. PMOXA(y)-PDMS(x)-PMOXA (y1) which is a poly(2-methyloxazoline)-block-poly(dimethylsiloxane)-block-poly(2-methyloxazoline) which may be symmetric (y = y1) or assymmetric; PMMA-b-PIB-b-PMMA Poly(methyl methacrylate) (PMMA) and polyisobutylene (PIB). PLGA-PEO-PLGA triblock Polymers of poly(DL-lactic acid-co-glycolic acid) copolymer (PLGA) and PEO. Sulfonated styrene/ ethylene- butylene/styrene (S-SEBS) triblock copolymer proton conducting membrane Poly(1-lactide)-block-poly(ethylene oxide)-block-poly(1-lactide) triblock copolymer Poly-ester-ester-ester triblock copolymer PLA/PEO/PLA triblock copolymer The synthesis of the triblock copolymers can be prepared by ring-opening polymerization of DL-lactide or e- caprolactone in the presence of poly(ethylene glycol), using no-toxic Zn metal or calcium hydride as co-initiator instead of the stannous octoate. The composition of the copolymers can be varied by adjusting the polyester/polyether ratio. The above polymers can be used in mixtures of two or more of polymers in the same or different class. For example, in two polymer mixtures measured in weight percent of the first polymer, such mixtures can comprise 10-15%, 15-20%, 20-25%, 25-30%, 30- 35%, 35-40%, 40-45% or 45-50%. Or, for example where three polymers are used: the first can comprise 10-15%, 15-20%, 20-25%, 25-30%, 30-35%, 35- 40%, 40-45% or 45-50% of the whole of the polymer components, and the second can 10-15%, 15-20%, 20-25%, 25-30%, 30-35%, 35-40%, 40-45% or 45-50% of the remainder. Block co-polymers can be custom synthesized and obtained, e.g. from the following

http://www.encapson.eu/index.php?option=com_content&task=view&id=17&Itemid=32
http://www.polymer.de/services/custom-synthesis/#
http://www.pkasynthesis.com/
http://www.akinainc.com/
http://www.polysciences.com/

Application of membrane scaffold

The invention relates in a further aspect to a filtration device for filtering essentially pure water comprising a composite biomimetic membrane comprising aquaporin water channels as described above. The advantages of using the composite membrane in said filtering device is closely related to the possibility of up-scaling the functional membrane area by the manufacturing of large, flexible, and relatively thin sheets having a large multitude of discrete membrane units. In addition, the composite membrane ensures that filtering ability is maintained even though one or more discrete membrane units have failed. This situation may especially apply to a filtration device having multi layer stacking of the individual composite membranes or 2D-aperture-arrays. The final dimensions of the stacked composite membranes will depend on overall robustness and on intrinsic permeability of the chosen membrane material/membrane composition.

Examples of how functional aquaporins can be incorporated into a water membrane have been described, however the present invention is not limited by these examples. The present invention relates to any composite biomimetic water membrane comprising a membrane scaffold as described herein with a biomimetic membrane comprising functional (channel) molecules reconstituted in its apertures. Other useful applications of said composite membrane include biosensor applications, such as a transmembrane protein functioning as receptor or channel, labeled with a fluorophore to make a protein-based biosensor sensitive to ligands, solutes or small molecules. Said biosensors incorporated into bimimetic membranes can be used for ligand-receptor interactions used in high throughput screening assays for diagnostic or prognostic pur-

poses prepared in 96-multi well plates, lab-on-a-chip devices or build into point-of-care measuring devices, or serve as quantitative measuring devices of solutes or small molecules such as heavy metal ions e.g. cadmium, copper, lead, etc., or antibiotics and other polluting agents for quantitative on-the-spot water analysis, or blood analysis of animals and humans.

Membrane formation

Furthermore, the invention relates to a novel method of forming auto-painted membranes (APM) in said scaffold to prepare a composite biomimetic memrane, and a chamber for the preparation and holding of said composite biomimetic membrane. Surprisingly, the inventors have found that the principle of the Auto-Painted membrane (APM) technique which uses a narrow reservoir of a concentrated, limited volume of amphiphilic membrane forming solution (e.g. DPhPC lipid mixed with an apolar solvent, e.g. a hydrocarbon solvent) in direct connection with a buffer volume on the front side (cis chamber) of the vertically positioned scaffold/partition is able to facilitate preparation of a composite biomimetic membrane. When raising said buffer solution the amphiphilic membrane forming solution will be raised completely past the scaffold (Teflon partition) and in the process be deposited into the multiple apertures, which have been pre-painted with a solution of amphiphilic substance in an apolar solvent, to create a composite membrane in said scaffold apertures. This method involves spraying the membrane scaffold with a solution of amphiphilic lipid in a hydrocarbon solvent prior to step a) above. The amphiphilic lipid is dissolved at a concentration of from about 10 mg/mL to about 100 mg/mL in an apolar solvent. Preferably the lipid is DPhPC and the apolar solvent is selected from the group comprising hexane, octane, decane, and hexadecane.

The invention further relates to the use of a composite biomimetic membrane of the invention comprising aquaporin water channels in pressure retarded osmosis for the production of salinity power, or the use of a composite biomimetic membrane comprising aquaglyceroporin water channels in pressure retarded osmosis for the extraction of salinity

power.

The hydrophobic nature of the scaffold surface ensures deposition of the apolar membrane forming solution into said multiple apertures. An optional feature of the APM method is that the composite membrane is supported and stabilized on the back side (trans chamber) by a preferably hydrophilic, porous support material that allows fluid connection between the membrane and the buffer solution in the trans chamber. In the APM-1 setting which is shown in fig. 9 the 15 trans buffer level is just above the central perforated area of the scaffold where a negligible hydrostatic pressure will not result in flow of solution through the apertures. One advantage of the APM technique as compared to the folding and painting methods described in the art is the ease of up-scalability to create membranes in multi-aperture partitions without loss of reproducibility.

A general method of preparing a composite biomimetic membrane according to the invention comprises the steps of (reference numbers refer to Fig. 12):

a) providing a two-cell chamber wherein each cell has an opening allowing for access to the cell, and a membrane scaffold according to any one of the claims 1 to 6, which provides a partition between the two cells to form a cis chamber and a trans chamber;

b) providing a porous support which is a functional water barrier at atmospheric pressure;

c) providing a first volume of aqueous buffer solution in the trans chamber opposite the partial separation where said volume covers said central area of said scaffold;

d) providing a second volume of aqueous buffer solution in the cis cell opposite the partial separation where said volume covers said central area of said scaffold;

e) providing means to perfuse a volume (bolus) of membrane forming solution in the trans chamber thereby impregnating said functional area resulting in fluid membranes in said area; and

f) adding an extra volume of said aqueous buffer into either chamber to remove bolus leaving membranes in said functional area facing the trans

and cis cell aqueous buffer.

The method described above is suitable for fabrication of composite biomimetic membranes in both the horizontal and in the vertical position and any position therein between

In another method of the invention a composite biomimetic membrane is prepared following the steps of (reference numbers refer to Fig. 12):

a) providing a two-cell chamber wherein each cell has an upper opening to allow access to the cell, and a membrane scaffold according to any one of the claims 1 to 6, which provides a partition between the two cells to form a cis chamber and a trans chamber,

b) providing a partial separation (7) in the cis chamber which extends from the top of said chamber to below said functional area thus forming a relatively narrow space with said scaffold (4),

c) providing a porous support (3) which is a functional water barrier at atmospheric pressure opposite the partial separation (7),

d) providing a first volume of aqueous buffer solution in the trans chamber opposite the partial separation (7) where said volume extends above said central area of said scaffold (4),

e) providing a second volume of aqueous buffer solution in the cell having the partial separation (7) where said volume does not reach the lower level of said functional area of said scaffold (4),

f) providing a volume of membrane forming solution in the space between the partial separation (7) and the scaffold (4), and

g) adding an extra volume of said aqueous buffer into said cis chamber to raise the buffer level above said functional area thereby raising the membrane forming solution completely past said apertures to form a fluid membrane therein.

A spacer (5) may be provided between said partial separation (7) and said scaffold (4), said spacer having an upper opening to allow insertion of a syringe; and elastic seals (2, 6) may be inserted between parts 1 and 3, 4 and 5, 5 and 7, 7 and 8, 8 and 9, and between 9 and the annular sealing screw, said elastic seals being of a chemically resistant material, such as a fluoroelastomer, e.g. Viton®.

The invention further relates to an apparatus for testing the function of a transmembrane molecule comprising the composite biomimetic membrane of the invention and having the following features:

A two-cell chamber wherein each cell has an upper opening to allow access to the cell, and a membrane scaffold of the invention comprising said composite biomimetic membrane, which provides a partition between the two cells to form a cis chamber and a trans chamber, a partial separation (7) in the cis chamber which extends from the top of said chamber to below said functional area thus forming a relatively narrow space with said scaffold (4), a porous support layer (3) which is a functional water barrier at atmospheric pressure opposite the partial separation (7), a first volume of aqueous buffer solution in the trans chamber opposite the partial separation (7) where said volume extends above said central area of said scaffold (4), a second volume of aqueous buffer solution in the cell having the partial separation (7) where said volume does not reach the lower level of said functional area of said scaffold (4), a spacer (5) is provided between said partial separation (7) and said scaffold (4), said spacer having an upper opening to allow insertion of a syringe.

Elastic seals (2, 6) may be inserted between parts 1 and 3, 4 and 5, 5 and 7, 7 and 8, 8 and 9, and between 9 and the annular sealing screw, said elastic seals being of a chemically resistant material, such as a fluoroelastomer, e.g. Viton®; and an electrode may be inserted in each of said upper openings and in contact with said first and second "buffer" solutions.

The apparatus described above may in an embodiment comprise a plurality of alpha-hemolysine oligomers incorporated in the biomimetic bilayer membrane, which enables the use of said apparatus for the testing of a compound having binding effect on alpha-hemolysine said testing comprising adding a solution of said compound to said cis chamber and measuring conductance through said electrodes. Positive reference measurements may be obtained in advance following addition of an inhibitor of alpha-hemolysine, e.g. beta-cyclodextrin and measuring the conductance.

Additional aspects of the invention relate to composite biomimetic membranes comprising aquaporins useful in the purification of a water source, or which can be used for pressure retarded osmosis (PRO), and in another aspect the present invention relates to the implementation of said membrane in a PRO system used in the production of salinity power, such as is described in WO /2007/033675.

EXAMPLES

Example 1. Array fabrication

To have an efficient membrane scaffold for, e.g. a filter membrane, the perforation level has to be as high as possible. Interactions from the production of neighbouring apertures in dense arrays influences the fabrication process when working with a $CO_2$ laser could be predicted. Due to be a thermal process, heat is coupled in the material each time the beam hits the surface of the film. This could lead to a lowering of the threshold where material is evaporated and thus result in bigger apertures in the middle of the array. Furthermore, when getting closer together, the bulges around the apertures could accumulate and so get higher in arrays than with single apertures. To investigate to what extent this may be the case, different arrays with different distances between the apertures and different parameters had to be designed and tested. To start the investigation and production of a highly perforated membrane, a simple 5x5 array of apertures was designed. It consisted of 5 rows of 5 apertures which were equally spaced. The term spacing refers to the distance between the centers of two neighbouring apertures. It was set to values of 500, 200 and 150 µm. With an average diameter of 96 µm this leaves an interspace of 404, 104 and 54 µm respectively between the apertures. The production parameters of the single aperture approach were transferred to the array - namely a power of 0.4 W and a spot lase duration (SLD) of 6 ms (see above). Furthermore, an Off Vector Delay of 600 µs was chosen to avoid tail formation like seen during the experiments with single apertures. The results confirmed the prediction of interactions between the apertures when coming closer together.

With 500 µm spacing every aperture has an individual bulge, but at 200 µm and below the bulges start to touch each other. This can be explained by the thermal characteristic of the ablation by $CO_2$ laser. When the beam hits the surface of the material it melts. In addition, some parts are evaporated and the resulting gas ejects the melted material from the aperture. This is intensified by the heat which is coupled in and which makes the material softer and thus easier to deform. A series of experiments was set up with the previous design of a 5x5 array. This time the spacing was ranging from 250 down to 150 µm. Several experiments with changing laser powers and spot lase durations were performed. The results were investigated by optical microscopy. Here, the main criteria were the equality and the diameter of the apertures. The diameter was estimated with the help of a ruler integrated in the microscope's eyepiece. At the end of this test sequence the SLD could be reduced by 1 to 2 ms. It became obvious that it has to be changed within the grid. In the middle of the array the SLD could be lower than on the starting aperture to achieve the same results. This is again linked to the heat induced by the production. Since the apertures were close together and the time between production steps was short (600 µs), the material had no time to cool down. Due to the so preheated substrate less energy was needed to reach the melting point and the threshold of evaporation respectively. The optimization of the SLD resulted in an optimised array with smooth and almost round apertures. Furthermore, a decrease in the average aperture diameter could be observed. When producing single apertures the average diameter was ~96 µm but in the array of 5x5 apertures with a spacing of 150 µm and a reduced SLD this value decreased by 7 % to ~89 µm. This is again connected to the heat induced by the production of neighboring apertures. As found when reducing SLD the diameter of the aperture decreased as well, cf. Fig. 5 which shows a 5x5 rectangular array with spacing of 150 µm. Figure 6 shows SEM pictures of two scaffold arrays of the invention made in Tefzel 100LZ ETFE film (DuPont) with 140 µm spacing; the structure with the higher OVD (right side) has more circular holes whereas the one on the left side a more honeycomb like pattern.

Example 2. Geometrical examination of arrays

After having optimized the main production parameters, samples with spacing ranging from 150 µm to 120 µm were produced and examined to characterize the arrays and the apertures geometrically. It was found that the apertures at a center to center distance of 150 µm were completely round, however, their shape changed when decreasing the spacing. The cause was that every new aperture influenced its neighbours more and more with decreasing distance. The thermal energy induced by the laser melted and evaporated the material. Evaporating material built up a pressure which ejected melted parts but also pushed the softened boundaries. By having hexagonal arranged apertures this resulted in the formation of box like or even hexagonal shaped apertures, cf. Fig.6. Using the previous model an estimation of the bulge height could be made. The highest bulge will form at the spot where two apertures get closest to each other. However, it has to be noted that this time no single hole was investigated but two or more. Therefore, the displaced volume of two holes is accumulated at the interspace of two apertures. Consequently, Eq.(5.5) is altered to be:

$$h = \frac{d_i^{\,2} * h_i}{\pi * s * (d_i + s)} \qquad (7.9)$$

The diameter and the width of the bulge were again measured with the help of an SEM image. As mentioned earlier the ETFE foil had a thickness of about 25 µm. Applying Eq.(7.9) using a diameter of 84.6 µm and a bulge width of 34.1 µm, the bulge height could be estimated to be 14.1 µm. This theoretical value was again verified by a Dektak profilometer measurement, cf. Fig. 8. The measurement of the 120 µm spaced array with its apertures resulted in an average bulge height of 19.05 µm. The difference between the theoretical and the experimental value of about 26 % is caused by the assumptions made during the calculation. Furthermore, it is likely that material from the four other apertures surrounding the interspace was added to the measured bulge. An-

other method to verify the results is by turning the structure 49 degrees and take an SEM picture. The bulge can be seen clearly. However, it cannot be directly measured because of the angle in which the aperture is displayed. The actual bulge height is calculated by:

$$h = h_{turned} * \sin\alpha$$

h is the height measured on the picture and α was the angle with which the structure was turned. The result was a height of 17 µm. In summary, it may be concluded that the mathematical model developed is only applicable for a rough estimation of the bulge height when looking at single apertures. If more than one aperture contributes to the bulge, like it is the case in dense arrays, this estimation became too imprecise. The elements of uncertainty are the assumptions made to simplify the calculation and the unknown number of apertures which contribute to form the bulge at the interspace. To get a more exact value of the bulge height it is necessary to make a profilometer measurement or calculate it with the help of tilted SEM micrographs. 10 Fig. 8 shows an extract from the profilometer measurement of a horizontal row in a 120 µm spacing array; the displayed values are rounded off; the full graph has 18 peaks with an average height of 19 µm.

Example 3. Off Vector Delay and spacing consideration

The basic structure for this test was a hexagonal array with 10 apertures in each row and 11 rows. The distance from center to center (spacing) was chosen to be 250, 200, 150, 140, 130 and 120 µm. The optimal parameters for arrays with these spacings and an OVD of 1 µs were determined (Table 6).

Table 6: Overview of the optimized parameters for the production of apertures with an OVD of 1 µs with an intensity of 0.4 W

| Optimized parameters for the Off Vector Delay vs. spacing test | | |
|---|---|---|
| spacing in µm | Apertures | spot lase duration |

| | | |
|---|---|---|
| 250 | All | 5 ms |
| 200 | All | 5 ms |
| 150 | 1st of each row<br>2nd of 1st row | 5 ms |
| | Remaining | 4.8 ms |
| 140 | 1st of each row | 5 ms |
| | 2nd of first row | 4.8 ms |
| | 3rd of first row | 4.5 ms |
| | Remaining | 4 ms |
| 130 | 1st of each row | 5 ms |
| | 2nd of 1st row | 4.8 ms |
| | 3rd of 1st row | 4.5 ms |
| | Remaining | 4 ms |
| 120 | 1st of 1st row | 5 ms |
| | 1st hole of each row<br>2nd of 1st row | 4.8 ms |
| | 3rd of 1st row | 4.5 ms |
| | Remaining | 4 ms |

Example 4. Increased aperture diameter

The purpose of these partitions was to investigate the bilayer formation for which purpose the density of apertures over the area was not of importance. Hence, 5x5 and 8x8 arrays were designed. The settings regarding intensity and spot lase duration were established. By initially having optimized the process to production of apertures being as small as possible, the production of larger apertures was straightforward. For this purpose the 200 mm lens with a focal spot diameter of 290 µm was more suitable. Two different aperture diameters were supposed to be produced: Apertures around 400 µm which were arranged in a 5x5 array with a center to center distance of 600 µm, and apertures with a diameter of 300 µm which were positioned in an 8x8 array with a spacing of 400µm. Compared to the production of apertures with a diameter of 90 µm and below, here a higher power as well as a higher spot lase dura-

tion was needed. In the end, following parameters were found to fulfill the diameter requirements (Table 7).

Table 7: Production parameters for arrays of apertures with increased diameter

| Diameter | Power | spot lase duration |
|---|---|---|
| 400 µm | 9 % of cavity2 = 1.8 W | 12 ms |
| 300 µm | 6 % of cavity2 = 1.2 W | 8ms |

When fabricating these larger apertures care has to be taken to choose the right process direction. The effect of elliptical apertures mentioned above emerged. However, although structuring with the machine direction, the 400µm apertures still appeared to be slightly oval. Single scaffolds of the resulting samples were taken to be examined. Therefore, SEM micrographs were taken and the diameter was calculated to prove that the desired diameter of the apertures could be achieved. However, the largest apertures were slightly oval. This deformed shape is suspected to be the result of the previously parallel aligned polymer chains and the higher energy input compared to the small apertures. Another factor could also be the OVD. Since the spacing was increased to 600µm but the OVD was still at 1 µs, an influence of this parameter could not be excluded.

Example 5

During the process of optimizing the production parameters for every material, optical inspection and geometrical measurements were performed to follow the progress. The results were used to decide, whether a further optimization was useful or if the material was not suited and had to be discarded. A parameter here was the achievable diameter which could be from 400 µm down to below 100 µm. It was measured using SEM pictures of the aperture hole and the software IMAQ Vision Builder 6.1 (National Instruments). Here, a line could be drawn through the hole and its length was given as the number of pixels. By measuring the scale bar in the SEM picture and relate the resulting number of pixels with the one measured in the hole, the diameter of

the aperture could be calculated. This was done for the best results achieved with every material, i.e. PTFE, ETFE, FEP. With most materials the minimization of the aperture diameter stopped around the minimal focal spot diameter of 116 µm as given by the lens manufacturer and confirmed in the literature (Jensen et al. 2003 above). However, ETFE was an exception because minimal diameters of 100 µm or below could be made. With the help of the theoretical considerations made earlier above it was possible to estimate the height of the bulges surrounding the aperture. A SEM picture of an aperture in ETFE was used to measure both, bulge width and diameter of the actual hole. By using Eq.(5.5) the bulge height could be calculated. The production process was carried out using an OVD of 1000 µs. The intensity and spot lase duration had to be altered within the array. This resulted in having 4.2 W combined with 4 ms for the last row, 4.4 W and 5 ms for the first row and 4.4 W and 4 ms for the rows 2 to 7. By having an average aperture diameter of 303 µm, a bulge width of 65 µm and a thickness of the foil of 0.002 inch, the resulting bulge height should be 31 µm. This result was then verified by a measurement with a DekTak profilometer.The differences between the theoretical result and the measured value can be explained by the assumptions which were made to simplify the calculation. The actual bulges are neither completely elliptical nor evenly distributed. They are higher at the edge and gently flatten out on the outside. Furthermore, due to the nature of ablation, material is evaporated and thus not the entire volume of the hole is deposited as a bulge. In addition it is believed that the volume of the melted, ejected, and deposited polymer increases. This is caused by a lowering of the material's density during the heating process where polymer chains are cut into shorter chains without being ablated (SNAKENBORG, D., H. -KLANK, and J. P. - KUTTER. - Microstructure Fabrication with a $CO_2$/ Laser System. - *Journal of Micromechanics and Microengineering*. (- 2), pp – 182). However, the measurement shows that the theoretical model is applicable to roughly estimate bulge heights.

Example 6. Use of $CO_2$ laser ablation in the preparation of a membrane

scaffold from an ETFE film

General introduction to operation and laser parameters: The $CO_2$ Laser and therefore the fabrication of arrays, is controlled by the software package Win-Mark Version 4.6.2.5245 (SYNRAD Inc. Mulkiteo, WA, USA). This software is provided by the manufacturer of the laser. The most important settings for fabricating described structures are the intensity of the laser beam, the Off Vector Delay (OVD) and the Spot Lase Duration (SLD). The intensity (or also referred to as power) controls how much of the overall power is used for the production. It can be chosen between 0 and 100 % in steps of 0.1 %. The specified output power of 50 W given by the machine supplier equals a value of 70 to 80 %. The Off Vector Delay (OVD) sets the time when the laser is switched off between two production steps. Thus it gives the mirrors time to get settled over the starting point of a new structure before giving the command to "fire". The software allows the OVD to be set to values between 0 and 80,000 µs. The last parameter of importance is the Spot Lase Duration (SLD). It defines the time for how long the laser stays on one spot. It can be chosen in ms and the maximum value equals 1 s. The following working example states the used values of all three of these important parameters: The used material was the Tefzel® 200LZ (DuPont®), an ETFE foil with a thickness of 0.002 inch (50.8 µm). The structure which was fabricated consisted of 64 apertures which were arranged in a rectangular array of 8 columns times 8 rows. The average diameter of the apertures was estimated to be 300 µm +/-5 µm and the center to center distance of the apertures (also referred to as spacing) was chosen to be 400 µm. The task of having equally sized apertures over the whole structure made it necessary to change the laser parameters within the array. This can be explained by the thermal energy which is introduced by the production of neighbouring apertures – this means that apertures in the middle and at the end of the array can be produced with less energy than at the beginning. This relationship between the apertures influences all three main laser settings. The OVD was chosen to be 1000 µs instead of 1 µs like it is used with the thinner Tefzel 100LZ foils. The purpose was to give the material time to cool down before "shooting" the

next aperture to avoid deformation of the apertures. The SLD was chosen to be 5 ms for the first horizontal row and 4 ms for all subsequent rows. The power was altered from 22% (4.4 W) to 21% (4.2 W) for the last row. These settings (Table 5) made it possible to produce an array with the preferred characteristics including a smooth rim with a bulge of about 17 µm (see also Fig. 8):

Table 8: Summary of the used settings for the preparation of a membrane scaffold with 8x8 apertures of 300 µm ± 5 µm diameters and 400 µm spacing in a rectangular array in ETFE foil with a thickness of 0.002 inch

| Location | Intensity | SLD | OVD |
|---|---|---|---|
| first row horizontal | 22 % | 5 ms | 1000 µs |
| last row horizontal | 21 % | 4 ms | |
| all others | 22 % | 4 ms | |

The same laser settings, except using an OVD of 1 µs, were used in the fabrication of membrane scaffolds having the same array configuration but prepared in Tefzel® 100LZ (DuPont®) foil having a thickness of 0.001 inch (25.4 µm). Laser settings will ideally have to be optimized for the preparation of membrane scaffolds having other specifications. Typically, OVD settings are increased with increasing thickness of the ETFE film to avoid deformation of the apertures. Due to higher power and SLD settings when structuring thicker films more thermal energy is absorbed by the material and thus a longer cooling time between the productions of two neighbouring apertures is preferred. Figure 4 is a SEM picture of the central aperture array (average diameter about 300 µm ) of a scaffold of the invention, where the left side is a section of a 8x8 array; right side is a single aperture of such an array. The pictures were taken using a FEI Nova 600 NanoSEM. The use of a low vacuum made it possible to take clear pictures of the non-conducting polymer by scanning electron microscopy (SEM). An array of near circular apertures having perfectly smooth rims is shown. The lighter shades of the rims indicate bulging to an extent of about 10 to 40 µm above original foil. The actual bulges are

a bit wider than the visible lighter shades. These lighter shades show the inside (the raising) part of the bulge. As can be seen on the right picture the lighter shade stops almost at the top and the other side of the bulge is darker again.

Conclusion:

The $CO_2$ laser enables preparation of the membrane scaffolds of the invention having apertures with diameters in the range from about slightly less than 80 µm to about 400 µm and above, the desired rim smoothness and rim bulging, and it also enables very close spacing of the apertures, i.e. producing an aperture area of up to 44 % using the rectangular arrangement of the apertures and 47% using a hexagonal arrangement relative to the entire functional area of the scaffold. Moreover, the laser enables fast production of smaller samples, e.g. the production of a scaffold having an 8x8 aperture array is done in less than 3 seconds.

Example 7. Method and device for the preparation of Auto Painted Membrane

Preparation of a composite bio-mimetic membrane using a circular disk (diameter 29 mm) scaffold of the invention having a rectangular 8x8 aperture array (each aperture has an average diameter of 300µm) with a centre to centre distance of 400µm formed in ETFE film (EthyleneTetraFlouroEthylene, 100LZ ETFE of 0.001 inch (25.4µm) film thickness, DuPont®) using the $CO_2$ laser ablation according to the procedures described in Example 6.

The APM principle: The APM principle is sketched in fig. 9 and in fig. 23 where the basics of the Auto- Painted Membrane (APM) technique is shown with one or 64 apertures respectively. Figure 9 shows a sectioned schematic side view through the middle of an assembled two-cell Teflon chamber (the APM-1 chamber, cf. Fig.13). In steps 1-3 the buffer level in the cis chamber (left-hand chamber in fig. 9) is raised above the aperture, thus creating a lipid bilayer (red line, step 3) by the parallel raising of the DPhPC/decane layer (red square, step 1-3). It has been found

that prepainting the aperture array of the scaffold with a solution of the amphiphilic substance (block co-polymer or lipid) in a suitable solvent, such as decane, hexane, etc., before mounting in the APM chamber facilitates the formation of membranes in the apertures.

Cleaning APM-1 chamber parts: The Teflon parts of the APM-1 chamber were cleaned with 3 successive washes in 96% ethanol, Folch mixture and chloroform, followed by a thorough rinse in Millipore water. Viton A (flourodipolymer, DuPont) seals were cleaned once in 50% (v/v) ethanol for 10 minutes in an ultrasonic bath (BRANSON 1510, Buch&Holm) followed by a 10 minute ultrasonic rinse in Millipore water. Scaffolds were washed 3 times successively in 60% (v/v) ethanol, hexane, and water.

Pre-painting ETFE scaffolds: The pre-painting solution used in this study consisted of 1,2-Diphytanoyl-sn-Glycero-3-Phosphocholine (DPhPC, Avanti Polar Lipids, Inc., Alabaster, Alabama) (50 mg/ml) dissolved in n-decane (Sigma®). The same lipid solution was used as bilayer forming solution (BFS). Cleaned and dried ETFE scaffolds were first pre-painted once on both sides by adding and distributing a small droplet of pre-painting solution and then leaving the scaffold to dry under a fume hood. The following 4 pre-paints involved maintaining open apertures with a stream of N2: By carefully blowing on the apertures of the scaffold with a stream of N2 after addition of the pre-paint droplet the solvent could be evaporated from the pre-painting solution, while keeping the apertures open.

Assembling APM-1 chamber parts: The assembly of the individual inner elements of the APM-1 -chamber is shown below (Figures 12, 12a). The inner elements all have approximately a 29,9mm outer diameter to fit snugly into the cylindrical 30 mm diameter tube of the cis chamber (left-hand chamber in Fig. 12a), and rest upon the ledge created by the interface of the cis chamber and the cylindrical 20mm diameter tube of the trans chamber. A 5 mm thick Teflon cylindrical tube (arrow 8 in fig.12, see also fig. 14) provides the link to the annular brass screw (perimeter thickness 7 mm) generating sufficient pressure from

the exterior of the chamber to obtain water tight sealing. Thus both the cis and trans chambers have identical inner diameters of 20mm when the APM chamber is assembled.

A circular, 2 mm thick Teflon spacer (arrow 5 in fig. 12) with a 2 mm slit is positioned with the opening at the top to allow for entering membrane forming solution behind the cut glass (arrow 7 in fig. 12) with a Hamilton inserted through a 3mm cylindrical opening through the top part of the APM chamber (fig 13).

The inner diameter of the inner Viton seals (arrows 2 in fig 12) and Teflon spacers (arrows 1 and 5 in fig 12) as shown here is about 8 mm to better stabilize the scaffold (arrow 4 in fig 12) when made of the thin 100LZ film. The scaffold support material (arrow 3 in fig 12) is comprised of a about 250µm thick sheet of regenerated cellulose sheet having a molar mass cut off of 10kDa and a contact angle of 10.3 °, DSS-RC70PP, Alfa Laval, Denmark.

When sealed the chamber space between the cover slip (arrow 9 in fig 12) and the scaffold (arrow 4 in fig 12) constitutes the cis chamber. When using scaffolds made of thicker film material, e.g. about 50 µm (0.002 inches), the parts 1, 2, and 5 can be of the same inner diameter as the other parts. Optimal sealing is achieved by applying a thin layer of silicone grease (High Vacuum Grease, Dow Corning) to the inner Viton seals (arrows 2 in fig 12) prior to assembly.

The annular brass screw having an inner diameter of 20 mm (not shown, cf. Fig. 15) secures tight sealing from the right end as shown by the arrow. It is possible to visually follow the lowering and raising of buffer levels in the cis chamber through the opening in the annular sealing screw.

Example 8. Incorporation of functional valinomycin into Auto-Painted Membranes (APM's)

In a 8x8 ETFE membrane array having aperture diameters of about 300 µm In this study we incorporated the potassium ionophore valinomycin (Mary Pinkerton, L. K. Steinrauf and Phillip Dawkins: "The molecular structure and some transport properties of valinomycin". Bio-

chemical and Biophysical Research Communications VOL 35 Issue 4 512-518) in very stable (>100 hours) DPhPC membrane systems (lipid bilayers) formed in a membrane scaffold of the present invention, and subsequently we reversed the valinomycin induced increase in conductivity by adding tetraethylammonium chloride (TEA), a known inhibitor of potassium ionophores (Robert J. French, Jay B. Wells: "Sodium Ions as Blocking Agents and Charge Carriers in the Potassium Channel of the Squid Giant Axon". BIOPHYS. J. VOL 54 1053-1063). Voltage clamp measurements were performed in an in-house manufactured Faraday cage. The primary electrical setup consisted of a headstage (HS-2A, Eastern Scientific LLC) and an amplifier (PICOAMP-300, Eastern Scientific LLC). Data acquisition was done with a combined oscilloscope/analog-digital converter (ADC-212, Pico technology. A 200mM KCl solution served as electrolyte. Valinomycin powder (Sigma) was dissolved in 96% ethanol to yield a 2mg/ml (1,8mM) working solution (WS), which was stored at 4°C. A 16 mM TEA working solution was prepared in 200mM KCl and stored at 4°C. 2-10µl Valinomycin WS was added to the small APM-1 chamber volume through the slit in Teflon spacer (arrow 5 in Fig. 12) between the ETFE scaffold and the first glass coverslip (≈ 0,5mL), cf. Fig. 12, in APM-1 setups where the APM's displayed constant membrane characteristics over several days. To reverse the valinomycin-induced conductance, TEA working solution was added to the small chamber volume in molar excess. Results: The graph in Fig. 16 shows reversing valinomycin induced increase in conductance by adding TEA. Experiments performed on 13 day old membrane. 10µL 1,8mM valinomycin WS added to the small chamber volume (0,5mL) at t=52min corresponding to ~32µM final valinomycin concentration. 500µL 16mM TEA WS added to the small chamber volume between t=69min and t=2min corresponding to ~8mM final TEA concentration. The graph Fig. 17 shows the reversal of valinomycin induced increase in membrane conductance by adding TEA in molar excess. Experiments were performed on a 4 day old composite membrane. 10µL 1,8mM valinomycin was added to the small chamber volume (0,5mL) at t=0 min corresponding to ~32µM final valinomycin concentration. 200µL 16mM

TEA WS added to the small chamber volume at t=5min corresponding to ~4,5mM final TEA concentration.

Conclusion: In this study we have demonstrated facilitation of incorporation of valinomycin into Auto-Painted Membranes created in ETFE 8x8 300µm diameter aperture diameter arrays, and subsequently reversal of the Valinomycin induced increase in conductance by adding TEA. Control experiments have shown that addition of and TEA alone does not significantly affect membrane characteristics (not shown). Our results in this study confirm that we can manipulate membranes in ETFE arrays created by use of the APM technique.

Upon reversing the valinomycin induced increase in membrane conductance by adding TEA, we observe again a significant increase in membrane conductance, which is followed by membrane failure (not shown). It is believed that this increase in membrane conductance followed by membrane failure to be a result of an excessive amount of valinomycin in an unstirred layer close to the membrane.

Example 9. A diagnostic kit for detection of serum CD 95/Fas ligand

A composite biomimetic membrane will be prepared in the APM-1 chamber as described in Example 8. A fluorescently labeled, e.g. with an environmentally sensitive probe, such as BadanR or LaurdanR, CD-95 receptor (Fas protein, 5 catalogue No.198749, ICN Biochemicals & Reagents 2002- 2003) will be prepared in an emulsion according to Beddow et al. (Anal. Chem. 2004, 76, 2261- 2265) and added to the membrane through the slit in Teflon spacer (5) for direct reconstitution in the membrane. A serum sample extract containing Fas ligand to be tested will be added to the membrane. Following binding of the Fas ligand extract to the prepared membrane the membrane will be transferred to either a microscope or a spectrophotometric plate reader (Wallac Victor2) for examination. Quantification of binding will be based on an internal standard of known fluorescence.

Example 10. Preparation of membranes with functional valinomycin

A Synrad Duo 48-5S Duo Lase carbon dioxide laser with a specified power output of 50 W (Mulkiteo, WA, USA) and equipped with a 200 mm 20 focal length lens was used to fabricate partitions with 8x8 rectangular arrayed apertures in ETFE LZ200 film (50.8 µm thickness). The average 5 diameter was 301 ± 5 µm (n=5) positioned in the array with an aperture centre-to-centre spacing of 400 µm. The 8x8 array was placed in the middle of a circle with a diameter of 29 mm. The apertures were produced with an intensity of 1.2 W and a spot lase time (impact time of the beam) of 8 ms. The ETFE film was placed in a custom produced sample 10 holder made of polymethyl methacrylate. A clearance was situated in the middle of this fixture where the laser beam hit the sample. Thereby, it was assured that no underlying material interfered with the production process.

A scanning electron microscope (SEM) (Jeol JSM 5500 LV SEM from 15 GN nettest) was used for imaging. It is capable of a lateral resolution of 30–50 nm and a magnification up to x300,000. The acceleration voltage can be set between 1 to 30 kV. The SEM has a reproducibility and accuracy in lateral distance measurements better than 5.0 %. SEM images of the produced $CO_2$ laser percussion drilled EFTE partitions showed that 20 the apertures were symmetrically positioned in the 8x8 array with slight elliptical apertures having nicely rounded edges (Figure 22).

The lipid bilayer chamber design is depicted in Figures 12 to 15. The complete chamber setup consists of a main Teflon chamber with two asymmetrical drilled holes having diameters of 20 and 30 mm respec- 25 tively, a 30 mm diameter cylindrical Teflon tube (5 mm thickness), two 30 mm circular Teflon inter spacers where one has a 2 mm slit, six Viton O-ring seals, two coverslip glasses where one is cut, and a brass screw to tighten the bilayer chamber. The inner elements consisting of a porous cellulose support, ETFE partition, Teflon spacers, circular glass 30 cover slips and Viton O-rings fit into the cylindrical 30 mm diameter tube of the cis chamber, and rest upon the ledge created by the interface of the trans chamber and the cylindrical 20 mm diameter tube of the cis chamber. The 5 mm thick cylindrical Teflon tube provides the link to the 20 annular brass screw (perimeter thickness 7 mm) generating sufficient

pressure from the exterior of the chamber to obtain a water tight sealing. Thus the cis and trans chambers have identical volumes. A circular, 2 mm thick circular Teflon spacer with a 2 mm slit is positioned with the opening at the top of the chamber that allows for entering bilayer forming solutions into the lipid bilayer chamber with a Hamilton syringe.

Pre-painting of scaffold using the airbrush technique

The lipid solution for pre-treatment of ETFE LZ200 partitions (pre-painting) and for the bilayer forming solution consisted of 50 mg/ml of 1,2-Diphytanoyl-sn-Glycero-3-Phosphocholine (DPhPC) in decane. 30 DPhPC (2 ml) in chloroform (10 mg/ml stock) was evaporated under nitrogen gas and the dry lipid was resuspended in 400 mL decane. The bilayer forming solutions were stored at −20°C until use. For fluorescent microscopy the lipid solutions were added 1 mol% of 1-Oleoyl-2-[6-[(7-nitro-2-1,3-benzoxadiazol-4-yl)amino]hexanoyl]-sn-Glycero-3-Phosphocholine (NBD-PC).Pre-painting of ETFE partitions was carried out by the addition of approximately 5 mL of DPhPC in decane (50 mg/ml) using a glass Pasteur pipette to both sides of the ETFE partition. The ETFE partitions were left to dry for 10 min followed by applying a gentle stream of nitrogen gas to both sides the partition to ensure opened apertures. The prepainting step was repeated five times, and the pre-treated ETFE partitions were stored in a vacuum desiccator until use. Another pre-painting strategy was developed to provide a more controlled and uniform deposition of the pre-painting solution (50 mg/ml DPhPC in decane) to the ETFE partition aperture arrays, and was based on airbrushing the pre-painting solution onto the ETFE partition sides. The airbrush setup consisted of an airbrush (type: MAS G41, TCPGlobal) connected to a nitrogen gas flask and mounted onto an aluminum track with a ruler. The airbrush was positioned with a distance of 45 mm from the airbrush nozzle to the ETFE partition. The partition was mounted on a brass housing that was connected to a low capacity vacuum pump. Partitions were placed on the brass housing and the vacuum pump turned on briefly to fix the partition in position during the pre-painting procedure. The 0.6 ml gravity feed cup of the airbrush was filled with

pre-painting solution (100 µl) and the pre-painting solution was deposited onto the ETFE partitions as a fine mist using a nitrogen pressure of 15 psi. The partitions were applied pre-painting solution on each side consequitive times with an interval of 30 s to give a thin uniform coverage of prepainting solutionon the ETFE partitions.

Fluorescent imaging was performed on a Zeiss Axiovert 200M epifluorescence microscope (Carl Zeiss, Jena, Germany) equipped with a monochrome Deltapix DP450 CDD camera (Deltapix, Maalov, Denmark). Imaged were acquired using Deltapix DpxView Pro acquisition software (Deltapix, Maalov, Denmark). Objectives used were air corrected Plan-Neofluar 2.5x/0.075 Numerical Aperture (NA), 10x/0.25 NA and 20x/0.40 NA respectively. Fig. 19 shows 6 fluorescent images of traditional and airbrush pretreated multiple apertures. Epifluorescence images of the ETFE 8x8 apertures array partitions pre-treated with pre-painting solution (50 mg/ml DPhPC in decane) with 1mol% of the fluorescent lipid NBD-PC with two different methods. Images A), B), and C) show the pre-treatment of the ETFE partition by the traditional pre-painting method using a glass Pasteur pipette for 5 consecutive times on both sides. Objectives used were A) 2.5x, B) 10x and C) 20x. Images D), E), and F) show the pre-treatment of ETFE partitions by the air-brushing the pre-painting solution on both sides for 20 consecutive times with 30 s intervals. Objectives used were 15 D) 2.5x, E) 10x, and F) 20x.

The lipid bilayer chamber was assembled with the ETFE partition prepainted using the traditional method and a circular regenerated cellulose sheet (DSS-RC70PP, Alfa Laval) with diameters of 29 mm. The regenerated cellulose was included in the multiple bilayer formation technique to provide a porous support structure for BLM formation. This semisupported bilayer formation strategy was chosen to minimize the hydrostatic pressure between the trans and cis chamber upon establishment of lipid bilayers. Once assembled, the ETFE partition was by design located at the center of the circular interface between the cis and trans lipid bilayer chamber. The trans and cis chambers were filled with 7.5 ml of a 200 mM KCl, pH 7.0 solution, and the lipid bilayer chamber

was then placed in a Faraday cage and the silver/silver chloride electrodes placed in the electrode wells. The level in the cis chamber was lowered to the beginning of the cut glass coverslip by aspiration of approximately 7 ml aqueous KCl solution using a plastic Pasteur pipette (Figure 23A). A Hamilton pipette was filled with 100 mL of DPhPC in decane (50 mg/ml), and the bilayer forming solution was applied to the space between the cut cover slip glass and the combined partition and regenerated cellulose support of the cis chamber through the 2 mm slit in circular Teflon spacer of the assembled chamber. The level of the aqueous solution in the cis chamber was slowly raised by adding approximately 7 ml aqueous KCl solution using a plastic Pasteur pipette (Figure 23B-C). During the raising of the aqueous KCl solution the stepwise formation of BLMs in the partition aperture arrays was recorded by measurements of the capacitance and conductance signals. The primary electrical setup consisted of a Model 2400 Patch Clamp Amplifier with a headstage containing 10G/10M feedback resistors (A-M 15 Systems, Inc., WA, USA) and a Thurlby Thandar Instruments model TG2000 20MHz DDS function generator (RS components Ltd, Northants, UK).

Data acquisition was done with a combined oscilloscope/analogdigital converter (ADC-212/50, Pico technology) connected to a laptop computer. Sampling frequency was 50 Hz and the low pass filter corner frequency of 1 kHz. Capacitance and conductance measurements were performed by applying triangular and rectangular voltage clamp waveforms. Reference measurements of the combined regenerated cellulose and ETFE partition were made prior to formation of the multiple BLMs. Formation of planar lipid bilayers across multiple aperture ETFE partitions was performed by the method outlined in Fig. 23. This method proved to be reliable in the sense that multiple BLMs (64 apertures) were generally established by a single or two lowering and raisings (Figure 23), and with a success rate above 95%. For all multiple aperture bilayer experiments initial conductance values were in the range of 250–900 nS and capacitance values in the range of2000–6000 pF. We evaluated the capacitance and conductance contributions of regenerated cellulose, and of ETFE film without apertures and regenerated

cellulose mounted in the bilayer chamber respectively. The regenerated cellulose had a conductance of 9165.9 ± 23.0 nS and no measurable capacitance (n=5), whereas the ETFE film plus cellulose had a conductance of 127.0 ± 1.6 nS and a capacitance of 2336.4 ± 19.0 pF (n=5). Given that the capacitance and conductance values for the multiple bilayer experiments are comparable to the reference values of the overall system, the initial measured capacitance and conductance values in the multiple aperture bilayer experiments are interpreted as being from the system alone and is due to the effective sealing of the apertures by the bilayer forming solution. The observed fluctuations in the initial conductance and capacitance values were due to variations in chamber assembly (e.g. tightening of the brass screw, silicone grease deposition, etc). Thus, the initial capacitance and conductance values and the initial value fluctuations observed for formation of multi array lipid bilayers reflect the inherent capacitance and conductance properties of the bilayer chamber and assembly. Following lipid membrane sealing across the apertures, lipid bilayers start to form and expand inside the apertures. The thinning of lipid membranes into bilayers give rise to an increase in the observed capacitance (Fig. 18A), while an increase in conductance is observed when the sealing properties of the BLMs start to fail (Figure 18B). Interestingly, some membranes (~10%) exhibited a capacitative discharge and recharge cycling behaviour with a time course of approximately 500 min, which is also reflected in the time course of the conductance. This behaviour of BLMs formed across multiple aperture partitions was observed as a repetitive cycling in capacitance and conductance values from the initial lipid bilayer formation values of around 2000–5000 pF and 250–900 nS, and to lipid bilayer values of 26000–38000 pF and 2500–5800 nS respectively (Figure 18C and 18D). In general, lipid bilayers formed across multiple aperture ETFE partitions were stable for 200–300 min before breakdown, while some membranes (approx. 40%) lasted for 1–3 days when left with voltage potentials ≤ ±100 mV. However, the membrane thinning curves varied considerably between experiments with average capacitance and conductance values of 31607.6 ± 13425.7 pF and 2947.0 ± 2898.8 nS (n=5) at 250 min (Figure 18A

and 18B).

A reason for the low experimental reproducibility of BLM characteristics from establishment of the lipid membranes to lipid bilayers could be influenced significantly by variations in the amount and homogeneity of lipid depositions during the pre-treatment process. Therefore, fluorescent images were acquired of 8x8 array ETFE partitions following pre-painting with DPhPC in decane (50 mg/ml) with 1 mol% of the fluorescent lipid NBD-PC for five consecutive times on each side followed by opening of apertures under a gentle stream of nitrogen gas. Results showed that the pre-painting solution was deposited inhomogeneous on the partition surface, and several apertures were consistently partial or completely occluded by the prepainting solution in spite of the applied nitrogen to open the apertures (Figure 19A, 19B and 19C). Although the majority of apertures were open, they had a varied degree of lipid deposition around the rim of the apertures protruding into the aperture, thus reducing the effective aperture diameter. This could also be a factor negatively influencing the reproducibility (Figure 23B and 23C). To circumvent the inhomogeneous lipid pre-treatment depositions, an airbrushing pre-treatment technique was developed. The airbrush technique for pre-treatment of partitions, e.g. as described above, was able to deposit lipids onto the ETFE partition in a homogenous and controlled manner by using a nozzle to partition distance of 45 mm, a nitrogen pressure of 15 psi and painting intervals of 30 s. Fluorescent images of ETFE partitions pretreated for twenty consecutive times on each side showed that apertures were homogeneously covered by a fine thin layer of lipids (Figure 19D, 19E, and 19F). Apertures were coated with lipid without being occluded, and aperture rims exhibited a uniform coating without lipid depositions protruding into the apertures (Figure 19E, and 19F). Multiple aperture bilayer experiments revealed that enhanced reproducibility were achieved by establishing BLMs across the airbrush pre-treated multi aperture ETFE partitions (Figure 20A). Following a short lag phase (~2–10 min) the multiple formed lipid membranes thinned in a time dependent manner reaching maximum capacitance values of 28529.7 ± 1421.7 pF at around 250 min (n=5) (Figure 20A).

The conductance values were relatively stable (540.9 ± 128.2 nS) during the time course of 100 min at which point the conductance increased 15 to 2323.3 ± 460.9 nS during the time course from 100 min to 250 min. In the minutes prior to membrane rupture an abrupt increase in conductivity was commonly observed.

Valinomycin was dissolved in 96% ethanol to yield a 1.8 mM working solution, which was stored at 4 °C until use. Tetraethylammonium (TEA) working solution (16 mM) was prepared in 200 mM KCl and prepared immediately before use. Valinomycin (1.8 mM) was added (10 µl) to the small chamber volume between the ETFE partition and the first glass coverslip in the chamber setup (volume 0.5ml), corresponding to a final valinomycin concentration of ~32 µM. Valinomycin incorporation was only performed on multiple BLMs displaying constant membrane characteristics for more than 60 min. To reverse the valinomycin-induced conductance, TEA working solution was added (200 µl) to the small chamber volume, corresponding to ~4.5 mM TEA. To ensure that bilayers are formed across the multi aperture partitions the potassium ion-selective cyclodepsipeptide valinomycin were added (32.0 µM final concentration) to lipid bilayers displaying a stable conductivity for more than 60 min. Following addition of valinomycin to the chamber an abrupt increase was immediately observed indicating functional reconstitution of valinomycin cyclodepsipeptides into the bilayers formed across the array of 8x8 aperture (300 µm diameters) partitions. The effect of valinomycin could effectively be reversed by the addition of 5 the channel blocker TEA (4.5 mM final concentration) (Figure 21). In contrast, addition of ethanol or TEA alone to formed lipid bilayers to final chamber concentrations of up to 1% and 5.9 mM, respectively, did not significantly affect membrane characteristics (data not shown). Combined, these results strongly indicates that stable lipid bilayers are in fact formed across the multi array aperture partitions and that lipid bilayer spanning channels can be functionally inserted into the formed lipid bilayers. Giving the total aperture area of 0,045 $cm^2$ for 64 apertures with average diameters of 300 µm and a specific capacitance of 0.4–0.6 µF/ $cm^2$ previously determined for solvent containing lipid bilayers, the capacitance for multi-

ple formed bilayer lipid membranes were expected to be in the range of 18095 to 27143 pF. Therefore, the capacitance values of 29126.6 ± 691.9 pF found in this study (Figure 20A) indicate that the total lipid bilayer area is somewhat 6.4–37.6 % larger than expected with a specific bilayer capacitance of 0.4–0.6 μF/ $cvm^2$. This indicates that either the membranes formed by the technique presented herein is thinner compared to the conventional manually painted lipid membranes or a reservoir of lipid is present on the sides of the partition when bilayer lipid membranes are formed across the multi aperture ETFE partitions, or a combination of both.

Example 11. Testing of different ETFE films as scaffold material.

Scaffolds having 300 μm diameter apertures in a rectangular 8x8 arrays and a centre-to-centre distance of 400 μm were prepared in two different ETFE film materials: Fluon 50N and Tefzel LZ200 both having a 50.8 μm thickness. BLMs were prepared in these scaffolds to make composite biomimetic membranes using the lipid, solvent, and aqueous electrolyte solution materials described in Example 10 above in a horizontal chamber setup,cf. Fig. 26 without scaffold prepainting and where a hydrophobic fluorescent material, i.e. NBD-PC (a fluorescent lipid analogue) had been added to the lipid setup adapted for microscopic visualisation. Fluorescence images were obtained using a 2.5x objective and virtually identical BLMs were observed, cf. Fig. 25 wherein it can be seen that identical composite membrane arrays can be formed in different ETFE brands.

Example 12. Incorporation of alpha-hemolysin in composite biomimetic membrane

Aim of experiment was to show that functional establishment of black lipid membranes (BLMs) can be performed by inserting membrane spanning peptides and proteins. A protein that inserts spontaneously into functional BLMs is α-hemolysin (αHL), which forms a heptameric protein complex when reconstituted into established membranes. Protein incorporation can be followed because the insertion of a functional protein has a conductance of approx 35 pA. The sequential insertion of the pro-

tein is observed as a stair-like voltage clamp trace.

*Materials and Chemicals*

- 8x8 array on ETFE LZ200 partition
- 25mg/ml DPhPC + NBD-PC (1-oleoyl-2- [6-[ (7-nitro-2–1, 3-benzoxadiazol-4-yl) amino]hexanoyl]-sn-glycero-3-phosphocholine) (Avanti Polar Lipids Inc. (Alabaster, AL, USA)
- 0,5mg/ml α-hemolysin (αHL) solution diluted 20X (Sigma-Aldrich Denmark ,Brøndby, Denmark).
- KCl buffer solution 1M

*Equipment & Required laboratory working time*

- Inverted fluorescence microscope
- BLM amplifier and signal generator: The experimental setup consisted of a Model 2400 Patch Clamp Amplifier with a head stage containing 10 G/10 M feedback resistors (A–M Systems, Inc., WA, USA) and a Thurlby Thandar Instruments model TG2000 20 MHz DDS function generator (RS Components Ltd, Northants, UK). The electrodes were placed in the trans and cis compartments of the bilayer formation chamber with the ground electrode positioned in the trans compartment. Data acquisition was done with a combined oscilloscope/analog–digital converter (ADC-212/50, Pico Technology, Cambridgeshire, UK) connected to a laptop computer.
- Chamber shown in Fig. 26.
- DPhPC has to be prepared the day before and stored at -20ºC

Preparing black lipid membrane arrays:

- Mount the chamber as described in example 10 and fill the centre chamber with 3ml 1 M KCl and the outer chamber accordingly.
- With the tip of a small Finnpipette, and the amount of lipid that is left when emptying the tip, "draw" the membranes on the array An air/lipid bubble is blown out from the pipette tip and positioned close to the array. The pipette tip is then swept across the array in a painting-like motion to establish BLMs across the apertures.

- Repair any broken membranes with the tip while waiting for the membrane to stabilize.

Preparation of αHL solutions:

- αHL is supplied as a lyophilized powder with a content of 0.5 mg per vial.
- To make a stock solution, add 1 ml Milli-Q water to the vial with αHL, this gives a stock concentration of 0.5 mg/ml.
- Dilute the stock solution with water or an appropriate buffer by 20 fold to make a 25 µg/ml working solution.
- Store at -20ºC until use.

Data acquisition and incorporation of αHL:

- When a stable BLM array has been established (check by capacitance and conductance measurements), apply a 60 mV DC offset using the menu on the signal generator. It is convenient to store this as a program.
- In pico scope set the axes for the membrane output to 20V on the y-axis amplitude and 50 div/s on the x-axis. This gives a voltage clamp trace running for 500 s.
- Leave the DC offset on for approx 5-10 min before adding the protein solution to ensure a stable membrane array. If single apertures rupture, then repair and wait for another 5-10 min with the DC offset turned on.
- For protein incorporation apply 10 µl of a 25 µg/ml αHL solution to the top chamber and away from the membrane array. This gives a final αHL concentration in the top chamber of approx 83.3 ng/ml.
- Follow the membrane trace on pico scope to see when protein is reconstituted into the membrane array.
- Store the trace after successful protein incorporation.

*Results and conclusion*

Fig. 25 shows that αHL was successfully inserted in a composite biomimetic membrane of the invention. A) shows the bilayer array used

in the αHL experiment using a 2.5x objective. B) shows a transmitted light image of a part of the bilayer array to demonstrate the prescense of bilayers, and C) shows the corresponding fluorescence image of the fluorescent NBD-PC lipid analog that is present in the bilayer forming solution.D) shows the functional incorporation of αHL proteins in the preformed bilayer array. The functional reconstitution of αHL proteins in the lipid bilayer array is observed as a stepwise increase in the conductance, where each functional incorporation results in an approx. 35 pA conductance increase. The resulting stair-like voltage diagram in Fig. 25 D shows that it is possible to insert functional transmembrane proteins in lipid bilayers established across the ETFE scaffold. Moreover, the fact that single channel events can be resolved with very low background noise shows that the scaffold is applicable to sensitive membrane protein-based biosensor applications such a drug screening.

An example of the usefulness of having access to an array of functional αHL transmembrane proteins is in testing of compound libraries for modulation, such as inactivation or antagonizing, of the protein. Beta-cyclodextrin can be used as a positive control since this molecule is a known αHL antagonist (Li-Qun Gu and Hagan Bayley, Interaction of the Noncovalent Molecular Adapter, b-Cyclodextrin, with the Staphylococcal a-Hemolysin Pore. Biophysical Journal Vol. 79 October 2000 1967–1975).

Example 13. Preparation of composite BPM membrane using the APM method

*Materials and Chemicals*

- KCl, 200 mM
- 30 mg of 4 PMOXA(y)-PDMS(x)-PMOXA(y) (poly(2-methyloxazoline)-block-poly(dimethylsiloxane)-block-poly(2-methyloxazoline)having 4 cross-linkers. Herein is used 5 = y = 15; 40 = x = 80, which can be custom synthesized by Polymer Source, Quebec, Canada. Nardin et al. Langmuir Vol. 16, p7708-12, 2000

- Photoinitiator: DAROCUR® 1173
- Solvent:
    - o Decane
    - o Choroform
    - o 1,2 butandiol diacrylate

*Equipment & Required laboratory working time*

- APM chamber fully assembled including 8x8 scaffold Tefzel LZ200
- Labware in general
- 90 min + membrane lifetime
- Instruments for voltage-clamp measurements:
- PicoScope data acquisition unit
- Generator and amplifier (Eastern Scientific)

*Standard operating procedure:*

Preparation of polymer solution:

Weight 30 mg of polymer in a small glass vial. Place the polymer stock back to the fridge. Dissolve completely (takes some time) the polymer by adding and shaking 50 µl of Chloroform. Add 250 (between 200 and 300) µl of Decane and shake again. Using a "plastic tip" pipette, add 50 µl of 1,2 butandiol diacrylate.

*Preparation of the electrolyte solution:*

Prepare a non-filtered 50 ml solution of KCl 200 mM. Using a "plastic tip"pipette add 50 µl of photoinitiator (Darocur). With the same pipette, add one droplet of photoinitiator in the polymer solution. Shake and than filter the electrolyte solution using a 200 µm filter connected to the syringe. Wrap the polymer solution + electrolyte solution's container with aluminium foil. Mount the chamber using quartz glass slides. Use a viton ring with a large hole in front of the ETFE partition.

*Rinsing the assembled chamber with buffer:*

Fill up the back chamber with the electrolyte solution, including the

shaft space. Discard the buffer and refill up to the level just below the shaft space. Fill up, gently, the front chamber and make sure the area in front of the partition and behind the cut inner glass cover; the 'capillary volume,' is wetted. Discard and refill with buffer until desired level is reached.

*Injecting polymer solution on top of buffer:*

Inject 150 µL of polymer solution (organic phase) by inserting a Hamilton-syringe into the injection shaft and gently place the organic phase volume on top of the buffer surface. Rinse immediately the Hamilton-syringe with chloroform: otherwise the metal piston will be glued to the glass syringe. Fill up the front chamber with buffer until the surface of the 'capillary volume'. Put the APM chamber inside a Faraday-cage.

*Set up for doing voltage-clamp measurements:*

In short: Make sure the generator is on and the PicoScope data acquisition software is running. Position the head-stage mounted AgCl-electrodes in the front and back chamber. For ease, adjust the external off-set to align the blue (membrane signal) line just below the red line showing the external signal. Collect reference data for both triangular (capacitative signal) and square (resistance or conductive signal.) applied external signal.

Lowering and raising the buffer level in front of partition to form BPM's:

Use the principle of painting polymer membranes on the apertures grid. The organic phase containing polymers are painted over the partition thereby depositing and partitioning polymers into the apertures. As the aqueous phase subsequently surrounds the apertures and organic phase, the polymer molecules spontaneously self assemble into planar polymer thin membranes. Apply external signals, squared and triangular to record snapshots of the resulting electrical membrane characteristics.

Observe the membranes development for a few minutes (10 - 15). If the electrical signal are really low (cap < 25 mV), reform the membrane by lowering and raising the buffer level. If the electrical signals

evolve very fast ( +/- 5 mV per minute), the membrane is not stable. So it is better to reform a new one. When the electrical signals are nice and evolve slowly, cross-link the membrane following the instructions mention below.

*Formation of second 'generation' BPM's:*

Break first 'generation' membranes by switching generator power on and off. Lower the 'capillary vol.' and add 50µL of the polymer solution. Raise, lower and reraise the 'capillary vol.' Observe that an electrical seal has been achieved which is an indicator for successful membrane formation. If the membranes break within the first 30 minutes, repeat the lowering/raising and note accordingly in the experiment journal. Perform data recording in the following series:

- First 30 min. every 2 minutes
- Next 60 min. every 10 minutes
- Remaining time every 20 minutes

After formation of BPMs in the scaffold protein can be incorporated in the membranes according to the procedures disclosed in Ho et al. Nanotechnology Vol. 15 (2004) 1084-94 for incorporation of bacteriorhodopsin or COX in copolymer membranes, or according to Ho et al. Nanomedicine Vol 2 (2006) 103-12 for membrane insertion of OmpF solubilized in n-octylpolyoxyethylene.

Following protein incorporation and allowing for subsequent equilibration time of up to 1 hour, the membrane can be cross-linked according to the procedure below.

Polymer cross-linking

Since every components are already mixed, we just need to irradiate the whole chamber with UV to activate the photoinitator. Hold the UV lamp (EA-140/FE from Spectroline, 625µW/cm$^2$ at 6 inch distance) far as possible from the chamber. Switch on the UV lamp and place it in front of the chamber. Wait 7 minutes, place the lamp as far as possible and switch it off. After 4 days the 8x8 composite membranes attained a steady state conductance value of 500 nS, and a steady state capacitance value of about 3000 pF. The composite membranes were stable for

at least 6 days. Thus, we have shown that a composite biomimetic membrane where the amphiphilic membrane forming compound is a co-polymer can be formed using the scaffold of the invention.

Further aspects of the invention relates to the following statements:

A membrane scaffold comprising a planar material having a hydrophobic surface (water contact angle greater than about 100°, such as a Teflon, e.g an ETFE film) wherein a central functional area comprising a plurality of apertures have been formed using an optically guided thermal process, and wherein the apertures in said film are essentially of a circular shape and have an essentially perpendicular position relative to the plane of said planar material, and further characterized in that the aperture rims are smooth and formed into bulges; and said membrane scaffold wherein the perforated area covers from about 30 % to about 60 % of said central functional area; said membrane scaffold wherein said apertures have a diameter of > 200 µm to about 3000 µm, preferably > 250 µm to about 450 µm; said membrane scaffold wherein the aperture rim further has a toroidal bulging; said membrane scaffold wherein said bulging is from about 8 µm to about 20 µm above the scaffold surface; said membrane scaffold wherein the spacing between the apertures is from about 150 µm to about 500 µm; said membrane scaffold wherein the central perforated area is about 2 cm x 2 cm; said membrane scaffold where said planar material has a thickness of from about 25 µm to about 200 µm; said membrane scaffold wherein said planar material is an ETFE film having a thickness of between about 50 µm to about 75 µm; said membrane scaffold where said optical or thermal process is a $CO_2$ laser ablation.

A composite biomimetic membrane comprising

a) the membrane scaffold as defined in any one of the preceding claims, and

b) a biomimetic membrane formed in said apertures, where functional channel forming molecules have been incorporated in said membrane;

said biomimetic membrane wherein said channel forming molecules are selected from the group consisting of ion channel molecules, such as valinomycin and gramicidin monomers and dimers, transmembrane proteins, such as porins, aquaporin water channels, and the CD family of receptors; said biomimetic membrane wherein said channel forming molecules cover at least 1 to 10 % of the bilayer area; said biomimetic membrane wherein said channel forming molecule is an aquaporin molecule, and said biomimetic membrane being useful in a filtration device for purification of a water source or a liquid, aqueous medium.

A biomimetic membrane according to any of the above statements, which is a bilayer lipid membrane wherein said lipid is selected from DPhPC and DPPC and derivatives thereof; said biomimetic membrane wherein said lipid is dissolved at a concentration of from about 10 mg/mL to about 100 mg/mL in an apolar solvent selected from hexane, octane, decane, hexadecane, etc.; said biomimetic membrane wherein said lipid bilayer further comprises a bilayer stabilising amount of cholesterol, dextran, etc.).

A filtration device for filtering essentially pure water comprising a composite biomimetic membrane according to any of the statements above.

A method of preparing a composite biomimetic membrane comprising the following steps where the reference numbers refer to Fig. 12 herein:

a) providing a two-cell chamber wherein each cell has an upper opening to allow access to the cell, and a scaffold with a central area having multiple apertures (4) according to claim 1 which provides a partition between the two cells to form a cis chamber and a trans chamber,

b) providing a partial separation (7) in the cis chamber which extends from the top of said chamber to below said central area thus forming a relatively narrow space with said scaffold (4) where a spacer (5) between said partial separation (7) and said scaffold (4) has an upper opening to allow insertion of a syringe ,

c) providing a porous support (3) which is a functional water barrier at atmospheric pressure opposite the partial separation (7),

d) providing a first volume of aqueous buffer solution in the trans chamber opposite the partial separation (7) where said volume extends above said central area of said scaffold (4) ,

e) providing a second volume of aqueous buffer solution in the cell having the partial separation (7) where said volume does not reach the lower level of said central area of said scaffold (4),

f) providing a volume of membrane forming solution in the space between the partial separation (7) and the scaffold (4), and

g) adding an extra volume of said aqueous buffer into said cis chamber to raise the buffer level above said central area thereby raising the membrane forming solution completely past said apertures to form a fluid membrane therein; said method may further require that elastic seals (2) and (6) are inserted between parts (1) and (3), (4) and (5), (5) and (7), (7) and (8), (8) and (9), and between (9) and the annular sealing screw, said elastic seals being made from a chemically resistant material, such as a fluoroelastomer, e.g. Viton®; said method wherein said scaffold has been pre-painted with a solution of amphiphilic lipid in a hydrocarbon solvent; said method wherein said lipid is DPhPC and where said solvent is n-decane.

The APM-1 chamber as defined herein or as shown in Figures 12, 12a, 13.

While the present invention has been described with reference to specific embodiments thereof, it will be appreciated that numerous variations, modifications, and embodiments are possible, and accordingly, all such variations, modifications, and embodiments are to be construed as being within the spirit and scope of the present invention. All references cited herein are incorporated in their entirety by reference. Additional aspects, features and embodiments of the invention will be more fully apparent from the ensuing disclosure and appended claims.

C L A I M S

1. A membrane scaffold comprising a planar material having a hydrophobic surface and a functional area comprising a plurality of apertures the cross sections of said apertures in said film being of an essentially circular shape, wherein the apertures have a diameter of from about 80µm to about 3000 µm, preferably 800µm and the rims of the apertures comprise bulges extending above and/or below the surface level of the planar material.

2. The membrane scaffold according to claim 1, wherein the perforated area of the functional area is from about 20% to about 60 %.

3. The membrane scaffold according to claim 1 or 2, wherein the apertures have a diameter of 200 µm to about 300 µm, especially 250 µm to about 450 µm and the center-to-center distance of the apertures is from about 100µm to about 600µm, such as about 150 µm to about 500 µm.

4. The membrane scaffold according to any one of claims 1 to 3, wherein the planar material is a film of polyethylenetetrafluoroethylene (ETFE) or a derivative thereof.

5. The membrane scaffold according to any one of the claims 1 to 4, wherein the bulge extends about 6 µm or more, such as 8 µm or more, above the level of the planar material and wherein the bulges of neighbouring apertures may be merged into a common bulge.

6. The membrane scaffold according to any one of the claims 1 to 5, further comprising a homogeneous layer of a hydrophobic substance either deposited by solvent evaporation or covalently bonded by chemical activation.

7. A method for producing the membrane scaffold according to any one of the claims 1 to 6, comprising the steps of:

a. providing a planar material having a hydrophobic surface,

b. subjecting a spot of a functional area of the planar material to a laser beam having a wave length absorbed by the planar material for a time and an intensity sufficient for the planar material to melt and/or

vaporize at said spot,

c. allowing the melted material to solidify around the spot, thereby forming a bulging aperture rim,

d. displacing the planar material or the laser beam to another spot of the functional area and

e. repeating steps b. to d. until a plurality of apertures have been formed.

8. The method according to claim 7, wherein the planar material is a foil of polyethylenetetrafluoroethylene (ETFE) or a derivative thereof and the laser beam is provided by a $CO_2$ laser.

9. The method according to claims 7 or 8, wherein a neighbouring spot is subjected to a laser beam before solidification of the melted material of a previous spot and/or wherein the apertures initially produced are receiving a higher spot lase duration and/or a higher power or intensity than the subsequently produced apertures.

10. A composite biomimetic membrane comprising the membrane scaffold as defined in any one of the claims 1 to 6, and a biomimetic membrane provided in the apertures.

11. A composite biomimetic membrane according to claim 10 wherein functional channel forming molecules have been incorporated in said membrane.

12. The composite biomimetic membrane according to claim 11, wherein said channel forming molecules are selected from the group consisting of ion channel molecules, such as valinomycin and gramicidin monomers and dimers; transmembrane proteins, such as porins, aquaporin water channels, alpha-hemolysin; and the CD family of receptors.

13. The composite biomimetic membrane according to claims 10 to 12, wherein the membrane comprises of a triblock copolymer.

14. The composite biomimetic membrane according to any one of claims 10 to 13, wherein the membrane is a lipid bilayer.

15. The composite biomimetic membrane according to any one of the claims 10 to 14, wherein the lipid of the lipid bilayer membrane is selected from DPhPC, DPhPE, DPPC, SOPC, DOPC, asolecithin, E. coli to-

tal lipid extract, SOPE, DOPE, DOPS and derivatives and mixtures thereof.

16. A method according to claim 15, comprising the steps of:

a) providing a two-cell chamber wherein each cell has an opening allowing for access to the cell, and a membrane scaffold according to any one of the claims 1 to 6, which provides a partition between the two cells to form a cis chamber and a trans chamber,

b) providing a porous support which is a functional water barrier at atmospheric pressure

c) providing a first volume of aqueous buffer solution in the trans cell opposite the partial separation where said volume covers said central area of said scaffold,

d) providing a second volume of aqueous buffer solution in the cis cell opposite the partial separation where said volume covers said central area of said scaffold,

e) providing means to perfuse a volume (bolus) of membrane forming solution in the trans cell thereby impregnating said functional area resulting in fluid membranes in said area; and

f) adding an extra volume of said aqueous buffer into either chamber to remove bolus leaving membranes in said functional area facing the trans and cis cell aqueous buffer.

17. A method according to claim 16, comprising the steps of:

a) providing a two-cell chamber wherein each cell has an upper opening to allow access to the cell, and a membrane scaffold according to any one of the claims 1 to 6, which provides a partition between the two cells to form a cis chamber and a trans chamber,

b) providing a partial separation in the cis chamber which extends from the top of said chamber to below said functional area thus forming a relatively narrow space with said scaffold,

c) providing a porous support which is a functional water barrier at atmospheric pressure opposite the partial separation,

d) providing a first volume of aqueous buffer solution in the trans chamber opposite the partial separation where said volume extends above said central area of said scaffold,

e) providing a second volume of aqueous buffer solution in the cell having the partial separation where said volume does not reach the lower level of said functional area of said scaffold,

f) providing a volume of membrane forming solution in the space between the partial separation and the scaffold, and

g) adding an extra volume of said aqueous buffer into said cis chamber to raise the buffer level above said functional area thereby raising the membrane forming solution completely past said apertures to form a fluid membrane therein.

18. The method according to claim 17, wherein a spacer is provided between said partial separation and said scaffold, said spacer having an upper opening to allow insertion of a syringe.

19. An apparatus for testing the function of a transmembrane molecule comprising the composite biomimetic membrane according to any one of claims 10 to 15 and having the following features:
A two-cell chamber wherein each cell has an upper opening to allow access to the cell, and a membrane scaffold according to any one of the claims 1 to 6 comprising said composite biomimetic membrane, which provides a partition between the two cells to form a cis chamber and a trans chamber, a partial separation (7) in the cis chamber which extends from the top of said chamber to below said functional area thus forming a relatively narrow space with said scaffold (4), a porous support layer (3) which is a functional water barrier at atmospheric pressure opposite the partial separation (7), a first volume of aqueous buffer solution in the trans chamber opposite the partial separation (7) where said volume extends above said central area of said scaffold (4), a second volume of aqueous buffer solution in the cell having the partial separation (7) where said volume does not reach the lower level of said functional area of said scaffold (4), a spacer (5) is provided between said partial separation (7) and said scaffold (4), said spacer having an upper opening to allow insertion of a syringe.

20. The apparatus of claim 19, wherein elastic seals (2, 6) are inserted between parts 1 and 3, 4 and 5, 5 and 7, 7 and 8, 8 and 9, and between 9 and the annular sealing screw, said rubber-like seals being of

a chemically resistant material, such as a fluoroelastomer, e.g. Viton®.

21. The apparatus of claim 19 or 20, wherein an electrode is inserted in each of said upper openings and in contact with said first and second buffer solutions.

22. The apparatus according to any one of claims 19 to 21, wherein said transmembrane molecule is alpha-hemolysine.

23. Use of the apparatus according to claim 22 for the testing of a compound having binding effect on alpha-hemolysine said testing comprising adding a solution of said compound to said cis chamber and measuring conductance through said electrodes.

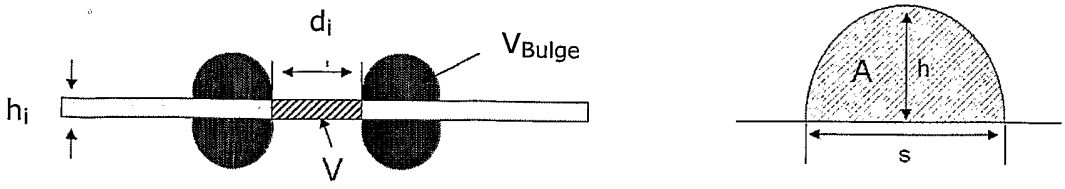


Fig. 1

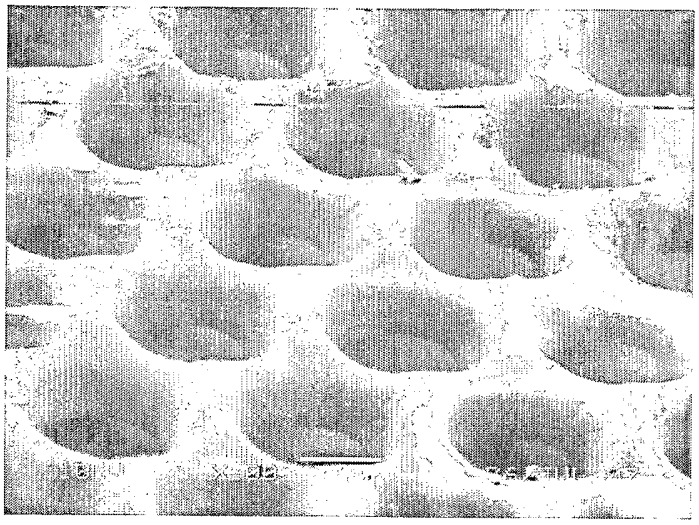

Fig. 2

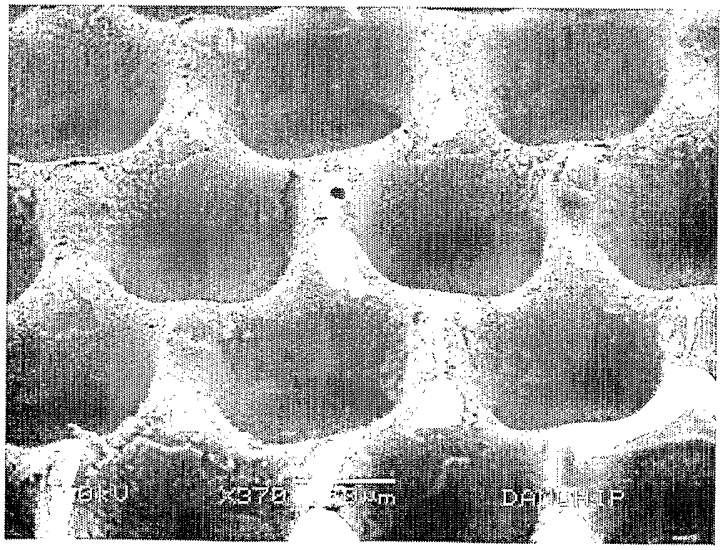

Fig. 3

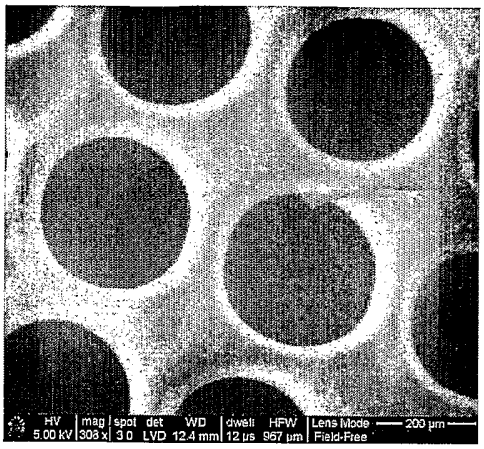


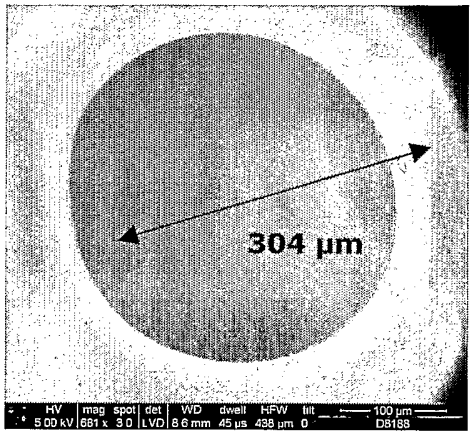


Fig. 4

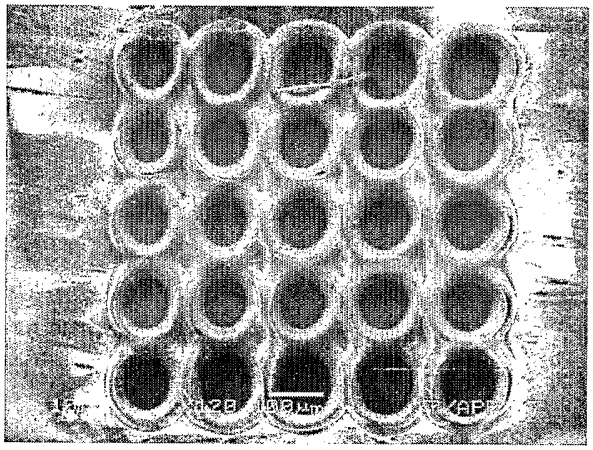

Fig. 5

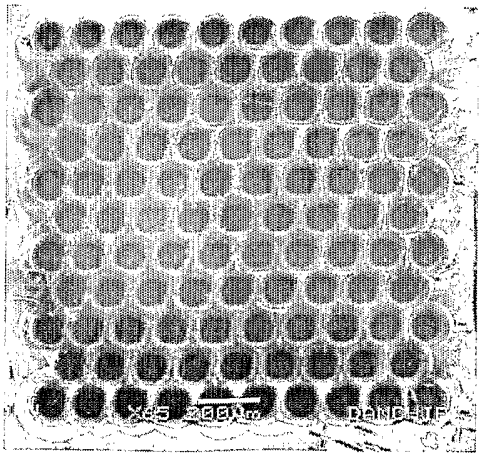

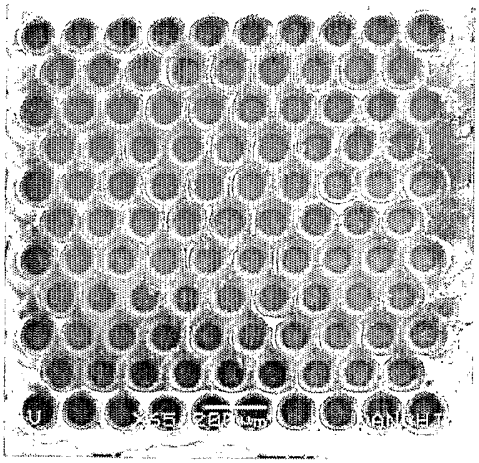

Fig. 6

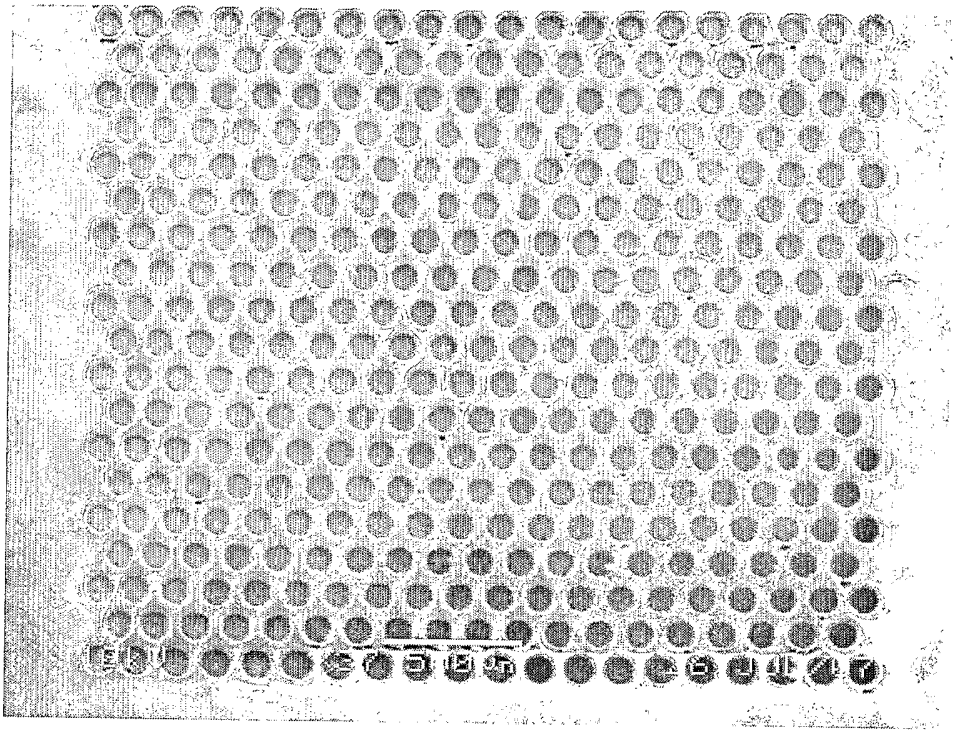

Fig. 7

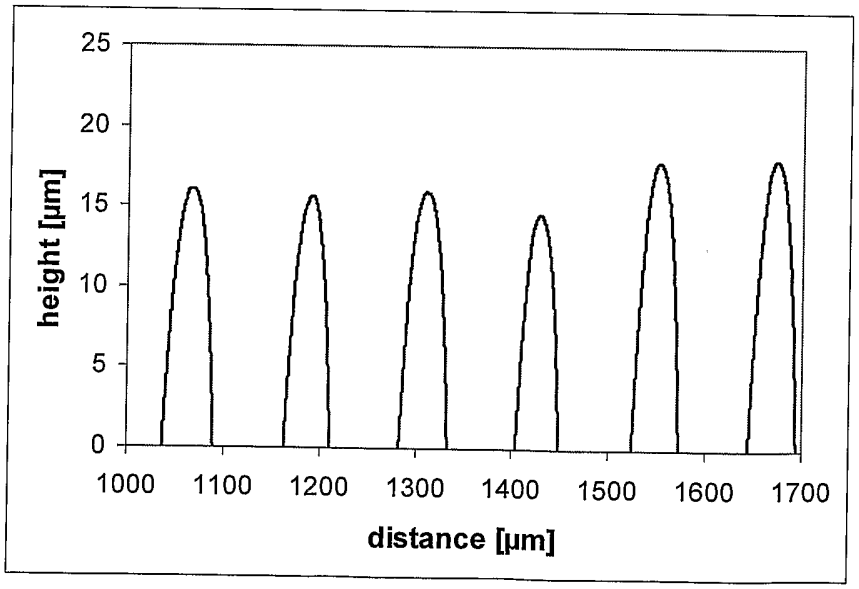
25
20
15
10
5
0
height [µm]
1000
1100
1200
1300
1400
1500
1600
1700
distance [µm]

Fig. 8

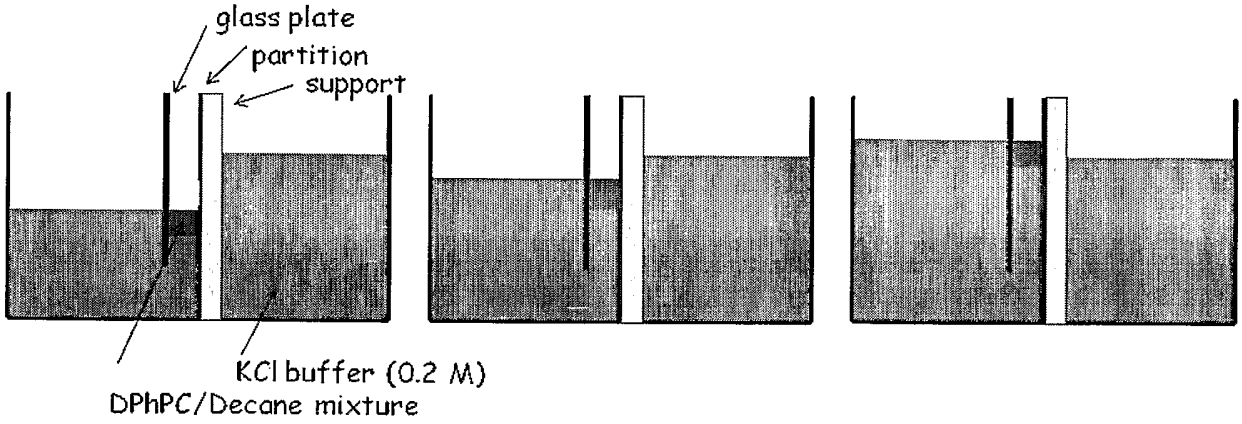


Fig. 9

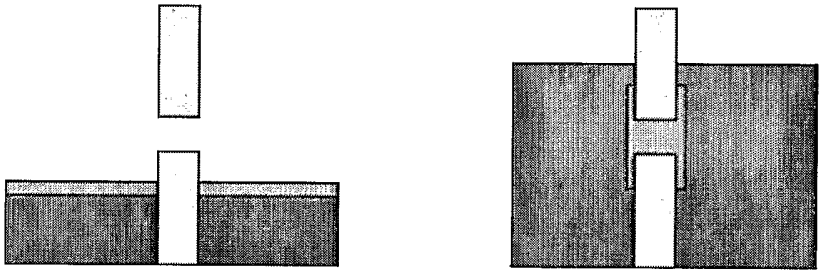

Fig. 10

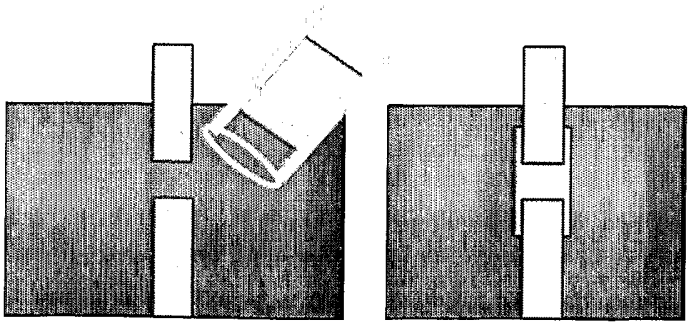

Fig. 11

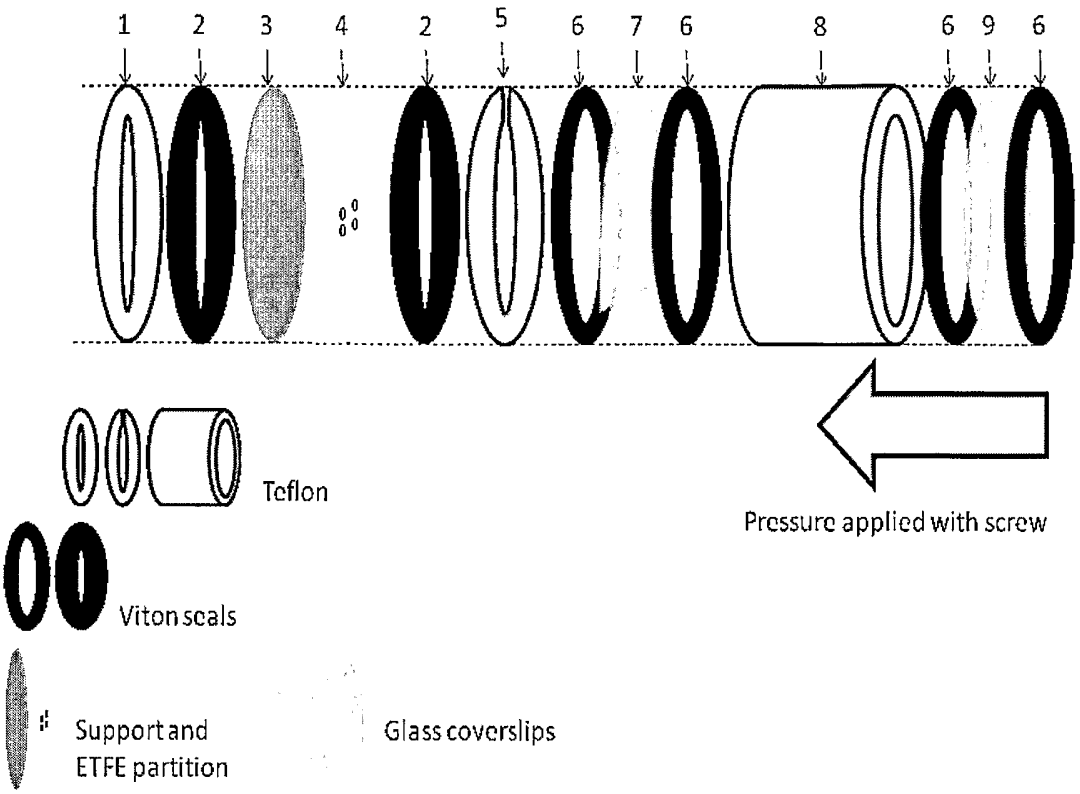


Fig. 12

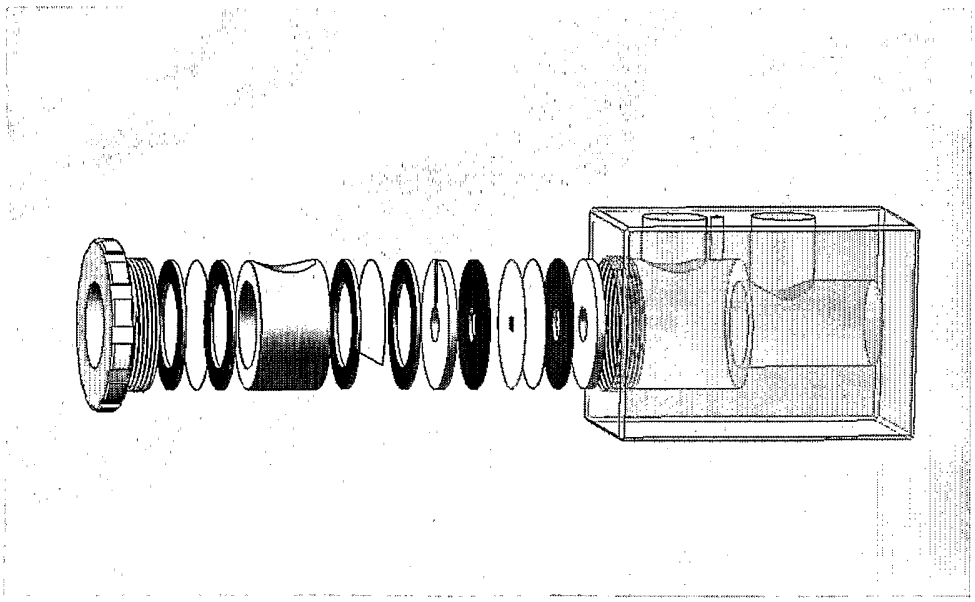

Fig. 12a

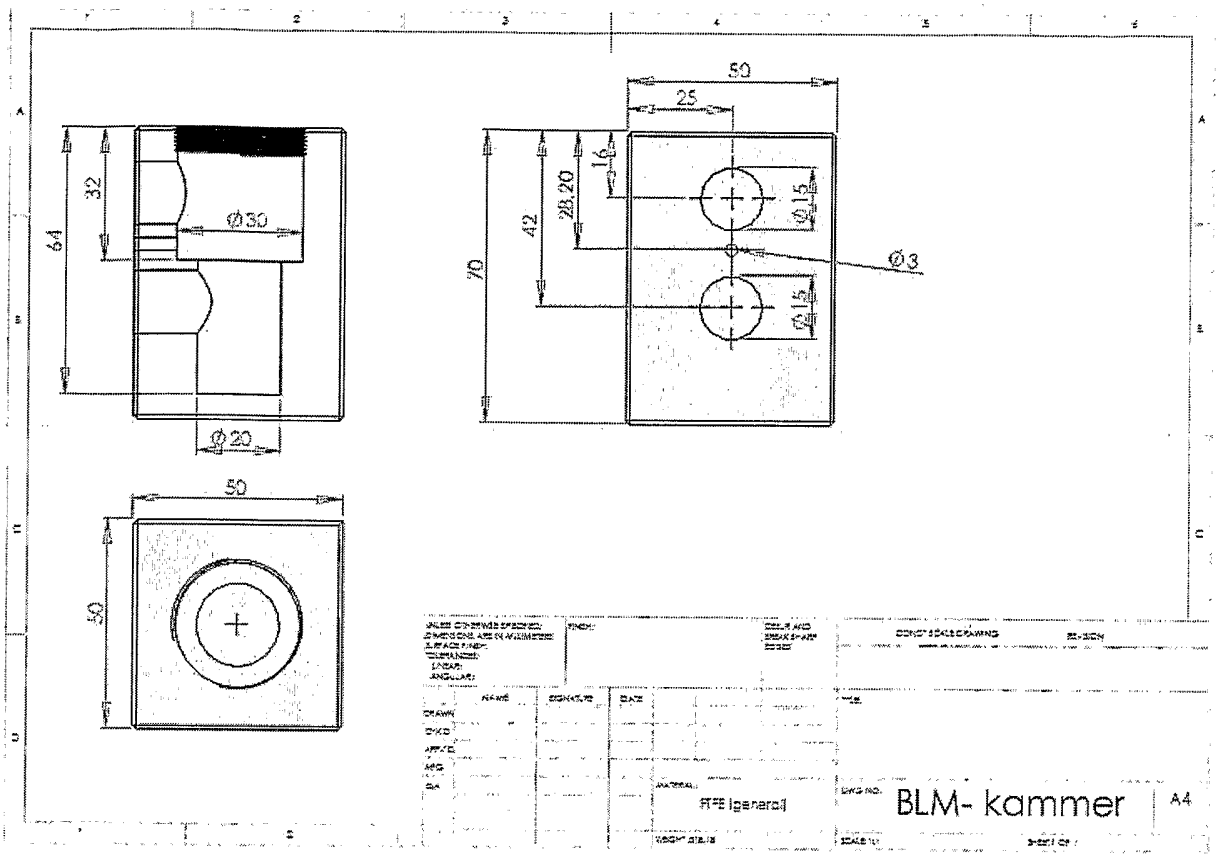


Fig. 13

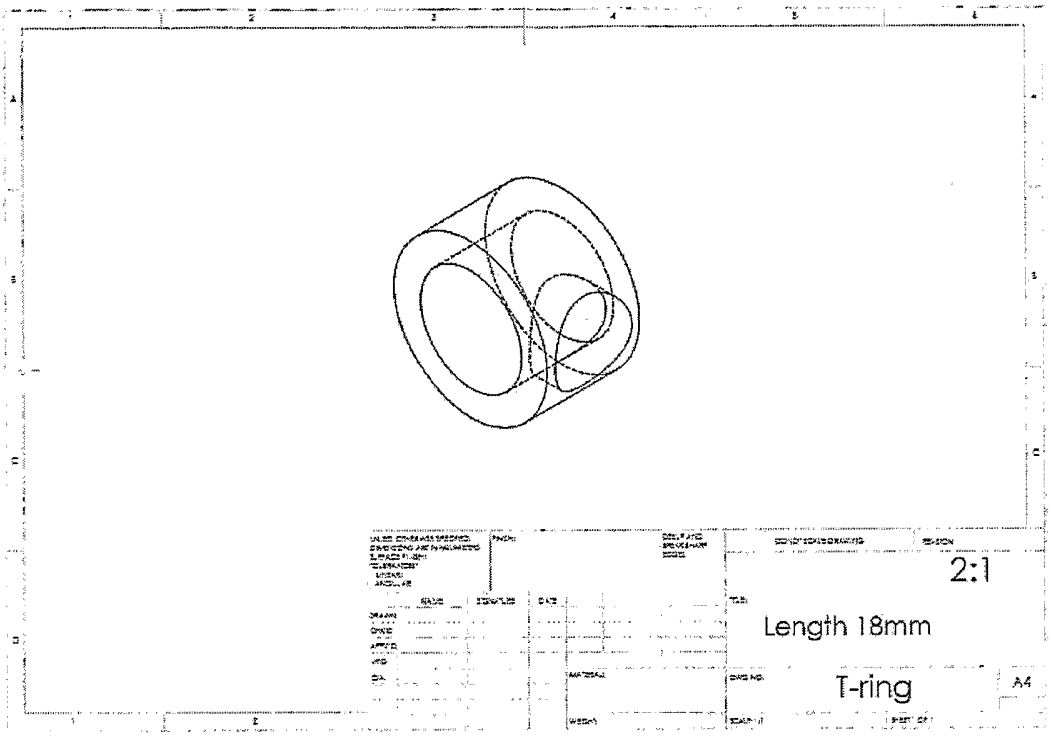


Fig. 14

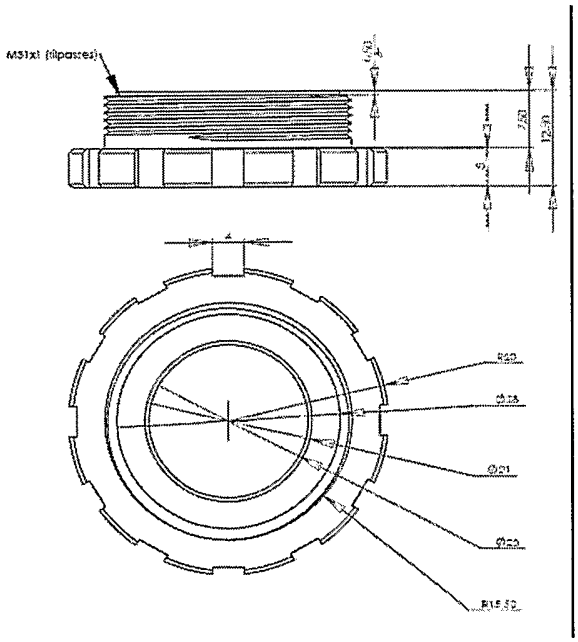


Fig. 15

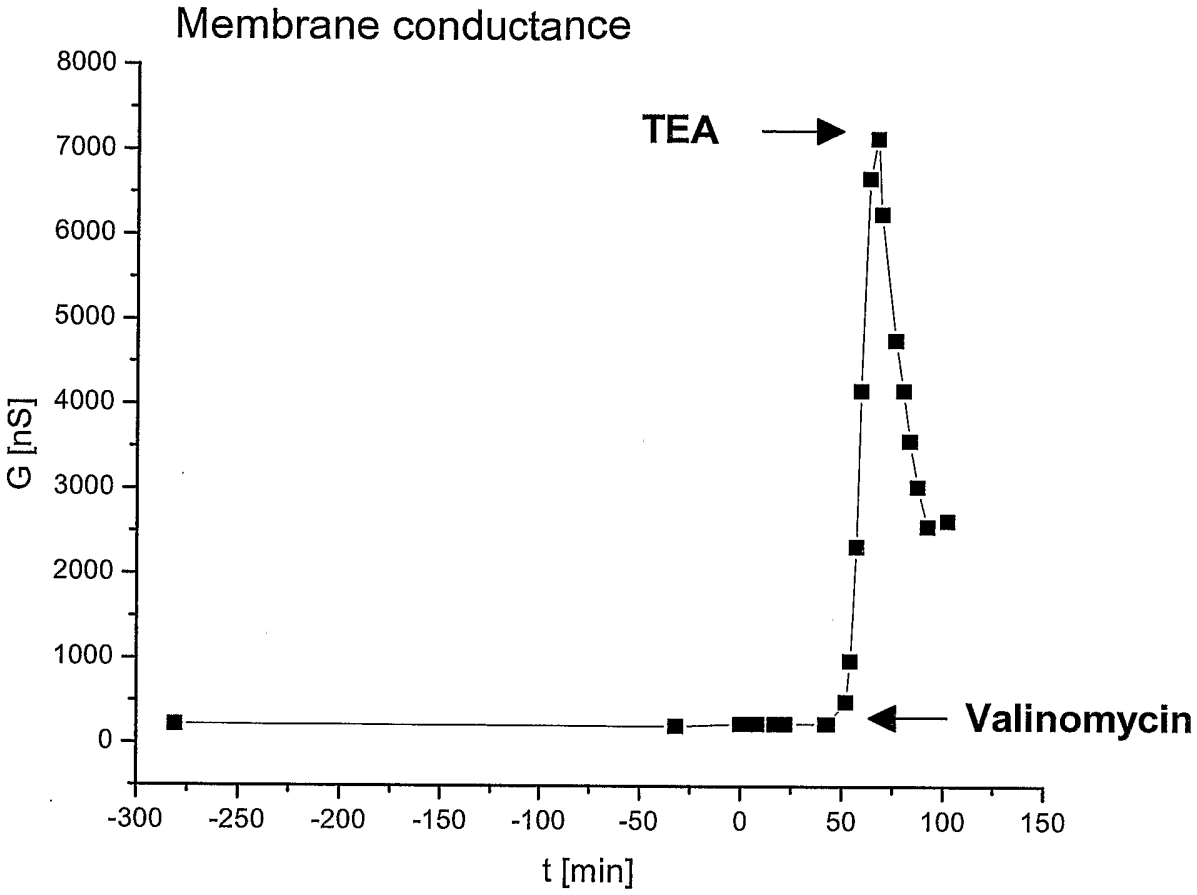
Membrane conductance
8000
7000
6000
5000
4000
3000
2000
1000
0
G [nS]
TEA
Valinomycin
-300
-250
-200
-150
-100
-50
0
50
100
150
t [min]

Fig. 16

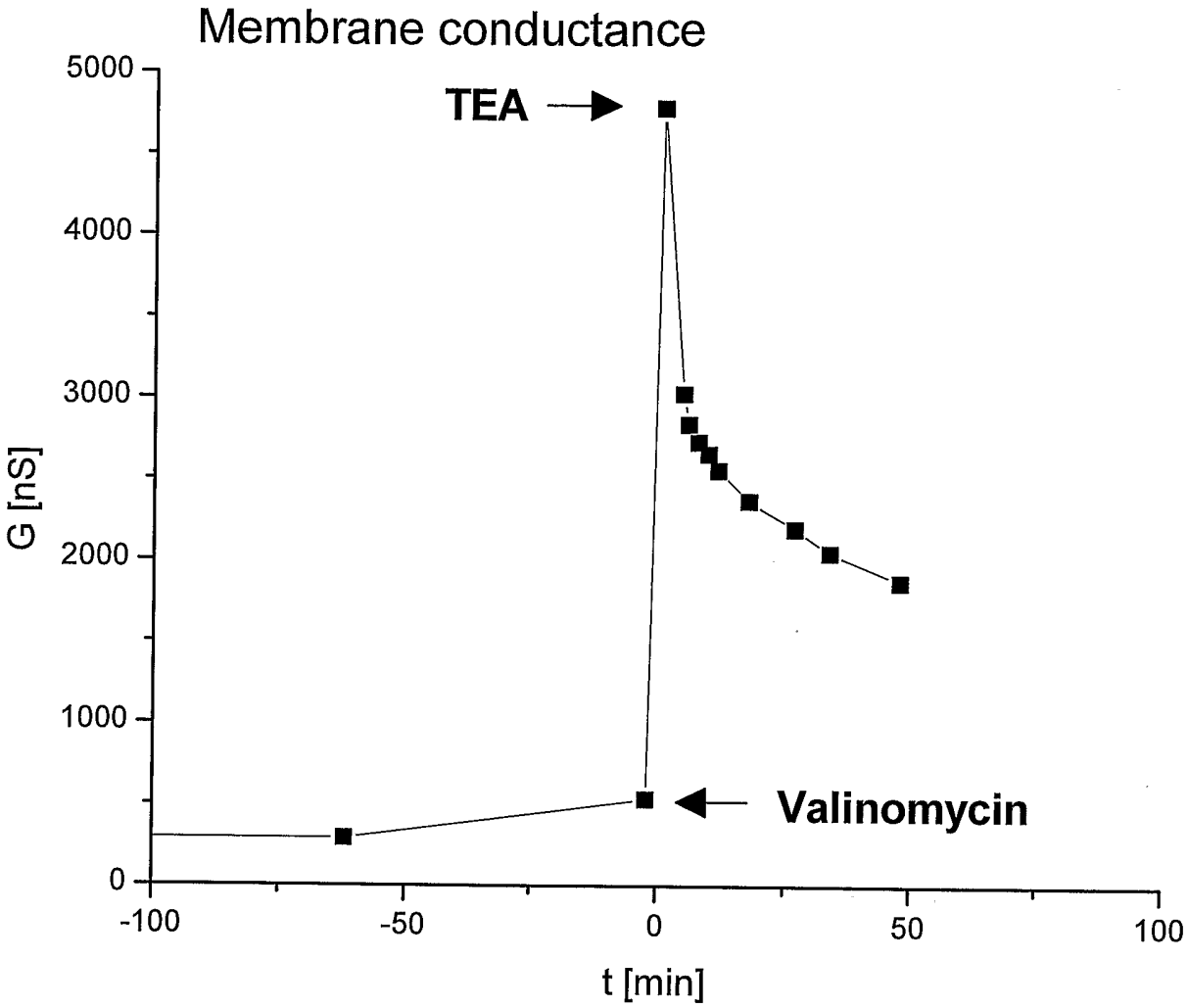
Membrane conductance
TEA
Valinomycin
G [nS]
5000
4000
3000
2000
1000
0
-100
-50
0
50
100
t [min]

Fig. 17

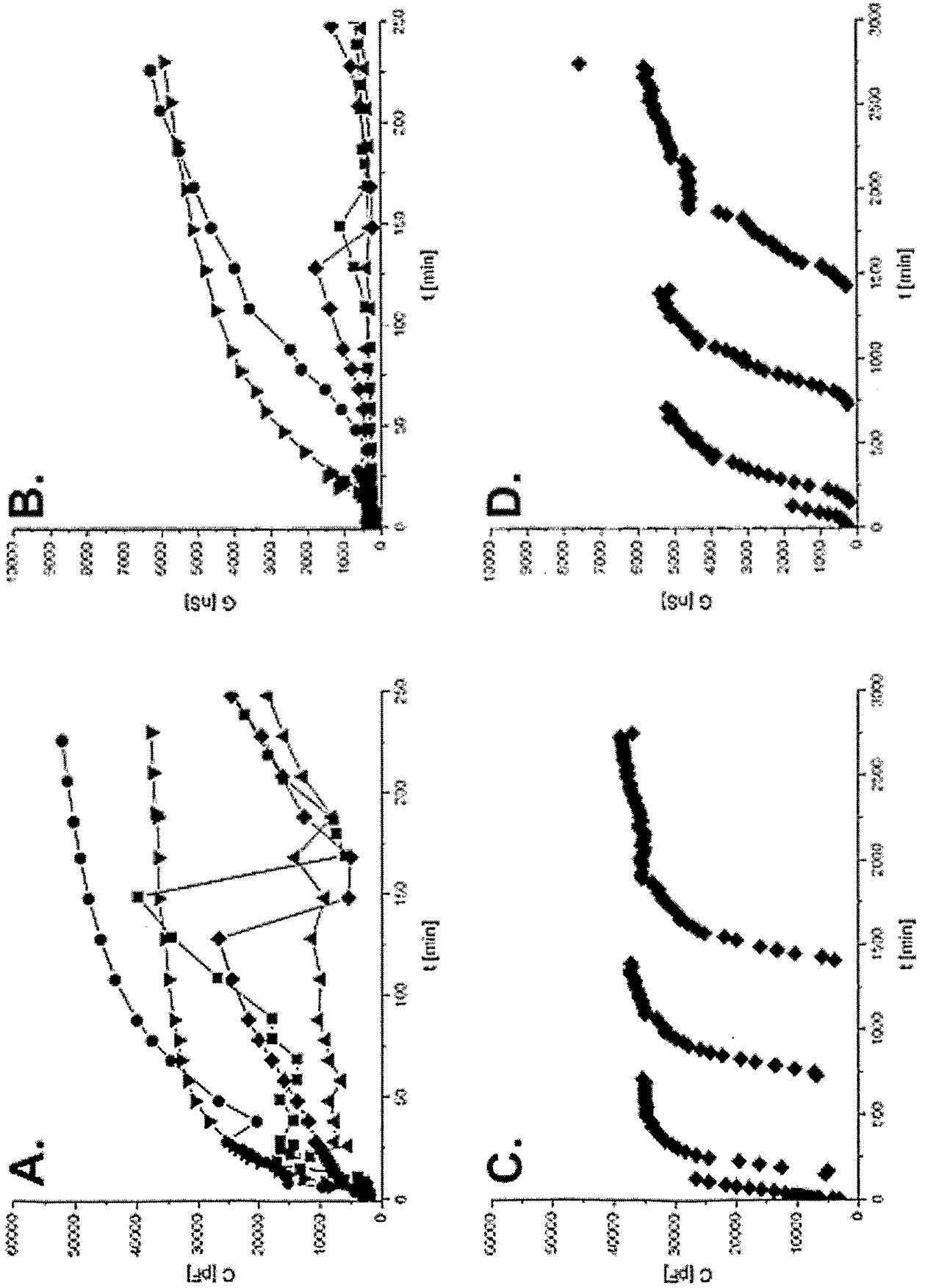


Fig. 18

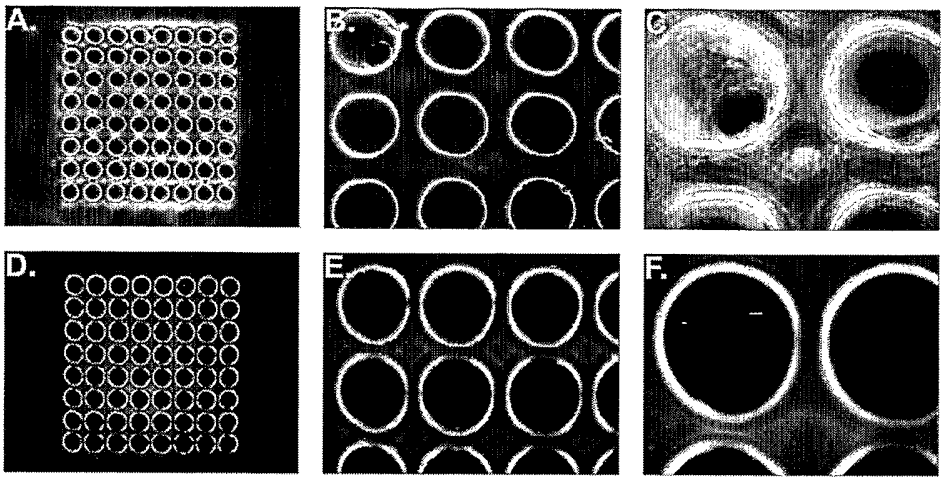


Fig. 19

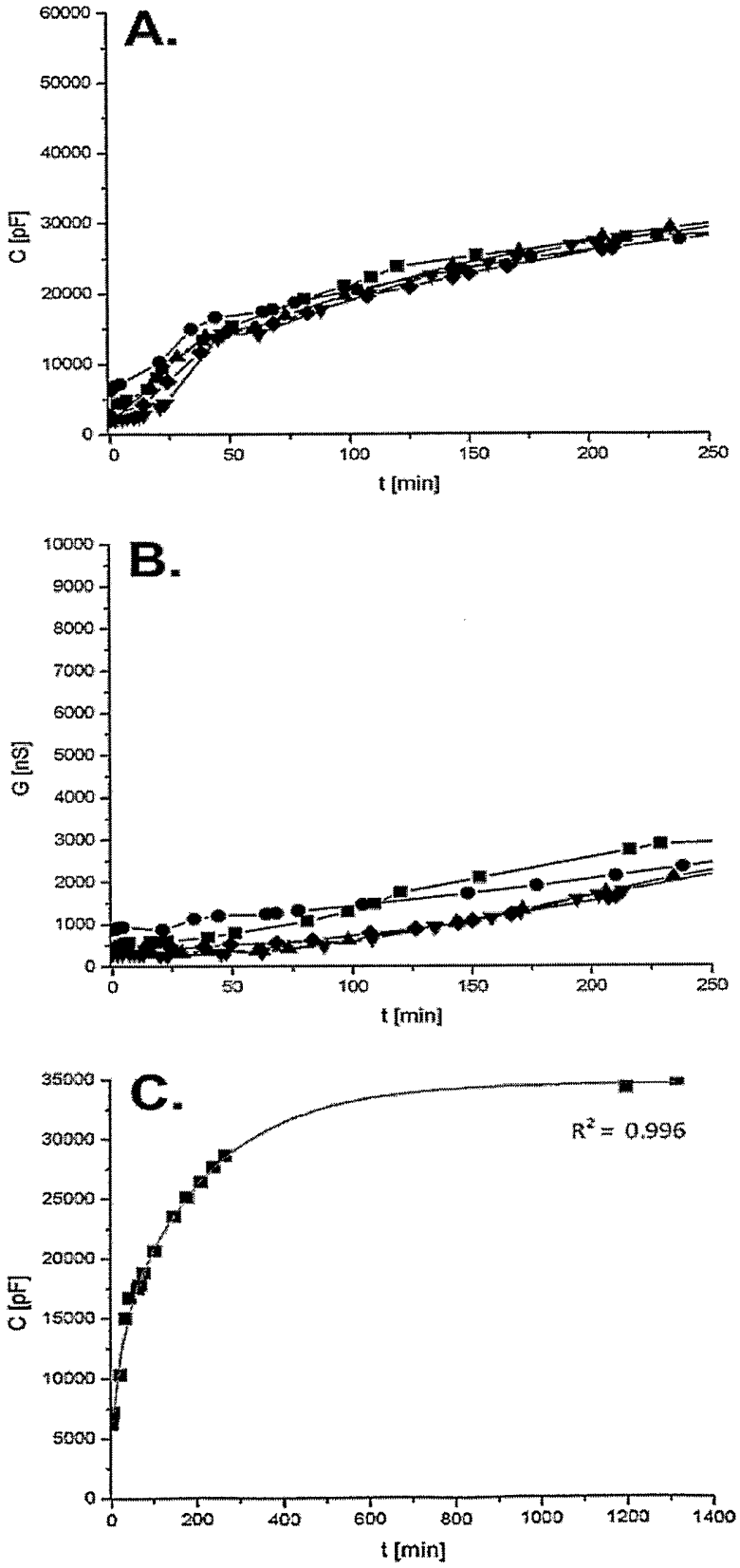


Fig. 20

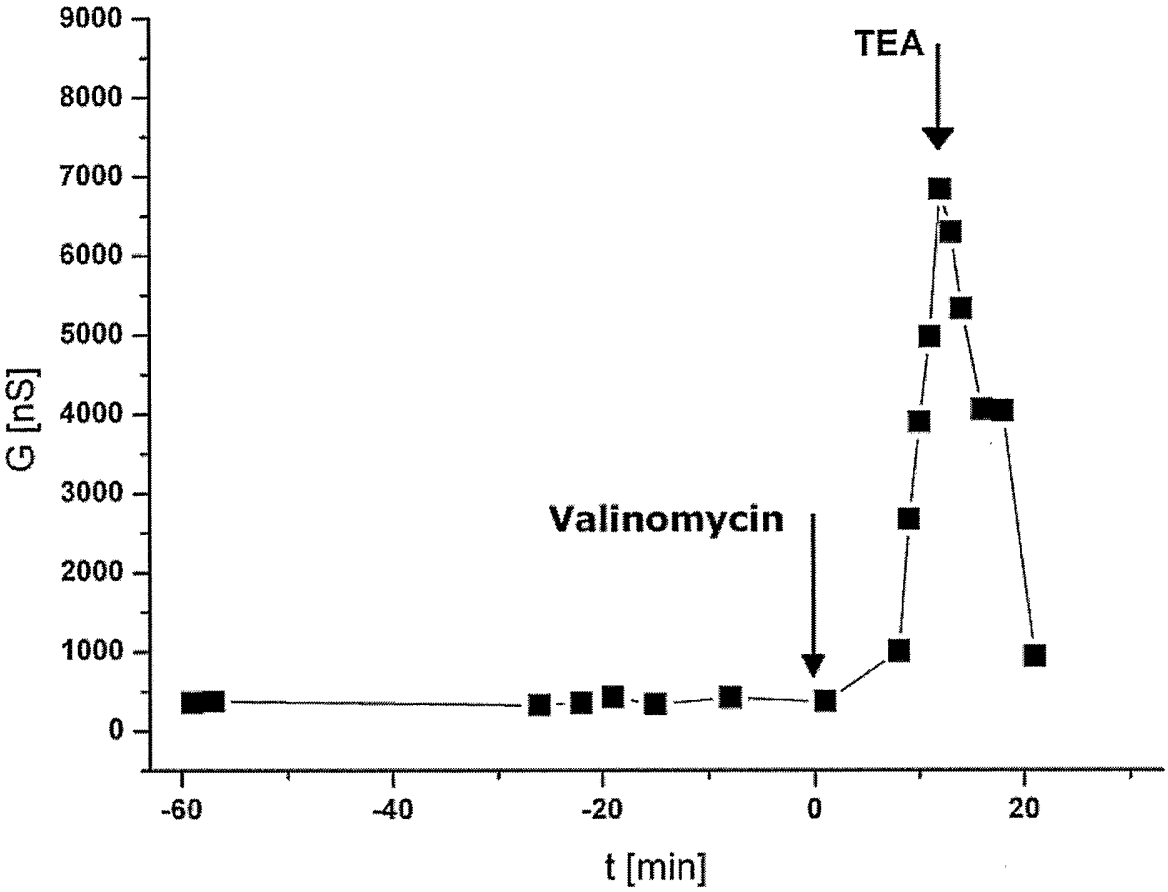
9000
8000
7000
6000
5000
4000
3000
2000
1000
0
G [nS]
TEA
Valinomycin
-60
-40
-20
0
20
t [min]

Fig. 21

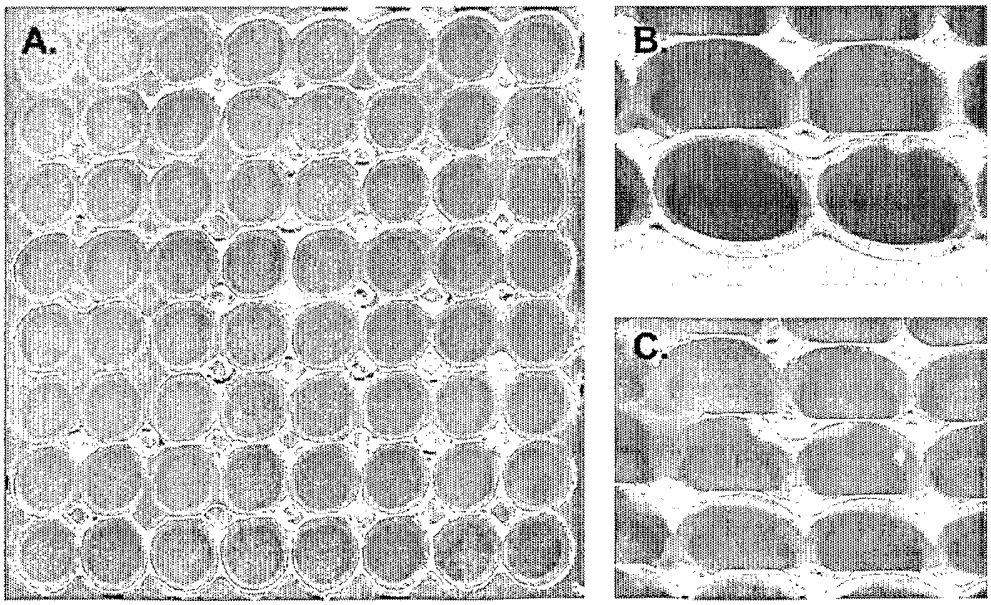
A.
B.
C.

Fig. 22

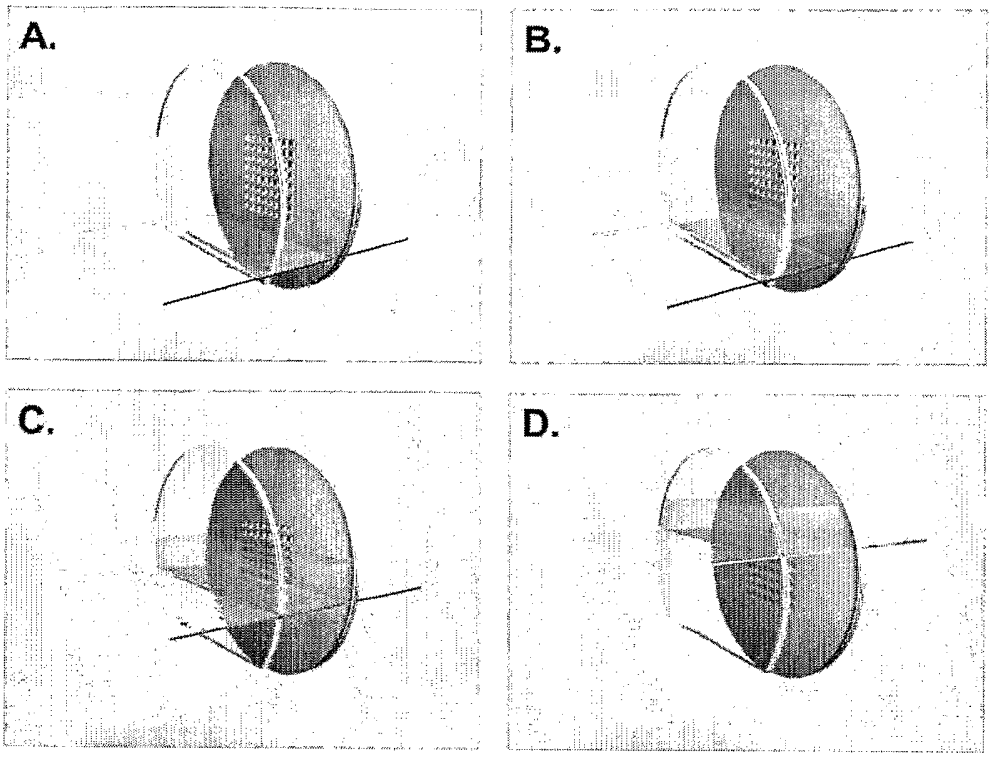


Fig. 23

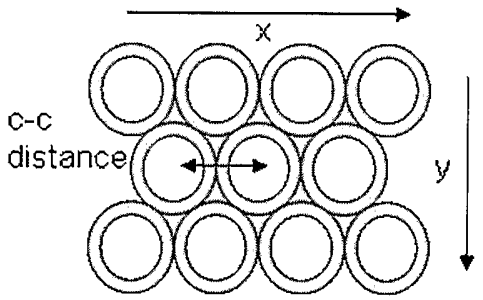


Fig. 24

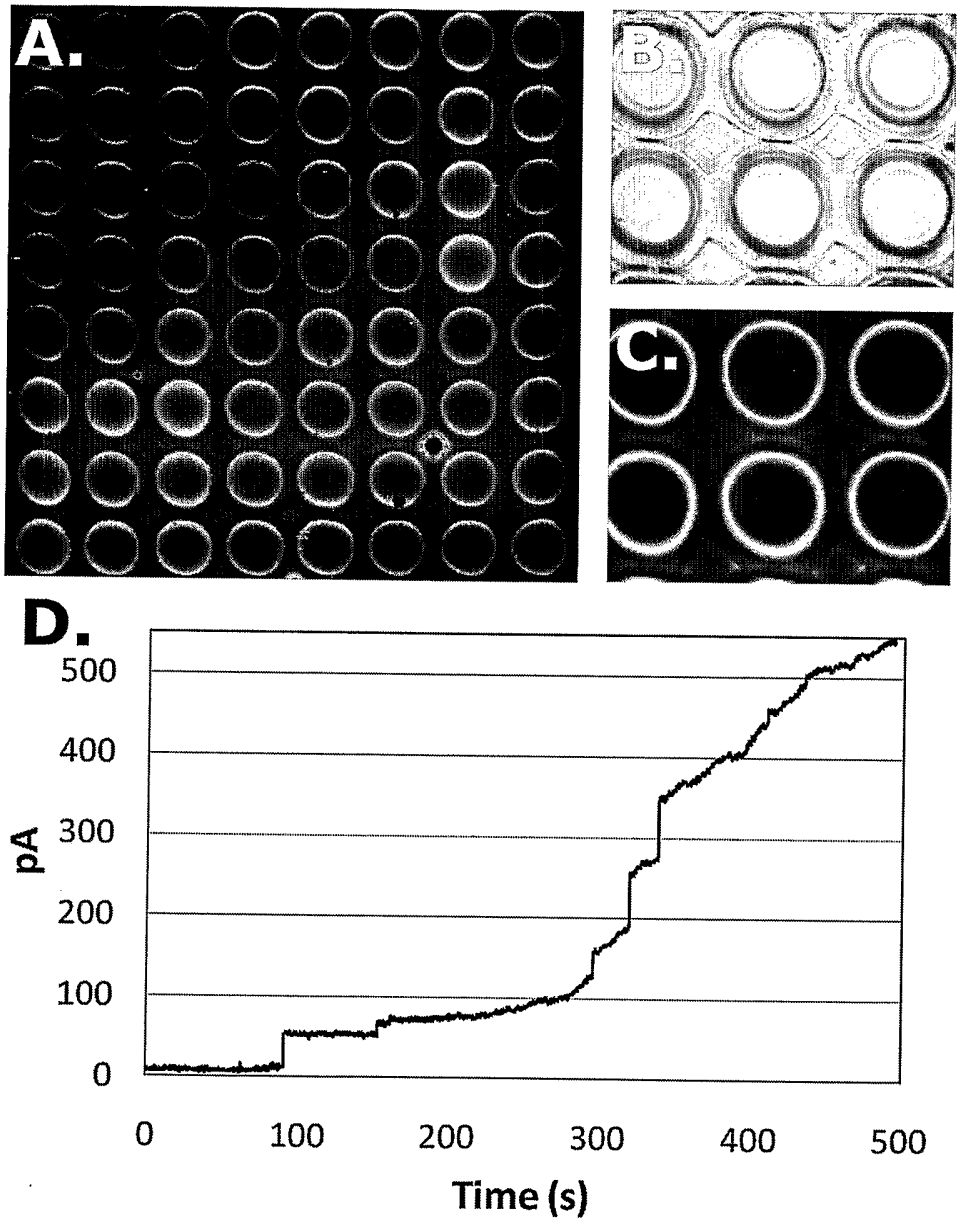


Fig. 25

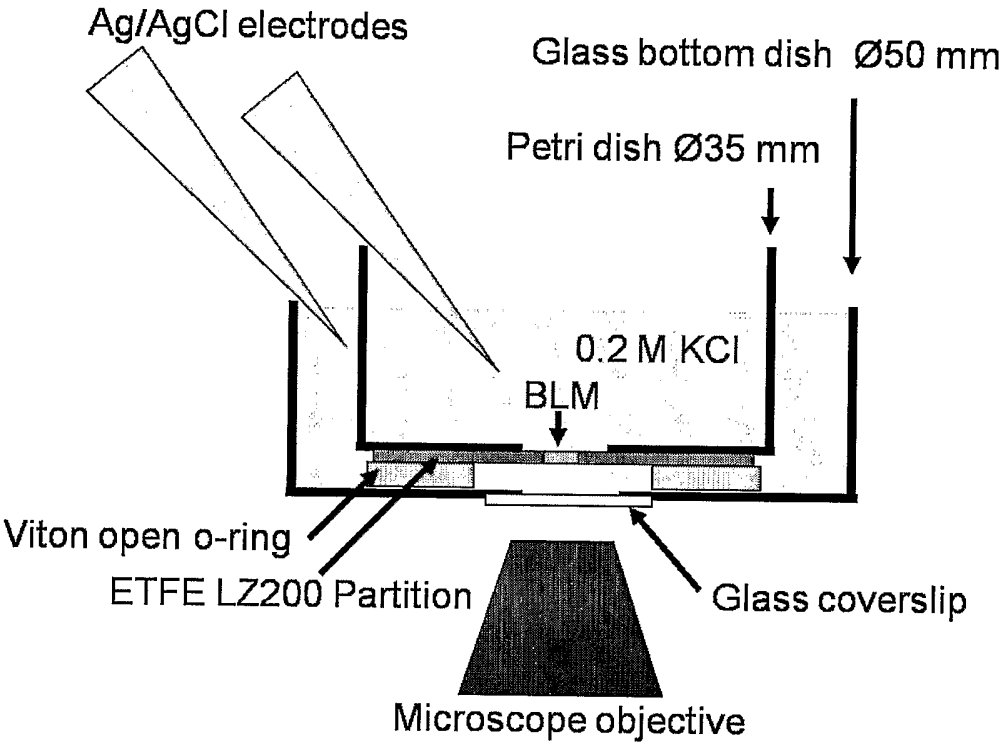
Ag/AgCl electrodes
Glass bottom dish Ø50 mm
Petri dish Ø35 mm
0.2 M KCl
BLM
Viton open o-ring
ETFE LZ200 Partition
Glass coverslip
Microscope objective

Fig. 26

# INTERNATIONAL SEARCH REPORT

International application No
PCT/DK2008/050303

A. CLASSIFICATION OF SUBJECT MATTER
INV. B01D69/14 B01D69/02 B01D69/10

According to International Patent Classification (IPC) or to both national classification and IPC

B. FIELDS SEARCHED

Minimum documentation searched (classification system followed by classification symbols)
B01D

Documentation searched other than minimum documentation to the extent that such documents are included in the fields searched

Electronic data base consulted during the international search (name of data base and, where practical, search terms used)
EPO-Internal, WPI Data

C. DOCUMENTS CONSIDERED TO BE RELEVANT

| Category* | Citation of document, with indication, where appropriate, of the relevant passages | Relevant to claim No. |
|---|---|---|
| X | WO 2006/122566 A (AQUAPORIN APS)<br>23 November 2006 (2006-11-23)<br>cited in the application<br>page 15, line 29 - page 17, line 6<br>page 27, line 16 - line 29; claims 1-16 | 1-23 |
| A | US 6 551 542 B1 (ARADIGM CORP.)<br>22 April 2003 (2003-04-22)<br>column 12, line 61 - column 13, line 26;<br>claims 1-24; figure 2 | 1-23 |
| A | US 2004/038105 A1 (V. HENNINGE ET AL.)<br>26 February 2004 (2004-02-26)<br>paragraph [0081] | 1-23 |

☐ Further documents are listed in the continuation of Box C.

☒ See patent family annex.

* Special categories of cited documents :

"A" document defining the general state of the art which is not considered to be of particular relevance

"E" earlier document but published on or after the international filing date

"L" document which may throw doubts on priority claim(s) or which is cited to establish the publication date of another citation or other special reason (as specified)

"O" document referring to an oral disclosure, use, exhibition or other means

"P" document published prior to the international filing date but later than the priority date claimed

"T" later document published after the international filing date or priority date and not in conflict with the application but cited to understand the principle or theory underlying the invention

"X" document of particular relevance; the claimed invention cannot be considered novel or cannot be considered to involve an inventive step when the document is taken alone

"Y" document of particular relevance; the claimed invention cannot be considered to involve an inventive step when the document is combined with one or more other such documents, such combination being obvious to a person skilled in the art.

"&" document member of the same patent family

| Date of the actual completion of the international search | Date of mailing of the international search report |
|---|---|
| 9 March 2009 | 25/03/2009 |

| Name and mailing address of the ISA/ | Authorized officer |
|---|---|
| European Patent Office, P.B. 5818 Patentlaan 2<br>NL - 2280 HV Rijswijk<br>Tel. (+31-70) 340-2040,<br>Fax: (+31-70) 340-3016 | Luethe, Herbert |

1

# INTERNATIONAL SEARCH REPORT

Information on patent family members

International application No
PCT/DK2008/050303

| Patent document cited in search report | Publication date | Patent family member(s) | Publication date |
|---|---|---|---|
| WO 2006122566 A | 23-11-2006 | AU 2006246841 A1 | 23-11-2006 |
| | | CA 2607371 A1 | 23-11-2006 |
| | | EP 1885477 A2 | 13-02-2008 |
| | | JP 2008540108 T | 20-11-2008 |
| | | NO 20075674 B | 12-02-2008 |
| US 6551542 B1 | 22-04-2003 | AU 1473000 A | 05-06-2000 |
| | | CA 2349712 A1 | 25-05-2000 |
| | | EP 1196263 A1 | 17-04-2002 |
| | | JP 2002529212 T | 10-09-2002 |
| | | MX PA01004914 A | 10-03-2003 |
| | | WO 0029167 A1 | 25-05-2000 |
| US 2004038105 A1 | 26-02-2004 | AU 2178302 A | 24-06-2002 |
| | | CA 2431057 A1 | 20-06-2002 |
| | | DE 10061959 A1 | 20-06-2002 |
| | | WO 0247802 A1 | 20-06-2002 |
| | | EP 1345675 A1 | 24-09-2003 |
| | | JP 2004515351 T | 27-05-2004 |
| | | NO 20032718 A | 13-06-2003 |
| | | PL 361848 A1 | 04-10-2004 |

# Appendix II

Manuscript to be submitted

K. Pszon-Bartosz, M. Perry, J. S. Hansen, J. Vogel, C. Hélix-Nielsen, J. Emnéus, O. Geschke; ***Microfluidic formation and regeneration of highly stable biomimetic membrane arrays***

# Microfluidic formation and regeneration of highly stable biomimetic membrane arrays

K Pszon-Bartosz[1,2], M Perry[1], J S Hansen[1,2], J Vogel[1,2], C Hélix-Nielsen[1,3], J Emnéus[2] and O Geschke[1,2]

[1]Aquaporin A/S, Ole Maaløes Vej 3, 2200 Copenhagen N, Denmark
[2]Technical University of Denmark, Department of Micro- and Nanotechnology, DTU Nanotech building 345 east, DK-2800 Kongens Lyngby, Denmark
[3]Technical University of Denmark, Department of Physics, DTU Physics 309, DK-2800 Kongens Lyngby, Denmark

E-mail: kps@aquaporin.dk

**Abstract**

Biochemical analysis of membrane proteins is still a difficult task and requires a method for formation of stable and long lasting lipid membranes; the natural platform to sustain protein functionality. A fully automated and closed microfluidic device for the formation, regeneration and investigation of an array of planar lipid membranes was developed using $CO_2$ laser technique. The device comprised five layers clamped together, rendering the devices cleanable and reusable. By voltage clamp measurements, it was shown that the device allowed the formation and regeneration of an array of lipid bilayers across a perforated (8 x 8 apertures) ETFE partition and that microfluidic pumping enabled thinning of the thick lipid-solvent to form the lipid bilayer. Voltage clamp measurements showed moreover that the pore-forming heptameric α-HL membrane protein could successfully be reconstituted into the bilayer lipid array by simple injection into the microfluidic system.

**Abbreviations**

| | |
|---|---|
| α-HL | α-Hemolysin |
| BFS | Bilayer Forming Solution |
| BLM | Black Lipid Membrane |
| DPhPC | 1,2-Diphytanoyl-*sn*-Glycero-3-Phosphocholine |
| ETFE | Ethylene Tetrafluoroethylene |
| NBD-PC | 1-Oleoyl-2-[6-[(7-nitro-2–1,3-benzoxadiazol-4-yl)amino]hexanoyl]-*sn*-glycero-3-phosphocholine |
| PDMS | Polydimethylsiloxane |
| PMMA | Poly(methyl methacrylate) |
| PTFE | Polytetrafluoroethylene |

## 1. Introduction

There is a growing interest in trying to mimic biological membranes by creating artificial lipid bilayers (biomimetic membranes) that can be used in sensor and separation devices [1]. However, there are still many difficulties to be overcome; amongst these are the inherent fragility of lipid membranes and the challenge of up-scaling the effective membrane area. Various methods for the formation of membrane arrays with long lifetimes (>days) have recently been investigated [2, 3]. Conventionally, lipid membranes are formed across apertures in a hydrophobic material separating two aqueous compartments. In principle they can be established by two different methods; the Mueller-Rudin painting method [4] and the Montal-Mueller folding method [5]. In the folding method, a lipid monolayer is spread at the air-water interface in each compartment. Raising the aqueous solution results in membrane formation across the aperture. In the painting method, lipid membranes are formed by self-assembly of an initially thick lipid-solvent film spread over one side of an aperture submerged in aqueous solution. The lipid layer gradually thins down to form a bilayer. However, this spontaneous process is rather slow and several ways to induce the thinning process have been presented, e.g. manual thinning [3], solvent extraction [6], pressure induced thinning [7-9], agitation by removing and re-injection of the buffer solution in one of the compartment [10], removing excess lipid solution [8], air-exposure technique and a device architecture that promote spontaneous thinning [11] and thinning aided by microfluidics [11]. Suzuki et al. applied either air pressure [7] or hydrostatic pressure [9] to the lipid solution, while Ide and Ichikawa [8] mechanically pressed the thick membrane on an agarose gel to facilitate membrane thinning. To eliminate the problem of removing excess of lipid solution, Sandison et al. [12] developed an air-exposure technique to form an array of lipid membranes within a microfluidic device with fluidic perfusion only on one side of the membrane, still however, requiring manual intervention in the top compartment [2, 13]. Several of the approaches

mentioned above have been performed in microfluidic systems, the motivation being that it enables rapid exchange of electrolytes, use of small quantities of materials, rapid transport of material to and from the lipid membranes and finally the possibility for automation [11, 14]. Automated formation of lipid bilayers in a microfluidic system was proposed by Malmstadt et al. [6], presenting a method using solvent extraction through the walls of a microfluidic channel, and by Funakoshi et al. [15] by contacting two lipid monolayers in a microfluidic device. In both cases the bilayers were formed inside the microfluidic channels perpendicular to the channel wall and therefore electrolyte exchange was not possible. Several studies on membrane formation in a microfluidic system, enabling liquid exchange on both sides of the membrane, have been presented with a microfluidic channel on one side of the membrane, leaving the top compartment of the device open. Open systems like this may however lead to problems with solvent evaporation and limited membrane stability. Sandison et al. [11] proposed a closed system fully accessible via microfluidic channels on both sides of the membrane and also showed that they were able to form a single lipid bilayer membrane by spontaneous thinning of the lipid solution, encouraged by buffer agitation in both channels. Mach et al. [14] designed a microfluidic device for automated formation of a single lipid bilayer by giant liposome adsorption across a micron-sized aperture in a glass slide, sandwiched between two polydimethylsiloxane (PDMS) channels, allowing fast perfusion on each side of the membrane.

Based on earlier work [18] we hypothesized that it should be possible to create bilayers by microfluidic pumping of a lipid solution across an aperture or array of apertures. Subsequent pumping of electrolyte would then induce lipid film thinning. Here we developed a microfluidic system in order to enable continuous formation, thinning, and regeneration of an array of bilayer lipid membranes in a fully closed and automated microfluidic device, as well as the automated reconstitution of a membrane protein inside. The device was entirely fabricated by the $CO_2$ laser technology, which is a quick and inexpensive alternative to existing technologies. The device provides an environment for reconstitution of proteins that is similar to their native one, with the bilayer membrane surrounded by water on both sides, and with the possibility for control of electrolytes on both sides of the membrane and fast and precise exchange/regeneration of the membrane itself.

## 2. Materials and methods

### *2.1 Reagent and materials*

Poly(methyl methacrylate) (PMMA) raw material was used (Nordisk Plast A/S, Denmark) in various plate thicknesses: (1.5, 1.75 and 4) mm. Ethylene tetrafluoroethylene (ETFE) Tefzel LZ200 fluoropolymer for the fabrication of multi-aperture partitions, and Viton® A

fluoroelastomer for the production of microchannels were both from DuPont Fluoropolymers (Detroit, U.S.A.). Double adhesive acrylic tape (ARcare® 90819, Adhesives Research, Ireland) was used for the production of device sealing parts. PDMS (Polydimethylsiloxane– Sylgard® 184 Silicone Elastomer Kit) from DowCorning (Midland, USA**)** was used to fabricate inverse replicas of the produced microchannels. A conventional laboratory oven (Memmert GmbH, Schwabach, Germany) was used for the annealing process of PMMA plates in order to avoid stress cracks.

Ethanol [analytical grade, 97%] was purchased from Merck KGaA (Darmstadt, Germany). A 5 mg/ml lipid-solvent solutions of 1,2-diphytanoyl-sn-glycero-3-phosphocholine (Avanti Polar Lipids, USA) in n-decane, doped with 1 mol% 1-oleoyl-2-[6-[(7-nitro-2-1,3-benzoxadiazol-4-yl)amino]hexanoyl]-*sn*-glycero-3-phosphocholine (Avanti Polar Lipids, USA), was used for membrane formation. Staphylococcus aureus α-Hemolysin (Sigma), n-decane (Fluka) and potassium chloride powder were purchased from Sigma-Aldrich Denmark (Brøndby, Denmark). All electrolyte solutions were prepared using MiliQ water.

### *2.2 $CO_2$ laser setup*

The laser micromachining was carried out using a Synrad Inc. (Mukilteo, WA, USA) 48-5S Duo Lase carbon dioxide laser. A computer aided design program WinMark Pro® version 4 from Synrad Inc. (Mukilteo, WA, USA) was used to set the movements of the laser beam, number of laser beams passing over a given design, laser beam speed and laser output power. The laser had a maximum output power of 65 W, which could be varied linearly. The laser system was equipped with a marking head containing a field lens and two swivel-mounted mirrors. The lens was able to focus the laser beam to a 290 μm diameter spot at a focal distance of 190 mm. The mirrors allowed the placement of the focused laser beam anywhere on a 110 by 110 mm large working area. The maximum speed of the beam was 1000 mm $s^{-1}$.

### *2.3 Device design, fabrication and assembly*

The microfluidic device design is depicted in figure 1. Each part (including tape and holders) was fabricated using $CO_2$ laser technology. Laser settings (number of laser beam passes, laser power and velocity) were adjusted individually to each microfluidic device part. Microchannels were fabricated in two 1 mm thick fluoroelastomeric (Viton®) parts (47 mm x 32 mm), which were then sandwiched with double adhesive tapes on both sides of a 50 μm ETFE partition (47 mm x 32 mm). The sandwich was then covered on both sides with 1.75 mm thick PMMA plates (47 mm x 32 mm), each sealed by tape and then clamped with 4 mm thick PMMA holders (48 mm x 48 mm), using four screws. The two Viton® parts had square chambers in the middle (10 mm x 10 mm) connected to the microchannels, enabling liquid injection and removal. The microchannel system is presented in Figure 1b and the

typical Gaussian profile of the cross-section of one of the Viton® channels is shown in figure 1d and figure 1e. The central 50 µm thick ETFE partition, with an array of 8 x 8 apertures (300 µm - diameter of each, 400 µm - centre-centre distance between two of them), was laser micromachined as previously described [16]. The ETFE surface was covalently modified by plasma treatment with lower-carbon-chain-length alkanes, predominantly hexanes, resulting in a hydrophobic surface coating. This surface modification was applied to provide a molecular anchoring for establishing the lipid membranes across the micro-structured arrays.

Prior to alignment and assembly the different parts were cleaned by flushing or sonication with ethanol and water. The most crucial step was the sealing of the Viton® parts with the ETFE partition, since placing the double adhesive tapes around the microchannel edges required high precision. To enable connection of the Viton® microchannels to the outer world, prior to sealing, 10 µl Eppendorf tips (Eppendorf Nordic, Denmark) were put into holes made by 0.7 mm in diameter needles on two sides of the Viton® material. The plastic tips provided flexible but stable interconnection between the Viton® microchannels and PTFE tubing with an inner diameter of 0.8 mm and an outer diameter of 1.6 mm (Bohlender GmbH, Germany). In order to improve fluidic sealing, thick PMMA plates were used to clamp the device together.

### *2.4 Characterization of Viton® micro-channels*

Two methods were used to characterize the black non-transparent Viton® fluoroelastomeric material: laser scanning confocal microscopy (LSCM) and optical microscopy. The first method involved the fabrication of PDMS replicas of the structured Viton® micro-channels, i.e. PDMS was poured on top of the micro-channels, cured and released. The PDMS replica was then placed in a Rhodamine B solution to make it fluorescent for further analysis with LSCM. The second method involved measuring the channel depth and width by taking pictures of the channel cross-section using a Leica DML optical microscope and a built-on Canon Power Shot S40. The pictures were analysed using the freeware software ImageJ. The channel depth and width was measured using a built-in measurement function, relating the acquired length in pixels to a scale.

### *2.5 Connection with injector, pumps and electrical set up*

The microfluidic system set-up, with pumps, injector, syringe barrels and electrodes is illustrated in figure 2. The device consisted of two compartments, each one with its own inlet and outlet. The inlet of the top and bottom compartment was connected to each a syringe pump (1 and 3)(model: 540060, TSE system GmbH, Germany). The bottom compartment was in addition connected to a six-valve rotary injector (2)

(IDEX Health & Science, Germany) equipped with a 40 µl injection loop for injection of small quantities of different liquids. Both outlets were further connected to Ag/AgCl electrodes inserted in two syringe barrels (4 and 5) with the same level of liquid to minimize the pressure difference on each side of the ETFE partition.

The microfluidic device, injector and syringe pumps were placed in an in-house manufactured Faraday cage in which Voltage clamp measurements were performed. The electrical setup consisted of a headstage (HS-2A, Eastern Scientific LLC), an amplifier (PICOAMP-300, Eastern Scientific LLC), and an oscilloscope (IDS710, ISO-TECH). Data acquisition was performed with a combined oscilloscope/analogue-digital converter (ADC-212, Pico technology). A 200 mM or 1 M KCl solution served as an electrolyte for membrane and protein incorporation characterisation, respectively. By applying triangular and rectangular voltage clamp wave forms across the BLMs, and measuring the resulting responses, the capacitance and conductance of the membrane array could be calculated respectively, as previously described [17]. To measure protein incorporation electrically, a potential of +60 mV was applied, and the resulting membrane output current was filtered through 1 kHz on the amplifier and subsequently further filtered through a low-pass Bessel filter with 50 Hz cut-off (Frequency Devices, IL, USA) before data acquisition.

### *2.6 Flow rate tests*

Different flow rates with either electrolyte or n-decane were tested through the upper and bottom compartments to ensure that no leakage took place in the system. Pumping was carried out at increasing flow rates from 5 to 50 µl/min with increments of 5 µl/min, until leakage was observed or for 10 min if the device was not leaking.

### *2.7 Preparation of lipid solutions for BLM experiments*

The bilayer forming solution (BFS) consisted of 1,2-diphytanoyl-*sn*-glycero-3-phosphocholine (DPhPC) in n-decane (5 mg/ml), doped with 1 mol% 1-oleoyl-2-[6-[(7-nitro-2-1,3-benzoxadiazol-4-yl)amino]hexanoyl]-*sn*-glycero-3-phosphocholine (NBD-PC) to enable visual inspection of the BFS. The BFS was prepared the day before, and stored at −20 °C until use.

### *2.8 Procedure for bilayer membrane formation*

Planar lipid membranes were established across the laser microfabricated ETFE partition array by a modification of the lipid bilayer painting method [4]. The main difference was that the lipid bilayer was automatically formed and thinned aided by microfluidics. The procedure is illustrated in figure 3: (a) the electrolyte was pumped at a flow rate of 50 µl/min, through both compartments of the microfluidic device, (b) 40 µl of the BFS was then injected into the

bottom compartment. As the BFS passes the ETFE array partitioning, it is painted onto the array, (c) the excess BFS is removed and the membrane thinning process induced by the continuous flow of electrolyte through the top and bottom compartments, (d) finally, electrical measurements on the formed bilayer lipid membranes were performed.

*2.9 Reconstitution of transmembrane protein*

*S. aureus* α-hemolysin (α-HL) was reconstituted into the 8 × 8 bilayer membrane array by injecting 40 µl of a 10 µg/ml stock solution in 1.0 M KCl into the bottom chamber of the microfluidic system. In this case the aqueous solution pumped through the microfluidic compartments was 1.0 M KCl.

## 3. Results and discussion

A closed microfluidic device for automated formation, regeneration and subsequent investigation of an array of planar lipid membranes, incorporating reconstituted protein inside, was developed and investigated. The device was entirely fabricated by $CO_2$ laser ablation; therefore of low cost with a production time of only a few minutes. The device consisted of two compartments separated by a perforated ETFE partition, across which bilayer lipid membranes were formed. Fast injection and removal of liquids above and below the ETFE partition was possible using continuous pumping of electrolyte and injection of the bilayer forming solution followed by the protein solution, and where the lipid membrane thinning process was induced by the microfluidic process. Since the microchannels were created in a fluoroelastomer material (Viton®), which is chemically resistant to hydrocarbons, n-decane containing bilayer forming solutions were not detrimental to the system.

Conventional painting methods for lipid bilayer formation are slow and require that a thick bulky membrane spontaneously thin into a bilayer membrane. Current methods for lipid bilayer formation also usually require manual application of the BFS across the membrane support. So far utilization of a microfluidic system with a fully closed chamber for automated formation, regeneration of an array of bilayer lipid membranes, as well reconstitution of protein therein, has to our knowledge not yet been implemented.

*3.1 Establishment of long-life biomimetic membranes in the microfluidic device by pumping induced thinning process*

The procedure for bilayer membrane formation in the microfluidic device is shown in figure 3. A pre-defined volume of the BFS was injected into the lower compartment of the device, covering the entire membrane support; a process that could be repeated many times ($1^{st}$, $2^{nd}$ $3^{rd}$ generation membrane). Continuous monitoring of membrane capacitance and conductance over time indicated whether the BFS thinned into lipid bilayers in the ETFE

partitioning using microfluidic pumping. By continues pumping electrolyte into the two compartments of the device, excess of BFS was removed and the thinning process was electrically studied. After a first portion of BFS was injected, an increase in membrane capacitance was observed after approximately 25 min (increase in effective bilayer area) while the membrane conductance remained at the same level (indicating a tight membrane)(figure 4, 1st generation membrane). Further pumping resulted in membrane leaking, which finally resulted in breakage of the membrane (an increase in membrane capacitance was concomitant with an increase in membrane conductance indicating an increase in ionic leak across the membrane). A 2nd generation membrane was created by injecting a new portion of BFS. As seen in figure 4, the same behaviour of capacitance and conductance over time was observed as for the 1st generation membrane. When injecting a 3rd BFS portion (figure 5), it can be seen that membrane life time (3rd generation membrane) was significantly increased, however, (the effective membrane area did not change) (the same capacitance value as for the 1st and 2nd generation membranes). Successful formation of the 3rd generation membrane was thus likely enabled by the pre-painting (1st and 2nd generation membranes) of the ETFE partition by the BFS, similarly as previously described [18]. The lipid bilayer arrays established under these conditions had a lifetime of ~42 h and exhibited capacitance and conductance values of ~4300 pF and ~250 nS, respectively. The specific membrane capacitance for n-decane containing lipid bilayer membranes is ~0.4 μF $cm^{-2}$ [19], which indicated that the bilayer area constituted around ~24 % of the aperture area. A future optimisation of the microfluidic system could prove important in order to obtain a uniform lipid flow through the device and to have a better control of the pressure applied to the system; in this way possibly increase the effective lipid bilayer area.

### *3.2 Incorporation of the pore-forming heptameric α-HL membrane protein demonstrates that functional lipid bilayers were established*

To evaluate if functional lipid bilayers were established in the microfluidic device, the pore-forming heptameric α-HL membrane protein was reconstituted into the lipid bilayer membrane array. The membrane pore of α-HL can be created in a lipid bilayer upon assembly of seven 33 kDa monomeric polypeptides on the membrane surface [20, 21]. The α-HL membrane protein was injected into the bottom compartment of the microfluidic system incorporating in pre-formed bilipid membrane arrays, and the obtained current trace recorded (figure 6). Stepwise current increases could be observed and compared with previously presented results [22], Scaling the literature single channel incorporation current value [~35pA] to our experimental conditions [~70pA] according to electrolyte conductivity, our results demonstrate that α-HL pores were inserted into a lipid bilayer at the timeThis strongly confirmed that functional lipid bilayers were established in the microfluidic device.

## 4. Conclusion

A fully automated and closed microfluidic device for the formation, regeneration and investigation of an array of planar lipid membranes with reconstituted α-HL membrane protein was described. The benefits of this automated and closed microfluidic device include controlled deposition of lipid solution into the apertures, thick lipid film thinning facilitated by microfluidic pumping, improvement of the membrane stability and lifetime (42 hours), and solution exchange on both sides of the membrane. The device was entirely fabricated by $CO_2$ laser technology, which is a quick and inexpensive alternative to existing technologies. The system provides an environment for reconstituting proteins that is similar to their native one, having the bilayer surrounded on both sides by water, thus providing the possibility of fast and precise measurement of exchange of analytes and ligands through transmembrane protein pores and channels. The developed system shows the potential for formation of biomimetic membrane arrays that could be useful for biochemical studies of proteins and for the development of future sensor arrays and separation technologies.

## 5. Acknowledgments

The work was supported by MEMBAQ (STREP, NMP4-CT-2006-033234) and The Danish National Advanced Technology Foundation (023-2007-1).

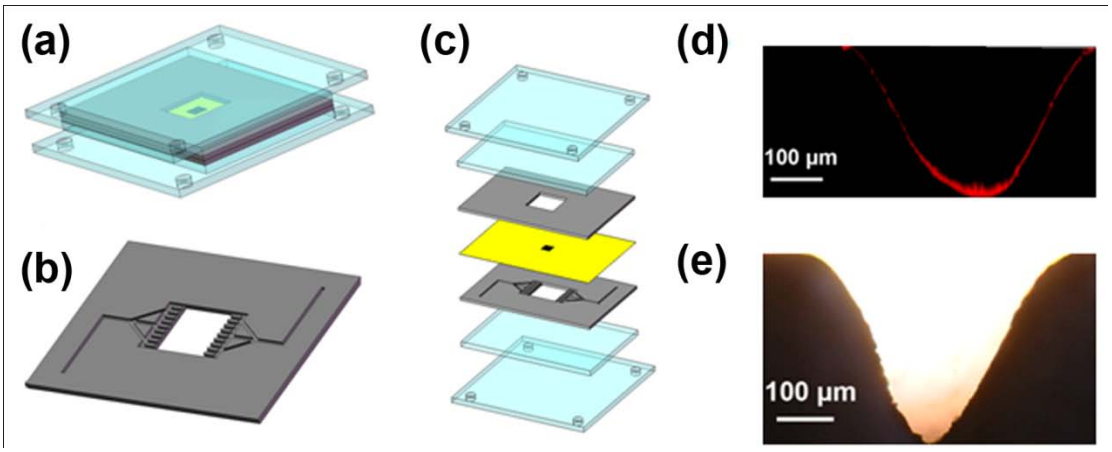


OR

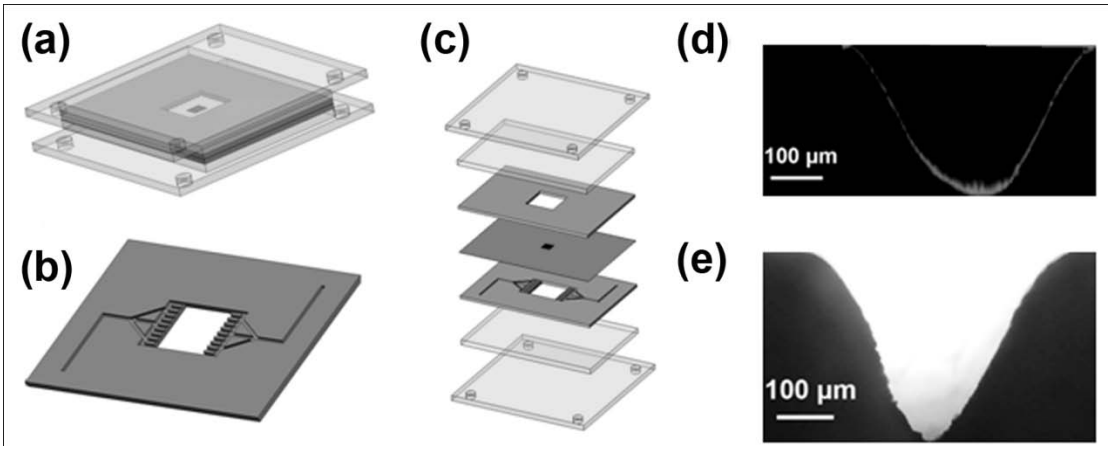


**Figure 1** The microfluidic device; (a) an assembled device, (b) a Viton® with micro-channels system, (c) exploded view of the device. The component order of the assembly is from bottom to top: a PMMA clamping holder, a PMMA plate, a Viton® with microchannels, an ETFE partition, a Viton® with microchannels, a PMMA plate, a PMMA clamping holder, (d) a cross-section of a Viton® microchannel inverse copy in PDMS in a confocal laser scanning microscope, (e) a cross-section of a Viton® microchannel in an optical microscope.

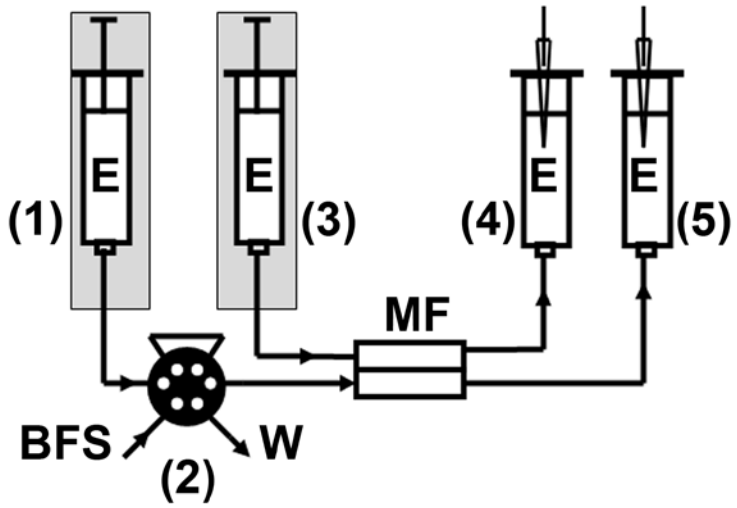


**Figure 2** The microfluidic system set-up containing: (1), (3) syringe pumps delivering electrolyte (E) to both microfluidic device compartments; (2) six-valve rotary injector enabling electrolyte (E) and bilayer forming solution (BFS) injection into the bottom compartment and waste (W) removing; (4), (5) syringe barrels collecting liquids from the top and bottom compartments enabling electrical measurements of the lipid membrane formed within the device.

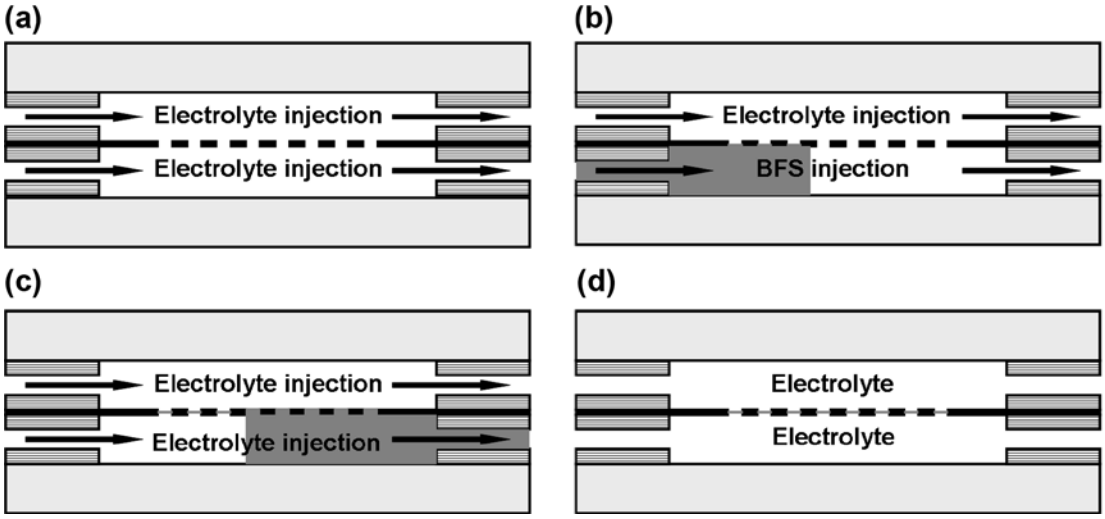


**Figure 3** The procedure for bilayer membrane**s** formation in the microfluidic device; (a) the electrolyte is pumped at a flow rate of 50 µl/min, through both compartments of the microfluidic device, (b) 40 µl of the BFS is then injected into the bottom compartment, (c) the excess BFS is removed and the membrane thinning process induced by the continuous flow of electrolyte through the top and bottom compartments, (d) finally, electrical measurements on the formed bilayer lipid membranes can be performed.

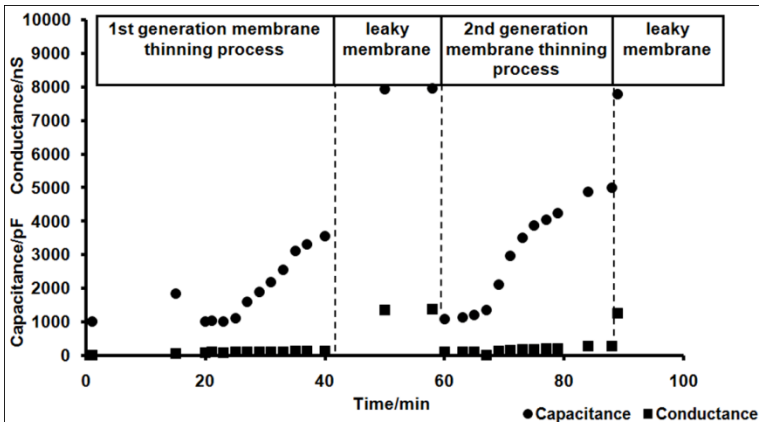


**Figure 4** Capacitance and conductance versus time created in the microfluidic device 1st and 2nd generation membranes. Membrane thinning was induced by microfluidic pumping.

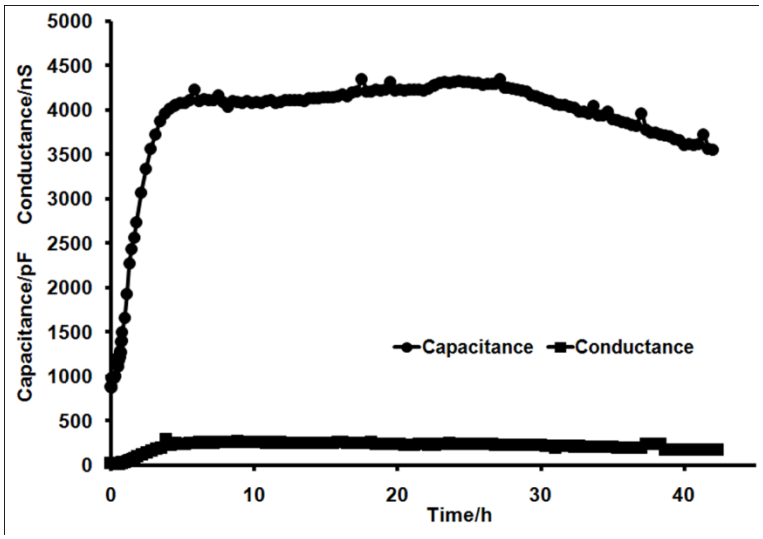


**Figure 5** Capacitance and conductance versus time created in the microfluidic device 3rd generation membrane. Membrane thinning was induced by microfluidic pumping.

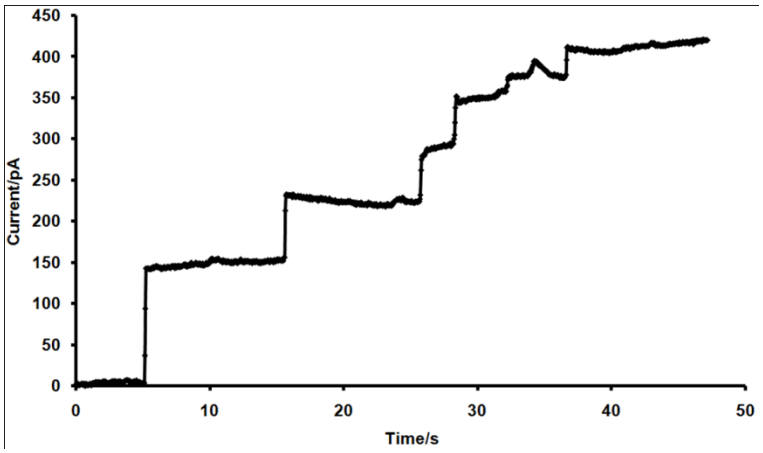


**Figure 6** Current trace of the reconstitution of the pore-forming heptameric α-HL membrane protein in established in the microfluidic device 8×8 bilayer arrays.

## 6. References

[1] Nielsen CH. Biomimetic membranes for sensor and separation applications. Analytical and Bioanalytical Chemistry. 2009;395[3]:697-718.

[2] Zagnoni M, Sandison ME, Morgan H. Microfluidic array platform for simultaneous lipid bilayer membrane formation. Biosensors and Bioelectronics. 2009;24[5]:1235-40.

[3] Hansen JS, Perry M, Vogel J, Groth JS, Vissing T, Larsen MS, et al. Large scale biomimetic membrane arrays. Analytical and Bioanalytical Chemistry. 2009;395[3]:719-27.

[4] Mueller P, Rudin Do. Bi molecular lipid membranes techniques of formation study of electrical properties and induction of ionic gating phenomena. 1969:141-56.

[5] Montal M, Mueller P. Formation of bimolecular membranes from lipid monolayers and a study of their electrical properties. Proc Natl Acad Sci U S A. 1972;69[12]:3561-6.

[6] Malmstadt N, Nash MA, Purnell RF, Schmidt JJ. Automated formation of lipid-bilayer membranes in a microfluidic device. Nano Letters. 2006;6[9]:1961-5.

[7] Suzuki H, Tabata KV, Noji H, Takeuchi S. Highly reproducible method of planar lipid bilayer reconstitution in polymethyl methacrylate microfluidic chip. Langmuir. 2006;22[4]:1937-42.

[8] Ide T, Ichikawa T. A novel method for artificial lipid-bilayer formation. Biosensors and Bioelectronics. 2006;21[4]:672.

[9] Suzuki H, Tabata KV, Noji H, Takeuchi S. Electrophysiological recordings of single ion channels in planar lipid bilayers using a polymethyl methacrylate microfluidic chip. Biosensors and Bioelectronics. 2007;22[6]:1111-5.

[10] Sandison ME, Zagnoni M, Abu-Hantash M, Morgan H. Micromachined glass apertures for artificial lipid bilayer formation in a microfluidic system. J Micromech Microengineering. 2007;17[7]:S189-96.

[11] Sandison ME, Morgan H. Rapid fabrication of polymer microfluidic systems for the production of artificial lipid bilayers. J Micromech Microengineering. 2005;15[7]:S139-44.

[12] Sandison ME, Zagnoni M, Morgan H. Air-exposure technique for the formation of artificial lipid bilayers in microsystems. Langmuir. 2007;23[15]:8277-84.

[13] Zagnoni, Sandison, Marius, Lee, Morgan. Controlled delivery of proteins into bilayer lipid membranes on chip. Lab on a Chip. 2007;7[9]:1176-83.

[14] Mach T, Chimerel C, Fritz J, Fertig N, Winterhalter M, Futterer C. Miniaturized planar lipid bilayer: Increased stability, low electric noise and fast fluid perfusion. Analytical and Bioanalytical Chemistry. 2008;390[3]:841-6.

[15] Funakoshi K, Suzuki H, Takeuchi S. Lipid bilayer formation by contacting monolayers in a microfluidic device for membrane protein analysis. Anal Chem. 2006;78[24]:8169-74.

[16] Vogel J, Perry M, Hansen JS, Bolinger P, Nielsen CH, Geschke O. A support structure for biomimetic applications. J Micromech Microengineering. 2009;19[2]:025026.

[17] Perry M, Vissing T, Boesen TP, Hansen JS, Emneus J, Nielsen CH. Automated sampling and data processing derived from biomimetic membranes. Bioinspiration. 2009;4[4]:044001.

[18] Hansen JS, Perry M, Vogel J, Vissing T, Hansen CR, Geschke O, et al. Development of an automation technique for the establishment of functional lipid bilayer arrays. J Micromech Microengineering. 2009;19[2]:025014.

[19] Benz R, Janko K. Voltage-induced capacitance relaxation of lipid bilayer membranes effects of membrane composition. Biochimica et Biophysica Acta [BBA]/Biomembranes. 1976;455[3]:721-38.

[20] Dinges MM, Orwin PM, Schlievert PM. Exotoxins of staphylococcusaureus. Clin Microbiol Rev. 2000;13[1]:16-34.

[21] Fink D, Contreras ML, Lelkes PI, Lazarovici P. Staphylococcus aureus α-toxin activates phospholipases and induces a Ca2+ influx in PC12 cells. Cell Signal. 1989;1[4]:387-93.

[22] Hemmler, Bose, Wagner, Peters. Nanopore unitary permeability measured by electrochemical and optical single transporter recording. Biophys J. 2005;88[6]:4000-7.